

University of Alberta

**Synthesis and Properties of Graphyne Model Compounds and an
Electrochemical Study of Substituted Pentacenes**

by

Adrian Harrison Murray

A thesis submitted to the Faculty of Graduate Studies and Research
in partial fulfillment of the requirements for the degree of

Doctor of Philosophy

Chemistry

©Adrian Harrison Murray

Spring 2013
Edmonton, Alberta

Permission is hereby granted to the University of Alberta Libraries to reproduce single copies of this thesis and to lend or sell such copies for private, scholarly or scientific research purposes only. Where the thesis is converted to, or otherwise made available in digital form, the University of Alberta will advise potential users of the thesis of these terms.

The author reserves all other publication and other rights in association with the copyright in the thesis and, except as herein before provided, neither the thesis nor any substantial portion thereof may be printed or otherwise reproduced in any material form whatsoever without the author's prior written permission.

Abstract

The work described in this thesis focuses on two central topics: (1) the synthesis of carbon-rich macrocycles as model compounds of the carbon allotrope graphyne and the study of their electronic properties, and (2) the electrochemical investigation of the properties of substituted pentacene molecules. To this end, Chapter 1 first offers an introduction to conjugated organic materials, focusing on acetylene-rich macrocycles. Subsequently, the theoretical structures of graphyne are introduced, and their potential properties described. Previous synthetic efforts to prepare model compounds for graphyne are also discussed.

Chapter 2 focuses on the synthesis of 12,12,12-graphyne. Described first are the syntheses of small molecules based on four molecular scaffolds: (1) aryl triazenes, (2) dibromoolefins, (3) tetraethynylethenes, and (4) vinyl triflates. These molecules are characterized using standard methods, including ^1H and ^{13}C NMR, IR, and mass spectrometries. These molecules are then used as building blocks toward the synthesis of expanded radialenes, which would serve as model compounds for 12,12,12-graphyne.

Chapter 3 focuses on the use of small molecules prepared in Chapter 2 as building blocks toward a series of radiannulene oligomers, which serve as model compounds for 6,6,12-graphyne. Several synthetic routes are explored in an effort to optimize preparation of the series of radiannulenes. The products are characterized by ^1H and ^{13}C NMR, IR and mass spectrometries, as well as by X-ray crystallography. The electronic properties are investigated using UV-vis spectroscopy and cyclic voltammetry to provide insight into the potential properties of 6,6,12-graphyne.

Chapter 4 focuses on the electrochemical properties of substituted pentacenes. A brief introduction to pentacene and functionalized pentacene is provided. The syntheses of several pentacene derivatives is outlined, and the synthesis of conjugated pentacene-

thiophene molecules is described. The effect of the substituents on the HOMO and LUMO energy levels and band gaps of the pentacene molecules is described, based on results from cyclic voltammetry.

The thesis concludes with a brief summary, an outlook for the synthesis graphyne model compounds, and a description of how radiaannulenes might serve as useful materials in the synthesis of other conjugated organic molecules.

Acknowledgements

I would first like to thank my supervisors, Prof. Rik R. Tykwinski and Prof. Jonathan G. C. Veinot, for their guidance, feedback, and support over the course of my degree. They both gave me the opportunity to be an independent researcher, while providing insight and encouragement when needed.

I have also been given the opportunity to work with many friendly and talented chemists over the course of my degree. I would like to thank my fellow Tykwinski group members at the University of Alberta. Thanks to Erin Sullivan, Khalid Azyat, and Thanh Luu for their help and assistance with courses, exams, and presentations. Thanks to Sharwatie Ramsaywack and Mojtaba Gholami for their discussions on radialenes. Thanks to BJ Medos, Dan Lehnerr and Wesley Chalifoux for their guidance, mentoring, and great discussions. Thanks to Dan Lehnerr for assistance with the synthesis of conjugated pentacenes for electrochemical analysis.

I would like to thank the entire Veinot research group, for graciously welcoming me into the fold and making me an active member of their group. Thanks to the “organic group”, Brenna Brown and Leah Coumont, for their discussions, assistance, and of course sharing their lab space with me.

I would like to express my gratitude to all of the department analytical services; especially Wayne Moffat and Marc-Andre Hoyle for their assistance with IR, TGA, and DSC, and Dr. Randy Whittal, Dr. Angie Morales-Izquierdo, and Jing Zheng for their assistance with mass spectrometry.

I also have to thank the Arbeitskreis Tykwinski, at the Friedrich-Alexander-Universität Erlangen-Nürnberg, Germany. Thanks to Dr. Alex Scherer, Dr. Eike Jahnke, and Dr. Gabor Borzsonyi for being friendly, familiar faces when I arrived, and for your insightful discussions. Thanks to Pamela Hampel for all of her assistance with the move

to and from Germany. Thanks to Dr. Frank Hampel for the X-ray crystallographic structures he solved. Thanks to the other “visiting” researchers, Dr. Norbert Grzegorzec, Sylvia Kunakom, Anna-Chiara Salle, Patricia Garcia Catala, Kensuke Kiyokawa, and Akihito Konishi. Special thanks to Andreas Waterloo, Dominik Prenzel, Vincent Oerthel, Maximilian Krempe, Matthias Adam, Julia Tyrach, Katrin Schmidt, Matthias Schulze, Stephanie Frankenberger, Johanna Januszewski, Dominik Wendinger, Michael Franz, Andrea Radwansky, Ute Meinhardt, Martin Pröller, and Vroni Walter; they welcomed me with open arms, invited me to everything, and made what could have been a difficult period of my degree a fantastic and unforgettable experience.

I also have to thank my family for all of their love and encouragement during my many years as a student. Finally, I have to thank my wife Laura. She has been tremendously supportive over the course of my degree, even when it forced us continents apart. Without her understanding, patience, and love I could not have completed this feat.

Table of Contents

Chapter 1 – Introduction to Conjugated Materials and Graphyne	1
1.1 Introduction to Conjugated Materials.....	1
1.2 Conjugated Hydrocarbons: All Carbon and Carbon-rich materials.....	2
1.3 Hybrid Structures: Materials Based on sp^2 -Carbon and sp -Carbon.....	3
1.3.1 Acetylene-rich Macrocycles: Expanded Radialenes, Radiaannulenes and Dehydroannulenes.....	4
1.3.2 Phenylacetylene Based Molecules and Macrocycles: Models of Graphyne.....	15
1.3.3 Physical Properties of Graphyne Model Compounds.....	28
1.4 Conclusion.....	29
1.5 References.....	30
Chapter 2 - Model Compounds of 12,12,12-Graphyne Based on Expanded Radialenes	35
2.1 Introduction.....	35
2.2 Synthesis of Building Blocks.....	41
2.2.1 Synthesis of Aryl Triazenes.....	41
2.2.2 Synthesis of Dibromoolefins.....	43
2.2.3 Synthesis of Tetraethynylethenes (TEEs).....	45
2.2.4 Synthesis of Vinyl Triflates.....	49
2.2.5 Synthesis of <i>iso</i> -Polydiacetylenes (PDAs).....	53
2.3 Conclusion.....	56
2.4 References.....	57
Chapter 3 - Model Compounds of 6,6,12-Graphyne Based on Radiaannulenes	61
3.1 Introduction.....	61

3.2 Synthesis of Radiannulenes Using a One-pot Approach	64
3.3 Synthesis of a Di-Radiaannulene Using a One-pot Approach	67
3.4 Synthesis of Radiannulenes Using a Stepwise Approach.....	72
3.5 Synthesis of Substituted Radiannulenes	85
3.6 Physical Properties of Radiannulenes	87
3.7 Conclusion	104
3.8 References	105
Chapter 4 – Electrochemical Investigations of Functionalized Pentacenes	
and Pentacene Oligomers	107
4.1 Introduction	107
4.1.1 Introduction to Pentacene	108
4.2 Synthesis and Electrochemical Properties of Polarized Pentacenes	112
4.3 Synthesis and Electrochemical Properties of Pentacene/Polycyclic	
Aromatic Hydrocarbon Dyads	123
4.4 Electrochemical Properties of Conjugated Pentacene Oligomers.....	127
4.5 Synthesis and Electrochemical Properties of Conjugated Dimers of	
Diethynylpentacene Linked by π -Spacers	133
4.6 Attempted Electrochemical Polymerization of 4.19j	143
4.7 Conclusion	144
4.8 References	145
Chapter 5 – Conclusions and Future Outlook	147
5.1 Conclusions	147
5.2 Outlook	148
5.3 References	153
Chapter 6 – Experimental Section	155
6.1 General Experimental Details	155

6.2 Experimental Details for Chapter 2	158
6.3 Experimental Details for Chapter 3	176
6.4 Experimental Details for Chapter 4	204
6.5 References	209

List of Tables

Table 2-1. Conditions used toward optimizing the synthesis of 2.47	55
Table 3-1. Thermal properties of mono-radiaannulenes.	88
Table 3-2. UV-vis spectral data for compounds 3.7a–c and 3.30–3.32 in THF.	91
Table 3-3. UV-vis spectral data for compounds 3.21 , 3.35a , and 3.35b in THF.	92
Table 3-4. Electrochemical properties of compounds 3.7a , 3.7b , 3.33–3.34 , and 3.35a–b in CH ₂ Cl ₂ (vs Fc/Fc ⁺ couple).....	94
Table 3-5. Selected bond angles for radiaannulenes 3.7a , 3.9 , 3.7b , 3.35a , and 3.35b (°).	101
Table 3-6. Selected bond lengths and interplanar distances for radiaannulenes 3.7a , 3.9 , 3.7b , 3.35a , and 3.35b (Å).	102
Table 4-1. Electrochemical properties of pentacene copolymers 4.16–4.18	112
Table 4-2. Electrochemical properties (vs Fc/Fc ⁺ couple) and optical band gap of pentacenes 4.10 , 4.23a–n , and 4.27a–b	118
Table 4-3. Electrochemical properties (vs Fc/Fc ⁺ couple) and optical band gap of pentacene-PAH dyads 4.23e and 4.31a–e	125
Table 4-4. Electrochemical properties of conjugated pentacene oligomers 4.33–4.35 in THF (vs Fc/Fc ⁺ couple).....	129
Table 4-5. Electrochemical properties of conjugated pentacene oligomers 4.33–4.35 in CH ₂ Cl ₂ (vs Fc/Fc ⁺ couple).	132
Table 4-6. Electrochemical properties (vs Fc/Fc ⁺ couple) and optical band gap of pentacenes 4.37a–n	138

List of Figures

Figure 1-1. Common conjugated organic polymers.	2
Figure 1-2. Structural representation of select examples of two-dimensionally conjugated molecules.	4
Figure 1-3. Structures of functionalized expanded [4]radialenes with yields of final cyclization step as prepared by Tykwinski and Gholami (1.46a–d).....	13
Figure 1-4. Theoretical structures of graphynes as reported by Baughman and coworkers.....	17
Figure 1-5. Absorption spectra of 1.64 , 1.74a–c , and 1.98 . Adapted with permission from Johnson II, C. A.; Lu, Y.; Haley, M. M. <i>Org. Lett.</i> 2007 , <i>9</i> , 3725–3728. Copyright 2007 American Chemical Society.....	29
Figure 2-1. Schematic representation of expanded [4]-, [5]-, and [6]radialenes.....	36
Figure 2-2. Retrosynthetic routes to substituted 4[ER] _s , where R ₁ and R ₂ are desired functional groups.....	36
Figure 2-3. Structure of 12,12,12-graphyne and its corresponding model compound based on a [6]ER.....	37
Figure 2-4. Schematic representations of (a) aryl triazenes, (b) dibromoolefins, (c) TEEs, and (d) vinyl triflates.....	40
Figure 2-5. Structures of dibromoolefins 2.25 and 2.26	44
Figure 3-1. Structure of 6,6,12-graphyne and its corresponding model compound 3.1 based on a radiaannulene.....	62
Figure 3-2. Examples of known radiaannulenes prepared by Diederich (3.2a–b), Zhao (3.3a–b), Nielsen (3.4), Tykwinski (3.5a–b), and Mazki (3.6).....	63
Figure 3-3. Oligomeric series of mono-, di-, and tri-radiaannulenes 3.7a–c as model compounds of 6,6,12-graphyne.....	64

Figure 3-4. TLC analysis for the selective desilylation of 3.32 (silica gel, 4:1 Hex/CH ₂ Cl ₂).....	82
Figure 3-5. High-resolution MALDI mass spectrum of 3.7c (M ⁺) recovered from preparative TLC.	85
Figure 3-6. UV-vis spectra of compounds 3.32–3.34 as measured in THF. (Spectra normalized by assigning absorption at $\lambda_{\max} = 1$).....	90
Figure 3-7. UV-vis spectra of compounds 3.7a–c as measured in THF. (Spectra normalized by assigning absorption at $\lambda_{\max} = 1$).....	90
Figure 3-8. Scheme showing increase in λ_{\max} versus structure for compounds a) 3.32 , b) 3.7a , c) 3.33 , d) 3.7b , e) 3.34 , and f) 3.7c , as measured in THF.....	91
Figure 3-9. UV-vis spectra of compounds 3.21 , 3.35a , and 3.35b as measured in THF....	93
Figure 3-10. CV plots for compounds (a) 3.7a , (b) 3.7b , (c) 3.33 , (d) 3.34 , (e) 3.35a and (f) 3.35b as measured in CH ₂ Cl ₂ (vs Ag/AgCl)..	95
Figure 3-11. OSWV plot of radiaannulene 3.7a as measured in CH ₂ Cl ₂	96
Figure 3-12. ORTEP representation of X-Ray data for radiaannulenes 3.7a and 3.9 (atoms are represented by Gaussian ellipsoids at the 50% probability level, hydrogen atoms omitted for clarity).	98
Figure 3-13. X-ray crystallographic structures of radiaannulenes 3.7a and 3.9 illustrating solid-state packing (atoms are represented by Gaussian ellipsoids at the 50% probability level, hydrogen atoms omitted for clarity).	98
Figure 3-14. (a) ORTEP representation of X-Ray data for di-radiaannulene 3.7b (b) Edge- on view illustrating solid-state packing (atoms are represented by Gaussian ellipsoids at the 50% probability level, hydrogen atoms omitted for clarity).	100
Figure 3-15. (a) ORTEP representation of X-Ray data for radiaannulene 3.35a and 3.35b (b) Edge-on view for 3.35a and 3.35b illustrating solid-state packing (atoms are represented by Gaussian ellipsoids at the 50% probability level, hydrogen atoms and	

co-crystallized solvent molecules omitted for clarity).....	103
Figure 4-1. CV plots of pentacenes (a) 4.10 , (b) 4.23a , (c), 4.23b , (d), 4.23c , (e) 4.23d , (f) 4.23e , (g) 4.23f , and (h) 4.23g as measured in 3:1 benzene/MeCN (vs Ag/Ag ⁺).	121
Figure 4-2. CV plots of pentacenes (a) 4.23h , (b) 4.23i , (c), 4.23j , (d), 4.23k , (e) 4.23l , (f) 4.23m , (g) 4.27a , and (h) 4.27b as measured in 3:1 benzene/MeCN (vs Ag/Ag ⁺)...	122
Figure 4-3. HOMO-LUMO energy levels of polarized pentacenes 4.10 , 4.23a–m and 4.27a–b	123
Figure 4-4. CV plots of pentacenes (a) 4.23e , (b) 4.31a , (c) 4.31b , (d) 4.31c , (e) 4.31d , and (f) 4.31e as measured in 3:1 benzene:acetonitrile (vs Ag/Ag ⁺).....	126
Figure 4-5. HOMO-LUMO energy levels of pentacene-PAH dyads 4.23e and 4.31a–e	127
Figure 4-6. Structures of conjugated pentacene oligomers 4.33–4.36	128
Figure 4-7. CV plots of pentacenes (a) 4.33 , (b) 4.34 , and (c) 4.35 as measured in THF (vs Ag/Ag ⁺).	130
Figure 4-8. HOMO-LUMO energy levels of conjugated pentacenes 4.33–4.35 as measured in THF.	131
Figure 4-9. CV plots of pentacenes (a) 4.33 , (b) 4.34 , and (c) 4.35 as measured in CH ₂ Cl ₂ (vs Ag/Ag ⁺).	133
Figure 4-10. CV plots of pentacenes (a) 4.37a , (b) 4.37b , (c) 4.37c , (d) 4.37d , (e) 4.37e , and (f) 4.37n as measured in CH ₂ Cl ₂ (vs Ag/Ag ⁺).	141
Figure 4-11. CV plots of pentacenes (a) 4.37g , (b) 4.37h , (c) 4.37k , (d) 4.37i , and (e) 4.37j as measured in CH ₂ Cl ₂ (vs Ag/Ag ⁺).	142
Figure 4-12. HOMO-LUMO energy levels of conjugated pentacene dimers 4.37a–n	143
Figure 4-13. Attempted electrochemical polymerization of 4.23j using CV as measured in CH ₂ Cl ₂ (vs Ag/Ag ⁺).	144

List of Schemes

Scheme 1-1. Synthesis of expanded radialenes 1.1 , 1.2 , and 1.3	5
Scheme 1-2. Synthesis of expanded radialenes 1.7 , 1.8 , and 1.9	6
Scheme 1-3. Synthesis of dehydroannulenes 1.10 and 1.11	6
Scheme 1-4. Attempted synthesis of radiannulene 1.13 and formation of 1.16	7
Scheme 1-5. Synthesis of bicyclic radiannulenes 1.20a and 1.20b	8
Scheme 1-6. Synthesis of expanded radialenes 1.27 and 1.28	10
Scheme 1-7. Synthesis of perphenylated <i>iso</i> -PDA oligomers 1.31–1.34	11
Scheme 1-8. Synthesis of expanded radialenes 1.36–1.39 and hybrid radialene 1.40	11
Scheme 1-9. Synthesis of bicyclic radiannulene 1.42	12
Scheme 1-10. Synthesis of bicyclic radiannulene 1.43 and bis-expanded radialene 1.44	12
Scheme 1-11. Synthesis of functionalized expanded [3]radialenes 1.45a–e	13
Scheme 1-12. Synthesis of functionalized expanded [4]radialenes 1.48a–1.48d	14
Scheme 1-13. Synthesis of donor substituted expanded [4]radialene 1.50 and donor / acceptor substituted expanded [4]radialenes 1.51 and 1.52	14
Scheme 1-14. Step-wise synthesis of bis-expanded radialene 1.44	15
Scheme 1-15. Synthesis of hexaethynylbenzene 1.61	18
Scheme 1-16. Synthesis of hexakis(arylethynyl)benzene 1.62	19
Scheme 1-17. Cyclotrimerization of 1.65 to dehydrobenzannulene 1.64	19
Scheme 1-18. Stepwise synthesis of dehydrobenzannulene 1.64	20
Scheme 1-19. Synthesis of “bow-tie” bis-dehydrobenzannulene 1.70	21
Scheme 1-20. Synthesis of substituted “bow-tie” dehydrobenzannulenes 1.74a–c	22
Scheme 1-21. Synthesis of substituted “bow-tie” bis-dehydrobenzannulene 1.75	22
Scheme 1-22. Synthesis of “diamond” dehydrobenzannulene 1.78	23

Scheme 1-23. Synthesis of “bow-tie” bis-dehydrobenzannulene 1.83	24
Scheme 1-24. Synthesis of “trefoil” tris-dehydrobenzannulene 1.86	25
Scheme 1-25. Synthesis of “boomerang” and “trapezoid” dehydrobenzannulenes 1.91 and 1.92 , respectively.....	27
Scheme 1-26. Synthesis of tris-dehydrobenzannulene 1.98	28
Scheme 2-1. Retrosynthetic route to expanded [6]radialene model compound 2.1	39
Scheme 2-2. Retrosynthetic route to [4]ER 2.10 , an expanded version of quadrannulene (inset).	40
Scheme 2-3. Syntheses of <i>o</i> -iodoaryl triazenes 2.14a–c	41
Scheme 2-4. Synthesis of DTBP substituted <i>o</i> -iodoaryl triazene 2.20 and <i>o</i> -ethynylaryl triazene 2.21	43
Scheme 2-5. A typical synthesis of a symmetrical dibromoolefin.	44
Scheme 2-6. Synthesis of an unsymmetrical dibromoolefin 2.34	45
Scheme 2-7. Synthesis of differently protected TEE 2.31	45
Scheme 2-8. Synthesis of orthogonally protected TEEs 2.32–2.33	46
Scheme 2-9. Synthesis of unsymmetrically substituted TEE 2.34	47
Scheme 2-10. Synthesis of aryl triazene containing TEEs 2.35a–c	48
Scheme 2-11. Synthesis of unsymmetrically substituted TEEs 2.36a–b containing aryl triazenes.	49
Scheme 2-12. Synthesis of vinyl acetate 2.39 and vinyl triflate 2.37	49
Scheme 2-13. Attempted synthesis of vinyl acetate 2.40	50
Scheme 2-14. Proposed coarctate cyclization of diyne 2.41 to form dimer 2.42	51
Scheme 2-15. Attempted Negishi cross-coupling reaction of 2.21 and 2.38	52
Scheme 2-16. Attempted synthesis building block 2.43 for a of Suzuki-Miyaura cross-coupling.....	53
Scheme 2-17. Desilylation of 2.21 and observed coarctate side product 2.45	53

Scheme 2-18. Attempted synthesis of <i>iso</i> -PDA 2.46	54
Scheme 2-19. Synthesis of <i>iso</i> -PDA 2.47	55
Scheme 2-20. Attempted synthesis of [4]ER 2.48	56
Scheme 3-1. Attempted synthesis of 3.7a using TEE 2.31 and 1,2-diiodobenzene.	65
Scheme 3-2. Attempted synthesis of 3.8 using TEE 2.32 and 1,2-diiodobenzene.	66
Scheme 3-3. One-pot syntheses of 3.7a and 3.9 via the cross-coupling reaction of either dibromoolefin 2.25 or 2.24 with 1,2-diethynylbenzene.	67
Scheme 3-4. Retrosynthetic route to di-radiaannulene 3.7b (PG = protecting group).	68
Scheme 3-5. Synthesis of 3.13 via triazene decomposition with MeI.	69
Scheme 3-6. Synthesis of 3.13 via a modified Sandmeyer reaction of aniline 3.15	69
Scheme 3-7. Synthesis of 3.17 via Sonogashira cross-coupling reaction of 3.13 and TES- acetylene, followed by selective desilylation.	70
Scheme 3-8. Four-fold Sonogashira cross-coupling reaction of 3.17 with tetrabromoethene and subsequent desilylation to give 3.10	71
Scheme 3-9. Synthesis of TEE 3.19 and proposed synthesis of 3.18 from TEE 3.19	71
Scheme 3-10. Synthesis of di-radiaannulene 3.7b via a four-fold Sonogashira cross- coupling reaction.	72
Scheme 3-11. Retrosynthetic route to tri-radiaannulene 3.7c via unsymmetrical radiaannulene 3.21 (PG = protecting group).	74
Scheme 3-12. Synthesis of iodo-ethynylbenzene 3.23 and diethynylbenzene 3.24	75
Scheme 3-13. Synthesis of compound 3.25	75
Scheme 3-14. Synthesis of 3.22 via cleavage of 2-HP groups of 3.25	76
Scheme 3-15. Synthesis of 3.22 via the formation of 3.26 and subsequent selective desilylation.	77

Scheme 3-16. Synthesis of unsymmetrical radiannulene 3.21 , symmetrical radiannulene 3.7a , and radiannulene 3.7d	78
Scheme 3-17. Synthesis of radiannulene 3.28 from unsymmetrical radiannulene 3.2	79
Scheme 3-18. The synthesis of 3.29 starting from diethynylbenzene 3.17	80
Scheme 3-19. Synthesis of precursor 3.32 from 3.29 via a Sonogashira cross-coupling reaction.....	81
Scheme 3-20. Synthesis of radiannulene 3.33 via the selective desilylation of 3.32 and subsequent Sonogashira cross-coupling reaction with 3.29	82
Scheme 3-21. Synthesis of di-radiannulene 3.7b via the selective desilylation of 3.33 and subsequent Sonogashira cross-coupling reaction with dibromoolefin 2.25	83
Scheme 3-22. Synthesis of 3.34 via the selective desilylation of 3.33 and subsequent Sonogashira cross-coupling reaction with 3.29	83
Scheme 3-23. Synthesis of tri-radiannulene 3.7c via the selective desilylation of 3.34 and subsequent Sonogashira cross-coupling reaction with 2.25	84
Scheme 3-24. Synthesis of radiannulenes 3.33a–e via Sonogashira cross-coupling reaction with aryl-iodides.....	86
Scheme 3-25. Attempted synthesis of radialene 3.36	87
Scheme 4-1. Synthesis of pentacene 4.1	108
Scheme 4-2. Synthesis of 6,13-bis(ethynyl)pentacenes by Anthony and coworkers (4.5–4.11).....	109
Scheme 4-3. Synthesis of pentacene-fluorene copolymers 4.14 and 4.15	110
Scheme 4-4. Synthesis of pentacene copolymers 4.16–4.18	111
Scheme 4-5. Synthesis of unsymmetrically substituted pentacenes 4.23a–i	114
Scheme 4-6. Synthesis of unsymmetrically substituted pentacene 4.23j	114
Scheme 4-7. Synthesis of unsymmetrically substituted pentacenes 4.23k–m	115

Scheme 4-8. Synthesis of unsymmetrically substituted pentacene 4.23n	115
Scheme 4-9. Synthesis of polarized pentacenes 4.27a and 4.27b	116
Scheme 4-10. Synthesis of pentacene-polycyclic aromatic hydrocarbon dyads 4.31a–e	124
Scheme 4-11. Synthesis of conjugated pentacene dimers 4.37a–j	135
Scheme 4-12. Synthesis of conjugated pentacene dimers 4.37k–m	136
Scheme 4-13. Synthesis of conjugated pentacene dimer 4.37n via a Cadiot-Chodkiewicz reaction.....	136
Scheme 4-14. Attempted electrochemical polymerization of pentacene 4.23j	144
Scheme 5-1. Proposed synthesis of donor functionalized radiannulene 5.2 and donor / acceptor radiannulene 5.3	149
Scheme 5-2. Proposed synthesis of fused radiannulene 5.4	150
Scheme 5-3. Proposed synthesis of compound 5.9	151
Scheme 5-4. Proposed synthesis to east-west radiannulene oligomers.	152
Scheme 5-5. Proposed synthesis of dibenzo[A,J]coronene 5.14 via Bergman cyclization of 3.7a	153

List of Symbols

\AA	Angstrom
$^{\circ}\text{C}$	degrees Celsius
Δ	heat
δ	chemical shift in parts per million
ε	molar absorption coefficient
λ_{exc}	excitation wavelength
λ_{max}	lowest energy absorption wavelength with maximum absorption
$\lambda_{\text{max,em}}$	maximum intensity emission wavelength
μ	micro
$E_{\text{g}}^{\text{electro}}$	electrochemical band gap
$E_{\text{g}}^{\text{opt}}$	optical band gap
E_{ox1}	first oxidation potential
E_{ox2}	second oxidation potential
E_{ox3}	third oxidation potential
E_{pa}	anodic electrochemical polymerization
E_{red1}	first reduction potential
E_{red2}	second reduction potential
E_{red3}	third reduction potential
E_{red4}	fourth reduction potential
E_{red5}	fifth reduction potential
E_{red6}	sixth reduction potential
J	coupling constant
M_{r}	formula weight
R_{f}	retention factor

List of Abbreviations

2-HP	2-hydroxypropyl
AcO	acetate
APPI	atmospheric pressure photoionization
aq	aqueous
Ar	aryl
Bn	benzyl
br	broad (IR/NMR spectroscopy)
Bu	butyl
calcd.	calculated
cm	centimeter(s)
cm ⁻¹	wavenumber(s)
Cmpd	compound
CV	cyclic voltammetry
d	doublet (NMR spectroscopy)
D	distance
dba	dibenzylideneacetone
DBA	dehydrobenzannulene
<i>o</i> -DCB	<i>ortho</i> -dichlorobenzene
DCTB	<i>trans</i> -2-[3-(4- <i>tert</i> butylphenyl)-2-methyl-2-propenylidene]malononitrile
DME	1,2-dimethoxyethane
DMF	<i>N,N</i> -dimethylformamide
DPDEE	diphenyldiethynylethene
DSC	differential scanning calorimetry
DTBP	3,5-di- <i>tert</i> -butylphenyl

EI	electron impact
ER	expanded radialene
ESI	electrospray ionization
Et	ethyl
eV	electron volt(s)
FBW	Fritsch–Buttenberg–Wiechell
Fc	ferrocene
Fc ⁺	ferrocenium
g	gram(s)
GPC	gel permeation chromatography
h	hour(s)
Hex	hexanes
Hexyl	<i>n</i> -hexyl
HexLi	<i>n</i> -hexyllithium
HOMO	highest occupied molecular orbital
HRMS	high-resolution mass spectrometry
Hz	hertz
<i>i</i>	<i>iso</i>
ITO	indium tin oxide
IR	infra-red spectroscopy
kcal	kilocalorie(s)
L	liter(s)
LDA	lithium diisopropylamide
LUMO	lowest unoccupied molecular orbital
m	medium (IR spectroscopy)

m	multiplet (NMR spectroscopy)
<i>m</i>	<i>meta</i>
m	meter(s)
M	molar
MALDI	matrix assisted laser desorption ionization
Me	methyl
mg	milligram(s)
MHz	megahertz(s)
mL	milliliter(s)
mM	millimolar
mmol	millimole(s)
mol	mole(s)
Mp	melting point
MS	mass spectrometry
mV	millivolt(s)
<i>m/z</i>	mass-to-charge ratio
<i>n</i>	<i>normal</i>
NBS	<i>N</i> -bromosuccinimide
nm	nanometer(s)
NMR	nuclear magnetic resonance
<i>o</i>	<i>ortho</i>
ORTEP	Oak Ridge thermal ellipsoid plot
OSWV	Osteryoung square wave voltammetry
<i>p</i>	<i>para</i>
PA	polyacetylene

PAH	polyaromatic hydrocarbon
PANI	polyaniline
PCBM	phenyl-C ₆₁ -butyric acid methyl ester
PCC	pyridinium chlorochromate
PDA	polydiacetylene
PEDOT	polyethylenedioxythiophene
PF	polyfluorene
PG	protecting group
Ph	phenyl
PhMe	toluene
PLED	polymer light emitting diode
POSS	polyhedral oligomeric silsesquioxane
PPE	poly(phenylene ethynylene)
ppm	parts per million
PPP	polyparaphenylene
PPV	poly(phenylene vinylene)
PPy	polypyrrole
Pr	propyl
PT	polythiophene
Pyr	pyridine
q	quartet (NMR spectroscopy)
RA	radiaannulene
rt	room temperature
s	singlet (NMR spectroscopy)
s	strong (IR spectroscopy)

sept	septet (NMR spectroscopy)
t	triplet (NMR spectroscopy)
<i>t</i>	tertiary
TBAF	tetrabutylammonium fluoride
TEE	tetraethynylethene
TES	triethylsilyl
TfO	triflate
TGA	thermogravimetric analysis
THF	tetrahydrofuran
TIPS	triisopropylsilyl
TLC	thin layer chromatography
TMEDA	<i>N,N,N',N'</i> -tetramethylethylenediamine
TMS	trimethylsilyl
TPEB	tetrakis(phenylethynyl)benzene
TTF	tetrathiafulvalene
UV	ultraviolet
vis	visible
NIR	near infra-red
V	volt(s)
vs	versus
w	weak (IR spectroscopy)

Chapter 1 – Introduction to Conjugated Materials and Graphyne

1.1 Introduction to Conjugated Materials

We live in a digital world. Tremendous technological advancements have been made in the past century, and we now live in an era in which we rely heavily upon computers to complete everyday tasks. As a result of our dependence on electronics to aid us in our daily lives, the demand for faster computers and more efficient electronic devices is increasing rapidly. Many areas of research aim to address this issue, and the use of organic semiconducting materials is a topic of increasing importance toward developing the next generation of technologies.

One of the most influential discoveries in the field of organic semiconductors was that of conjugated organic polymers. The discovery and study of one of the simplest conjugated polymers, polyacetylene (PA) ($\text{H}-[\text{C}=\text{C}]_n-\text{H}$), resulted in the 2000 Nobel Prize in Chemistry, which was awarded to Heeger, MacDiarmid, and Shirakawa.¹⁻³ Numerous other conjugated polymers have been developed (Figure 1-1), such as polythiophene (PT), polypyrrole (PPy), polyaniline (PANI), polyparaphenylene (PPP), polyfluorene (PF) poly(phenylene vinylene) (PPV), and poly(phenylene ethynylene) (PPE).⁴⁻¹⁰

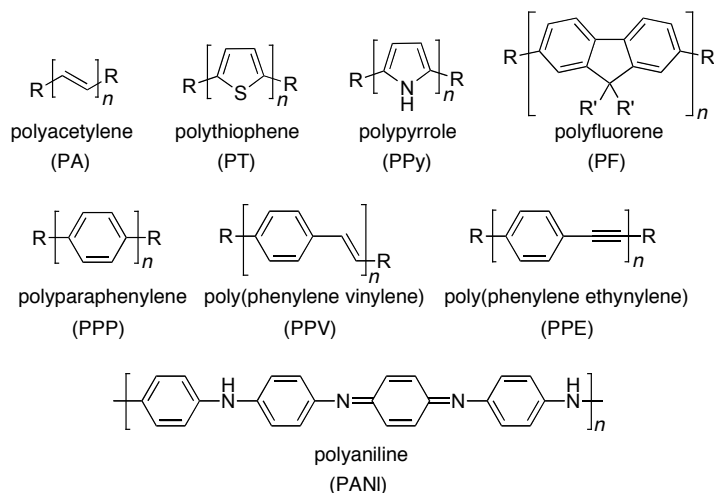


Figure 1-1. Common conjugated organic polymers

1.2 Conjugated Hydrocarbons: All Carbon and Carbon-rich

Materials

Conjugated materials prepared solely or predominantly from carbon are a unique class of materials, with many fascinating properties. For example, the carbon allotrope graphite is comprised of layers of two-dimensional sheets of sp^2 -carbon atoms bonded in a hexagonal (honeycomb) lattice and has been commonly used in electrodes and as a solid lubricant.¹¹ A single sheet of graphite, known as graphene, has become the focus of significant research efforts in the past couple of years due to its remarkable properties, highlighted by the awarding of the Nobel Prize in Physics to Geim and Novoselov in 2010 for their work on graphene.¹² Graphene has been prepared by numerous methods, such as exfoliation from graphite or by oxidation of graphite. In addition, there have been many attempts to synthesize graphene and smaller molecular segments to serve as models of graphene.¹³ The physical and electronic properties of graphene have been extensively studied, both theoretically and physically.¹³

In addition to the flat, two-dimensional structures of graphite and graphene, there

are spherical and tubular shaped allotropes such as the fullerenes and carbon nanotubes. The chemistry of fullerenes has been extensively explored since their discovery by Curl Jr., Kroto, and Smalley, which resulted in the Nobel Prize in Chemistry in 1996.¹⁴ In particular, fullerene derivatives such as phenyl-C₆₁-butyric acid methyl ester (PCBM) are of great value as electron acceptors for the formation of organic solar cells.¹⁵

Continuing in the series of conjugated carbon allotropes, one arrives to the sp-allotrope known as “carbyne”. Carbyne is a material of significant interest both theoretically and experimentally.¹⁶ This so far hypothetical material should consist of a linear chain of sp-hybridized atoms, that might be viewed as a conjugated wire with the thickness of a single sp-hybridized carbon atom. Although the existence of naturally occurring carbyne has yet to be confirmed, many defined length oligomers have been prepared in order to predict the properties of carbyne.¹⁶

1.3 Hybrid Structures: Materials Based on sp²-Carbon and sp-Carbon

In addition to materials based on either sp²- or sp-carbon, there are many conjugated materials that are constructed with a framework that contains a combination of both sp²- and sp-carbon. The use of sp-carbon allows for the extension of conjugation in a linear direction, while the inclusion of sp²-carbon allows for the formation of a two-dimensional network. There are several classes of molecules that feature two-dimensional conjugation, such as tetraethynylethenes¹⁷ (TEEs), tetrakis(phenylethynyl)benzenes¹⁸ (TPEBs), polydiacetylenes (PDAs), and *iso*-polydiacetylenes (*iso*-PDAs) (Figure 1-2).¹⁹ The synthesis of these molecules has been documented in the literature of the past decade or so, and these reports show that many of these molecules possess interesting optical and electronic properties.¹⁶⁻¹⁹ In addition, such molecules also serve as excellent building

blocks for the construction of larger structures, such as macrocycles.^{19c}

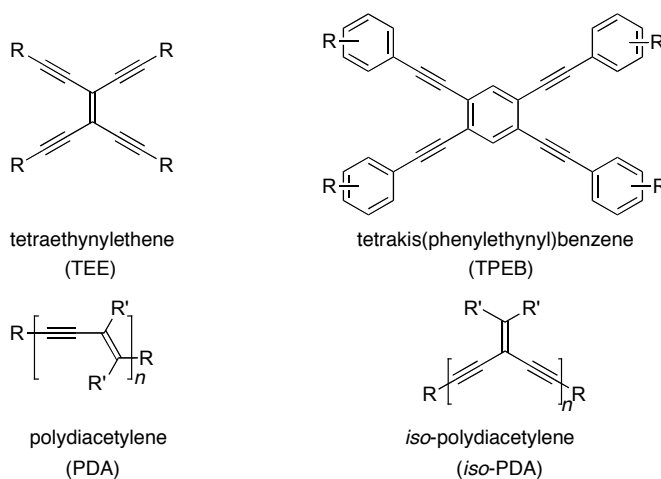


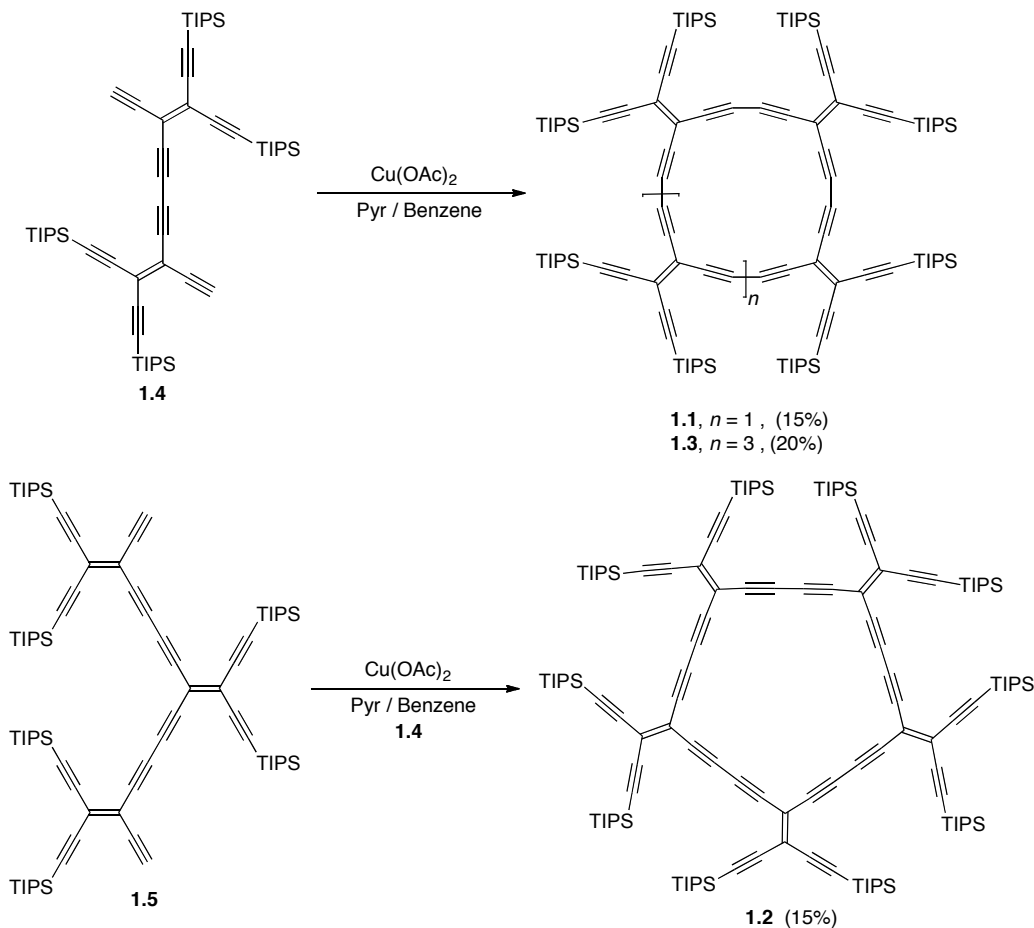
Figure 1-2. Structural representation of select examples of two-dimensionally conjugated molecules.

In the following sections, a brief study of enyne based macrocycles will be presented. The discussion is not meant to be comprehensive, but rather, examples have been chosen to highlight the scope of this evolving area of science. In particular, synthetic achievements are discussed, particularly those that lay the foundation for much of the work that appears in subsequent chapters of this thesis.

1.3.1 Acetylene-rich Macrocycles: Expanded Radialenes, Radiaannulenes, and Dehydroannulenes

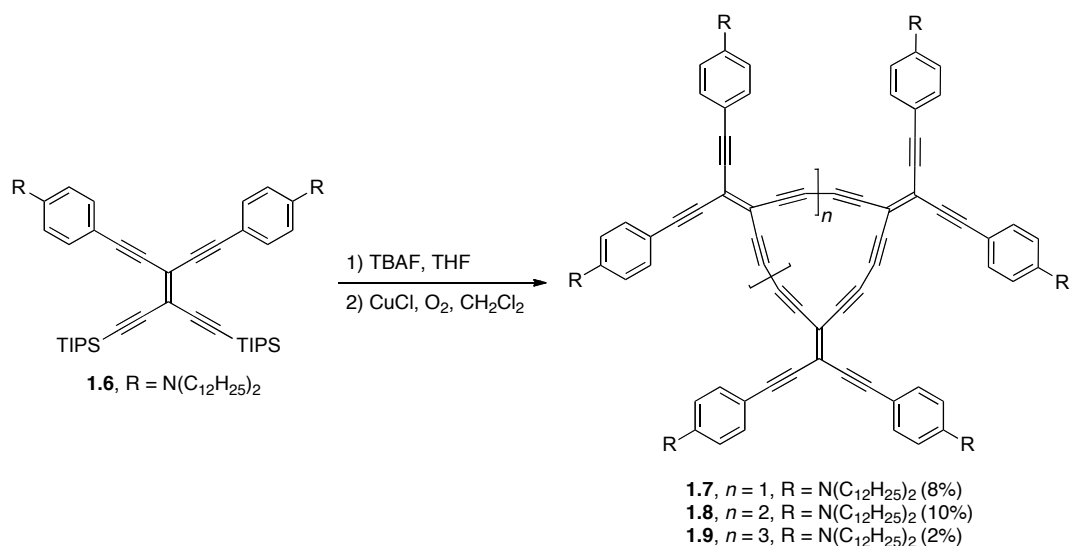
A variety of macrocycles have been synthesized using TEEs as the central building blocks, such as expanded [n]radialenes (ERs), radiaannulenes (RAs), and dehydroannulenes (DHAs).²⁰⁻²² The first syntheses of these macrocycles from a TEE building block relied on the use of a variety of inter- and intramolecular acetylenic homocoupling reactions. Using this homocoupling method, Diederich and coworkers were able to synthesize expanded [4]-, [5]- and [6]radialenes **1.1**, **1.2**, and **1.3** (Scheme 1-

1).^{24,25} Dimeric TEE **1.4** underwent oxidative coupling to yield [4]ER **1.1** and [6]ER **1.3** in 15% and 20% yield, respectively. The [5]ER **1.2** was prepared in 15% yield via an intermolecular oxidative coupling of trimeric TEE **1.5** with dimeric TEE **1.4**.



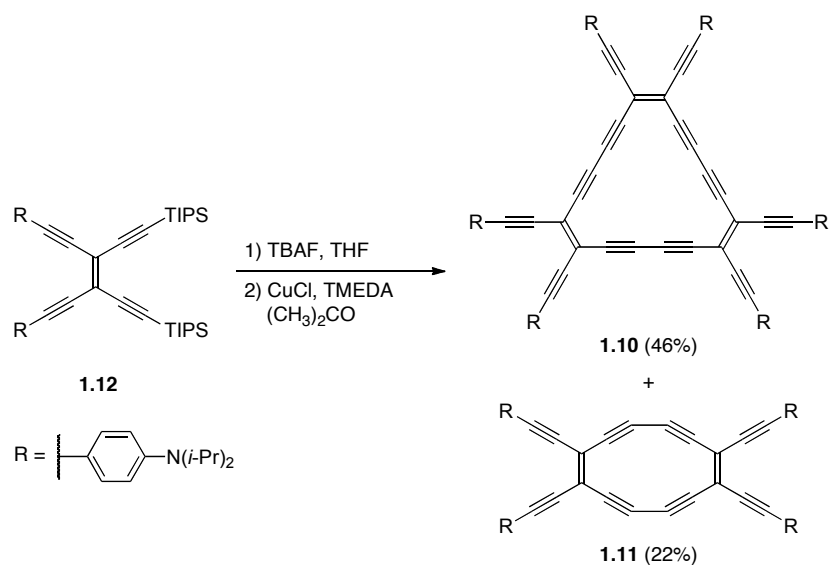
Scheme 1-1. Synthesis of expanded radialenes **1.1**, **1.2**, and **1.3**.

ERs capped with electron donating *N,N*-dialkylaniline groups were prepared using similar methodology (Scheme 1-2).²⁶ TEE **1.6** was stirred in the presence of tetrabutylammonium fluoride (TBAF) and the resulting product was subjected to a Hay homocoupling reaction, which furnished the [3]ER **1.7** in 8%, [4]ER **1.8** in 10% , and [5]ER **1.9** in 2% yield after separation by preparative gel permeation chromatography (GPC) and preparative thin layer chromatography (TLC).



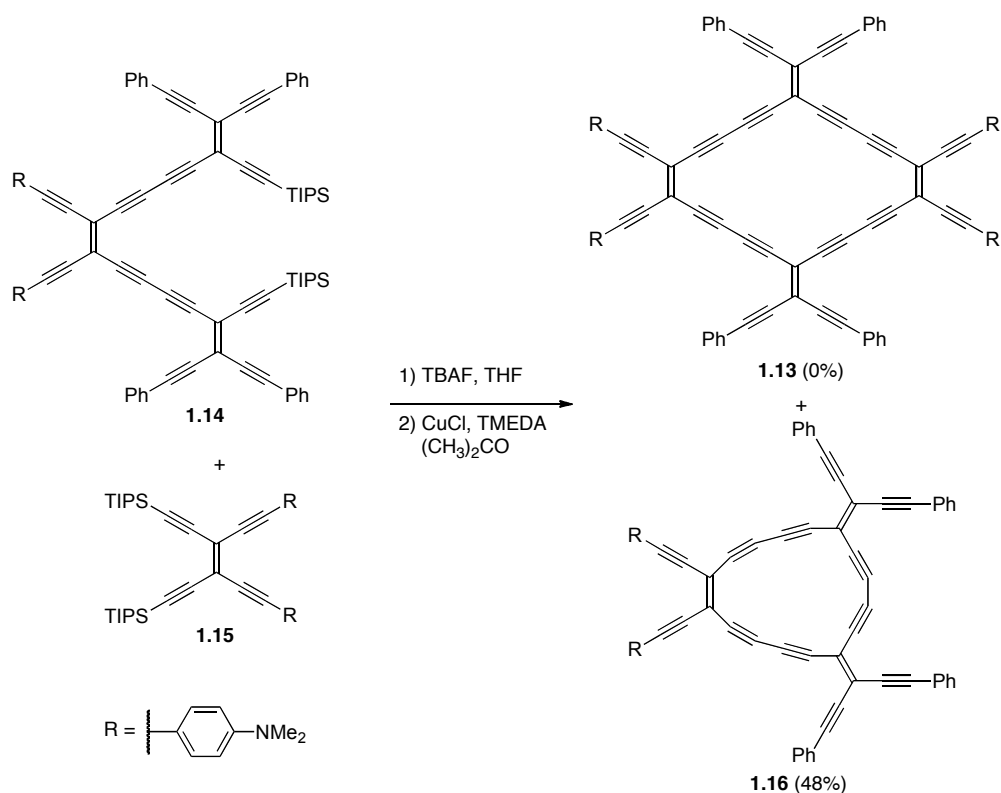
Scheme 1-2. Synthesis of expanded radialenes **1.7**, **1.8**, and **1.9**

Diederich and coworkers reported the synthesis of DHAs **1.10** and **1.11** (Scheme 1-3).²⁰ TEE **1.12** was stirred in the presence of TBAF and the resulting product subjected to a Hay homocoupling reaction using CuCl and tetramethylethylenediamine (TMEDA), which furnished the DHA **1.10** in 46% and DHA **1.11** in 22% yield following purification by column chromatography.



Scheme 1-3. Synthesis of dehydroannulenes **1.10** and **1.11**.

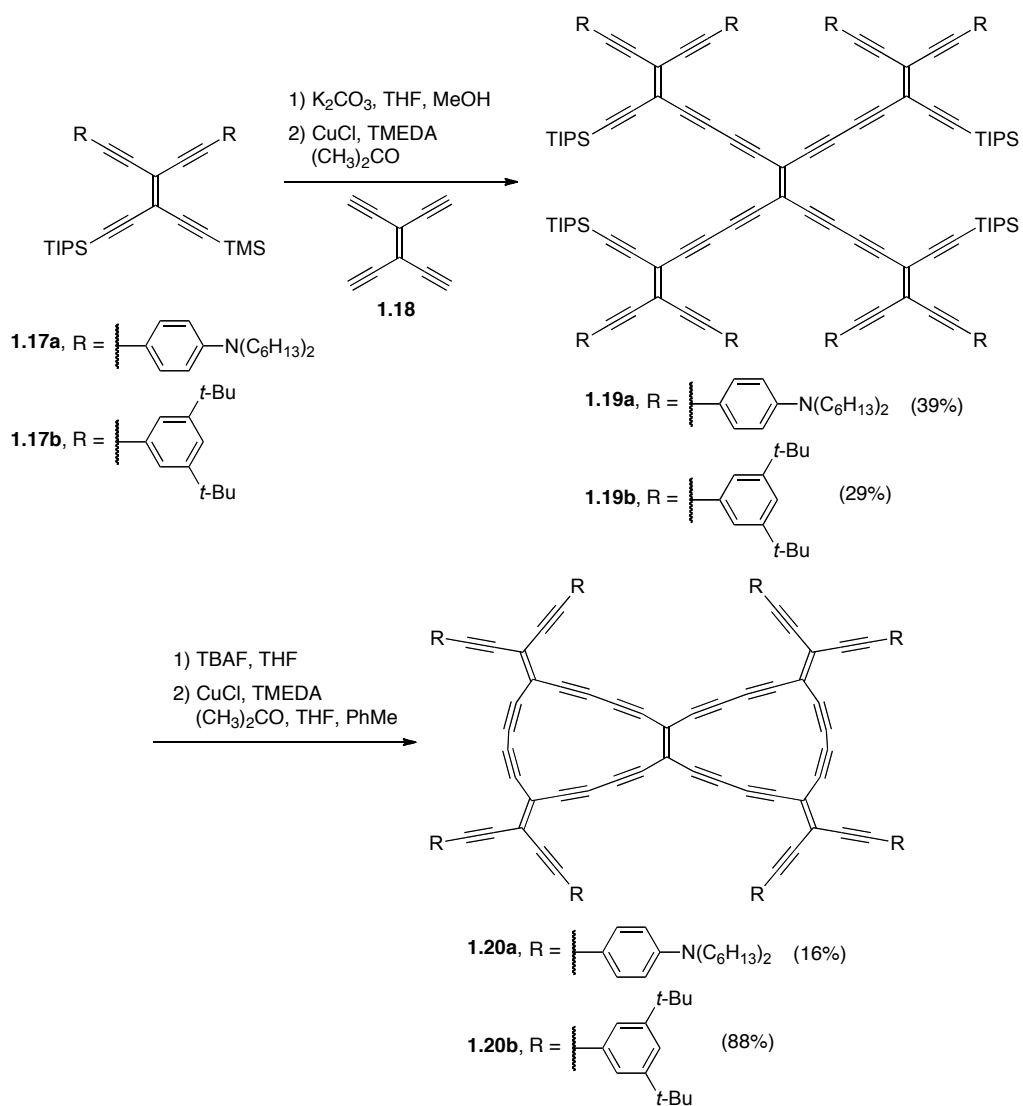
In an effort to prepare the expanded RA **1.13**, Diederich and coworkers first desilylated oligomer **1.14** and TEE **1.15** with TBAF, and the resulting products underwent a homocoupling reaction using CuCl and TMEDA (Scheme 1-4).²² While the expected product **1.13** was not observed, the smaller RA **1.16** was obtained in 48% yield, the result of an intramolecular homocoupling reaction of deprotected oligomer **1.14**.



Scheme 1-4. Attempted synthesis of radiannulene **1.13** and formation of **1.16**.

Diederich and coworkers also demonstrated that it is possible to synthesize bicyclic RAs using an oxidative homocoupling approach (Scheme 1-5).²² TEE **1.17a** was protodesilylated using K₂CO₃ and the resulting product added to a solution of tetraethynylethene **1.18**. The resulting products underwent intermolecular oxidative coupling in the presence of CuCl and TMEDA to give pentameric TEE **1.19a** in 39%

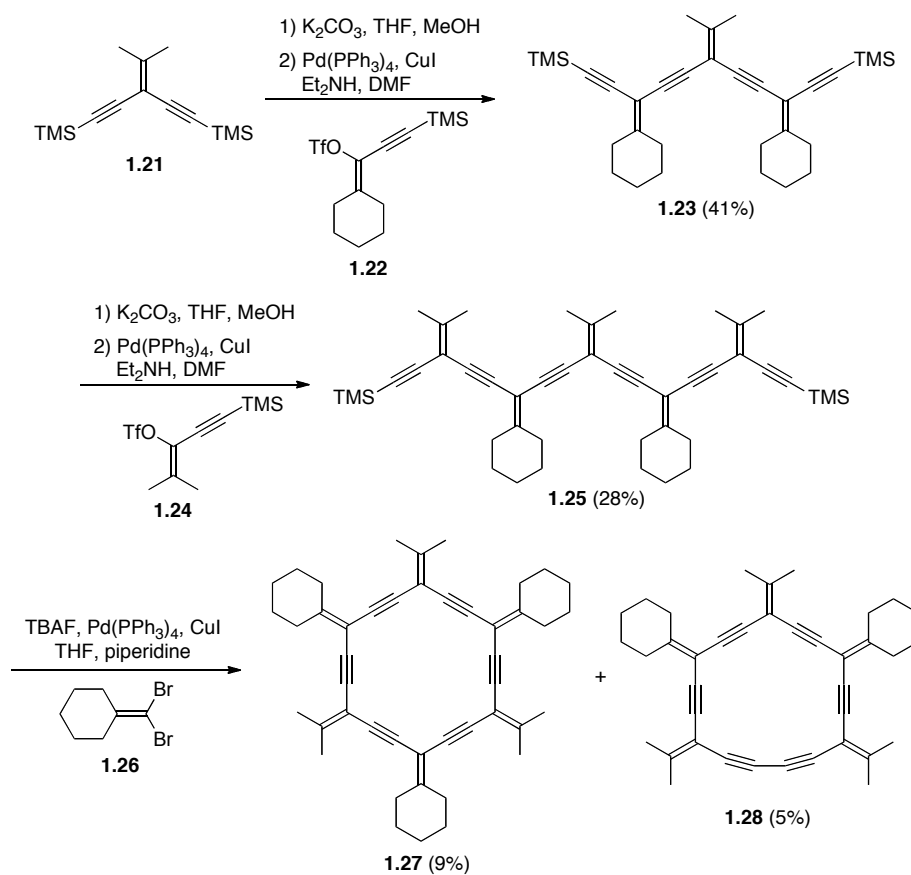
yield. Deprotection with TBAF and subsequent intramolecular oxidative coupling yielded bicyclic RA **1.20a** in 16% yield. An analogous procedure was used starting with TEE **1.17b**, giving the intermediate pentamer **1.19b** in 29% yield, and the final bicyclic RA **1.20b** in 88% yield.



Scheme 1-5. Synthesis of bicyclic radiannulenes **1.20a** and **1.20b**.

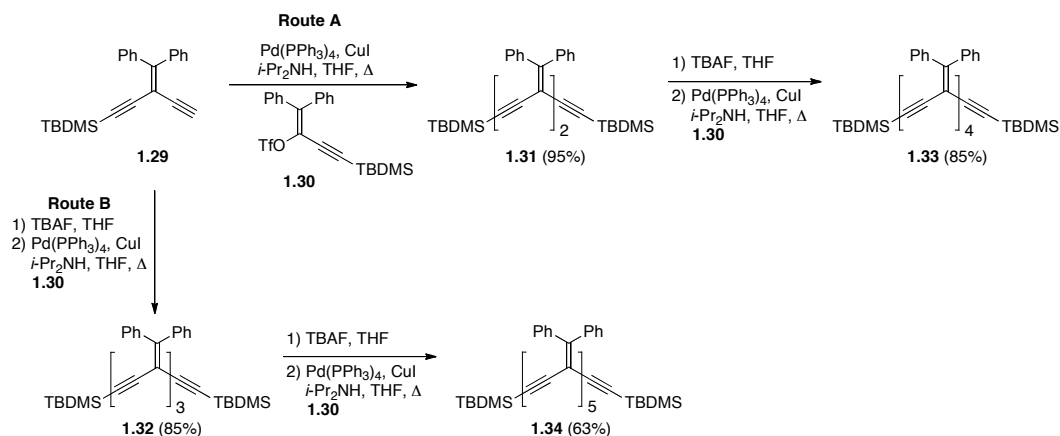
The oxidative coupling method has proved to be an effect method in the synthesis of macrocycles linked by butadiyne spacers. This protocol can also be

problematic, however, due to the formation of undesirable homocoupling side products, such as acyclic and cyclic oligomers, which can significantly hinder purification of the desired product.²³ In addition, the homocoupling route cannot be used to prepare smaller macrocycles based on acetylene spacers. To achieve such structures, Tykwinski and coworkers developed a synthetic route relying on the use of Sonogashira cross-coupling reactions to assemble the desired macrocycle. In 1999 the first ER consisting of acetylene spacers was prepared (Scheme 1-6).²⁷ *Iso*-PDA **1.21** was desilylated using K_2CO_3 , and the resulting product was added to a solution of vinyl triflate **1.22**. Sonogashira cross-coupling reaction of the product mixture afforded trimer **1.23** in 41% yield. Trimer **1.23** was desilylated using K_2CO_3 in MeOH, and the resulting product was transferred to a solution of vinyl triflate **1.24**. The subsequent Sonogashira cross-coupling reaction resulted in the formation of pentamer **1.25** in 28% yield. A final iteration of the desilylation/Sonogashira cross-coupling sequence was carried out with **1.25** in the presence of dibromoolefin **1.26** using TBAF and afforded the [6]ER **1.27** in 9% yield. In addition to the desired product **1.27**, a small amount of [5]ER **1.28** was also obtained (5% yield), as a result of an intramolecular oxidative coupling of the desilylated derivative of pentamer **1.25**. Unfortunately, ER **1.27** was not stable under ambient conditions. To date, empirical evidence suggests that an oxygen ene reaction occurs at the peripheral allylic positions and is the origin of the instability.²⁸



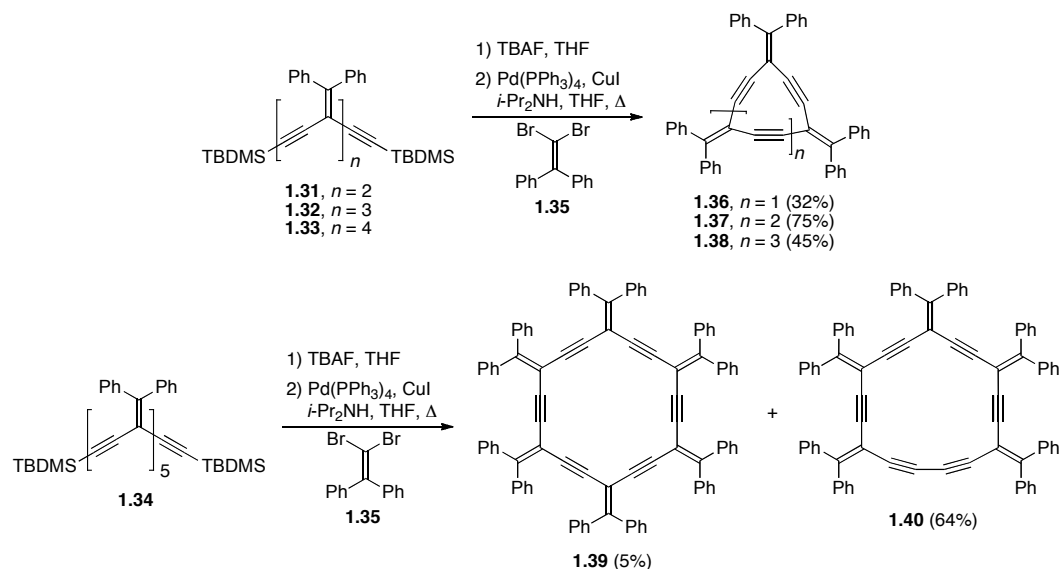
Scheme 1-6. Synthesis of expanded radialenes **1.27** and **1.28**.

Utilizing a similar approach to the [6]ER **1.27**, Tykwinski and coworkers prepared a series of perphenylated ERs in an effort to circumvent the instability observed in **1.27**. A series of phenyl-substituted *iso*-PDAs was prepared starting from enediyne **1.29** (Scheme 1-7).²⁹ Compound **1.29** underwent Sonogashira cross-coupling reaction with vinyl triflate **1.30** to yield dimer **1.31** in 95% yield (Route A). This was followed by desilylation and a second Sonogashira cross-coupling reaction with **1.30** to yield **1.33** in 85% yield. Alternatively, *iso*-PDA **1.29** was fully desilylated with TBAF prior to the Sonogashira cross-coupling reaction with **1.30** to yield trimer **1.32** in 85% yield (Route B). Following a second iteration of desilylation and Sonogashira cross-coupling reaction with vinyl triflate **1.30**, pentamer **1.34** was produced in 63% yield.



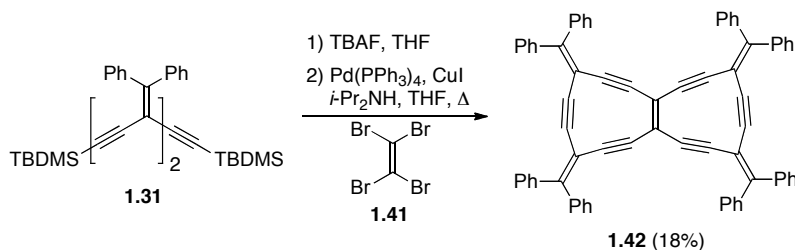
Scheme 1-7. Synthesis of perphenylated *iso*-PDA oligomers **1.31–1.34**.

Oligomers (**1.31–1.34**) were desilylated and subjected to a Sonogashira cross-coupling reaction with dibromoolefin **1.35** to yield ERs **1.36–1.39** (Scheme 1-8). In the case of smaller ERs, the products were isolated in reasonable yields ([3]ER **1.36** 32%, [4]ER **1.37** 75%, [5]ER **1.38** 45%). Unfortunately, [6]ER **1.39** was formed in a low yield of 5%, along with consistent formation of hybrid radialene **1.40** isolated in a much higher yield. All of the products were isolated as stable solids.

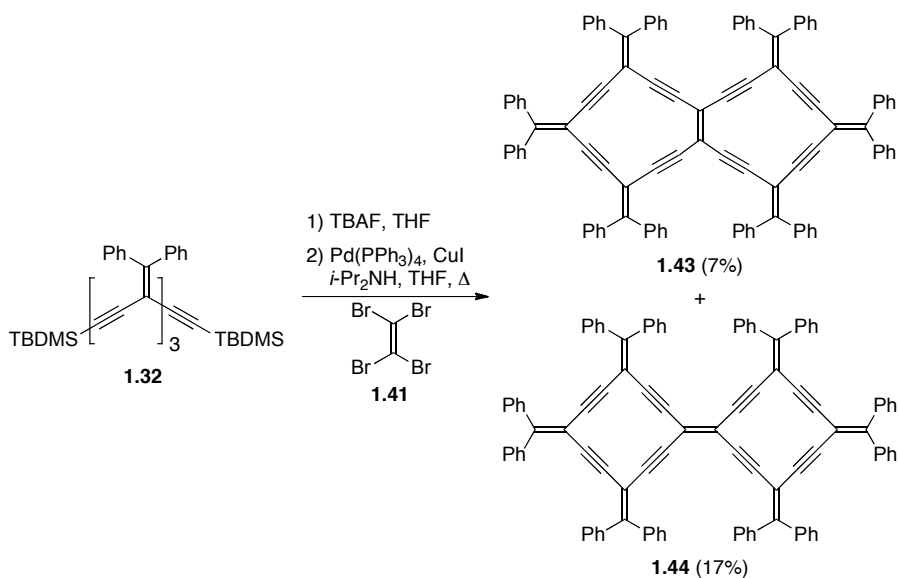


Scheme 1-8. Synthesis of expanded radialenes **1.36–1.39** and hybrid radialene **1.40**.

Following the successful synthesis of ERs **1.36–1.39**, Tykwinski and coworkers attempted the synthesis of bicyclic ERs.²⁹ Dimer **1.31** was desilylated with TBAF and the resulting product was used in a Sonogashira cross-coupling reaction with tetrabromoethene **1.41**, which resulted in the formation of bisRA **1.42** in 18% yield (Scheme 1-9). A larger bicyclic RA was prepared starting from trimer **1.32**. Initial desilylation and subsequent Sonogashira cross-coupling reaction with **1.41** resulted in the formation of two major products, bicyclic RA **1.43** and bis-ER **1.44** in 7% and 17% yield, respectively (Scheme 1-10).³⁰

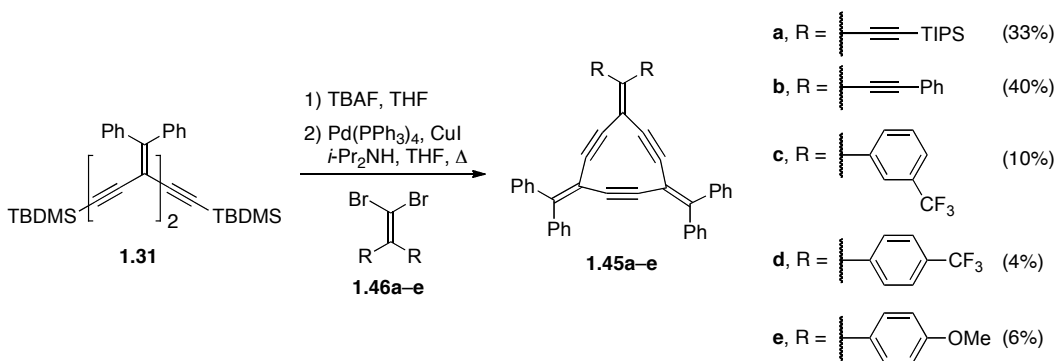


Scheme 1-9. Synthesis of bicyclic radiannulene **1.42**.



Scheme 1-10. Synthesis of bicyclic radiannulene **1.43** and bis expanded radialene **1.44**.

In addition to the perphenylated ERs, Tykwinski and coworkers have prepared a number of functionalized structures. The [3]ERs (**1.45a–e**) were synthesized from dimer **1.31** via desilylation and Sonogashira cross-coupling reactions with dibromoolefins **1.46a–e** (Scheme 1-11).³⁰ A similar approach was used for the synthesis of functionalized [4]ERs **1.47a–d** (Figure 1-3).³⁰



Scheme 1-11. Synthesis of functionalized expanded [3]radialenes **1.45a–e**.

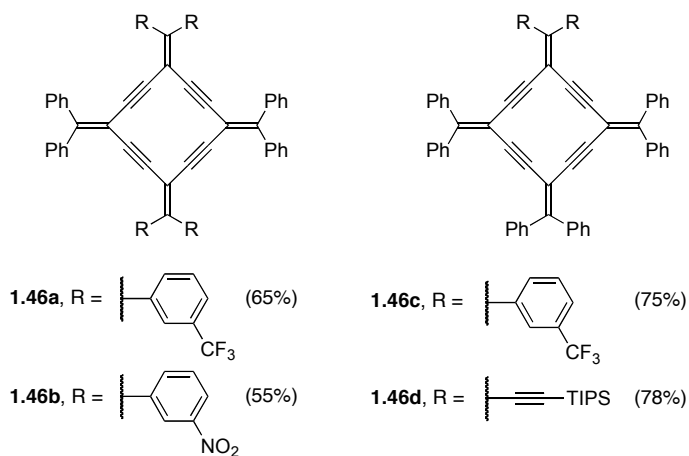
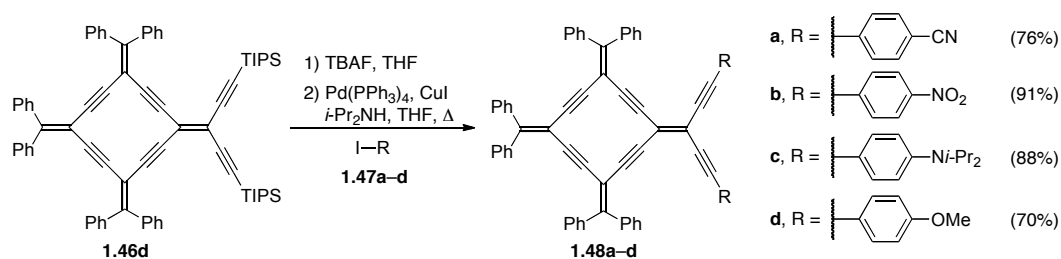


Figure 1-3. Structures of functionalized expanded [4]radialenes with yields of final cyclization step as prepared by Tykwinski and Gholami (**1.46a–d**).

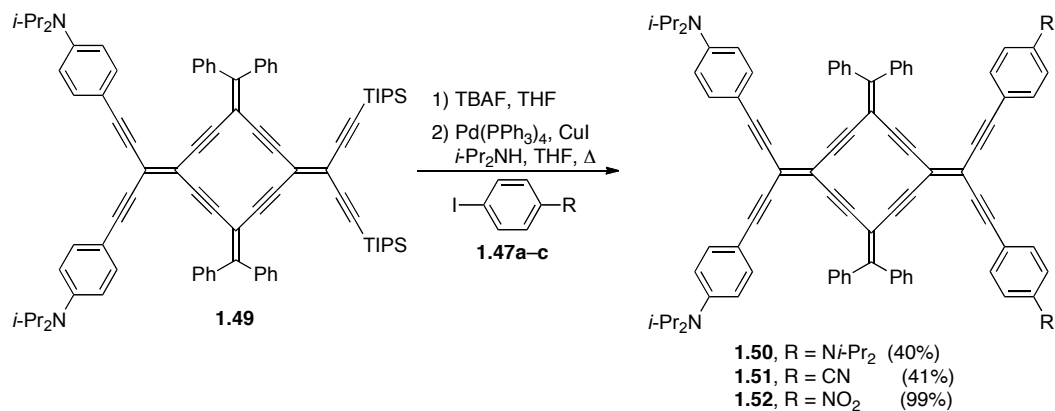
Tykwinski and coworkers have also demonstrated that derivatization of the framework of an [4]ER is also possible. Desilylation of [4]ER **1.46d** and a subsequent Sonogashira cross-coupling reaction with an aryl iodide (**1.47a–d**) led to the formation of

functionalized [4]ERs **1.48a–d** (Scheme 1-12).^{30,31} This functionalization of ERs via a Sonogashira cross-coupling reaction proved effective for both electron withdrawing (**1.48a** and **1.48b**), as well as electron donating substrates (**1.48c** and **1.48d**).



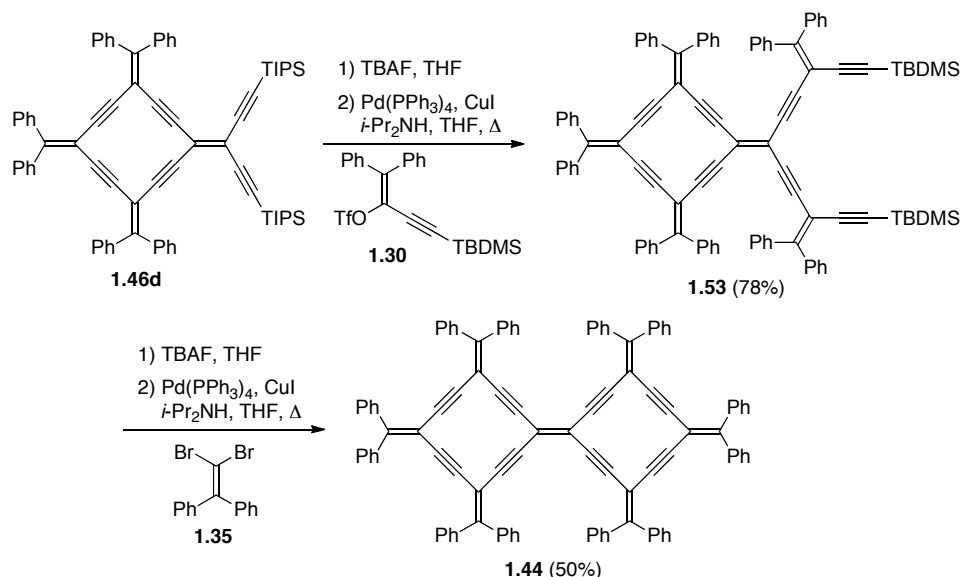
Scheme 1-12. Synthesis of differently functionalized expanded [4]radialenes **1.48a–1.48d**.

Further functionalization of ER **1.49** allowed for the formation of ERs **1.50–1.52** (Scheme 1-13).³¹ The TIPS groups of radialene **1.49** were removed using TBAF, and the resulting product underwent a Sonogashira cross-coupling reaction with aryl iodide **1.47c** to give the donor substituted radialene **1.50** in 40% yield. Donor-acceptor [4]ERs **1.51** and **1.52** were prepared in 41% and 99% yields, respectively, using an analogous route.



Scheme 1-13. Synthesis of donor substituted expanded [4]radialene **1.50** and donor / acceptor substituted expanded [4]radialenes **1.51** and **1.52**.

Taking advantage of the ability to functionalize the radialene skeleton, Tykwinski and coworkers developed a stepwise synthesis to bis-ER **1.44** (Scheme 1-14).³⁰ Desilylation of **1.46d** and subsequent Sonogashira cross-coupling reaction with vinyl triflate **1.30** led to the formation of compound **1.53** in a 78% yield. Compound **1.53** was desilylated using TBAF and the resulting product was used in a Sonogashira cross-coupling reaction with dibromoolefin **1.35** to yield bis-ER **1.44** in 50% yield. This improved upon their original one-pot procedure to the bis-ER, with an overall yield of 30% starting from trimer **1.32** and no formation of the bicyclic RA **1.43**.



Scheme 1-14. Stepwise synthesis of bis-expanded radialene **1.44**.

1.3.2 Phenylacetylene Based Molecules and Macrocycles: Models of Graphyne

Many interesting structures can be derived through the functionalization of aryl rings with acetylene units, and one of these structures, “graphyne”, is of particular interest. In 1987, Baughman and coworkers first proposed that graphyne is a planar, two-

dimensional structure comprised entirely of sp- and sp²-hybridized carbon atoms.³² Furthermore, by varying the ratio of sp:sp² carbon, a range possible structures are possible (Figure 1-4). The formal insertion of an acetylene bond between the phenyl rings of graphite results in the simplest possible graphyne structure, 6,6,6-graphyne (**1.54**, sp:sp² = 1:1). By increasing the ratio of sp-carbon in the structure, larger and more complex ring systems emerge, such as 6,6,12-graphyne (**1.55**, sp:sp² = 5:4), 6,6,14-graphyne (**1.56**, sp:sp² = 7:5), 12,12,12-graphyne (**1.57**, sp:sp² = 2:1), 14,14,14-graphyne (**1.58**, sp:sp² = 2:1), 14,14,18-graphyne (**1.59**, sp:sp² = 5:2), and 18,18,18-graphyne (**1.60**, sp:sp² = 3:1).

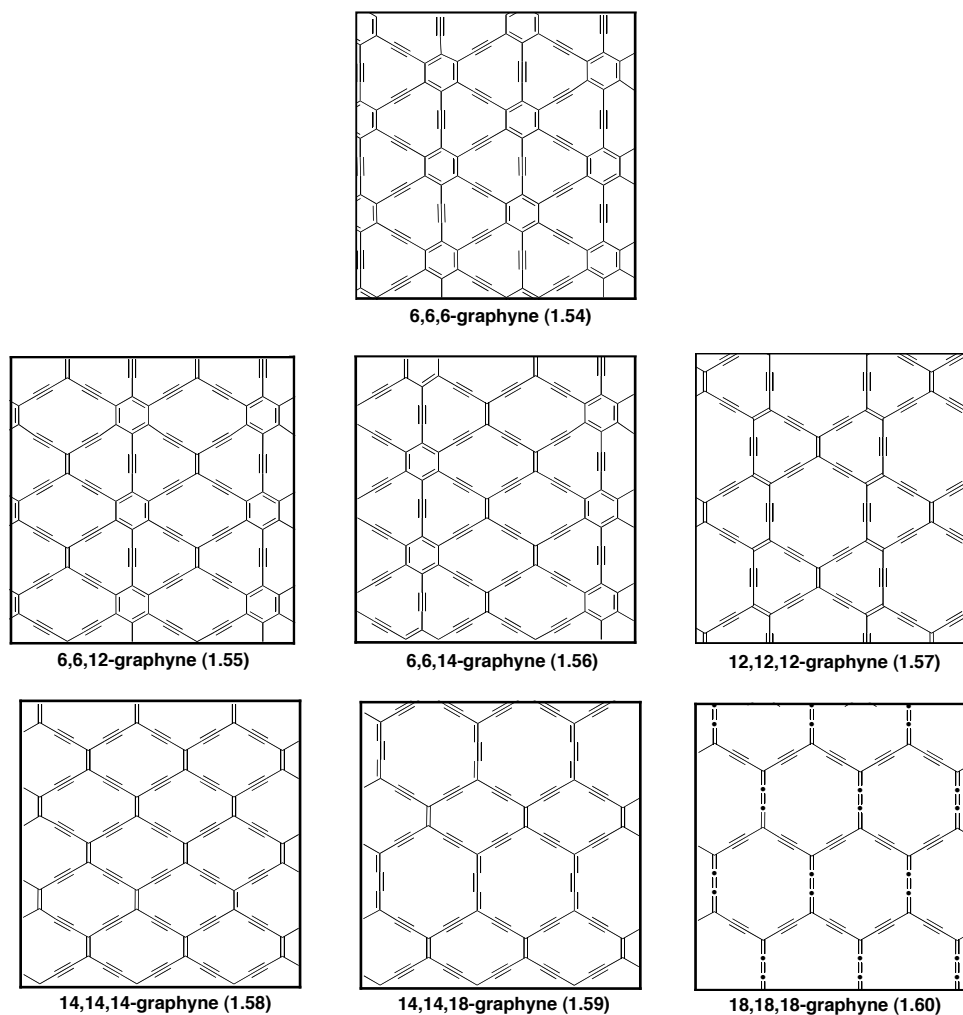
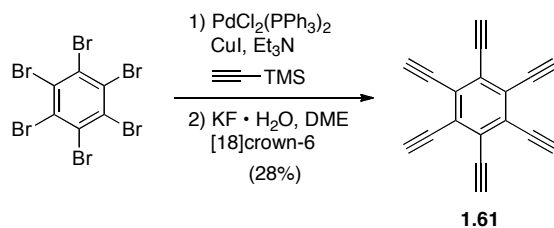


Figure 1-4. Theoretical structures of graphynes as reported by Baughman and coworkers.³²

While this initial study modeled the properties of several proposed structures, 6,6,6-graphyne was predicted to be the most stable. 6,6,6-Graphyne was predicted to have a crystalline state energy of formation of 12.4 kcal/g carbon, a value comparable to that determined for buckminsterfullerene (C_{60} , 10.16 kcal/g carbon).³³ 6,6,6-Graphyne was also proposed to have similar mechanical properties to graphite and was predicted to be a semiconductor with a band gap (E_g) of 1.2 eV. The formation of alkali metal charge

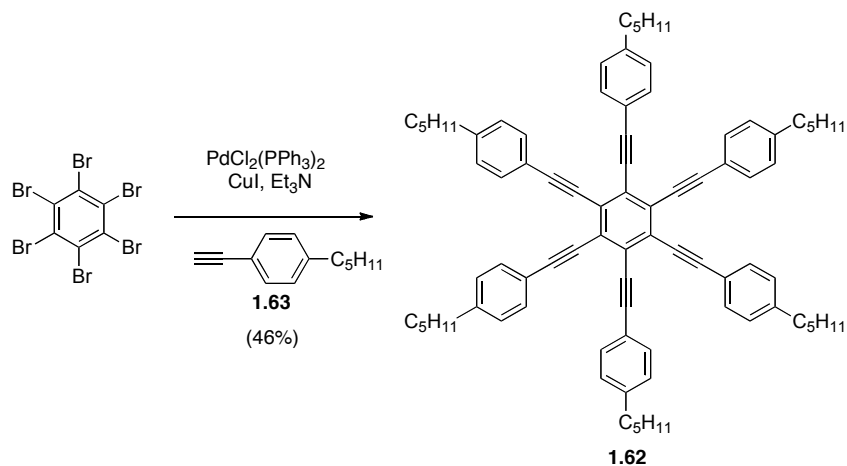
transfer complexes could render the structure metallic. The authors further postulated that 6,6,6-graphyne would exhibit interesting nonlinear optical properties. Since this original proposal, 6,6,6-graphyne has become the focus of much theoretical research, with studies further investigating the expected physical properties of the structure, as well as the properties of graphyne-based nanotubes and fullerenes.³⁴⁻⁴⁹ In recent years, more advanced computational methods have predicted that some versions of graphyne should exhibit properties similar to that of graphene. One of the remarkable properties of graphene is its conductivity, which derives from a band structure that features Dirac points and cones. At the Dirac point the valence and conduction bands of the material meet, which means the material can be considered a zero band gap semiconductor. Several structures of graphyne have been predicted to have band structures containing Dirac points.⁴⁹

Although the synthesis of bulk graphyne has not yet been achieved, many small molecules have been synthesized to serve as model compounds of graphyne, particularly for 6,6,6-graphyne. The simplest subunit prepared to model 6,6,6-graphyne is that of hexaethynylbenzene **1.61**. The pure hydrocarbon was first prepared by Vollhardt and coworkers, via the Sonogashira cross-coupling reaction of hexabromobenzene and trimethylsilyl-acetylene (TMS-acetylene), followed by desilylation to yield **1.61** in 28% yield (Scheme 1-15).⁵⁰ Compound **1.61** decomposed with heating or when exposed to air.



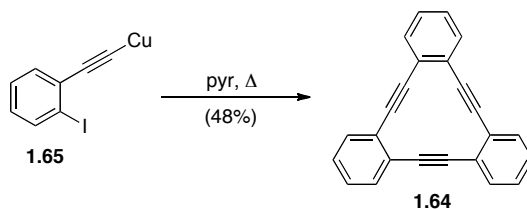
Scheme 1-15. Synthesis of hexaethynylbenzene **1.61**.

Hexakis(arylethynyl)benzene **1.62** was also prepared in a similar fashion, via the Sonogashira cross-coupling reaction with aryl acetylene **1.63** and hexabromobenzene (Scheme 1.16).⁵¹ Several other functionalized hexakis(arylethynyl)benzenes have been prepared using this method.^{51,52}



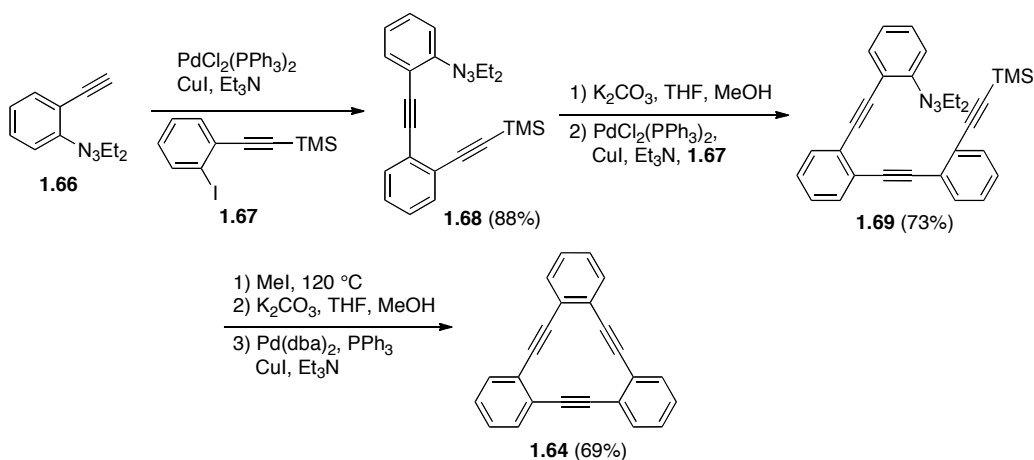
Scheme 1-16. Synthesis of hexakis(arylethynyl)benzene **1.62**.

In an effort to prepare larger model compounds of 6,6,6-graphyne, a series of macrocyclic oligomers was envisioned based on dehydrobenzannulene (DBA) **1.64**, which can be considered the smallest macrocyclic subunit of 6,6,6-graphyne. The synthesis of DBA **1.64** has been carried out in numerous ways over the past several decades. The initial approach involved the cyclotrimerization of copper acetylide **1.65** to yield DBA **1.64** in 48% yield, along with 10% of tetramer, and traces of larger macrocycles (Scheme 1-17).⁵²



Scheme 1-17. Cyclotrimerization of **1.65** to dehydrobenzannulene **1.64**.

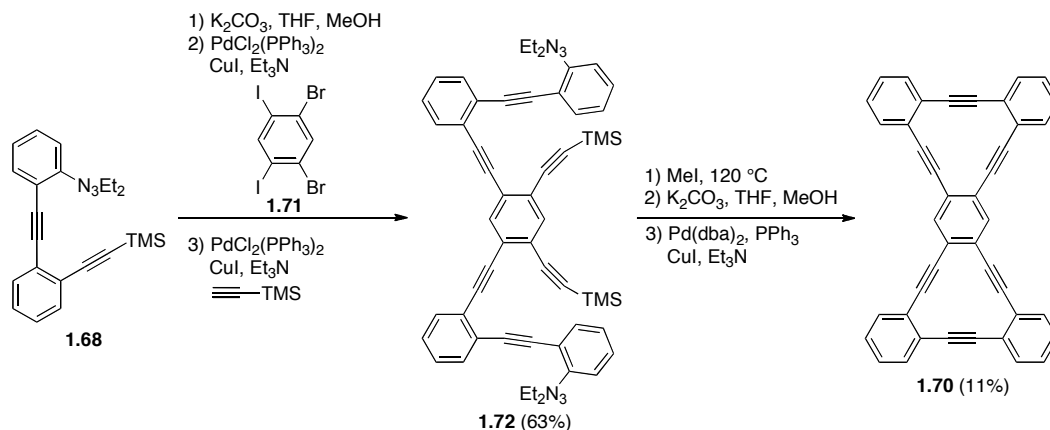
A stepwise approach to **1.64** was later developed by Haley and coworkers, in an effort to avoid the formation of larger macrocyclic side products. Sonogashira cross-coupling reaction of aryl triazene **1.66** with iodoarene **1.67** gave compound **1.68** in 88% yield (Scheme 1-18).⁵³ Desilylation of **1.68** and subsequent Sonogashira cross-coupling reaction with **1.67** gave the oligomer **1.69** in 73% yield. The aryl triazene was converted to an aryl iodide with MeI at high temperature, followed by desilylation. At this point, an intramolecular Sonogashira cross-coupling reaction was carried out in dilute solution to give DBA **1.64** in 69% yield, with no observed formation of larger cyclic side products.



Scheme 1-18. Stepwise synthesis of dehydrobenzannulene **1.64**.

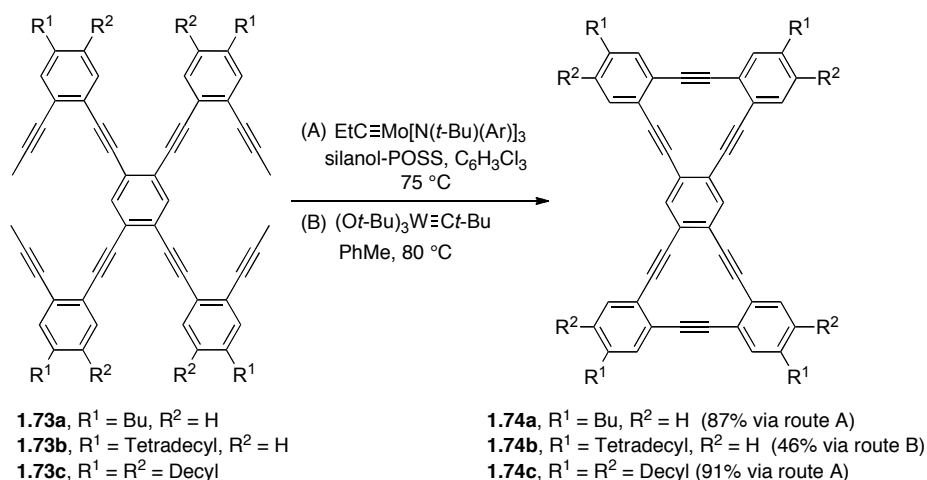
Turning to larger fragments of 6,6,6-graphyne, Haley and coworkers applied their intramolecular cross-coupling approach to the synthesis of “bow-tie” bis-DBA **1.70**. Compound **1.68** was desilylated and subsequently used in a Sonogashira cross-coupling reaction with 1,5-dibromo-2,4-diiodobenzene **1.71** (Scheme 1-19).⁵³ The reaction allowed for selective cross-coupling at the iodo positions of **1.71**, after which TMS-acetylene was added to complete the cross-coupling reaction at the bromo positions to give **1.72**. Conversion of the triazene into an iodide, desilylation, and an intramolecular Sonogashira

cross-coupling reaction afforded **1.70** in 11% yield. DBA **1.70** proved to be a highly insoluble compound, and the authors were unable to characterize the molecule using nuclear magnetic resonance (NMR) spectroscopy.



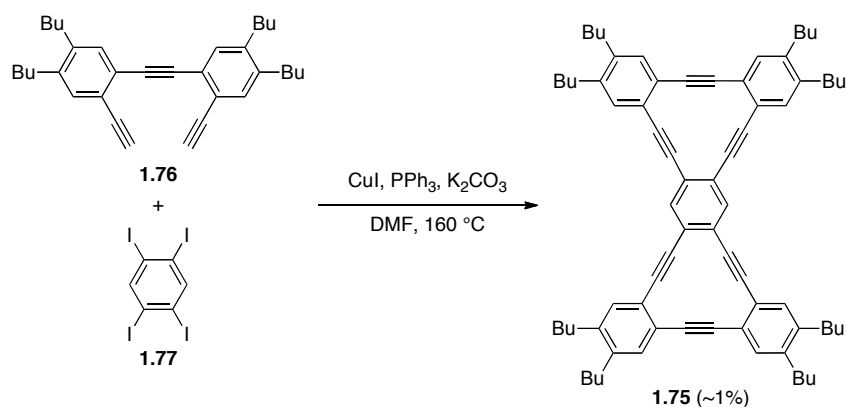
Scheme 1-19. Synthesis of “bow-tie” bis-dehydrobenzannulene **1.70**.

Haley and coworkers revised their synthetic strategy to improve the solubility of the “bow-tie” DBAs by appending alkyl chains to the molecule.⁵⁴ Octaynes **1.73a–c** underwent intramolecular alkyne metathesis using either (A) Schrock’s catalyst⁵⁵ (for **1.73b**) or (B) the Mo-amido catalyst developed by Moore and coworkers⁵⁶ (for **1.73a** and **1.73c**), to yield “bow-tie” DBAs **1.74a–c** (Scheme 1-20). It is noteworthy that both **1.74a** and **1.74b** also exhibited poor solubility despite the presence of the four C4 and C10 alkyl groups, while DBA **1.74c** displayed much improved solubility.



Scheme 1-20. Synthesis of substituted “bow-tie” dehydrobenzannulenes **1.74a–c**.

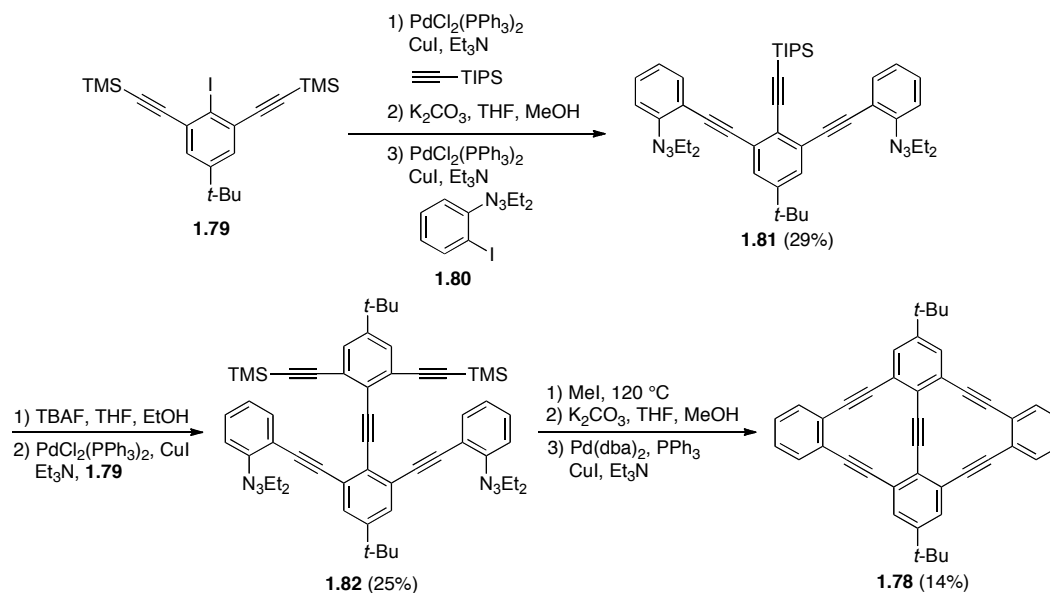
Iyoda and coworkers prepared “bow-tie” DBA **1.75** by an intermolecular Cu-mediated cross-coupling reaction (Scheme 1-21).⁵⁷ Triyne **1.76** and tetraiodobenzene **1.77** were heated in the presence of K_2CO_3 , CuI, and PPh_3 to yield DBA **1.75** in less than 1% isolated yield. Although the yield of **1.75** was extremely low, the eight alkyl substituents significantly improved the solubility of this derivative relative to **1.70**.



Scheme 1-21. Synthesis of substituted “bow-tie” bis-dehydrobenzannulene **1.75**.

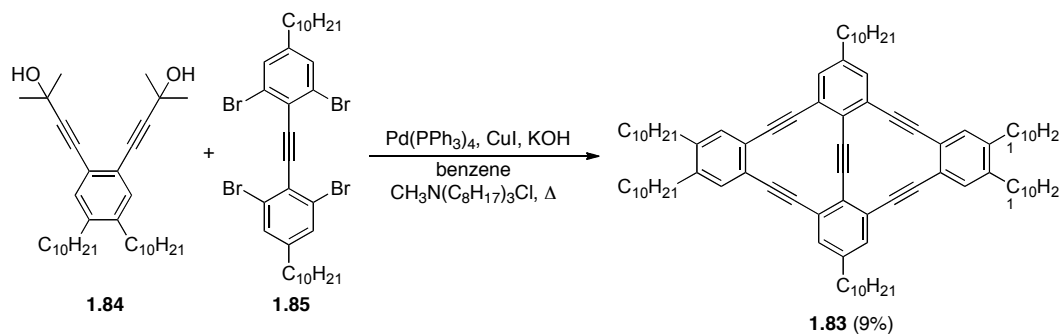
In addition to the “bow-tie” shaped DBAs, Haley and coworkers also pursued the “diamond” DBA **1.78** (Scheme 1-22).⁵³ Sonogashira cross-coupling reaction of diyne

1.79 and triisopropylsilyl-acetylene (TIPS-acetylene) followed by selective desilylation and additional Sonogashira cross-coupling reaction with triazene **1.80** led to triyne **1.81** in 29% yield. After removal of the TIPS group, the resulting product underwent a Sonogashira cross-coupling reaction with **1.79** to yield **1.82** in 25% yield. Conversion of the aryltriazene groups into aryl iodides, desilylation, and a two fold intramolecular Sonogashira cross-coupling reaction gave DBA **1.78** in 14% yield.



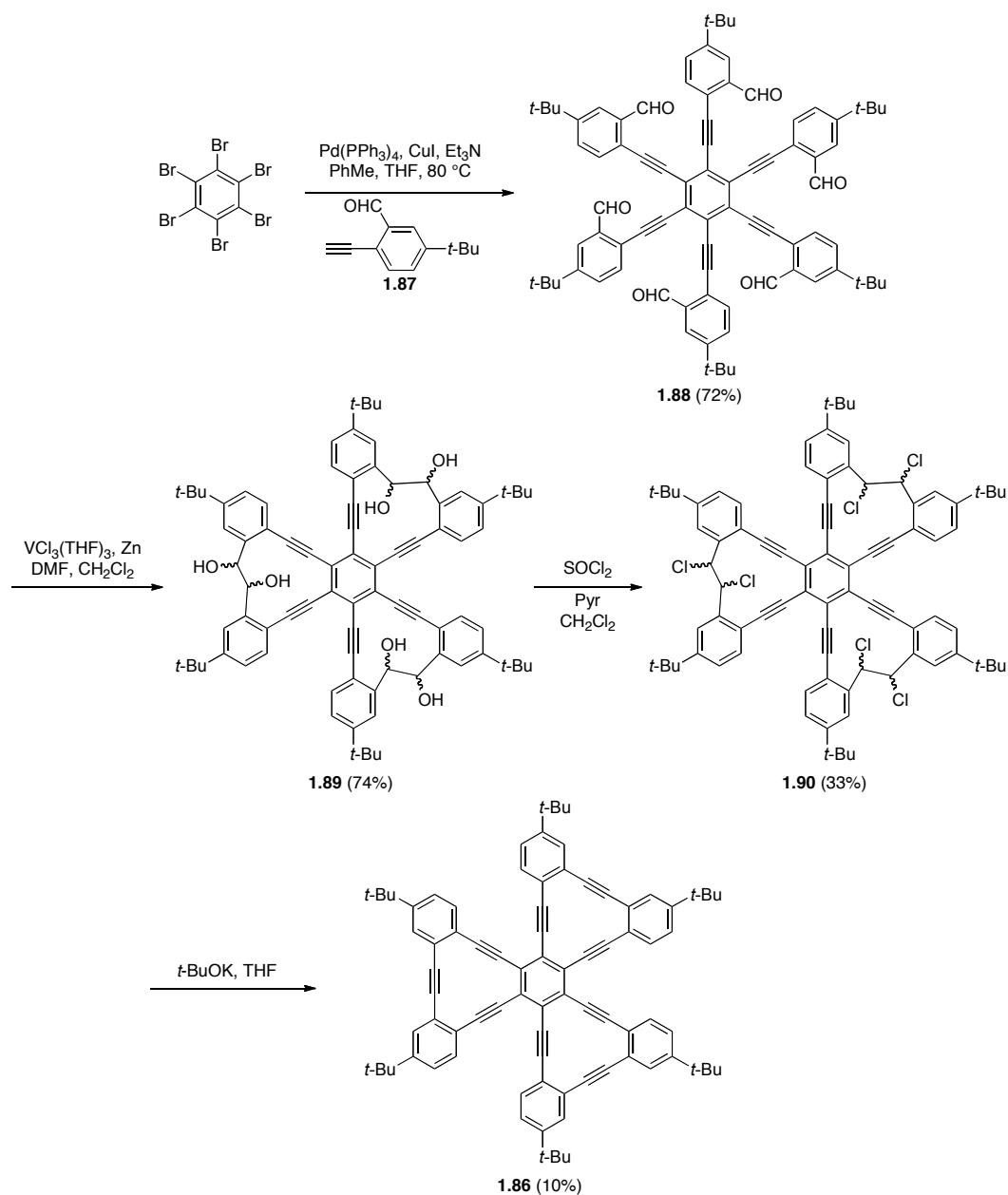
Scheme 1-22. Synthesis of “diamond” dehydrobenzannulene **1.78**.

Tobe and coworkers prepared a similar “diamond” DBA **1.83** using an intermolecular approach (Scheme 1-23).⁵⁸ Heating aryl diyne **1.84** in the presence of KOH gave the terminal alkynes, which underwent an intermolecular Sonogashira cross-coupling reaction with diarylacetylene **1.85** to give bis-DBA **1.83** in 9% isolated yield.



Scheme 1-23. Synthesis of “bow-tie” bis-dehydrobenzannulene **1.83**

In 2006, Tobe and coworkers prepared the large “trefoil” **1.86**, which consists of three DBAs fused to a central benzene ring (Scheme 1-24).⁵⁹ Starting from hexabromobenzene, a six fold Sonogashira cross-coupling reaction with aryl alkyne **1.87** led to the formation hexakis(arylethynyl)benzene **1.88** in 72% yield. Pinacol coupling using a vanadium reagent gave hexaol **1.89** in 74% yield as a mixture of isomers. Conversion of the alcohol groups to chlorides using thionyl chloride gave **1.90** in 33% yield, which underwent a six-fold elimination in the presence of potassium *t*-butoxide to give “trefoil” tris-DBA **1.86** in 10% yield.

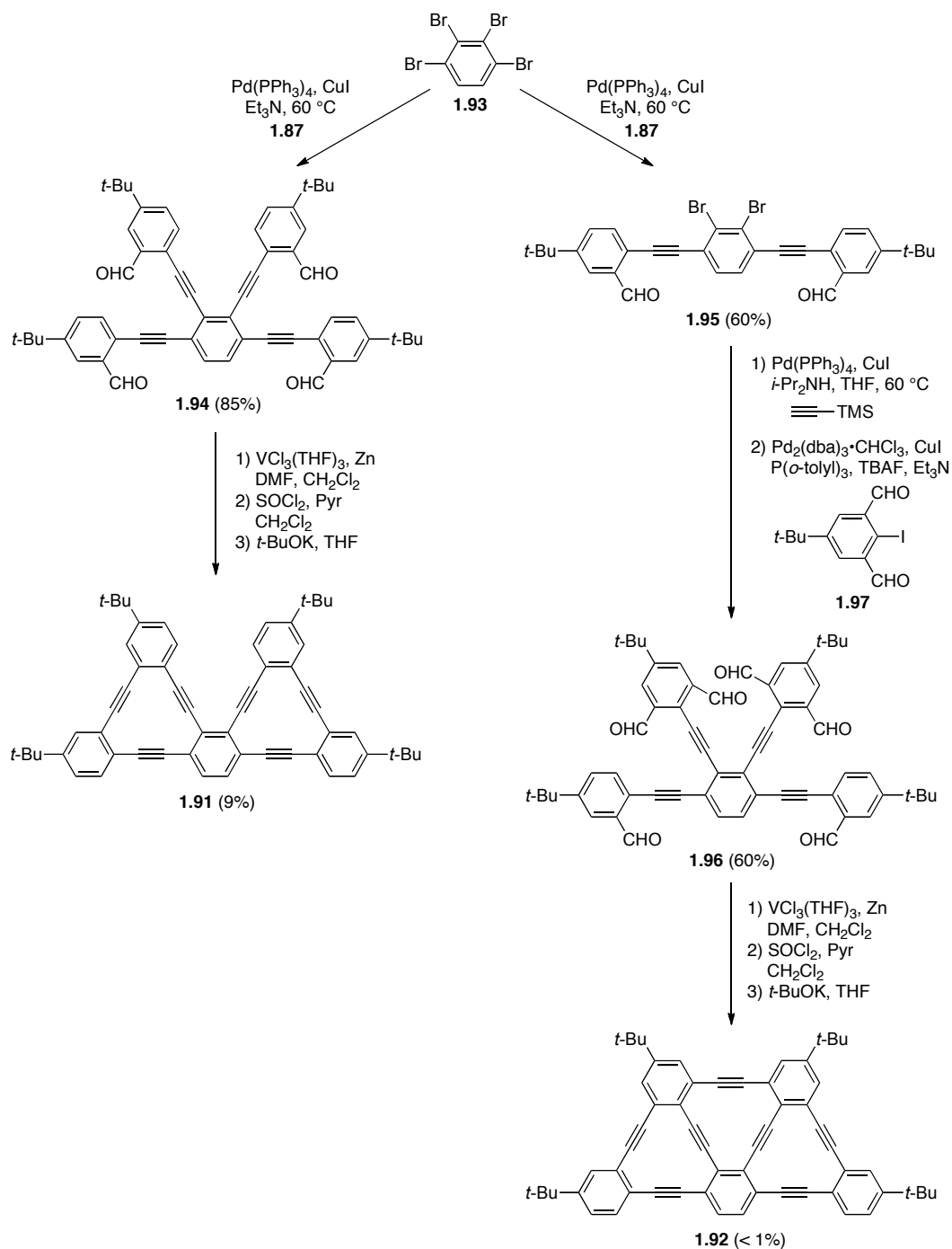


Scheme 1-24. Synthesis of “trefoil” tris-dehydrobenzannulene **1.86**

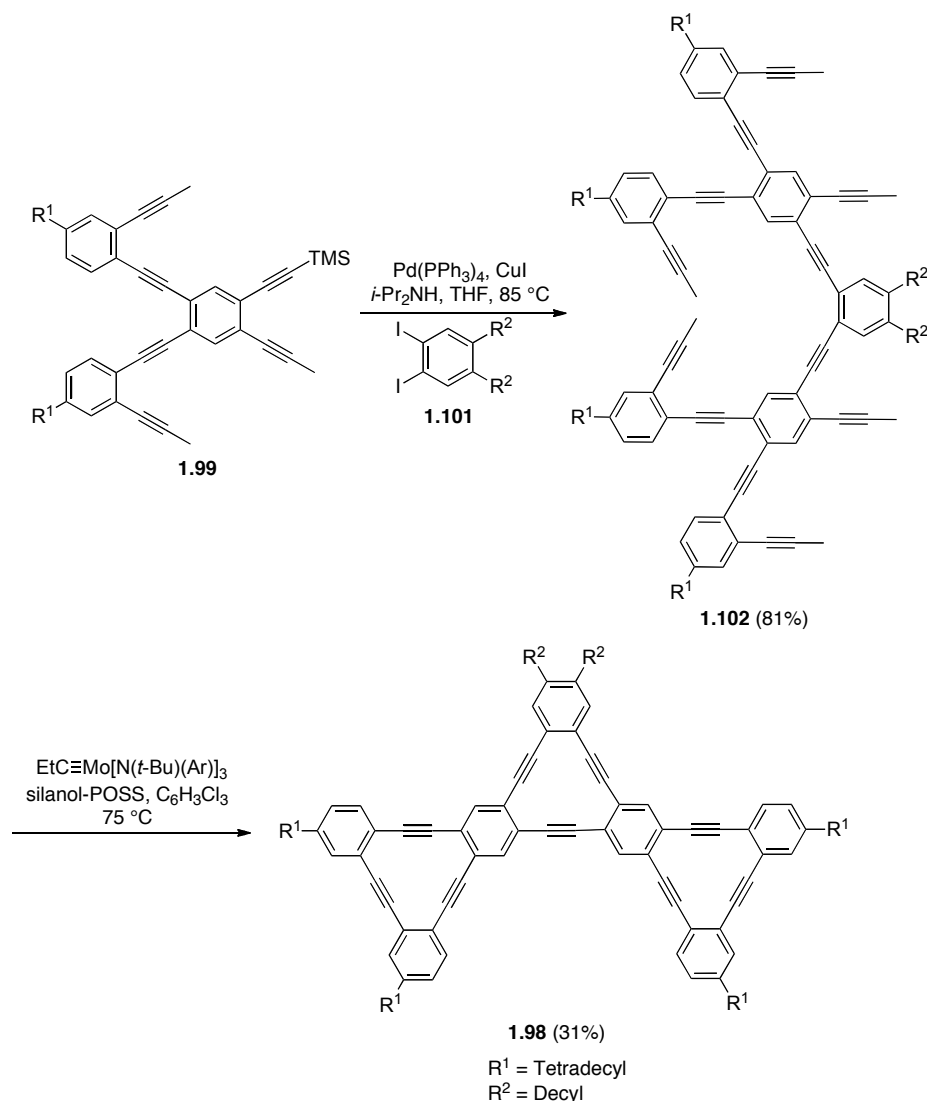
Tobe and coworkers utilized a similar approach to construct the “boomerang” bis-DBA **1.91** and “trapezoid” tris-DBA **1.92** (Scheme 1-25).⁶⁰ Starting from tetrabromobenzene **1.93**, a Sonogashira cross-coupling reaction with aryl acetylene **1.87** led to the formation of tetrayne **1.94** or diyne **1.95**, depending on the number of equivalents of **1.87** used in the reaction. An excess of **1.87** resulted in the formation of

1.94 in 85% yield, while using only two equivalents of **1.87** led to the preferential formation of **1.95** in 60% yield. Pinacol coupling, chlorination, and subsequent elimination of tetrayne **1.94** led to “boomerang” bis-DBA **1.91** in 9% yield over the three steps. Diyne **1.95** was converted to tetrayne **1.96** in 27% yield via a sequence of Sonogashira cross-coupling with TMS-acetylene, desilylation, and Sonogashira cross-coupling reaction with iodoformylarene **1.97**. Tetrayne **1.96** underwent a sequence of Pinacol coupling, chlorination, and elimination to yield “trapezoid” tris-DBA **1.92** in less than 1% yield over the 3 steps.

The longest linearly conjugated segment of 6,6,6-graphyne prepared to date, tris-DBA **1.98**, was assembled by Haley and coworkers (Scheme 1-26).⁵⁴ The synthesis began with **1.99**, which was desilylated and subjected to a Sonogashira cross-coupling reaction with diiodobenzene **1.100** to give polyynes **1.101** in 81% yield. Intramolecular alkyne metathesis of **1.101** using Moore’s catalyst afforded tris-DBA **1.98** in 31% yield. Efforts to prepare longer segments using this method have so far been unsuccessful.⁵⁴



Scheme 1-25. Synthesis of “boomerang” and “trapezoid” dehydrobenzannulenes **1.91** and **1.92**, respectively.



Scheme 1-26. Synthesis of tris-dehydrobenzannulene **1.98**.

1.3.3 Physical Properties of Graphyne Model Compounds

With the exception of **1.61**, all of the reported 6,6,6-graphyne model compounds are stable solids, with melting points of 250–300 °C, and they are generally stable toward heat, light and oxygen. Their electronic structure, as assessed by UV-Vis spectroscopy, is dominated by extension of the longest linear phenylene ethynylene chromophore,⁵⁴ as can be appreciated by the absorption spectra of DBAs **1.64**, **1.74**, and **1.98** that show bathochromic shifts in both λ_{cutoff} and λ_{max} with each successive ring fusion (Figure 1-5).

Thus, tris-DBA **1.98** possesses the longest linear diphenylacetylene pathway of all the model compounds, which results in the lowest energy absorption ($\lambda_{\text{cutoff}} = 525$ nm) of the series. Structural isomer of **1.98**, “trefoil” **1.86** possesses a shorter phenylene ethynylene pathway, which results a higher energy λ_{max} absorption ($\lambda_{\text{cutoff}} \sim 500$ nm). This preliminary evidence stresses the importance of the phenylene ethynylene pathway in the electronic properties of 6,6,6-graphyne, rather than cyclization.

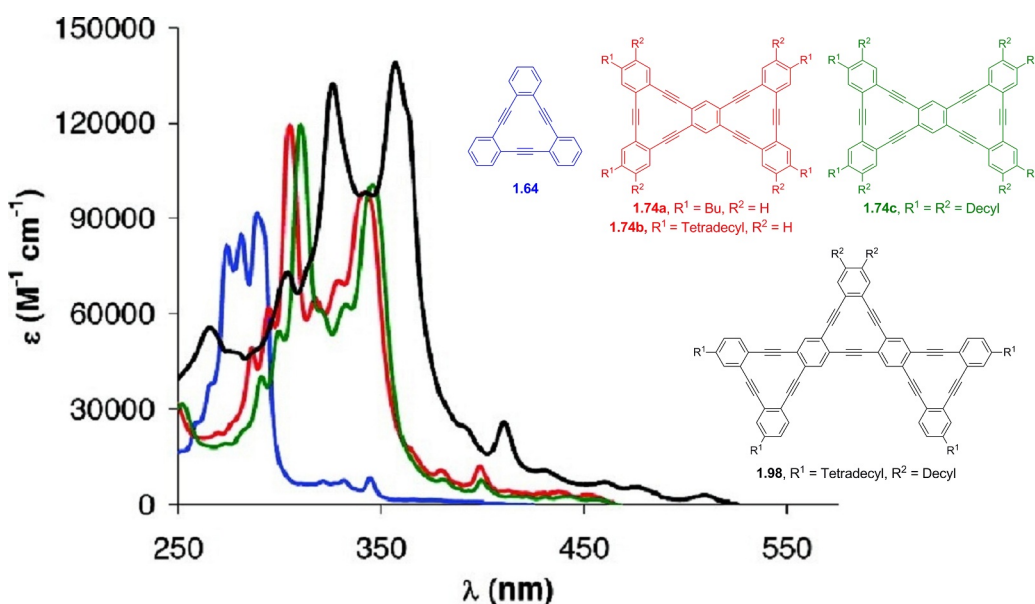


Figure 1-5. Absorption spectra of **1.64**, **1.74a–c**, and **1.98**. Adapted with permission from Johnson II, C. A.; Lu, Y.; Haley, M. M. *Org. Lett.* **2007**, *9*, 3725–3728. Copyright 2007 American Chemical Society.

1.4 Conclusion

A vast array of acetylene-rich molecules has been prepared over the past several decades. Interest in the carbon-rich material graphyne has further fueled the development of many of these structures. To date, however, synthetic efforts to model graphyne have focused on a single structural motif, 6,6,6-graphyne, while many other possible structures

of graphyne remain unexplored. Theoretical investigations suggest that several of these graphyne structures, such as 6,6,12-graphyne or 12,12,12-graphyne, are equally, and possibly more, promising materials than 6,6,6-graphyne.⁴⁹ Toward the realization of other graphyne structures, synthetic routes that have been established to prepare acetylene-rich macrocycles should serve as a solid foundation to realize the desired model compounds of graphyne.

1.5 References

1. Heeger, A. J. *Angew. Chem. Int. Ed.* **2001**, *40*, 2591–2611.
2. MacDiarmid, A. G. *Angew. Chem. Int. Ed.* **2001**, *40*, 2581–2590.
3. Shirakaw, H. *Angew. Chem. Int. Ed.* **2001**, *40*, 2574–2680.
4. Roncali, J. *Chem. Rev.* **1992**, *92*, 711–738.
5. Vernitskaya, T. V.; Efimov, O. N. *Russ. Chem. Rev.* **1997**, *66*, 443–457.
6. Sved, A. A.; Dinesan, M. K. *Talanta* **1991**, *8*, 815–837.
7. Hertei, D.; Setayesh, S.; Nothofer, H. G.; Scherf, U.; Müllen, K.; Bäessler, H. *Adv. Mater.* **2001**, *13*, 65–70.
8. Neher, D. *Macromol. Rapid Comm.* **2001**, *22*, 1365–1385.
9. Junkers, T.; Vandenberg, J.; Adriaensens, P.; Lutsen, L.; Vanderzande, D. *Polym. Chem.* **2012**, *3*, 275–285.
10. Hoeben, F. J. M.; Jonkheijm, P.; Meijer, E. W.; Schenning, A. P. H. J. *Chem. Rev.* **2005**, *105*, 1491–1546.
11. Kelly, B. T. *Physics of Graphite*, Applied Science Publishers: London, 1981.
12. Geim, A. K.; Novoselov, K. S. *Nat. Mater.*, **2007**, *6*, 183–191.
13. (a) Wu, J.; Pisula, W.; Müllen, K. *Chem. Rev.* **2007**, *107*, 718–747. (b) Rao, C. N. R.; Sood, A. K.; Voggu, R.; Subrahmanyam, K. S. *J. Phys. Chem. Lett.* **2010**,

- 1, 572–580.
14. (a) Kroto, H. W.; Heath, J. R.; O'Brien, S. C.; Curl, R. F.; Smalley, R. E. *Nature*, **1985**, *318*, 192–193. (b) Hirsch, A. (Ed) *The Chemistry of Fullerenes*, Wiley-VCH, Weinheim (**2002**) (c) Niyogi, S.; Hamon, M. A.; Hu, H.; Zhao, B.; Bhowmik, P.; Sen, R.; Itkis, M. E.; Haddon, R. C. *Acc. Chem. Res.* **2002**, *35*, 1105–1113.
 15. Dennler, G.; Scharber, M. C.; Brabec, C. J. *Adv. Mater.* **2009**, *21*, 1323–1338.
 16. Chalifoux, W. A.; Tykwinski, R. R. *C. R. Chimie* **2009**, *12*, 341–358.
 17. (a) Nielsen, M. B.; Diederich, F. *Chem. Rev.* **2005**, *105*, 1837–1867. (b) Tykwinski, R. R.; Gubler, U.; Martin, R. E.; Diederich, F.; Bosshard, C.; Gunter, P. *J. Phys. Chem. B* **1998**, *102*, 4451–4465.
 18. (a) Miller, J. J.; Marsden, J. A.; Haley, M. M. *Synlett* **2004**, 165–168. (b) Marsden, J. A.; Miller, J. J.; Shirtcliff, L. D.; Haley, M. M. *J. Am. Chem. Soc.* **2005**, *127*, 2464–2476. (c) Slepko, A. D.; Hegmann, F. A.; Tykwinski, R. R.; Kamada, K.; Ohta, K.; Marsden, J. A.; Spitler, E. L.; Miller, J. J.; Haley, M. M. *Opt. Lett.* **2006**, *31*, 3315–3317. (d) Samori, S.; Tojo, S.; Fujitsuka, M.; Spitler, E. L.; Haley, M. M.; Majima, T. *J. Org. Chem.* **2007**, *72*, 2785–2793. (e) Spitler, E. L.; Shirtcliff, L. D.; Haley, M. M. *J. Org. Chem.* **2007**, *72*, 86–96. (f) Spitler, E. L.; Haley, M. M. *Tetrahedron* **2008**, *64*, 11469–11474. (g) Spitler, E. L.; Monson, J. M.; Haley, M. M. *J. Org. Chem.* **2008**, *73*, 2211–2223.
 19. (a) Nielsen, M. B.; Diederich, F. *Chem. Rev.* **2005**, *105*, 1837–1868. (b) Gholami, M.; Tykwinski, R. R. *Chem. Rev.* **2006**, *106*, 4997–5027. (c) Diederich, F.; Kivala, M. *Adv. Mater.* **2010**, *22*, 803–812.
 20. Kivala, M.; Mitzel, F.; Boudon, C.; Gisselbrecht, J.-P.; Seiler, P.; Gross, M.; Diederich, F. *Chem. Asian J.* **2006**, *1*, 479–489.
 21. Nielsen, M. B.; Schreiber, M.; Baek, Y. G.; Seiler, P.; Lecomte, S.; Boudon, C.;

- Tykwinski, R. R.; Gisselbrecht, J. P.; Gramlich, V.; Skinner, P. J.; Bosshard, C.; Giinter, P.; Gross, M.; Diederich, F. *Chem. Eur. J.* **2001**, *7*, 3263–3280.
22. (a) Mitzel, F.; Boudon, C.; Gisselbrecht, J. P.; Seiler, P.; Gross, M.; Diederich, F. *Helv. Chim. Acta* **2004**, *87*, 1130–1157. (b) Mitzel, F.; Boudon, C.; Gisselbrecht, J.-P.; Seiler, P.; Gross, M.; Diederich, F. *Chem. Comm.* **2003**, 1634–1635.
23. Tykwinski, R. R.; Diederich, F. *Liebigs Ann. Recl.* **1997**, 649–661.
24. Boldi, A. M.; Diederich, F. *Angew. Chem. Int. Ed. Engl.* **1994**, *33*, 468–471.
25. Anthony, J.; Boldi, A. M.; Boudon, C.; Gisselbrecht, J. P.; Gross, M.; Seiler, P.; Knobler, C. B.; Diederich, F. *Helv. Chim. Acta* **1995**, *78*, 797–817.
26. Schreiber, M.; Tykwinski, R. R.; Diederich, F.; Spreiter, R.; Gubler, U.; Bosshard, C.; Poberaj, I.; Gunter, P.; Boudon, C.; Gisselbrecht, J. P.; Gross, M.; Jonas, U.; Ringsdorf, H. *Adv. Mater.* **1997**, *9*, 339–343.
27. Eisler, S.; Tykwinski, R. R. *Angew. Chem. Int. Ed.* **1999**, *38*, 1940–1943.
28. Orfanopoulos, M.; Stratakis, M.; Elemen, Y. *J. Am. Chem. Soc.* **1990**, *112*, 6417–6419.
29. Tykwinski, R. R.; Gholami, M.; Eisler, S.; Zhao, Y.; Melin, F.; Echegoyen, L. *Pure Appl. Chem.* **2008**, *80*, 621–637.
30. Gholami, M. Ph. D Thesis, University of Alberta, 2009.
31. Ramsaywack, S. Ph. D Thesis, University of Alberta, 2010.
32. Baughman, R. H.; Eckhardt, H.; Kertesz, M. *J. Phys. Chem.* **1987**, *87*, 6687–6699.
33. Beckhaus, H.-D.; Rückhardt, C.; Kao, M.; Diederich, F.; Foote, C. S. *Angew. Chem. Int. Ed. Engl.* **1992**, *31*, 63–64.
34. Narita, N.; Nagai, S.; Suzuki, S.; Nakao, K. *Phys. Rev. B* **1998**, *58*, 11009.
35. Narita, N.; Nagai, S.; Suzuki, S. *Phys. Rev. B* **2001**, *64*, 245408.
36. Coluci, V. R.; Braga, S. F.; Legoas, S. B.; Galvao, D. S.; Baughman, R. H. *Phys.*

- Rev. B* **2003**, *68*, 035430.
37. Coluci, V. R.; Braga, S. F.; Legoas, S. B.; Galvao, D. S.; Baughman, R. H. *Nanotechnology* **2004**, *15*, S142–S149.
 38. Enyashin, A. N.; Sofronov, A. A.; Makurin, Y. N.; Ivanovskii, A. L. *J. Mol. Struct. THEOCHEM* **2004**, *684*, 29–33.
 39. Kondo, M.; Nozaki, D.; Tachibana, M.; Yumura, T.; Yoshizawa, K. *Chem. Phys.* **2005**, *312*, 289–297.
 40. Tahara, K.; Yoshimura, T.; Sonoda, M.; Tobe, Y.; Williams, R. V. *J. Org. Chem.* **2007**, *72*, 1437–1442.
 41. Sebastiani, D.; Parker, M. A. *Symmetry* **2009**, *1*, 226–239.
 42. Zhang, H.; Zhao, M.; He, X.; Zhenhai, W.; Zhng, X.; Liu, X. *J. Phys. Chem. C* **2011**, *115*, 8845–8850.
 43. Li, C.; Li, J.; Wu, F.; Li, S.-S.; Xia, J.-B.; Wang, L.-W. *J. Phys. Chem. C* **2011**, *115*, 23221–23225.
 44. Zhou, J.; Lv, K.; Wang, Q.; Chen, X. S.; Sun, Q. *J. Chem. Phys.* **2011**, *134*, 174701.
 45. Pan, L. D.; Zhang, L. Z.; Song, B. Q.; Du, S. X.; Gao, H.-J. *Appl. Phys. Lett.* **2011**, *98*, 173102.
 46. Kim, B. G.; Choi, H. J.; *Condensed Matter* **2011**, arXiv:1112.2932v1
 47. Kang, J.; Li, J.; Wu, F.; Li, S.-S.; Xia, J.-B. *J. Phys. Chem. C* **2011**, *115*, 20466–20470.
 48. Cranford, S. W.; Buehler, M. J. *Carbon* **2011**, *49*, 4111–4121.
 49. Malko, D.; Neiss, C.; Vines, F.; Görling, A. *Phys. Rev. Lett.* **2012**, *108*, 086804.
 50. Diercks, R.; Armstrong, J. C.; Boese, R.; Vollhardt, K. P. C. *Angew. Chem. Int. Ed. Engl.* **1986**, *25*, 268–269.
 51. Praefcke, K.; Kohne, B.; Singer, D. *Angew. Chem. Int. Ed. Engl.* **1990**, *29*, 177–

179.

52. Kobayashi, K.; Kobayashi, N. *J. Org. Chem.* **2004**, *69*, 2487–2497.
52. Solooki, D.; Ferrara, J. D.; Malaba, D.; Bradshaw, J. D.; Tessier, C. A.; Youngs, W. J. *Inorg. Synth.* **1997**, *31*, 122.
53. Kehoe, J. M.; Kiley, J. H.; English, J. J.; Johnson, C. A.; Petersen, R. C.; Haley, M. M. *Org. Lett.* **2000**, *2*, 969–972.
54. Johnson II, C. A.; Lu, Y.; Haley, M. M. *Org. Lett.* **2007**, *9*, 3725–3728.
55. (a) Schrock, R. R. *Acc. Chem. Res.* **1986**, *19*, 342–348. (b) Schrock, R. R. *Polyhedron* **1995**, *14*, 3177–3195.
56. (a) Zhang, W.; Kraft, S.; Moore, J. S. *J. Am. Chem. Soc.* **2004**, *126*, 329–335. (b) Zhang, W.; Moore, J. S. *J. Am. Chem. Soc.* **2005**, *127*, 11863–11870. (c) Zhang, W.; Moore, J. S. *Adv. Synth. Catal.* **2007**, *349*, 93–120.
57. Iyoda, M.; Sirinintasak, S.; Nishiyama, Y.; Vorasingha, A.; Sultana, F.; Nakao, K.; Kuwatani, Y.; Matsuyama, H.; Yoshida, M.; Miyake, Y. *Synthesis* **2004**, 1524–1531.
58. Sonoda, M.; Sakai, Y.; Yoshimura, T.; Tobe, Y.; Kamada, K. *Chem. Lett.* **2004**, *33*, 972–973.
59. Yoshiura, T.; Inaba, A. I. Sonoda, M.; Tahara, K.; Tobe, Y.; Williams, R. V. *Org. Lett.* **2006**, *8*, 2933–2936.
60. Tahara, K.; Yoshimura, T.; Ohno, M.; Sonoda, M.; Tobe, Y. *Chem. Lett.* **2007**, *36*, 838–839.

Chapter 2 - Model Compounds of 12,12,12-Graphyne Based on Expanded Radialenes

2.1 Introduction

Over the past fifteen years, the Tykwinski group has been actively involved in the research of both linear and cyclic cross-conjugated molecules. An important structural motif that has been used in this area is that of radialenes, and in particular, expanded radialenes. A former Tykwinski group PhD student, Dr. Sarah Eisler, successfully developed a synthetic route to expanded radialenes ([*n*]ER), for which the π -spacer unit in the radialene structure was a single acetylene unit.¹ The [6]ER prepared using this method was also the first successful synthesis of this class of radialenes, containing a single acetylene unit as the π -spacer (Scheme 1-6). This synthetic strategy was then drawn upon for the synthesis of a modified series of expanded radialenes by another former Tykwinski group member Dr. Katie Campbell, for which the acetylene π -spacer unit was replaced by other π -conjugated subunits, such as aryl rings, pyridyl rings, and metallic bridges (Figure 2-1).² More recently, this same strategy was further exploited and refined by former Tykwinski group members Dr. Mojtaba Gholami and Dr. Sharwaite Ramsaywack in the synthesis of a series of [4]ERs, for which the periphery was decorated with phenyl rings, as well as donor and acceptor substituted phenyl rings.^{3,4}

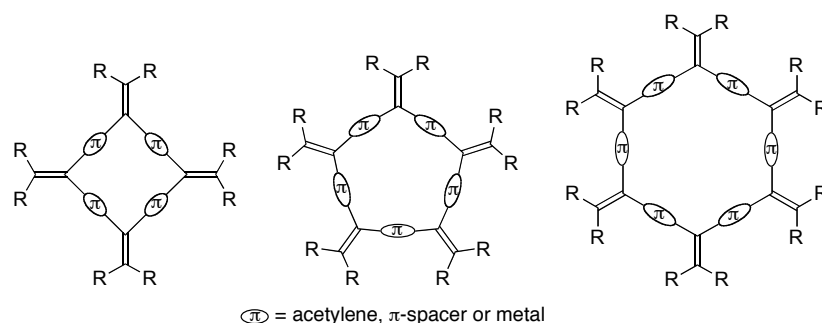


Figure 2-1. Schematic representation of expanded [4]-, [5]-, and [6]radialenes.

The synthesis of these substituted expanded radialenes, particularly the donor and acceptor substituted series, highlights the versatility of the synthetic route developed for the synthesis of these cross-conjugated macrocycles. For the donor and acceptor series, it was possible to introduce functionality onto the radialene framework by both the functionalization of the precursor building blocks via Path A and functionalization of the already formed radialene macrocycle itself via Path B (Figure 2-2).

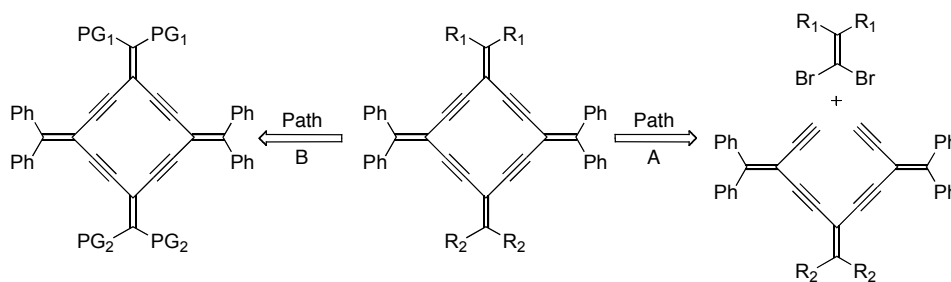


Figure 2-2. Retrosynthetic routes to substituted 4[ER]s, where R_1 and R_2 are the desired functional groups.

Utilizing methods similar to those established for [4]ERs, it becomes possible to substitute the periphery of the radialene core with functional groups to allow for the synthesis of sub-pieces 12,12,12-graphyne. In addition to structures based on [4]ERs, it

was hypothesized that this methodology could be applied in the synthesis of [6]ERs analogues.

12,12,12-Graphyne (sometimes referred to as β -graphyne) is one of the theoretically proposed structures of graphyne. It consists of a ratio of 2:1 $sp:sp^2$ hybridized carbon, made up entirely of acetylene and olefin bonds, arranged in a hexagonal lattice similar to graphene. It is one of the least dense forms of graphyne, with 0.232 carbons/Å.⁵ This form of graphyne is also one of the least studied, with only a handful of theoretical investigations and no synthetic models.^{5,6} Simplifying its structure, one of the smallest possible repeat unit that can be cut out of a 12,12,12-graphyne sheet consists of six dehydroannulenes fused to an expanded [6]radialene core (Figure 2-3). Using the synthetic methodology established within the Tykwinski group, it should be possible to synthesize this [6]ER in order to investigate its properties as a model compound of 12,12,12-graphyne.

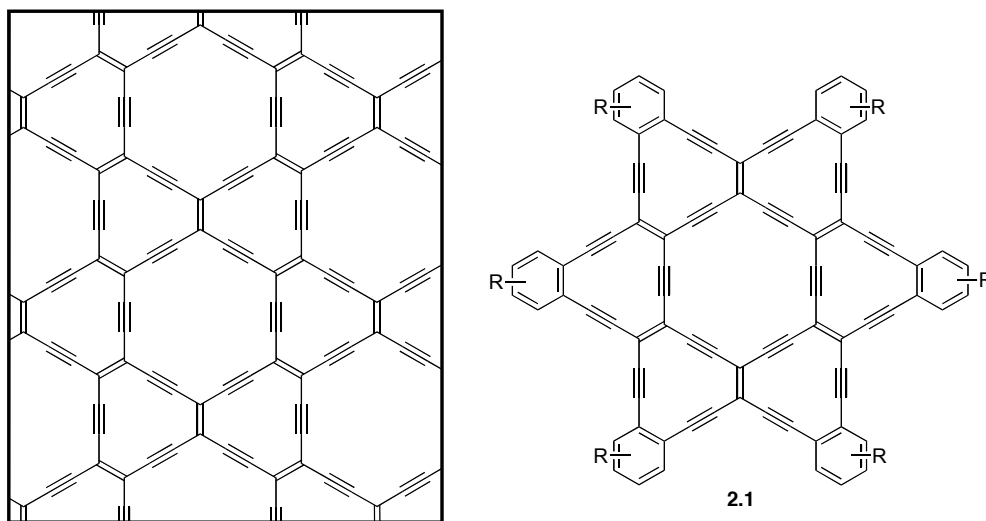
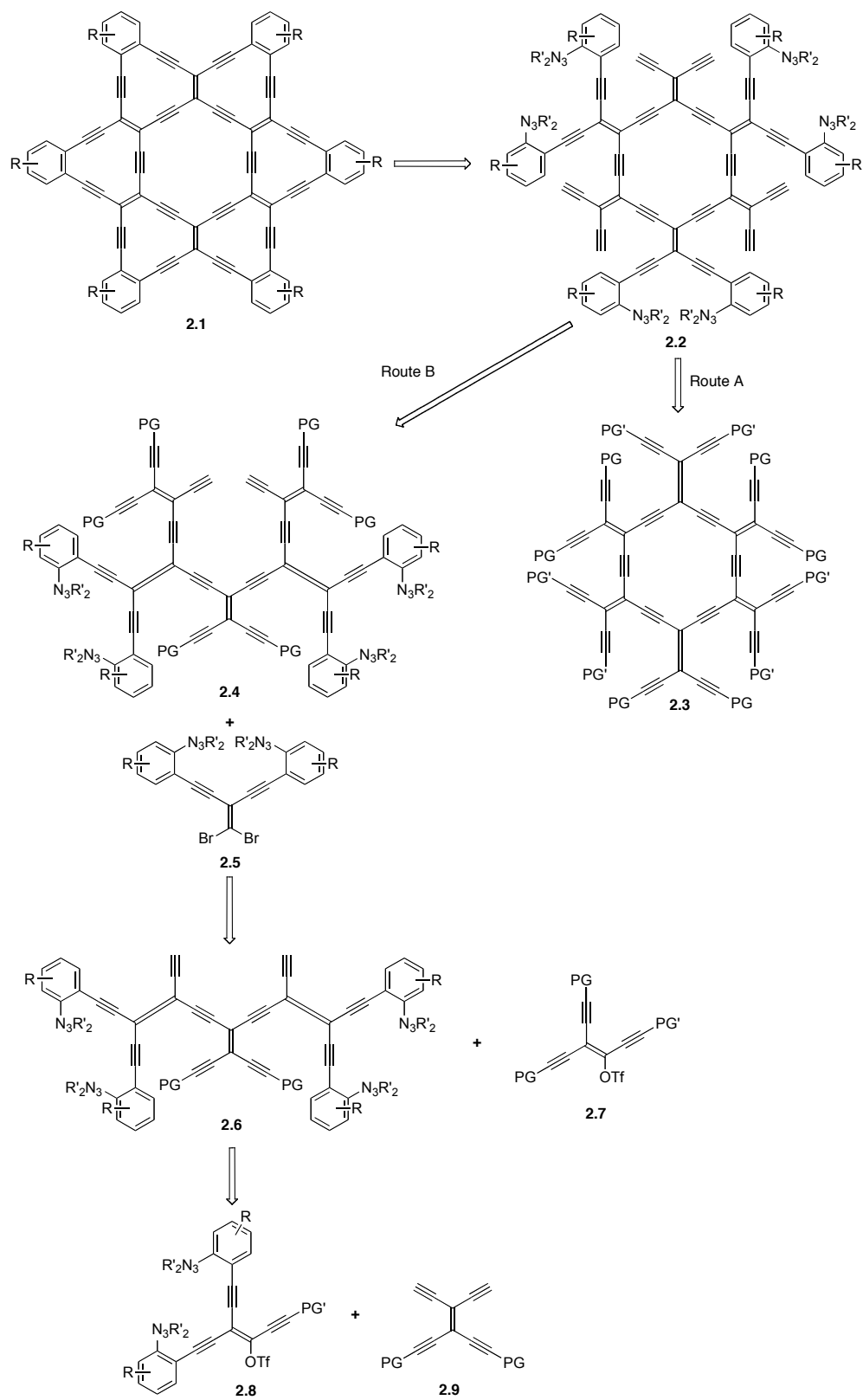


Figure 2-3. Structure of 12,12,12-graphyne and its corresponding model compound based on an expanded [6]radialene core.

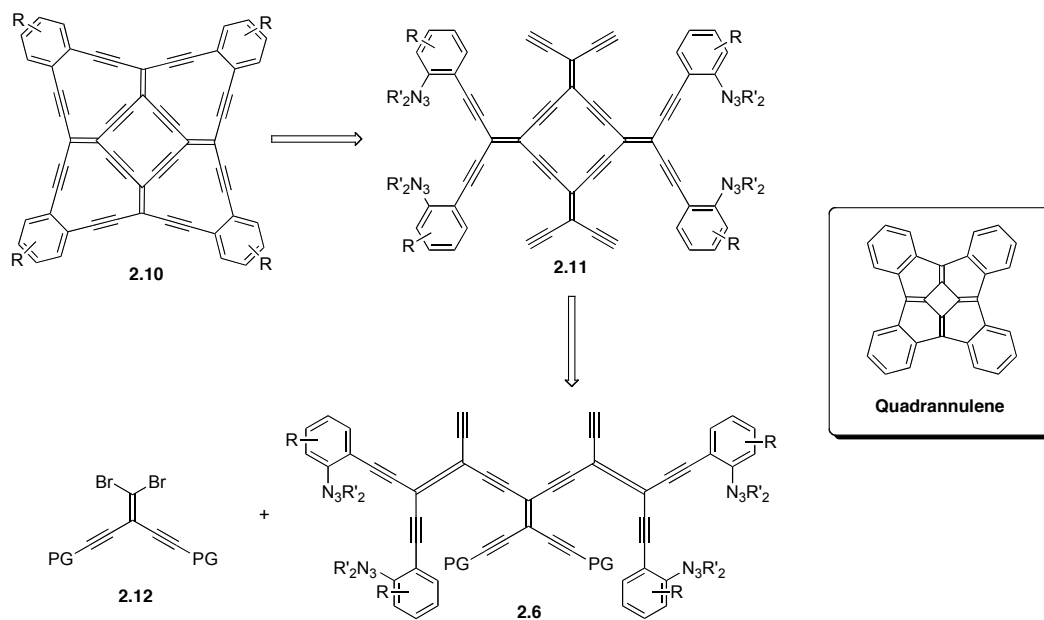
Analogous to the strategy used for the synthesis of the donor/acceptor functionalized [n]ERs, two general synthetic routes toward radialene **2.1** can be envisioned (Scheme 2-1). In both cases, target radialene **2.1** would be prepared from radialene **2.2**, via the transformation of the triazene groups to aryl iodides and a subsequent intramolecular Sonogashira cross-coupling reaction.^{7,8} The first route (Route A) relies heavily on a variety of orthogonally protected acetylenes (PG and PG') during the synthesis of the radialene core, which would then be functionalized after its assembly. Radialene **2.2** would arise from the orthogonally protected radialene **2.3**, which would allow for selective cross-coupling reactions to install the functional groups necessary to form the outer annulene rings.

The second route focuses on the incorporation of the desired functional groups into the building blocks of the target molecule **2.2** (Route B). Radialene **2.2** would be prepared via a two fold Sonogashira cross-coupling reaction of *iso*-polydiacetylene (*iso*-PDA) **2.4** and dibromoolefin **2.5**. Compound **2.4** can be further broken down into the smaller trimeric *iso*-PDA **2.6** and vinyl triflate **2.7**. Trimer **2.6** can be prepared from small key molecules, the tetraethynylethene (TEE) **2.8** and vinyl triflate **2.9**.

An important branching point should be noted at this stage, as trimer **2.6** is also a key intermediate in the synthesis of the smaller [4]ER **2.10** (Scheme 2-2). Radialene **2.10** could be prepared from radialene **2.11**, via the formation of aryl iodides and subsequent intramolecular Sonogashira cross-coupling reaction. Radialene **2.11** could be prepared from a Sonogashira cross-coupling reaction of **2.6** with dibromoolefin **2.12**. It is interesting to point out that radialene **2.10** is an expanded version of quadrannulene, a curved structure thought to be important in the formation of junctions in carbon nanotubes.⁹



Scheme 2-1. Retrosynthetic route to expanded [6]radialene model compound **2.1**.



Scheme 2-2. Retrosynthetic route to [4]ER **2.10**, an expanded version of quadrannulene (inset).

The key to both synthetic strategies in Scheme 2-1 is the synthesis of a variety of different small building blocks that will be pieced together in a stepwise process towards the larger radiannulenes. These building blocks are based on the four key structural motifs, (a) aryl triazenes, (b) dibromoolefins, (c) TEEs, and (d) vinyl triflates (Figure 2-4).

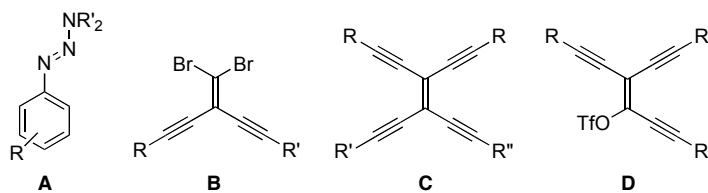


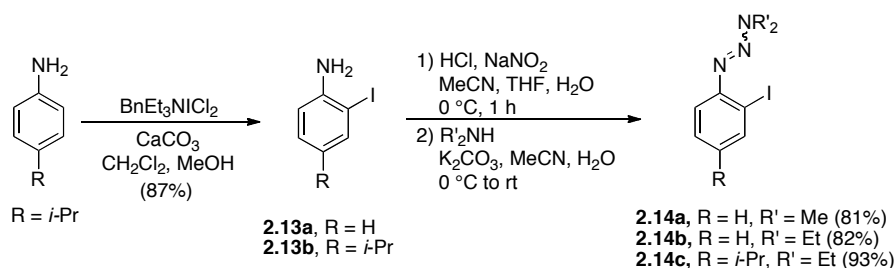
Figure 2-4. Schematic representations of (a) aryl triazenes, (b) dibromoolefins, (c) TEEs, and (d) vinyl triflates.

2.2 Synthesis of Building Blocks

2.2.1 Synthesis of Aryl Triazenes

In order to perform Sonogashira cross-coupling reactions late in the synthetic route, the required aryl halide must be protected throughout the synthetic route. Aryl triazenes, which have been shown to serve as masked iodides,^{8a} provide such a synthetic handle.

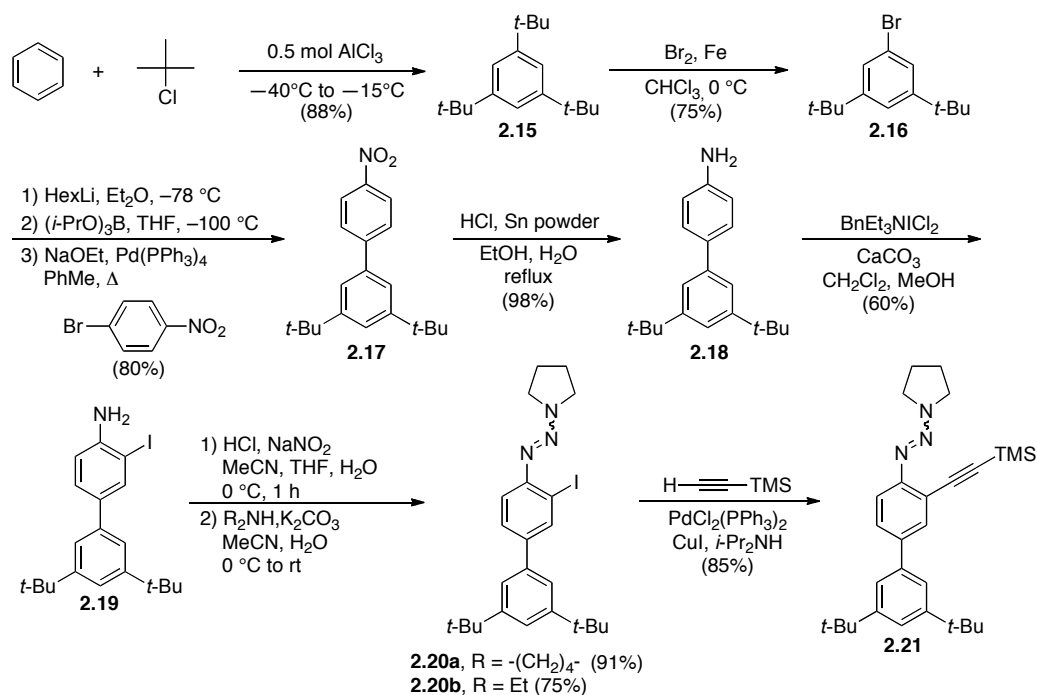
Considering the structure of radialene **2.1**, solubility of the large planar structure in common organic solvents is anticipated to be poor. Haley and coworkers encountered significant solubility problems during their synthesis of 6,6,6-graphyne models, such as **1.70**, which were addressed by appending solubilizing groups.^{10,11} As such, a similar strategy of appending solubilizing “tails” to the aryl triazene unit was designed for **2.1**. The general approach for triazene formation is shown in Scheme 2-3. The parent system is formed from *o*-iodoaniline **2.13a** using a sequence of diazotization, followed by quenching of the diazonium intermediate with either dimethyl- or diethylamine to give aryl triazenes **2.14a–b** in good yields.¹² The same process was used in the formation of **2.14c**, starting from iodoaniline **2.13b**. Iodoaniline **2.13b** was prepared in 87% yield by treatment of *p*-isopropylaniline with benzyltriethylammonium dichloroiodate.¹³



Scheme 2-3. Syntheses of *o*-iodoaryl triazenes **2.14a–c**.

The incorporation of a 3,5-di-*tert*-butylphenyl (DTBP) group was also investigated. DTBP was chosen as this bulky, branched substituent has previously used to

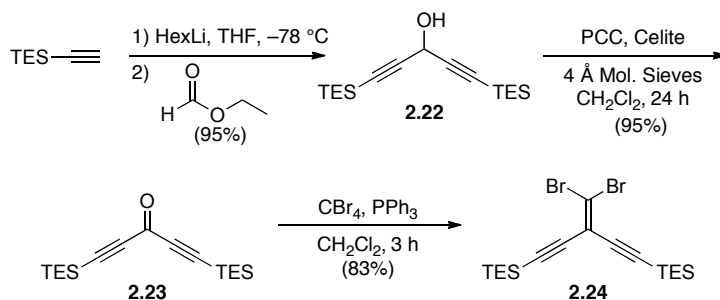
impart both good solubility and synthetic workability in the synthesis of graphdiyne model compounds.¹² The synthesis of this building block began with the synthesis of the DTBP portion of the molecule (Scheme 2-4). The three-fold Friedel Crafts alkylation of benzene with *tert*-butyl chloride yields 1,3,5-tri-*tert*-butylbenzene **2.15** in excellent yield.¹⁴ This was then treated with molecular bromine in the presence of iron to yield 1-bromo-3,5-di-*tert*-butylbenzene **2.16**, again in excellent yield.¹⁵ At this point, conversion to the boronic ester, followed by Suzuki-Miyaura coupling with 1-bromo-4-nitrobenzene, gave biphenyl **2.17**.¹⁶ The nitro group was then reduced to its corresponding aniline **2.18** using tin metal in refluxing hydrochloric acid. Iodination of **2.18** using benzyltriethylammonium dichloroiodate yielded **2.19**, followed by diazotization and trapping with an dialkyl amine to give either **2.20a** or **2.20b**. For **2.20a**, pyrrolidine was chosen as it has been reported to improve the crystallinity of the product, while still maintaining good solubility.^{8a} Iodides **2.20a–b** are designed to serve as both key intermediate building blocks for attachment to a radialene skeleton, as they can also be pushed forward to the alkynyl derivative via a cross-coupling reaction with TMS-acetylene to give, for example, the protected building block **2.21**.



Scheme 2-4. Synthesis of DTBP substituted *o*-iodoaryl triazenes **2.20a–b** and *o*-ethynylaryl triazene **2.21**.

2.2.2 Synthesis of Dibromoolefins

Dibromoolefins are very versatile building blocks. For example, they are highly valued as precursors to acetylenes via the Fritsch-Buttenberg-Wiechell (FBW) rearrangement, and as coupling partners for a variety of different metal catalyzed cross-coupling reactions.^{17,18} As previously mentioned, dibromoolefins are key pieces in the synthesis of the TEE building blocks as well as the final ring closure of the reaction to give radialene products (Scheme 2-1). The synthesis of dibromoolefins has been thoroughly described in the literature, and a typical synthesis is shown in Scheme 2-5.¹⁹



Scheme 2-5. A typical synthesis of a symmetrical dibromoolefin.

Two equivalents of triethylsilyl(TES)-acetylene was treated with *n*-hexyllithium (HexLi) at 0 °C and subsequently reacted with ethyl formate to yield alcohol **2.22** in excellent yield. The alcohol was readily oxidized to ketone **2.23** by treatment with pyridinium chlorochromate (PCC). The somewhat unstable ketone was then converted to dibromoolefin **2.24** using standard Ramirez reaction conditions.^{19a} The entire reaction sequence can be carried out in rapid succession with minimal purification between steps, and it can be readily scaled. Two known dibromoolefins were also prepared in this fashion (Figure 2-5), the TIPS-ethynyl substituted dibromoolefin **2.25** and TMS-ethynyl substituted dibromoolefin **2.26**.^{19c}

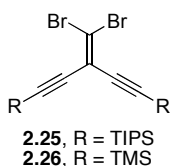
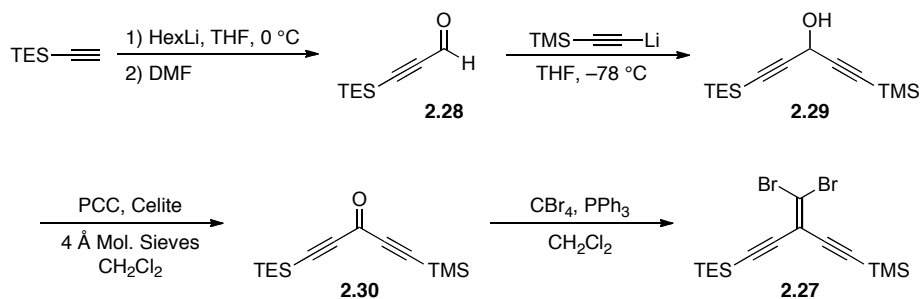


Figure 2-5. Structures of dibromoolefins **2.25** and **2.26**.

A slightly modified procedure was used to form unsymmetrical dibromoolefin **2.27** (Scheme 2-6). In this case, TES-acetylene was lithiated with HexLi and then reacted with dimethylformamide (DMF), to give aldehyde **2.28**. Aldehyde **2.28** was then treated with TMS-C≡C-Li to give the unsymmetrical alcohol **2.29**. Treatment of **2.29** with PCC

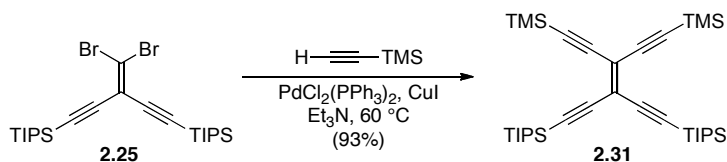
yields ketone **2.30**, followed by Ramirez dibromoolefination to give the unsymmetrical dibromoolefin **2.27**. The unsymmetrical product **2.27** was obtained pure from a co-worker, Dr. Wesley Chalifoux.²⁰



Scheme 2-6. Synthesis of an unsymmetrical dibromoolefin **2.34**.

2.2.3 Synthesis of Tetraethynylethenes (TEEs)

Starting from dibromoolefins **2.24–2.27**, it was possible to synthesize a variety of differently substituted and protected TEEs by a simple two-fold Sonogashira cross-coupling reaction. The procedure was based on that previously reported by Anthony and coworkers, and a typical example has been shown in Scheme 2-7.^{19c}

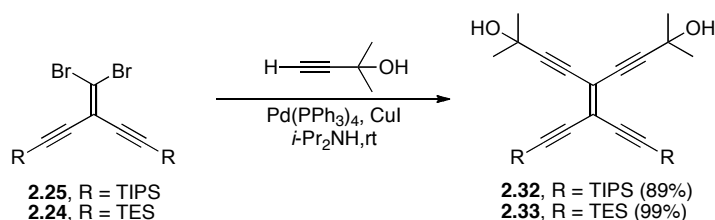


Scheme 2-7. Synthesis of differently protected TEE **2.31**.

Thus, dibromoolefin **2.25** was subjected a Sonogashira cross-coupling reaction, with a trimethylsilyl(TMS)-acetylene in triethylamine at 60 °C. This gave the TIPS/TMS protected TEE **2.31** in excellent yield and purity after recrystallization from

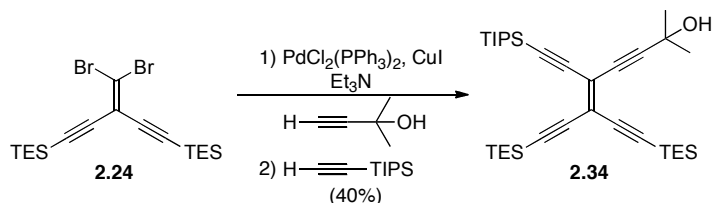
CH₂Cl₂/MeOH. The spectral properties of this compound were identical to those reported.^{19c}

An orthogonally protected TEE was also desirable, as this would allow for the selective deprotection of the alkyne moieties of the TEE by varying the reaction conditions. This cannot be achieved using typical silyl protecting groups, as the conditions required to cleave the TIPS group (TBAF, THF) would also cleave any of the more labile silyl protecting groups such as TMS or TES. To this end, the 2-hydroxypropyl (2-HP) protecting group was chosen toward forming TEE **2.32** and **2.33**. Not only the 2-HP group stable to TBAF, but the standard conditions required to cleave this protecting group (NaOH or KOH, benzene, reflux) will not remove a TIPS protecting group.²¹ An added benefit of this protecting group is that it also imparts polar functional groups to an otherwise apolar molecule, allowing for easier chromatographic purification from the apolar starting materials and byproducts. The synthesis of **2.32** was carried out using an analogous protocol as described for **2.31** (Scheme 2-8). Dibromoolefin **2.25** underwent a Sonogashira cross-coupling reaction with 2-methyl-3-butyn-2-ol at 60 °C to yield TEE **2.32** in good yield after column chromatography. The spectral properties of **2.32** were consistent with that previously reported.⁴ The related TEE **2.33** was prepared in a similar fashion starting from dibromoolefin **2.24**.



Scheme 2-8. Synthesis of orthogonally protected TEEs **2.32–2.33**.

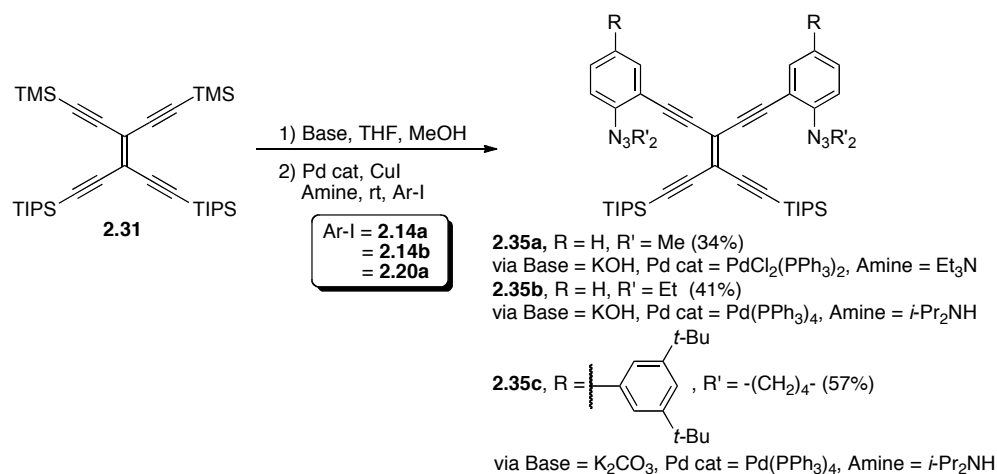
A TEE structure with an unsymmetrical substitution pattern was also desirable, such as TEE **2.34** (Scheme 2-9). This can be achieved the Sonogashira cross-coupling reaction of two different acetylenes to a symmetrically substituted dibromoolefin such as **2.24**. While this approach was expected to give a mixture of products, the 2-HP protected acetylene made it possible to separate the different structures with relative ease due to the polarity differences in each of the possible products.



Scheme 2-9. Synthesis of unsymmetrically substituted TEE **2.34**.

Thus, dibromoolefin **2.24** underwent a Sonogashira cross-coupling reaction with 2-methyl-3-butyn-2-ol at rt. After 2 hours, TIPS-acetylene was added to the reaction, and the mixture was left to stir at rt overnight. After aqueous work up, column chromatography allowed for the isolation of the unsymmetrical TEE **2.34** in 40% yield.

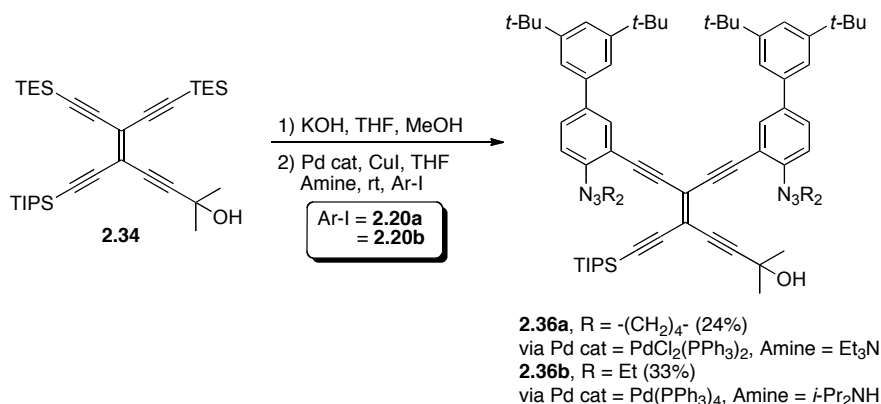
The final TEE targets contained the aryl triazene moiety. The synthesis of this class of TEE was carried via a functionalization of the TEE core, starting from either **2.31** or **2.34**.



Scheme 2-10. Synthesis of aryl triazene containing TEEs **2.35a–c**.

As shown in Scheme 2-10, selective removal of the TMS groups in **2.31** using KOH or K₂CO₃ furnished the terminal acetylene. Since the unprotected TEEs were expected to be unstable, the resulting products were kept in solution after the initial work-up and transferred directly into the flask containing the catalysts and corresponding *o*-iodoaryl triazene (**2.14a–b**, **2.20a**).^{17c} After stirring under argon overnight, the reactions were quenched, and purification by column chromatography yielded TEEs **2.35a–c** in modest, but acceptable, yields.

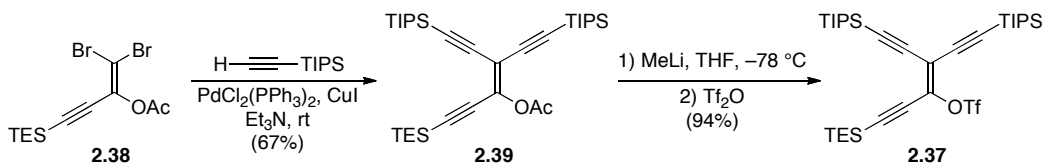
Unsymmetrical TEEs containing the aryl triazene moiety were prepared from TEEs **2.34** (Scheme 2-11). Selective desilylation with KOH furnished the terminal acetylene. The resulting product was kept in solution and, following workup, transferred to a flask containing the catalysts and corresponding *o*-iodoaryl triazene (**2.20a–b**). After stirring under argon overnight, the reactions were quenched via a standard aqueous workup, and purification by column chromatography furnished the desired TEEs **2.36a–b** in rather low yields.



Scheme 2-11. Synthesis of unsymmetrically substituted TEEs **2.36a–b** containing aryl triazenes.

2.2.4 Synthesis of Vinyl Triflates

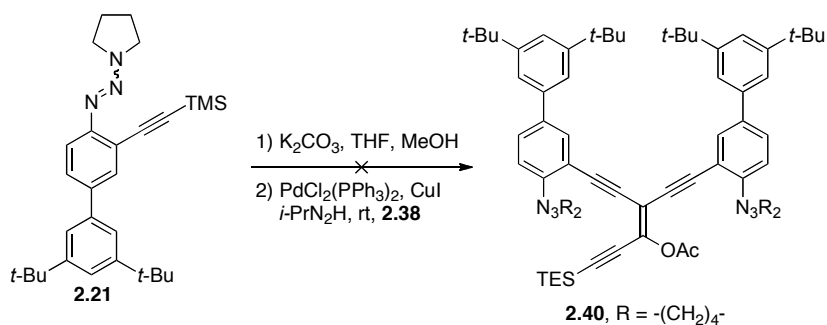
The final key building blocks needed for the assembly of the desired radialene frameworks was the vinyl triflate **2.37**. This was achieved via the known synthesis of the vinyl acetate precursor **2.38**, as previously described by Rankin and Tykwinski.²² Acetate **2.38** was prepared from TES-acetylene over three steps with a good overall yield of 56% (Scheme 2-12). A Sonogashira cross-coupling reaction between **2.38** and TIPS-acetylene yielded **2.39** in a 67% yield, which was converted to vinyl triflate **2.37** in a 94% yield the initial reaction with methyl lithium (MeLi) and quenching Tf_2O .



Scheme 2-12. Synthesis of vinyl acetate **2.39** and vinyl triflate **2.37**.

Several vinyl triflates were also envisioned with more elaborate functionalization (Scheme 2-13). The first attempt to prepare a triflate precursor containing the aryl

triazene moiety followed the standard Sonogashira procedure. Thus, *o*-ethynylaryl triazene **2.21** was desilylated and the resulting product reacted with the dibromo vinylacetate **2.38**. TLC analysis of the reaction mixture showed the formation of numerous products. Upon work-up, it was observed that the reaction had failed to generate the expected cross-coupled product **2.40**. Instead, a bright yellow, highly fluorescent solid was isolated.

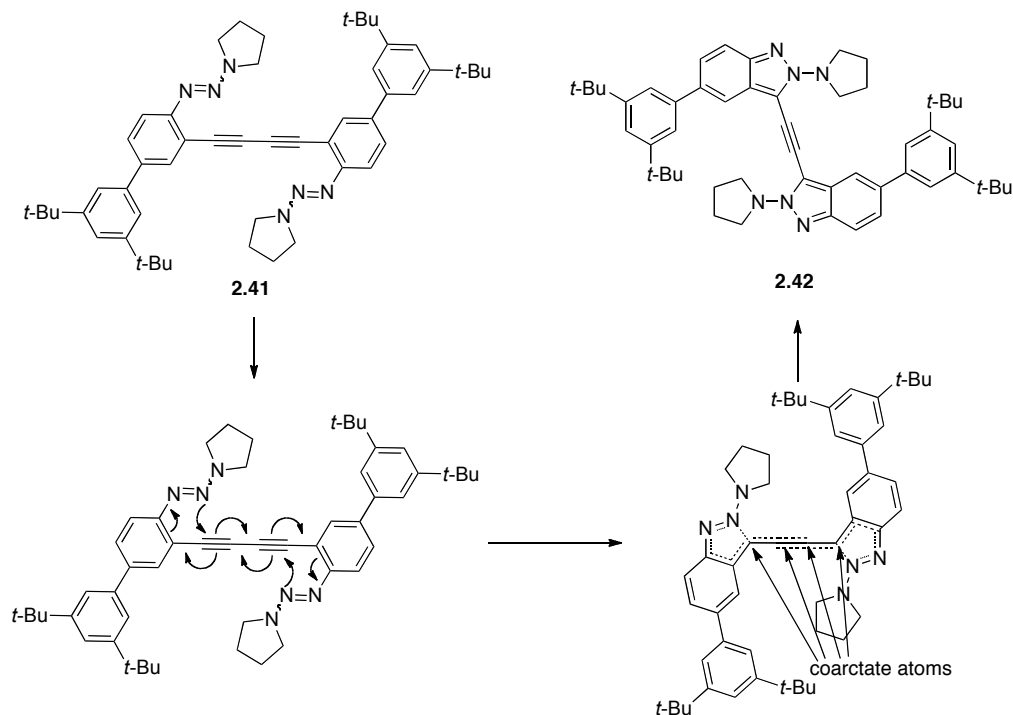


Scheme 2-13. Attempted synthesis of vinyl acetate **2.40**.

It was initially thought that the isolated product resulted from homocoupling of the terminal acetylenes to give diyne **2.41** (Scheme 2-14). A more detailed analysis of the ^{13}C NMR spectroscopic data, however, suggested that the product was the hetrocyclic dimer **2.42**. Thus, while an initial homocoupling reaction did occur, the resulting diyne had undergone an intramolecular cyclization with the triazene moieties on each aryl ring. This unexpected product was likely the result of a coarctate or pseudocoarctate cyclization of the resulting homocoupled side product **2.41**.

Coarctate reactions can be identified by an atom, or linear sequence of atoms, in which two bonds are broken and two bonds are formed in a single step.²³ This coarctate central atom, or linear chain of atoms, undergoing the reaction is only terminated by two loops, for which the electron arrow pushing results in a compressed cycle. The result of this compressed cycle is that the loops terminate to form odd membered rings and

exocyclic carbenes. Although concerted, coarctate reactions are not considered pericyclic due to the involvement of an exocyclic carbene.^{23d}

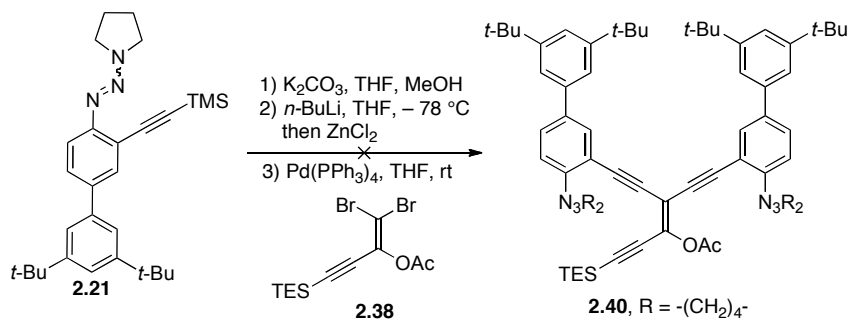


Scheme 2-14. Proposed coarctate cyclization of diyne **2.41** to form dimer **2.42**.

Coarctate cyclizations are known to occur in similar structures containing *ortho*-ethynyl and triazene units.²³ In these cases, high reaction temperatures are typically needed to drive forward the cyclization process. However, lower reaction temperatures of 50 °C, and in some cases rt, are also successful when using a catalytic system similar to that of the standard Sonogashira cross-coupling reaction conditions.^{24a} This prompted an investigation to determine if varying the standard Sonogashira conditions could promote the formation of the desired cross-coupling product while suppressing coarctate reactions.

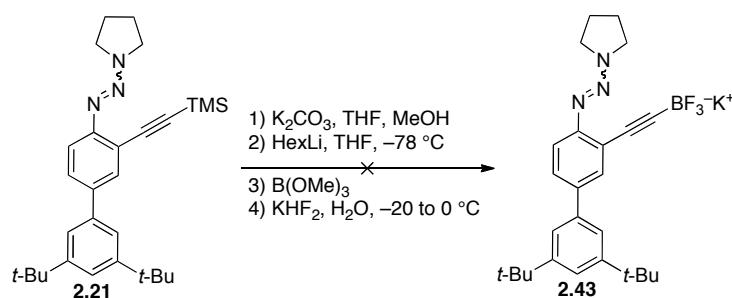
A modification of the Negishi method was thus attempted (Scheme 2-15).²⁵ Following the desilylation of **2.21**, the resulting acetylene solution in THF was cooled to

–78 °C and treated with *n*-BuLi. After stirring for 15 minutes a solution of ZnCl₂ was added dropwise. The solution was stirred at –78 °C for 1 hour, and then transferred to a flask containing a THF solution of catalyst and **2.38**. The reaction was allowed to warm to rt, stirred for 18 hours, and quenched via the addition of NH₄Cl_(aq). Analysis of the mixture of products by ¹H NMR spectroscopy showed only recovered starting material, as well as some products consistent with coarctate reactions.



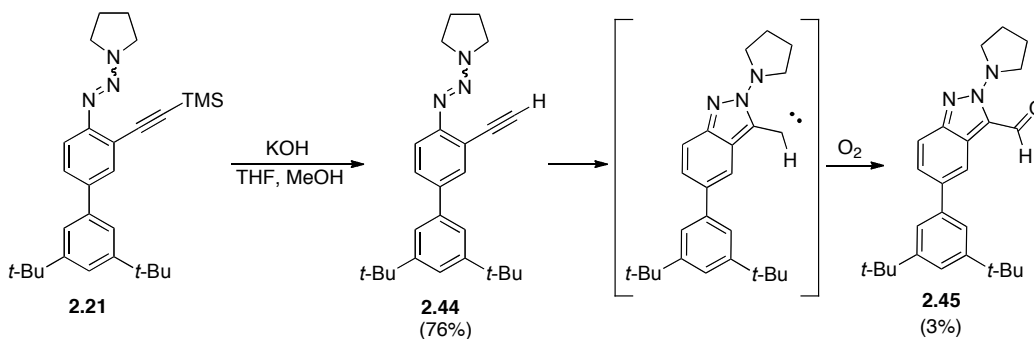
Scheme 2-15. Attempted Negishi cross-coupling reaction of **2.21** and **2.38**.

An attempt was made using a modified Suzuki-Miyaura cross-coupling reaction as described by Molander (Scheme 2-16).²⁶ Following desilylation of **2.21**, the resulting product was treated with HexLi in THF at –78 °C, and B(OMe)₃ was then added after 15 minutes. The solution was allowed to warm to approx. –20 °C and was then quenched via the addition of aqueous KHF₂. Following the workup, ¹H NMR spectroscopy showed no sign of the desired product **2.43**, and only recovered starting material could be isolated. The inability to form the trifluoroborate salt prevented any attempts at the palladium catalyzed cross-coupling reaction.



Scheme 2-16. Attempted synthesis building block **2.43** for a of Suzuki-Miyaura cross-coupling.

It was noted that during an attempt to isolate the deprotected acetylene **2.44** from the reaction of **2.21** with KOH, a small amount of a product consistent with **2.45** was observed. This product is likely the result of a coarctate intermediate reacting with molecular oxygen (Scheme 2-17).^{23b} This suggests that starting material itself might also be unstable and prone to undergo this cyclization, even at room temperature.

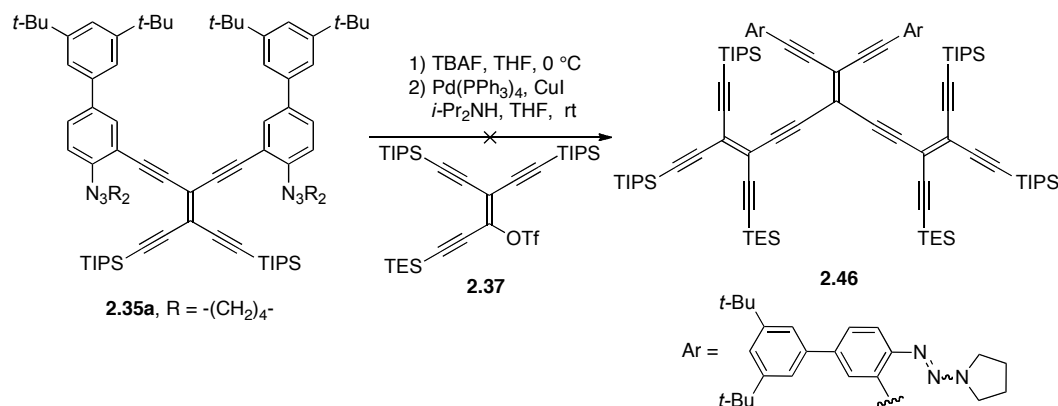


Scheme 2-17. Desilylation of **2.21** and observed coarctate side product **2.45**.

2.2.5 Synthesis of *iso*-Polydiacetylenes (PDAs)

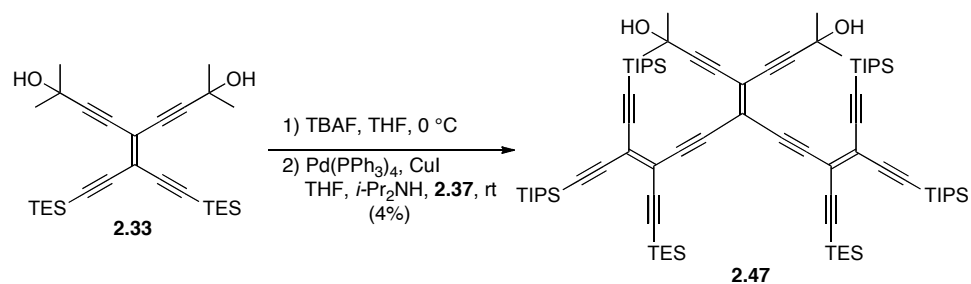
With the observed difficulties plaguing the coupling of *o*-arylethynyl trienes with **2.38**, it was decided to reverse the coupling order (Scheme 2-18). TEE **2.35a** was treated with TBAF to remove the TIPS groups. Following desilylation, the deprotected

intermediate was transferred to a flask containing vinyl triflate **2.37**. Unfortunately, in all attempts, cross-coupled product **2.46** was never observed. Instead, a large amount of baseline material resulted, and a significant amount of vinyl triflate **2.38** was recovered.



Scheme 2-18. Attempted synthesis of *iso*-PDA **2.46**.

The disappointing synthetic results using the ethynyl aryl triazene building blocks forced a rethinking of the synthetic strategy. Thus, the focus turned toward the assembly of the radialenes using the building blocks of Route A as previously described in this chapter. Starting from the 2-HP protected TEE **2.33**, desilylation using TBAF afforded the terminal acetylene, which was transferred to a flask containing an *i*-Pr₂NH solution of vinyl triflate **2.37**, Pd(PPh₃)₄, and CuI (Scheme 2-19). After stirring for 24 hours, the reaction was quenched with aq NH₄Cl, and the product purified via column chromatography. Gratifyingly, the desired product **2.47** was obtained in a low yield of 4%. A significant amount of the vinyl triflate **2.37** was also recovered.



Scheme 2-19. Synthesis of *iso*-PDA **2.47**.

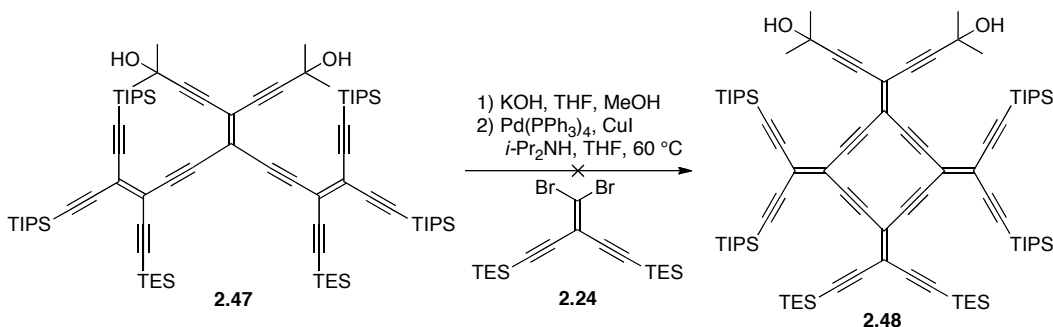
A variety of different cross-coupling reaction conditions were explored (Table 2-1) in an effort to improve and optimize the formation of *iso*-PDA **2.47**. Simple changes such as modifying the catalyst and reaction temperature seemed to have minimal affect on the yield of the reaction, with 10% isolated yield being the highest achieved. It is worth noting that previous attempts toward coupling TEEs with tri-ethynylated vinyl triflates such as **2.37** have also proven challenging, with no discernable trend in product yield versus reaction conditions.⁴

Table 2-1. Conditions used toward optimizing the synthesis of **2.47**.^[a]

Entry	Pd Catalyst / 5 mol %	Phosphine / 15 mol%	Temp. / °C	Time / hours	Yield / %
1	Pd(PPh ₃) ₄	–	rt	24	4
2	Pd(PPh ₃) ₄	–	50	24	0
3	PdCl ₂ (PPh ₃) ₂	<i>Pt</i> Bu ₃	0	24	4
4	PdCl ₂ (PPh ₃) ₂	<i>Pt</i> Bu ₃	rt	48	9
5	PdCl ₂ (PPh ₃) ₂	<i>Pt</i> Bu ₃	50	48	10

[a] Reactions performed in solutions of deoxygenated, dry THF and *i*-Pr₂NH with 10 mol % CuI, sealed under argon with a rubber septum.

Despite the low yields in the synthesis of the *iso*-PDA **2.47**, enough material was obtained so that the synthesis of radialene **2.48** could be attempted (Scheme 2-20). After selective removal of the TES groups of **2.47**, the deprotected oligomer was transferred to a THF/*i*-Pr₂NH solution of dibromoolefin **2.24**, Pd(PPh₃)₄, and CuI. The reaction was heated to 60 °C, stirred for 18 hours, and quenched via the addition of NH₄Cl_(aq). Unfortunately, after work-up, none of the desired radialene **2.48** was observed in the product mixture, by either NMR spectroscopy or mass spectrometry.



Scheme 2-20. Attempted synthesis of [4]ER **2.48**.

2.3 Conclusion

Several useful building blocks have been successfully prepared. These include a variety of dibromoolefins (**2.24–2.26**), TEEs (**2.31–2.36**) and a vinyl triflates (**2.37**). In addition, several differently substituted aryl triazenes (**2.14a–c**, **2.20a–b**, **2.21**) were prepared with the goal of using these pieces to assemble larger oligomers and ultimately radialenes.

Unfortunately, the side reaction involving a coarctate or pseudocoarctate cyclization of the triazene moiety onto the *ortho*-acetylene moiety proved to be surprisingly difficult to circumvent, preventing formation of the desired cross-coupled products. Nevertheless, building blocks such as **2.14a–c**, **2.20a–b**, and **2.21** can be

viewed as valuable and useful synthons in the synthesis of other acetylene rich structures, and these aspects will be discussed in Chapter 3.

In view of the difficulties encountered in the attempted coupling of aryl triazenes to vinyl acetate **2.38**, an alternate approach toward radialene formation was investigated using the 2-HP protected TEE **2.33**. This seemed a promising approach, since TEE **2.33** could undergo successful a Sonogashira cross-coupling reaction with vinyl triflate **2.38**, albeit in low yield. All attempts toward optimization of this reaction, however, led only to minor improvements in yield. The small amount of *iso*-PDA **2.47** that was obtained was used in an attempt to prepare radialene **2.48**, however, the reaction was unsuccessful.

The lack of any observed radialene product, combined with the difficulty in preparation of the required precursor, prevented efforts to move forward with the synthesis. With few alternatives available, this approach was abandoned.

2.4 References

1. Eisler, S.; Tykwinski, R. R. *Angew. Chem. Int. Ed.* **1999**, *38*, 1940–1943.
2. (a) Campbell, K.; Tiemstra, N. M.; Prepas-Strobeck, N. S.; McDonald, R.; Ferguson, M. J.; Tykwinski, R. R. *Synlett* **2004**, 182–186. (b) Campbell, K.; McDonald, R.; Branda, N. R.; Tykwinski, R. R. *Org. Lett.* **2001**, *3*, 1045–1048.
3. (a) Gholami, M.; Melin, F.; McDonald, R.; Ferguson, M.; Echegoyen, L.; Tykwinski, R. R. *Angew. Chem. Int. Ed.* **2007**, *46*, 9081–9085. (b) Gholami, M.; Chaur, M. N.; Wilde, M.; Ferguson, M. J.; McDonald, R.; Echegoyen, L.; Tykwinski, R. R. *Chem. Commun.* **2009**, 3038–3040. (c) Tykwinski, R. R.; Gholami, M.; Eisler, S.; Zhao, Y.; Melin, F.; Echegoyen, L. *Pure Appl. Chem.* **2008**, *80*, 623–639 (d) Gholami, M. Ph. D Thesis, University of Alberta, 2009.
4. Ramsaywack, S. Ph. D Thesis, University of Alberta, 2010.

5. Baughman, R. H.; Eckhardt, H.; Kertesz, M. *J. Phys. Chem.* **1987**, *87*, 6687–6699.
6. (a) Coluci, V. R.; Braga, S. F.; Legoas, S. B.; Galvao, D. S.; Baughman, R. H. *Phys. Rev. B* **2003**, *68*, 035430. (b) Coluci, V. R.; Braga, S. F.; Legoas, S. B.; Galvao, D. S.; Baughman, R. H. *Nanotechnology* **2004**, *15*, S142–S149. Kim, B. G.; Choi, H. J. *Condensed Matter* **2011**, arXiv:1112.2932v1. (d) Malko, D.; Neiss, C.; Vines, F.; Görling, A. *Phys. Rev. Lett.* **2012**, *108*, 086804.
7. Sonogashira, K.; Tohda, Y.; Hagihara, N. *Tetrahedron Lett.* **1975**, 4467–4470.
8. (a) Moore, J. S.; Weinstein, E. J.; Wu, Z. *Tetrahedron Lett.* **1991**, *32*, 2465–2466. (b) Kehoe, J. M.; Kiley, J. H.; English, J. J.; Johnson, C. A.; Petersen, R. C.; Haley, M. M. *Org. Lett.* **2000**, *2*, 969–972.
9. Bholra, B. R.; Bally, T.; Valente, A.; Cyranski, M. K.; Dobrzycki, L.; Spain, S. M.; Rempala, P.; Chin, M. R.; King, B. T. *Angew. Chem. Int. Ed.* **2009**, *48*, 1–5.
10. Kehoe, J. M.; Kiley, J. H.; English, J. J.; Johnson, C. A.; Petersen, R. C.; Haley, M. M. *Org. Lett.* **2000**, *2*, 969–972.
11. Johnson II, C. A.; Lu, Y.; Haley, M. M. *Org. Lett.* **2007**, *9*, 3725–3728.
12. Marsden, J. A.; Haley, M. M. *J. Org. Chem.* **2005**, *70*, 10213–10226.
13. Kosynkin, D. V.; Tour, J. M. *Org. Lett.* **2001**, *3*, 991–992.
14. Ditto, S. R.; Card, R. J.; Davis, P. D.; Neckers, D. C. *J. Org. Chem.* **1979**, *44*, 894–896.
15. Bartlett, P. D.; Roha, M.; Stiles, R. M. *J. Am. Chem. Soc.* **1954**, *76*, 2349–2353.
16. Miyaura, N.; Yamada, K.; Suzuki, A. *Tetrahedron Lett.* **1979**, *20*, 3437–3440.
17. (a) Fritsch, P. *Liebigs Ann. Chem.* **1894**, *279*, 319–323. (b) Buttenberg, W. V. *Liebigs Ann. Chem.* **1894**, *279*, 324–337. (c) Wiechell, H. *Liebigs Ann. Chem.* **1894**, *279*, 337–344. (d) Stang, P. J. *Chem. Rev.* **1978**, *78*, 383–405. (d) Knorr, R. *Chem. Rev.* **2004**, *104*, 3795–3849. (e) Kirmse, W. *Angew. Chem. Int. Ed.* **1997**,

- 36, 1164–1170. (e) Eisler, S.; Chahal, N.; McDonald, R.; Tykwinski, R. R. *Chem. Eur. J.* **2003**, *9*, 2542–2550.
18. Diederich, F.; Stang, P. J. (Eds.). *Metal-Catalyzed Cross-Coupling Reactions*, Wiley-VCH, Weinheim (1998).
19. (a) Ramirez, F.; Desai, N. B. McKelvie, N. *J. Am. Chem. Soc.* **1962**, *84*, 1745–1747. (b) Corey, E. J.; Fuchs, P. L. *Tetrahedron Lett.* **1972**, 3769–3772. (c) Anthony, J.; Boldi, A. M.; Rubin, Y.; Hobi, M.; Gramlich, V.; Knobler, C. B.; Seiler, P.; Diederich, F. *Helv. Chim. Acta* **1997**, *78*, 13–45.
20. Chalifoux, W. A.; PhD Thesis, University of Alberta, 2010.
21. (a) Harris, S. J.; Walton, D. R. M. *Tetrahedron*, **1978**, *34*, 1037–1042. (b) Swindell, C. S.; Fan, W.; Klimko, P. G. *Tetrahedron Lett.* **1994**, *35*, 4959–4962.
22. Rankin, T.; Tykwinski, R. R. *Org. Lett.* **2003**, *5*, 213–216.
23. (a) Herges, R. *Angew. Chem. Int. Ed.* **1994**, *33*, 255–276. (b) Herges, R. *Chem. Inf. Comput. Sci.* **1994**, *34*, 91–102. (c) McClintock, S. P.; Zakharov, L. N.; Herges, R.; Haley, M. M. *Chem. Eur. J.* **2011**, *17*, 6798–6806. (d) Young, B. S.; Herges, R.; Haley, M. M. *Chem. Comm.* **2012**, *48*, 9441–9455.
24. (a) Kimball, D. B.; Herges, R.; Haley, M. M. *J. Am. Chem. Soc.* **2002**, *124*, 1572–1573. (b) Shirtcliff, L. D.; Hayes, A. G.; Haley, M. M.; Köhler, F.; Hess, K.; Herges, R. *J. Am. Chem. Soc.* **2006**, *128*, 9711–9721. (c) Shirtcliff, L. D.; McClintock, S. P.; Haley, M. M. *Chem. Soc. Rev.* **2008**, *37*, 343–364. (d) Kimball, D. B.; Weakley, T. J. R.; Haley, M. M. *J. Org. Chem.* **2002**, *67*, 6395–6405. (e) Shirtcliff, L. D.; Weakley, T. J. R.; Haley, M. M. Köhler, F.; Herges, R. *J. Org. Chem.* **2004**, *69*, 6979–6985.
25. (a) Negishi, E.-I.; Qian, M.; Zeng, F.; Anastasia, L.; Babinski, D. *Org. Lett.* **2003**, *5*, 1597–1600. (b) Negishi, E.-I.; Anastasia, L. *Chem. Rev.* **2003**, *103*, 1979–2017. (c) Morisaki, Y.; Luu, T.; Tykwinski, R. R. *Org. Lett.* **2006**, *8*, 689–

692. (d) Luu, T.; Morisaki, Y.; Cunningham, N.; Tykwinski, R. R. *J. Org. Chem.* **2007**, *72*, 9622–9629. (e) Hoheisel, T. N.; Frauenrath, H. *Org. Lett.* **2008**, *10*, 4525–4528.
26. Molander, G. A.; Katona, B. W.; Machrouhi, F. *J. Org. Chem.* **2002**, *67*, 8416–8423.

Chapter 3 - Model Compounds of 6,6,12-Graphyne Based on Radiaannulenes

3.1 Introduction

To date, the majority of research towards the synthesis of graphyne model compounds has been focused on 6,6,6-graphyne. One of the most common scaffolds employed to investigate this form of graphyne is that of dehydrobenzannulenes. Looking at the larger structure 12,12,12-graphyne, as previously discussed in Chapter 2, one of the simplest model compounds is based on the expanded radialene framework. Intermediate between 6,6,6-graphyne and 12,12,12-graphyne is 6,6,12-graphyne (Figure 3-1). This particular form of graphyne is one of the least studied, both theoretically and experimentally. It contains a ratio of 5:4 $sp:sp^2$ hybridized carbon, consisting of acetylenes, olefins, and aromatic rings.¹ An interesting feature of this particular form of graphyne is that it does not adopt the hexagonal lattice found in graphene or 12,12,12-graphyne, but it is instead arranged with orthorhombic symmetry. A recent theoretical investigation has revealed that, despite the lack of hexagonal symmetry, 6,6,12-graphyne shows two unique Dirac points.² This is significant as the hexagonal symmetry and honeycomb lattice of graphene had been thought to be critical for the formation of Dirac points. Examining the structure of this form of graphyne, one of the core repeat units can be described as a hybrid structure between a dehydrobenzannulene and an expanded radialene, the structure known as a radiaannulene.

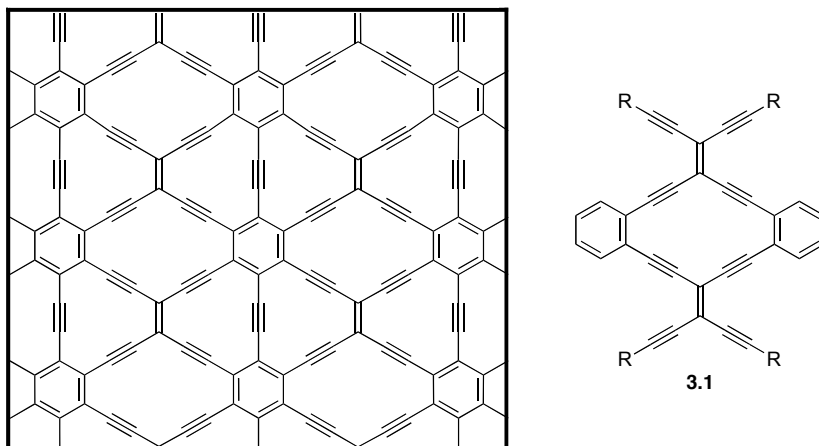


Figure 3-1. Structure of 6,6,12-graphyne and its corresponding model compound **3.1** based on a radiannulene.

A variety of different radiannulenes have been reported in the literature, but there are far fewer examples when compared with dehydrobenzannulenes (Figure 3-2). Diederich and coworkers have prepared donor/acceptor substituted radiannulenes **3.2a** and **3.2b** as small band-gap materials that show evidence of proaromaticity.³ Zhao and coworkers have used the radiannulene framework as a means of extending conjugation in the synthesis of tetrathiafulvalene (TTF) derivatives such as **3.3a** and **3.3b**.⁴ Nielsen and coworkers have also recently incorporated TTF moieties into the radiannulene framework, via the synthesis of **3.4**.⁵ The Tykwinski group has been interested in radiannulenes, with the phenyl substituted radiannulene **3.5a** and fluorenyl substituted **3.5b** prepared by former group member Dr. Mojtaba Gholami.⁶ Most recently, Mazaki and coworkers have prepared the cyano-substituted radiannulene **3.6**, which was determined to be a strong electron accepting molecule.⁷

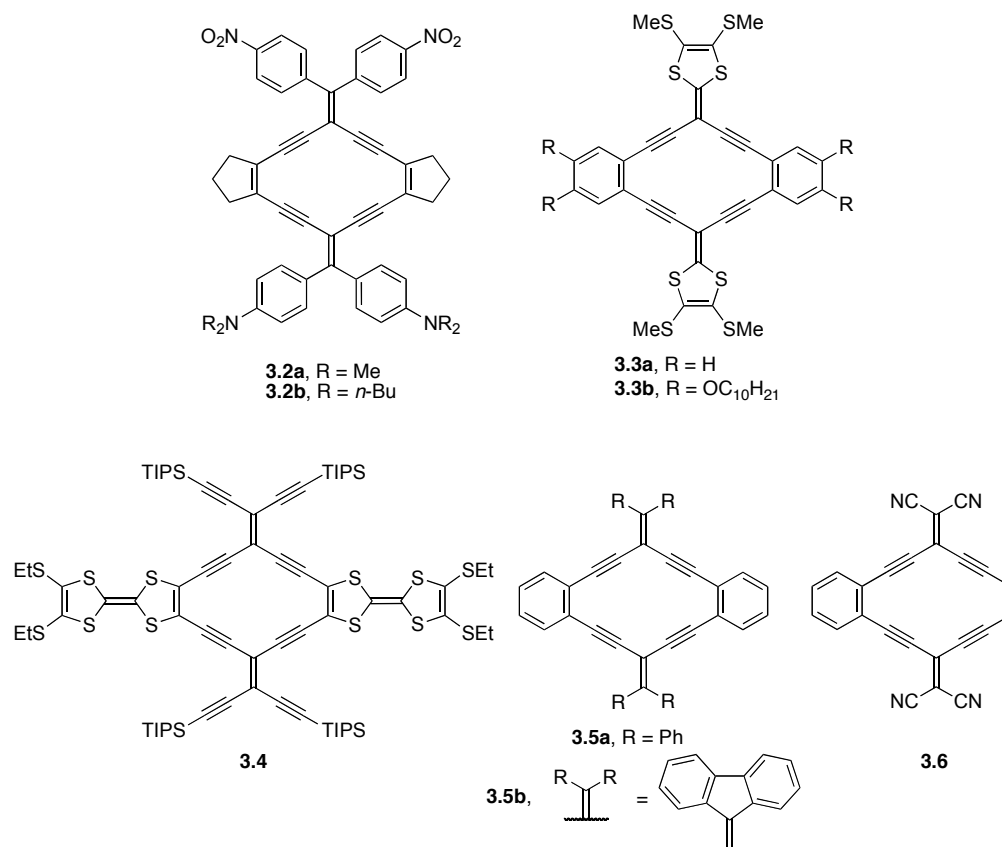


Figure 3-2. Examples of known radiannulenes prepared by Diederich (**3.2a–b**), Zhao (**3.3a–b**), Nielsen (**3.4**), Tykwinski (**3.5a–b**), and Mazki (**3.6**).

Considering radiannulene **3.1** as the primary model compound of 6,6,12-graphyne, it should be possible to prepare a series of oligomers based on this radiannulene core in order to explore the potential properties of 6,6,12-graphyne (Figure 3-3). This hypothesis has been explored, using methodology previously established in the Tykwinski group as well as many of the building blocks described in Chapter 2.

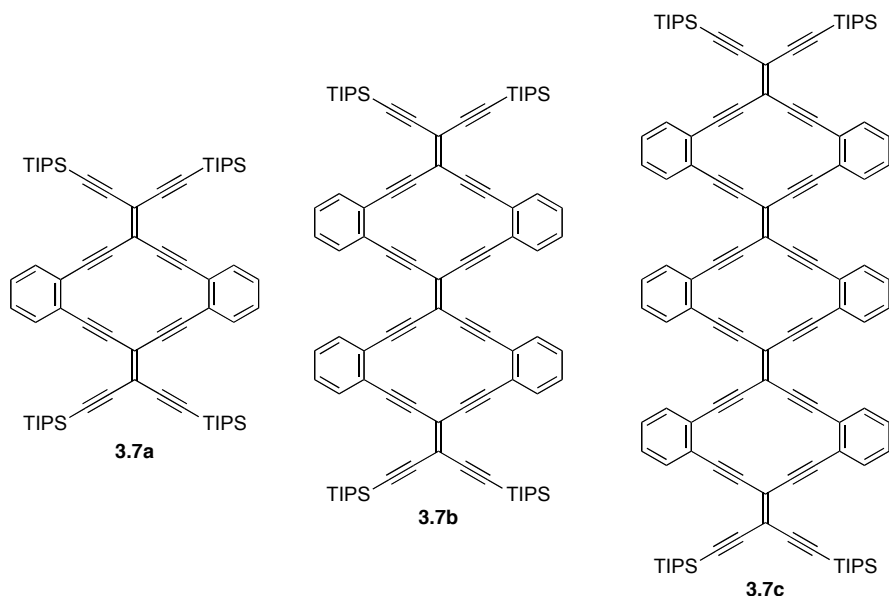
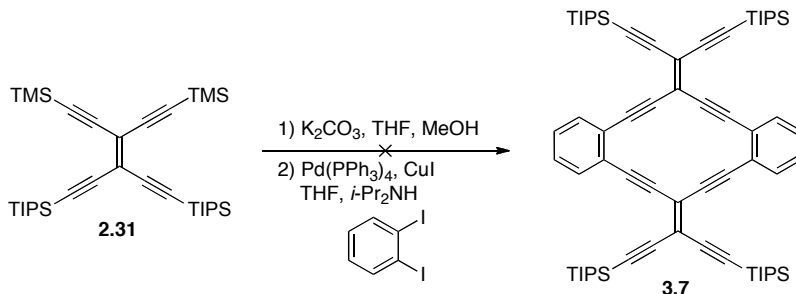


Figure 3-3. Oligomeric series of mono-, di-, and tri-radiaannulenes **3.7a–c** as model compounds of 6,6,12-graphyne.

3.2 Synthesis of Radiaannulenes Using a One-pot Approach

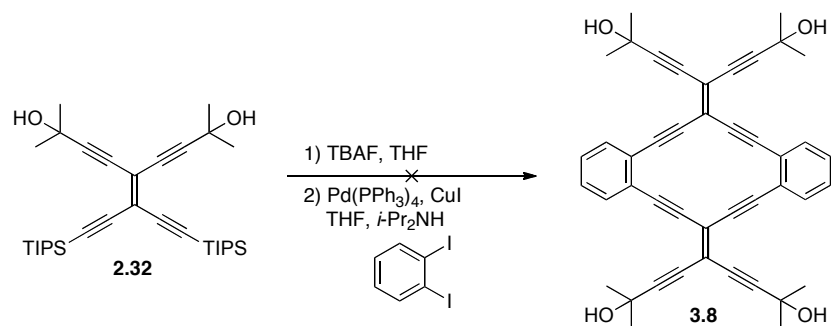
The initial approach taken for **3.7a** was a “one-pot” procedure that had been previously developed within the Tykwinski group for the synthesis of **3.5** (Scheme 3-1).^{6,8} A solution of TEE **2.31** dissolved in THF and MeOH was treated with K_2CO_3 for two hours. After aqueous work-up, the solution of the deprotected TEE was reduced to *ca.* 5 mL and care was taken to keep the product in solution to avoid decomposition. The resulting product was then transferred to a flask charged with 1,2-diiodobenzene dissolved in THF and *i*-Pr₂NH. The solution was purged with argon for several minutes, and Pd(PPh₃)₄ and CuI were added. The flask was sealed with a rubber septum and left to stir at rt for 24 hours. After work-up, isolation of radiaannulene **3.7a** using column chromatography and crystallization was attempted. Although formation of radiaannulene **3.7a** was suggested through analysis by matrix assisted laser desorption/ionization (MALDI) mass spectrometry, which showed a strong signal at m/z (M^+) 1020.6, the

desired product could not be isolated from the many side products formed during the reaction.



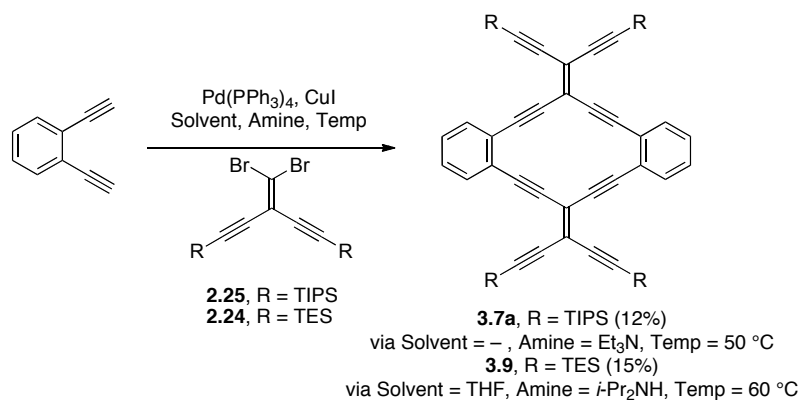
Scheme 3-1. Attempted synthesis of **3.7a** using TEE **2.31** and 1,2-diiodobenzene.

As a result, a second approach was explored, this time utilizing TEE **2.32** (Scheme 3-2). It was anticipated that the polar alcohol groups would facilitate separation of the desired product via column chromatography. A solution of **2.32** in THF was deprotected using TBAF, and the resulting product solution was reduced and transferred to a flask charged with 1,2-diiodobenzene dissolved in THF and $i-Pr_2NH$. The solution was purged with argon prior to the addition of the $Pd(PPh_3)_4$ and CuI. The flask was sealed using a rubber septum and the reaction left to stir for 24 hours. After work-up, purification of **3.8** was attempted using column chromatography. Unfortunately, none of the desired product **3.8** was obtained. Instead, a large amount of 1,2-diiodobenzene was recovered, and a significant amount of base-line material was observed by thin layer chromatography (TLC).



Scheme 3-2. Attempted synthesis of **3.8** using TEE **2.32** and 1,2-diodobenzene.

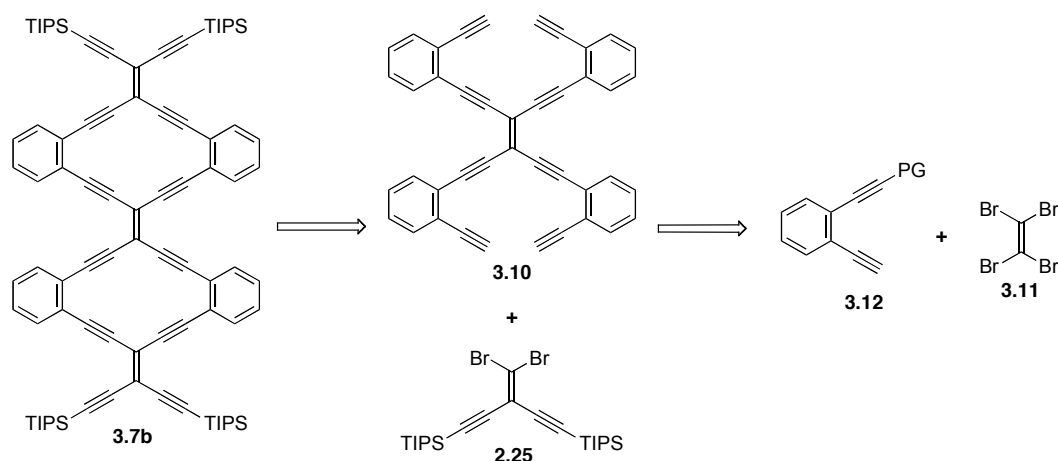
In view of the difficulty encountered when attempting to isolate the radiannulene product using a “one-pot” cross-coupling reaction of a TEE and 1,2-diodobenzene, an alternative cross-coupling reaction was investigated (Scheme 3-3). In this case, 1,2-diethynylbenzene was added to a solution of dibromoolefin **2.25** dissolved in Et₃N.⁹ Following an argon purge, Pd(PPh₃)₄ and CuI were added to the reaction mixture. The flask was then sealed under argon using a rubber septum and heated to 50 °C for 24 hours. After work-up, radiannulene **3.7a** was isolated by column chromatography. The product was further purified by precipitation from CH₂Cl₂/MeOH in order to remove impurities that were difficult to separate via column chromatography. The target radiannulene **3.7a** was isolated as a bright yellow solid in 12% yield. While the yield of this reaction is low, it allows for the synthesis of the target radiannulene to be carried out in a single step from two readily available starting materials. A similar reaction sequence was repeated using dibromoolefin **2.24**, containing TES protected acetylenes, to yield radiannulene **3.9** in 15% yield.



Scheme 3-3. One-pot syntheses of **3.7a** and **3.9** via the cross-coupling reaction of either dibromoolefin **2.25** or **2.24** with 1,2-diethynylbenzene.

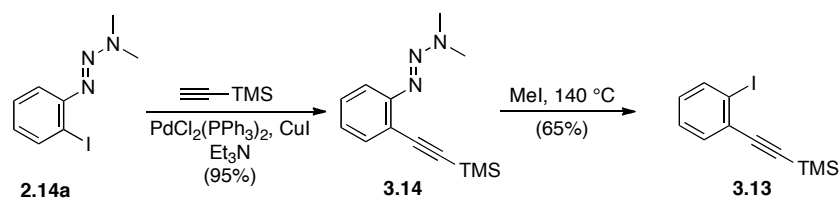
3.3 Synthesis of a Di-Radiaannulene Using a One-pot Approach

With the synthesis of the core radiaannulene complete, attention was then turned to the synthesis of a di-radiaannulene such as **3.7b**. It was supposed that di-radiaannulene **3.7b** could be formed via a one-pot reaction of dibromoolefin **2.25** with precursor **3.10** (Scheme 3-4). It was expected that **3.10** could be formed by the four-fold Sonogashira cross-coupling reaction of tetrabromoethene **3.11** and unsymmetrical diethynylbenzene **3.12**. Tetrabromoethene has been shown previously to be a valuable building block in the synthesis of radiaannulenes and bis-expanded radialenes via a somewhat similar four-fold cross-coupling reaction.⁸



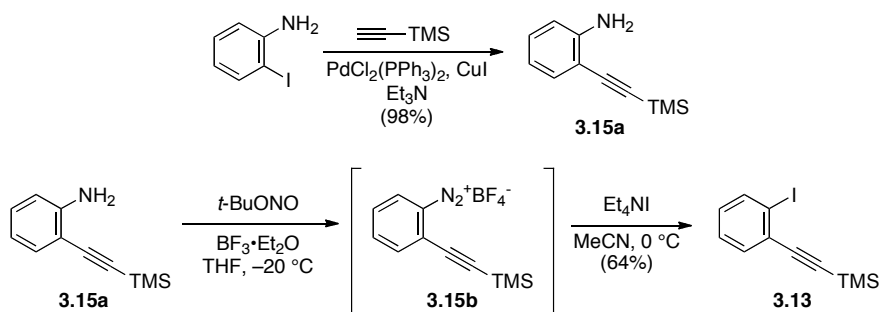
Scheme 3-4. Retrosynthetic route to di-radiaannulene **3.7b** (PG = protecting group).

The key building block required for this synthesis was unsymmetrical diethynylbenzene **3.12**, for which a variety of different synthetic approaches were available. The initial approach was designed to use aryl triazene **2.14a** as a precursor to 2-ethynyl-1-iodobenzene **3.13** (Scheme 3-5). The synthesis began with a Sonogashira cross-coupling reaction of aryl triazene **2.14a** with TMS-acetylene, to yield *o*-ethynylaryl triazene **3.14** in a 95% yield. Triazene **3.14** was then added to an argon purged glass pressure flask. The flask was charged with MeI, sealed, and heated to 140 °C for 18 hours as per Moore's protocol.¹⁰ The reaction was allowed to cool to rt, after which time the remaining MeI was removed under vacuum using a Schlenk line. The crude product was isolated using column chromatography to yield **3.13** in 65% yield.¹¹ Although the reaction gave an acceptable yield on a small scale (1.4 g of product), scaling this reaction to larger amounts of product proved difficult and dangerous, and thus an alternative route to **3.13** was desirable.



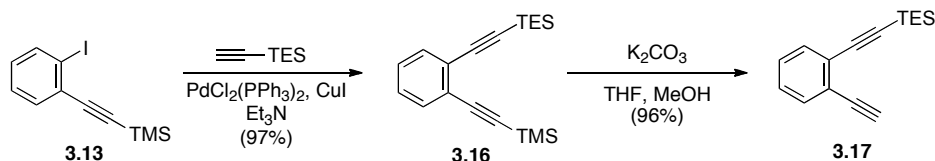
Scheme 3-5. Synthesis of **3.13** via triazene decomposition with MeI.

In an effort to provide a scalable synthesis of **3.13**, a modification of the Sandmeyer reaction was explored (Scheme 3-6).¹² First, a Sonogashira cross-coupling reaction between *o*-iodoaniline and TMS-acetylene under standard conditions afforded **3.15a** in 98% yield.¹³ Aniline **3.15a** was then dissolved in THF, and this mixture was added drop-wise to a solution of $\text{BF}_3 \cdot \text{Et}_2\text{O}$ in THF cooled to -20°C . The reaction was stirred for 20 minutes, after which a solution of *t*-BuONO in THF was slowly added. The reaction was allowed to warm to rt over one hour, after which time the diazonium intermediate **3.15b** precipitated by addition of Et_2O . The supernatant was carefully decanted, and the solid was quickly re-dissolved into MeCN. The diazonium solution was then reacted with Et_4NI for 30 minutes. Following aqueous work-up, column chromatography yielded **3.13** in 64% yield. This reaction proved much more scalable than the previous triazene/MeI decomposition route. It should be noted that although diazonium BF_4^- salts similar to **3.15b** are known to be stable, care should still be taken when handling these materials.^{12d}



Scheme 3-6. Synthesis of **3.13** via a modified Sandmeyer reaction of aniline **3.15a**.

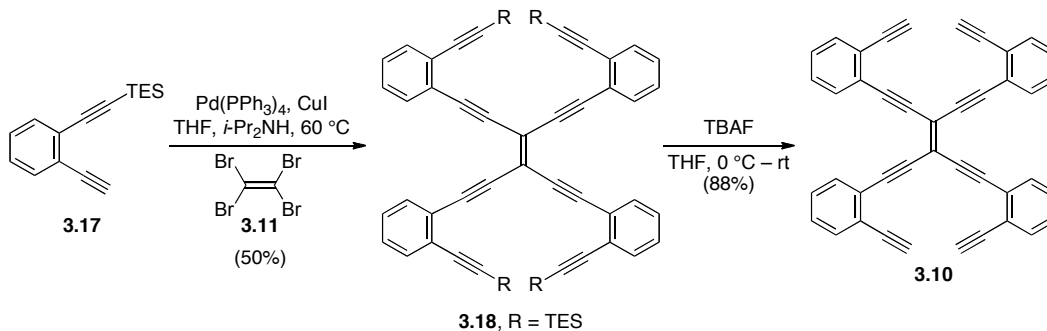
With 2-ethynyl-1-iodobenzene **3.13** in hand, the synthesis of an unsymmetrical diethynylbenzene could be carried out. This was done using the standard Sonogashira cross-coupling protocol (Scheme 3-7). A solution of **3.13** and TES-acetylene in Et₃N was purged with argon, and PdCl₂(PPh₃)₂ and CuI were added. The solution was stirred at rt for 18 hours. Following work-up and column chromatography, **3.16** was obtained in good yield (97%). Selective removal of the TMS group of **3.16** via a reaction with K₂CO₃ in THF and MeOH with gave diethynylbenzene **3.17** in 96% yield.



Scheme 3-7. Synthesis of **3.17** via Sonogashira cross-coupling reaction of **3.13** and TES-acetylene, followed by selective desilylation.

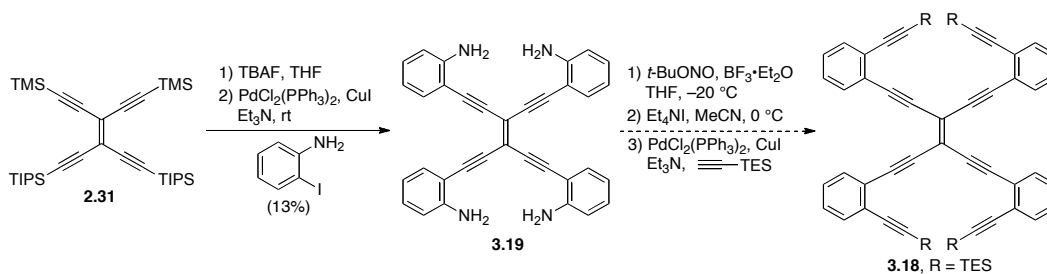
Diethynylbenzene **3.17** was then cross-coupled with tetrabromoethene **3.11** (Scheme 3-8). A solution of **3.17** and **3.11** in THF and *i*-Pr₂NH was stirred in the presence of Pd(PPh₃)₄ and CuI at 60 °C for 24 hours. After aqueous work-up, column chromatography allowed for the isolation of **3.18** in 50% yield. While this is a relatively low yield, it is worth noting that this four-fold cross-coupling reaction has not been optimized. In addition, the yield corresponded to *ca.* 84% yield per acetylene coupling. A four-fold desilylation of **3.18** with TBAF yielded **3.10** as a bright yellow crystalline solid that could be isolated in 88% yield simply by crystallization from hexanes. The sequence of four-fold cross-coupling reaction followed by desilylation could also be carried out in rapid succession without isolation of **3.18**. Passing crude **3.18** through a short silica gel

plug, followed by desilylation and subsequent crystallization of **3.10** allowed for a slightly improved yield of 48% over the two steps. The increased yield was likely due to the lack of product loss during the chromatographic separation of **3.18**.



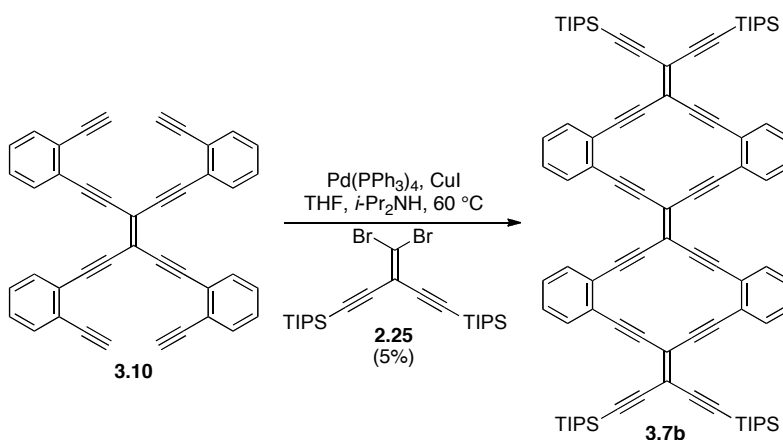
Scheme 3-8. Four-fold Sonogashira cross-coupling reaction of **3.17** with tetrabromoethene and subsequent desilylation to give **3.10**.

An alternate route to **3.18** was also explored in an effort to improve the overall synthetic yield (Scheme 3-9). TEE **2.31** was exhaustively desilylated with TBAF, and the resulting product was transferred to a solution of *o*-iodoaniline, PdCl₂(PPh₃)₂, and CuI in Et₃N. The product was purified using column chromatography to give **3.19** in 13% yield. Due to the poor yield of this reaction, the plan to convert the aniline moieties to iodides, and subsequent Sonogashira cross-coupling reaction with TES-acetylene to give **3.18** was abandoned.



Scheme 3-9. Synthesis of TEE **3.19** and proposed synthesis of **3.18** from TEE **3.19**.

At this point, the synthesis of di-radiaannulene **3.7b** could be attempted and this was carried out via a four-fold Sonogashira reaction between **3.10** and dibromoolefin **2.25**. The reaction was stirred at 60 °C for 18 hours, after which time the reaction was quenched and extracted into Et₂O (Scheme 3-10). The crude product was then purified using column chromatography. Unfortunately, the reaction yielded many side products and the isolation of the desired di-radiaannulene **3.7b** proved challenging. Chromatography using neutral alumina as the stationary phase proved to be the most effective. The isolated product, however, still contained impurities after chromatography. The residue was thus dissolved into a minimal amount of THF, and MeOH was added. The resulting dark red suspension was cooled to -78 °C and filtered, yielding **3.7b** as a deep red solid in 5% yield.

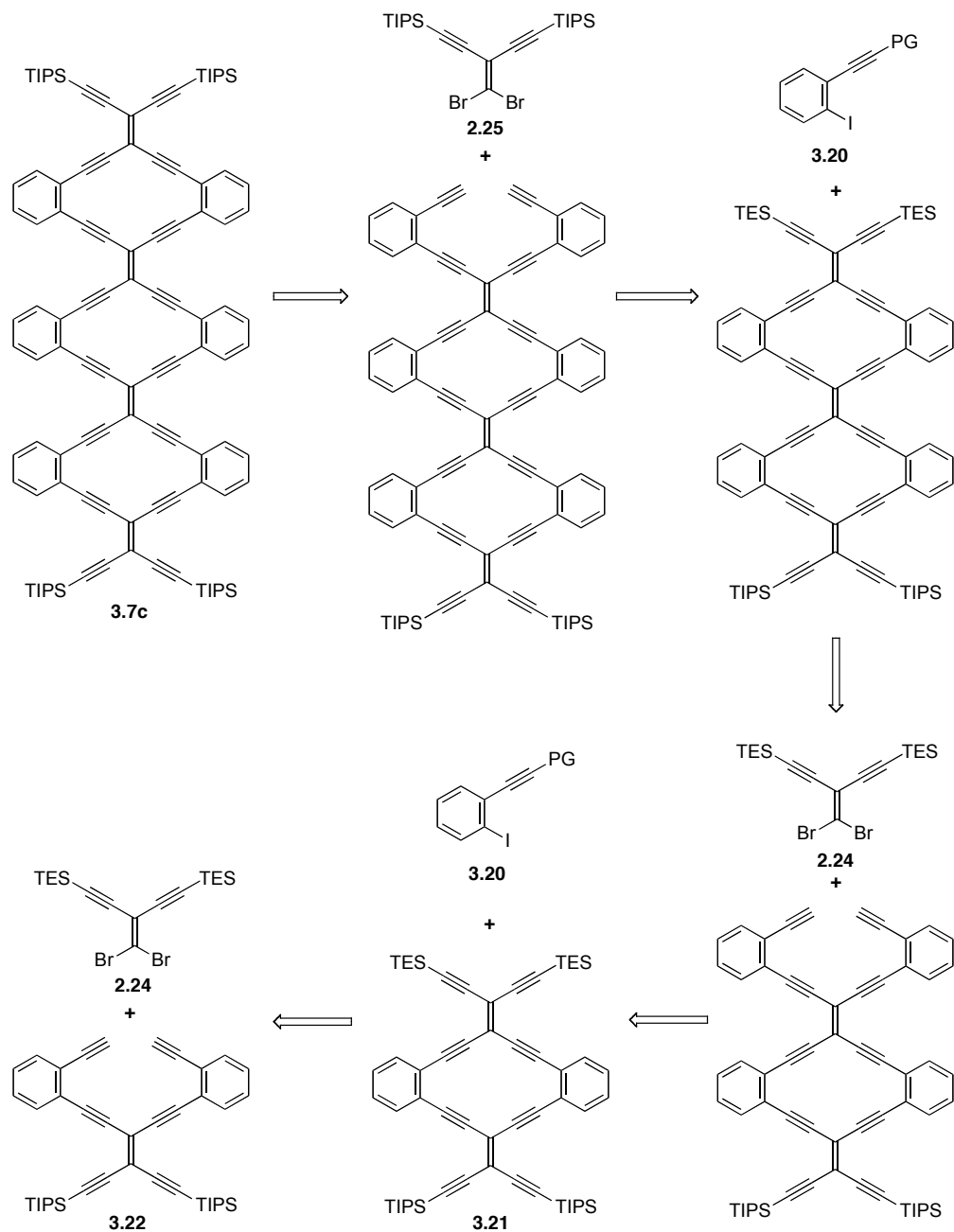


Scheme 3-10. Synthesis of di-radiaannulene **3.7b** via a four-fold Sonogashira cross-coupling reaction.

3.4 Synthesis of Radiaannulenes Using a Stepwise Approach

With the synthesis of di-radiaannulene **3.7b** complete, the focus then moved to the synthesis of the tri-radiaannulene **3.7c** (Scheme 3-11). Unfortunately, the poor yield of di-radiaannulene **3.7b** using the one-pot approach suggested that moving beyond this

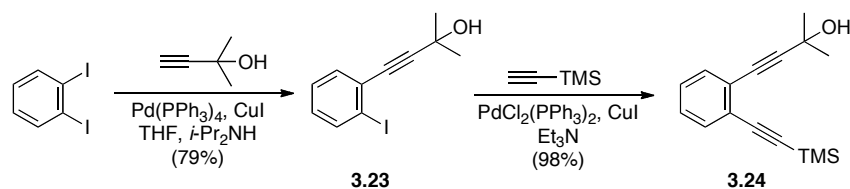
structure toward tri-radiaannulene **3.7c** would be ineffective. As such, it was decided to use a stepwise approach to build up **3.7c** piece by piece. It was envisioned that **3.7c** could be formed by an iterative series of cross-coupling reactions, radiaannulene expansion by cross-coupling with iodo-ethnylbenzene **3.20**, and ring closing onto dibromoolefin **2.25**. This reaction sequence could be repeated in a stepwise fashion starting from unsymmetrical radiaannulene **3.21**. Unsymmetrical radiaannulene **3.21** could then be formed from radiaannulene precursor **3.22** and dibromoolefin **2.24**.



Scheme 3-11. Retrosynthetic route to tri-radiaannulene **3.7c** via unsymmetrical radiaannulene **3.21** (PG = protecting group).

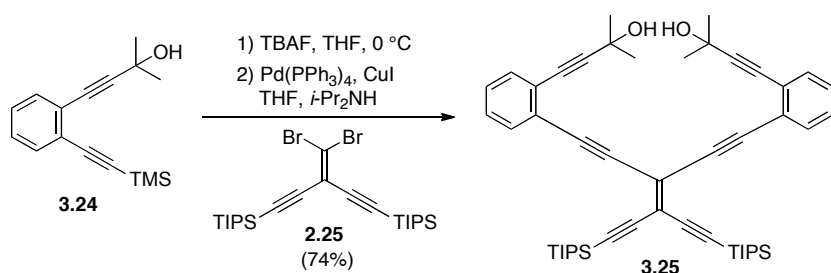
It was supposed that the optimal iodo-ethynylbenzene precursor for this reaction sequence would be **3.23**. This was due to the presence of the 2-HP protecting group, which impart a useful chromatographic handle to aid in the separation of intermediate

structures. The Sonogashira cross-coupling reaction of 2-methyl-3-butyn-2-ol with 1,2-diiodobenzene furnished **3.23** in a 79%, and the product could be readily purified using column chromatography (Scheme 3-12). Compound **3.23** was then reacted with TMS-acetylene again using a Sonogashira reaction to give **3.24** in a 98% yield.¹⁴



Scheme 3-12. Synthesis of iodo-ethynylbenzene **3.23** and diethynylbenzene **3.24**.

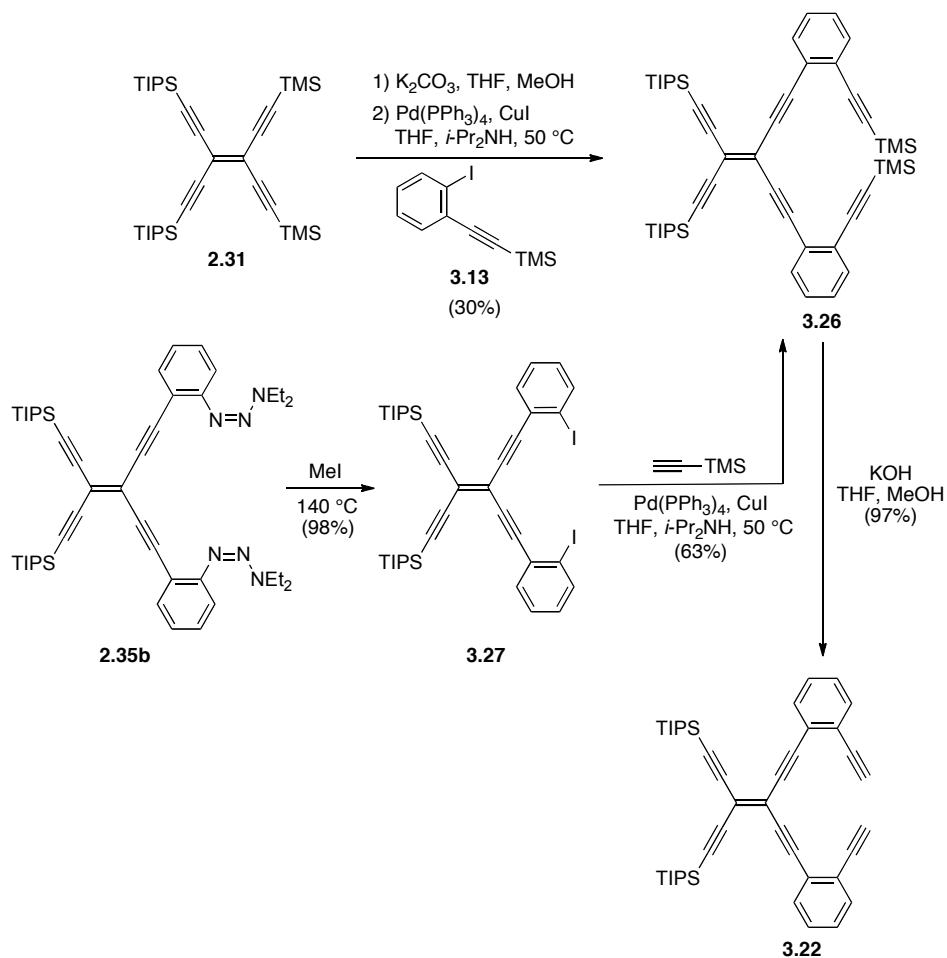
Unsymmetrical diethynylbenzene **3.24** was then subjected to TBAF at 0 °C for 30 min in order to selectively remove the TMS group. Following work up, the desilylated intermediate was used with dibromoolefin **2.25** in a Sonogashira cross-coupling reaction (Scheme 3-13). Purification of the resulting product by column chromatography yielded **3.25** in a 74% yield. It is worth noting that the chromatographic step for this reaction was particularly efficient as the starting material and impurities were significantly less polar than the desired product.



Scheme 3-13. Synthesis of compound **3.25**.

With the TEE **3.25** in hand, the synthesis of unsymmetrical radiannulene **3.21** could be attempted following the removal of the 2-HP groups. The removal of the 2-HP group was achieved via the reaction of **3.25** with KOH (Scheme 3-14),¹⁵ and it was

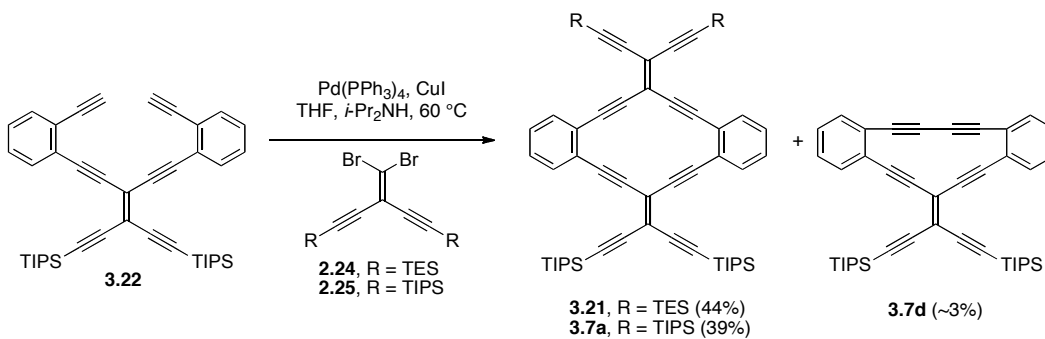
greater than about 100 mg. In either case, Subsequent desilylation of **3.26** using KOH afforded **3.22** in a nearly quantitative yield.



Scheme 3-15. Synthesis of **3.22** via the formation of **3.26** and subsequent selective desilylation.

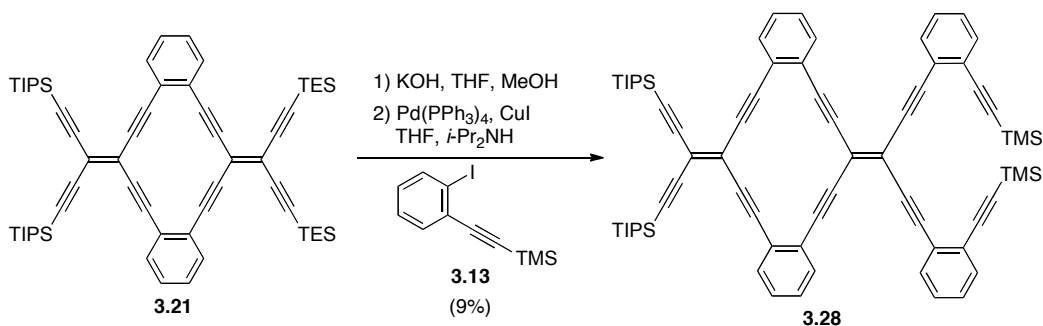
Despite low overall yields in the formation of **3.22**, the synthesis of unsymmetrical radiannulene **3.21** was nevertheless pursued. A solution of **3.22** and dibromoolefin **2.24** was combined with $Pd(PPh_3)_4$ and CuI and heated to $60\text{ }^\circ C$ for 24 h (Scheme 3-16). Following aqueous workup, the product mixture was separated by column chromatography using neutral alumina, which gave a dark yellow solid. The solid was then recrystallized from hexanes to yield the desired radiannulene **3.21** in just a

44% yield. The same procedure was repeated using dibromoolefin **2.25** to yield the symmetrical radiannulene **3.7a** in 39% yield. Radiannulene **3.7d** was occasionally isolated in low yields during the synthesis of **3.7a**, the result of an intramolecular homocoupling reaction of **3.22**.



Scheme 3-16. Synthesis of unsymmetrical radiannulene **3.21**, symmetrical radiannulene **3.7a**, and radiannulene **3.7d**.

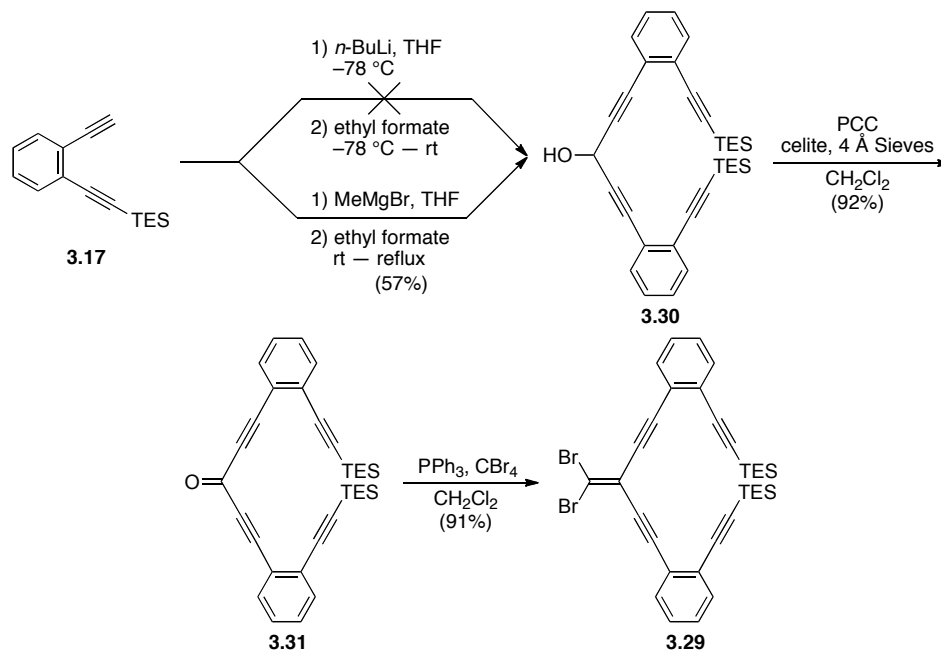
With unsymmetrical radiannulene **3.21** in hand, the synthesis of larger radiannulenes was attempted. A solution of **3.21** in THF and MeOH was stirred with KOH to remove the TES groups (Scheme 3-17). After 2 h the reaction was quenched and the product was transferred to a solution of **3.13** dissolved in THF and *i*-Pr₂NH. After purging with argon for 15 min, Pd(PPh₃)₄ and CuI were added and the reaction was stirred at rt for 24 h. Unfortunately, the reaction yielded a large mixture of products, and the desired compound **3.28** was isolated in only 9% yield by column chromatography.



Scheme 3-17. Synthesis of radiannulene **3.28** from unsymmetrical radiannulene **3.21**.

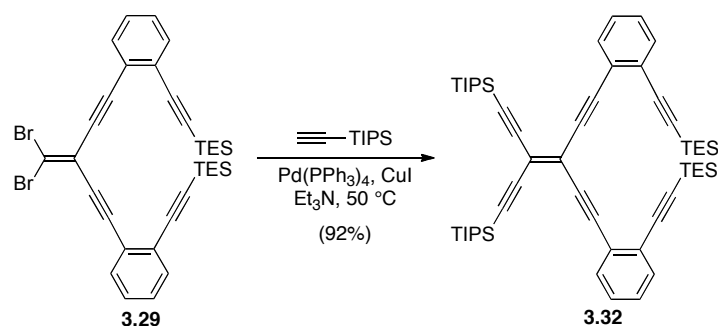
As a result of the poor yield **3.28**, there was insufficient material to continue with the reaction sequence toward di-radiannulene **3.7b**. The observed difficulty in the coupling of the deprotected analog of radiannulene **3.21** with iodo-ethynylbenzene **3.13** was disappointing, especially considering the improved yield achieved for formation of the radialene **3.21**. In light of this challenge a new building block was designed that contained the diethynylbenzene framework already attached to a dibromoolefin, namely **3.29** (Scheme 3-18). The synthesis of **3.29** began by lithiation of **3.17** and subsequent addition to ethyl formate. Initial reactions used *n*-BuLi to generate the acetylide nucleophile, but these attempts failed to generate the desired product **3.30**. Fortunately, switching to a Grignard reagent as the nucleophile proved successful. Thus, compound **3.17** was reacted with MeMgBr for 30 min, after which ethyl formate was added to the solution. After refluxing for 1 h, the reaction was cooled and quenched via the addition of aq NH₄Cl. The crude product could be easily purified using column chromatography to yield alcohol **3.30** in 56% yield. Alcohol **3.30** was then oxidized to ketone **3.31** in a 92% yield using PCC. The resulting ketone **3.31** was then converted to dibromoolefin **3.29** using PPh₃ and CBr₄ and the product isolated in 91% following purification via passing the reaction mixture through a plug of silica gel. The formation of **3.29** proved to be an extremely effective process. Despite the low yield of the nucleophilic addition step, **3.29**

was formed in a 48% yield over three steps, with minimal purification needed over the course of the synthesis.



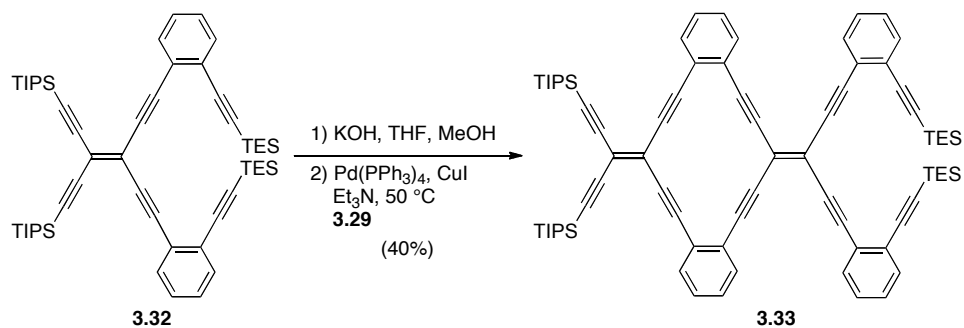
Scheme 3-18. The synthesis of **3.29** starting from diethynylbenzene **3.17**.

A portion of **3.29** was then converted to **3.32**, via reaction with TIPS-acetylene under Sonogashira cross-coupling reaction conditions (Scheme 3-19). The remaining portion of **3.29** was set aside to be used as the key component in an iterative radiannulene expansion process.



Scheme 3-19. Synthesis of precursor **3.32** from **3.29** via a Sonogashira cross-coupling reaction.

To begin the formation of the longer oligo-radiaannulenes, the TES groups of compound **3.32** removed using KOH in THF and MeOH (Scheme 3-20). The reaction was monitored using TLC and quenched after 6 h. The selective desilylation appeared to progress slowly based on TLC analysis, with the initial formation of two new products. Over time, these two spots faded to leave a single product spot (Figure 3-4). Presumably this is due to the formation of both the mono desilylated product, followed by conversion to bis-desilylated product. An appreciable amount of baseline material was also observed on the TLC plate, suggesting possible decomposition. Once the conversion to the bis-desilylated product was complete, the reaction was quenched via the addition of aq NH_4Cl . The resulting product was kept in a solution of THF, and transferred to a solution of **3.29** in Et_3N . $\text{Pd(PPh}_3)_4$ and CuI were added and the reaction was then heated to $50\text{ }^\circ\text{C}$ for 16 h. Following a standard aqueous work-up, the crude product was purified using column chromatography on silica gel to yield **3.33** as a bright orange solid in a 40% yield.



Scheme 3-20. Synthesis of radiannulene **3.33** via the selective desilylation of **3.32** and subsequent Sonogashira cross-coupling reaction with **3.29**.

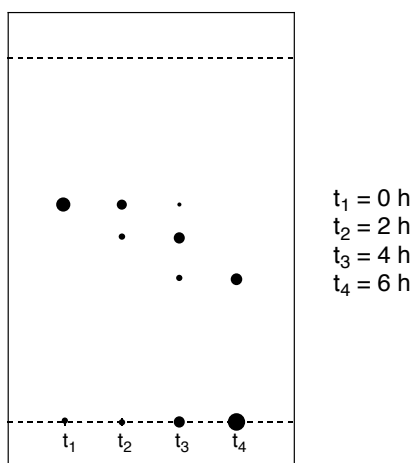
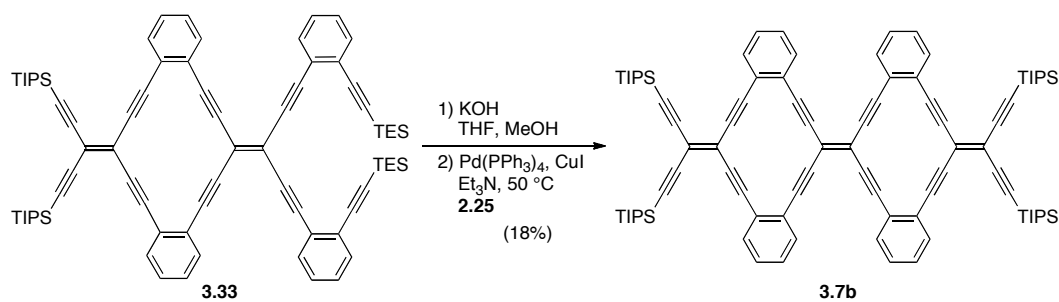


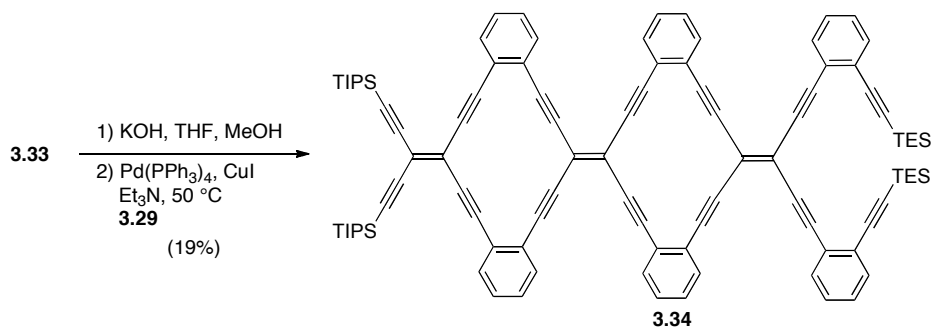
Figure 3-4. TLC analysis for the selective desilylation of **3.32** (silica gel, 4:1 Hex/ CH_2Cl_2).

A portion of **3.33** was then used for the synthesis of di-radiaannulene **3.7b** (Scheme 3-21). The TES groups of compound **3.33** were removed using KOH in THF and MeOH. The resulting product was kept in a solution of THF, and transferred to a solution of dibromoolefin **2.25** in Et_3N . $\text{Pd(PPh}_3)_4$ and CuI were added, and the reaction was heated to $50\text{ }^\circ\text{C}$ for 18 h. Following a standard aqueous workup, the crude product was purified by column chromatography on neutral alumina to yield **3.7b** in 18% yield as a deep red solid.



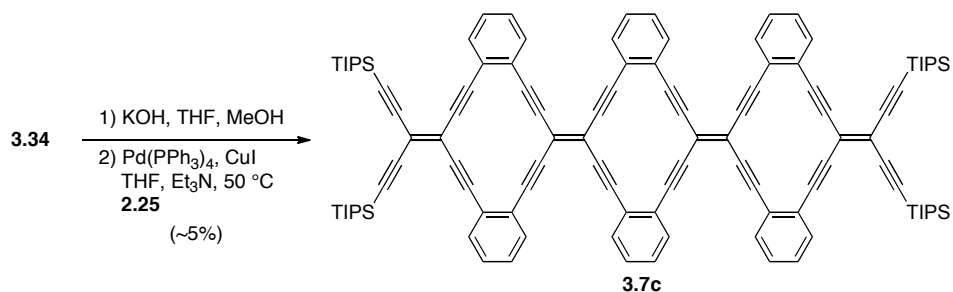
Scheme 3-21. Synthesis of di-radiaannulene **3.7b** via the selective desilylation of **3.33** and subsequent Sonogashira cross-coupling reaction with dibromoolefin **2.25**.

The remaining portion of compound **3.33** was then carried forward toward the tri-radiaannulene **3.7c**. The TES groups of compound **3.33** were removed using KOH in THF and MeOH (Scheme 3-22). The resulting product was kept in a solution of THF and transferred to a solution of dibromoolefin **3.29** in Et₃N. Pd(PPh₃)₄ and CuI were added, and the reaction was heated to 50 °C for 16 h. Following a standard aqueous workup, the product could be precipitated from THF by the addition of MeOH, but the resulting bright red suspension would pass through the filter during filtration attempts, regardless of the quality of the glass frit or filter. As a result, the product was purified by column chromatography on alumina to yield **3.34** in 19% yield as a fine, bright red solid.



Scheme 3-22. Synthesis of **3.34** via the selective desilylation of **3.33** and subsequent Sonogashira cross-coupling reaction with **3.29**.

The synthesis of tri-radiaannulene **3.7c** followed a similar path as that just described for **3.7b**. The TES groups of compound **3.34** were removed using KOH in THF and MeOH (Scheme 3-23). The resulting product was kept in a solution of THF and transferred to a solution of dibromoolefin **2.25** in Et₃N. Pd(PPh₃)₄ and CuI were added, and the reaction was heated to 50 °C for 16 h. Following aqueous workup, purification of the crude product by column chromatography was attempted. Unfortunately, the reaction yielded a significant number of side products, and traditional column chromatography proved ineffective to separate the target molecule. Isolation of the product containing fractions after column chromatography gave partial purification of the product **3.7c**, which was isolated as a deep red/brown solid. Preparative TLC gave further purification, and the product **3.7c** was then isolated as a bright red/pink solid in *ca.* 5% yield. Unfortunately, upon addition of CDCl₃ for NMR spectroscopic analysis, the product decomposed from a bright fluorescent orange solution to a dark brown solution. TLC analysis of the product from CDCl₃ showed only baseline material. A trace amount of the purified product, however, was recovered from the preparative TLC plate. High-resolution MALDI mass spectrometry confirmed to presence of **3.19** in the purified product (Figure 3-5). The only other signal present in the spectrum matched that of [M + Na]⁺. To date, the surprising instability of **3.7c** to CDCl₃ remains unexplained.



Scheme 3-23. Synthesis of tri-radiaannulene **3.7c** via the selective desilylation of **3.34** and subsequent Sonogashira cross-coupling reaction with **2.25**.

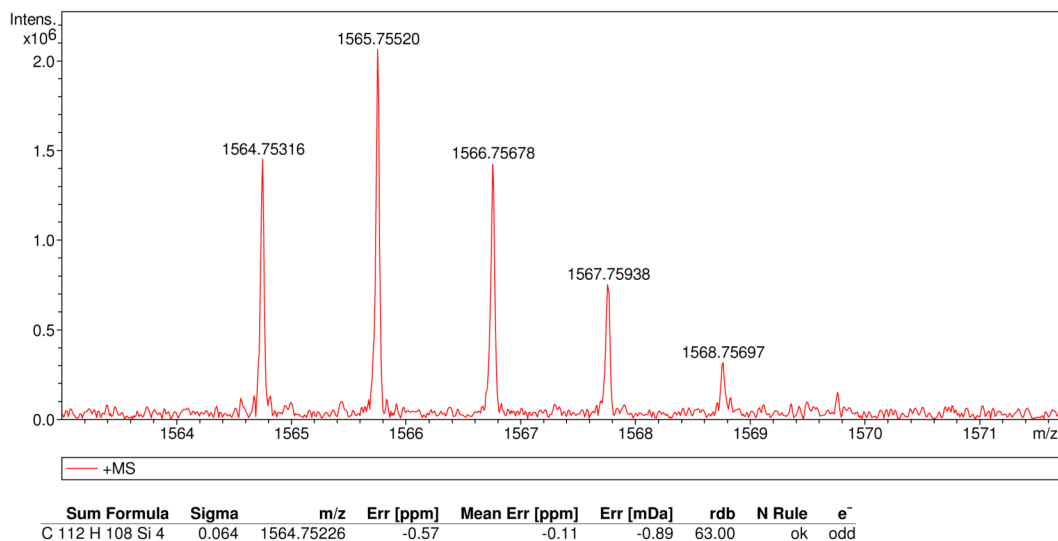


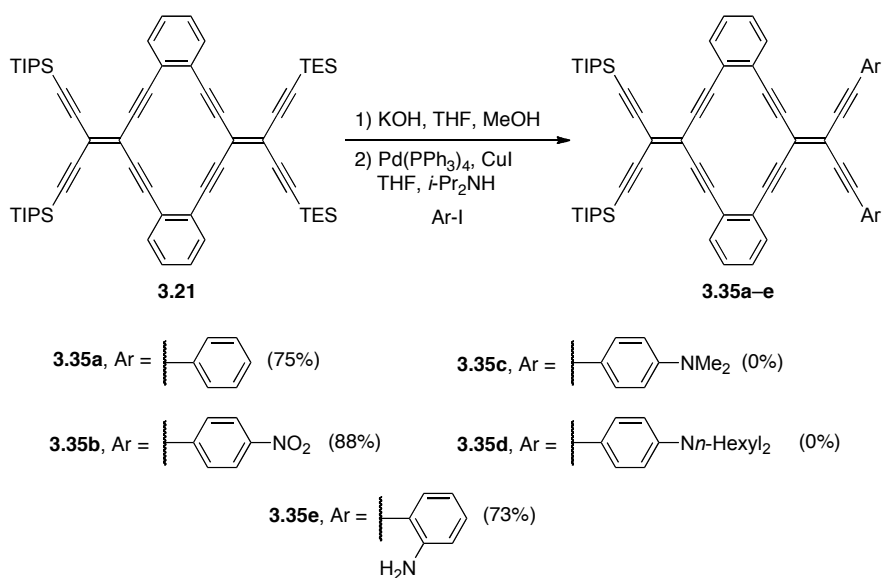
Figure 3-5. High-resolution MALDI mass spectrum of **3.7c** (M^+) recovered from preparative TLC.

3.5 Synthesis of substituted radiannulenes

In spite of the low yield obtained from the attempted formation of **3.28** from radiannulene **3.21** and iodo-ethynylbenzene **3.13** (Scheme 3-17), it was desirable to explore cross-coupling reactions with other iodoarenes. As such, the derivatization of **3.21** with several different substrates was used to determine the scope of this protocol, and to build a small library of substituted radiannulenes that might serve as interesting molecules for semiconductor applications. Electron donating and withdrawing substrates were chosen as a means of tuning the HOMO and LUMO energy levels of the radiannulenes, properties which are important when preparing devices such as solar cells.

Selective desilylation of **3.21** with KOH in THF and MeOH (1:1) was complete after 1 h (Scheme 3-24). The reaction was quenched via the addition of aq NH_4Cl , and the solution of the resulting product was then transferred to a flask containing an aryl-iodide in a solution of THF and $i\text{-Pr}_2\text{NH}$. $\text{Pd}(\text{PPh}_3)_4$ and CuI were added, and the reaction

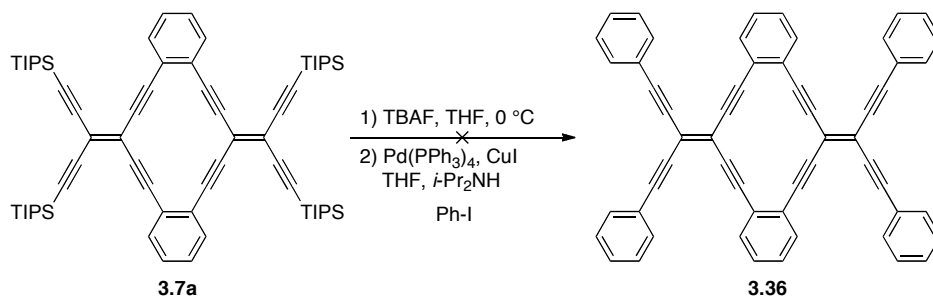
was left to stir until starting material was no longer observed by TLC analysis. Aqueous work-up, followed by purification via column chromatography yielded the products **3.35a–b** and **3.35e**, while products **3.33c–d** could not be isolated. The formation of the phenyl derivative **3.35a** proceeded smoothly in 1 h to yield the product 75% as a bright orange solid. The nitro-benzene substituted compound **3.33b** was also formed cleanly and isolated in 88% yield as a bright orange solid. The aniline substituted derivative **3.35e** was isolated in 73% yield as a dark orange semi-solid. Unfortunately, the formation of aryl amine substituted products **3.33c** and **3.33d** was not successful. In both cases, the reaction produced many products with similar R_f values, and reaction times were considerably longer when compared to the formation of **3.33a** and **3.33b**.



Scheme 3-24. Synthesis of radiannulenes **3.33a–e** via Sonogashira cross-coupling reaction with aryl-iodides.

The potential of symmetrical radiannulene **3.7a** to serve as a building block to substituted radiannulenes was also explored. Compound **3.7** was dissolved into THF and cooled to 0 °C (Scheme 3-25). TBAF was added and the reaction solution quickly turned

from bright yellow to black. TLC analysis suggested that the precursor had been completely converted to baseline material. Nevertheless, the reaction was quenched via the addition of aq NH_4Cl , and the resulting product solution was transferred to a Et_3N solution of iodobenzene. $\text{Pd}(\text{PPh}_3)_4$ and CuI were added, and the reaction was left to stir at rt for 4 h. The reaction was quenched via the addition of $\text{NH}_4\text{Cl}_{(\text{aq})}$, and the resulting product was passed through a short plug of silica gel. The resulting yellow/orange solid appeared to be a mixture of compounds, and the desired product **3.36** could not be isolated pure.



Scheme 3-25. Attempted synthesis of radialene **3.36**.

3.6 Physical properties of radiaannulenes

One consideration that must be taken into account when preparing planar π -systems is their resulting solubility. All mono-radiaannulenes (**3.7a**, **3.9**, **3.35a** and **3.35b**) exhibit good solubility ($\sim 10\text{--}15\text{ mg/mL}$) in most common organic solvents, such as Et_2O , CH_2Cl_2 , CHCl_3 , THF, toluene, and hexanes. The solubility of the larger structures (**3.7b**, **3.33**, and **3.34**) in these same solvents, however, begins to diminish with increasing oligomer length. Di-radiaannulene **3.7b** and its precursor **3.33** both show good solubility in Et_2O , CH_2Cl_2 , CHCl_3 , THF, and toluene ($\sim 10\text{--}15\text{ mg/mL}$), while solubility in hexanes

is somewhat diminished. While data for tri-radiaannulene **3.7c** is limited due to lack of material, **3.7c** appears to have good solubility in CH₂Cl₂ and THF.

All of the radiannulenes and their precursor compounds are isolated as stable oils or solids, with the notable exception of **3.7c**, which appears to rapidly decompose when dissolved into CDCl₃. The mono-radiaannulenes (**3.7a**, **3.9**, **3.21**, and **3.35a–b**) show good thermal stability, with decomposition temperatures near or above 200 °C. Differential scanning calorimetry (DSC) analysis (Table 3-1) of mono-radiaannulenes (**3.7a**, **3.9**, **3.21**, and **3.35a–b**) show exothermic events in the range of 195–266 °C, consistent with decomposition. Di-radiaannulene **3.7b** shows the highest thermal stability, with an exothermic transition at 285 °C.

Table 3-1. Thermal properties of mono-radiaannulenes.

Compound	M.p. ^[a] / °C	DSC (peak onset) ^[b] / °C	DSC (peak) ^[b] / °C
3.7a	304–305	254	266
3.9	225–230	232	236
3.21	215	231	234
3.33a	195–200	190	195
3.33b	224–225	221	228
3.7b	— ^[c]	280	285

[a] Uncorrected melting point. [b] Temperature measured under nitrogen.

[c] Insufficient material for analysis.

The electronic absorption spectra of radiannulenes **3.7a–c**, as well as their corresponding precursor compounds **3.32–3.34** have been acquired from THF solutions at room temperature. These results are summarized in Table 3-2, Figure 3-6, and Figure 3-7.

A common feature in the spectra is the strong, high-energy absorption at *ca.* 286 nm. The absorption at *ca.* 286 nm is notably missing from **3.32**, suggesting this transition is likely due to the radiannulene framework. In addition, each compound features two lower energy absorptions that significantly red shift and broaden as the conjugation length of the molecule increases. For example, the formation of the macrocycle core of **3.7a** from **3.32** results in a bathochromic shift in λ_{max} of 60 nm. The magnitude of this effect is diminished, however, as the size of the radiannulene increases: the bathochromic shift in λ_{max} for di-radiannulene **3.7b** from **3.33** is 34 nm, and for tri-radiannulene **3.7c** from **3.34** this shift is now only 6 nm. The decreasing bathochromic shift in λ_{max} vs conjugation length suggests that at the stage of the tri-radiannulene **3.7c**, the effective conjugation length for this series of graphyne model compounds has nearly been reached (Figure 3-8). The HOMO-LUMO gap for the radiannulene series ($E_{\text{g}}^{\text{opt}}$),¹⁶ calculated from the lowest energy λ_{max} , decreases from the monomer **3.7a** (2.76 eV) to dimer **3.7b** (2.46 eV) to trimer **3.7c** (2.38 eV). It is worth noting the HOMO-LUMO gap for radiannulene **3.7a** is significantly lower than that of dehydrobenzannulene **1.64** ($E_{\text{g}}^{\text{opt}} = 4.20$ eV), a model of 6,6,6-graphyne.¹⁷ As well, tri-radiannulene **3.7c** ($E_{\text{g}}^{\text{opt}} = 2.38$ eV) possesses a similar, albeit slightly lower, HOMO-LUMO gap when compared with the tri-dehydrobenzannulene (**1.98**, $E_{\text{g}}^{\text{opt}} = 2.43$ eV).¹⁷

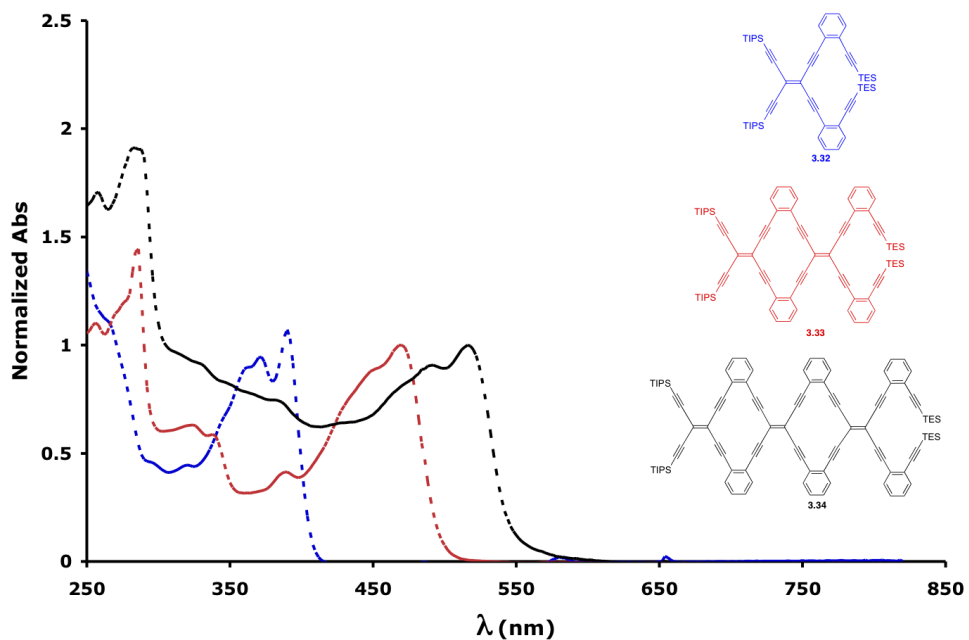


Figure 3-6. UV-vis spectra of compounds **3.32–3.34** as measured in THF. (Spectra normalized by assigning absorption at $\lambda_{\text{max}} = 1$)

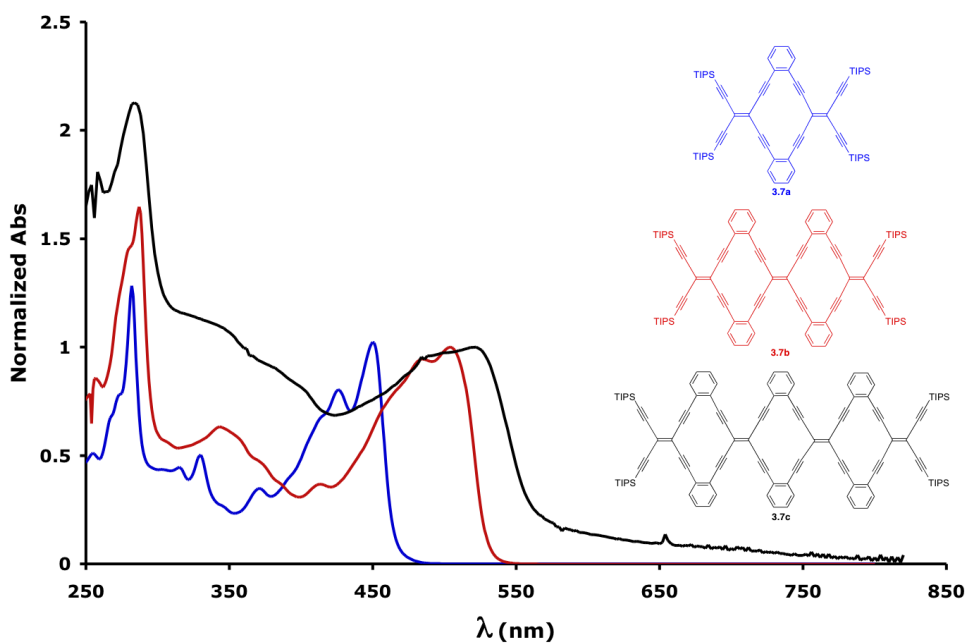


Figure 3-7. UV-vis spectra of compounds **3.7a–c** as measured in THF. (Spectra normalized by assigning absorption at $\lambda_{\text{max}} = 1$)

Table 3-2. UV-vis spectral data for compounds **3.7a–c** and **3.30–3.32** in THF.

Compound	λ_{\max} / nm ($\epsilon = \text{L mol}^{-1} \text{ cm}^{-1}$)			$E_g^{\text{opt [a]}}$ / eV
3.32 ^[b]	390	372	238	3.18
3.7a	450 (65 900)	426 (51 800)	282 (82 700)	2.76
3.33	470 (59 300)	450 (52 300)	286 (87 100)	2.64
3.7b ^[b]	504	485	287	2.46
3.34 ^[b]	516	494	288	2.40
3.7c ^[b]	522	490	284	2.38

[a] Calculated from the lowest energy λ_{\max} . [b] ϵ value not determined.

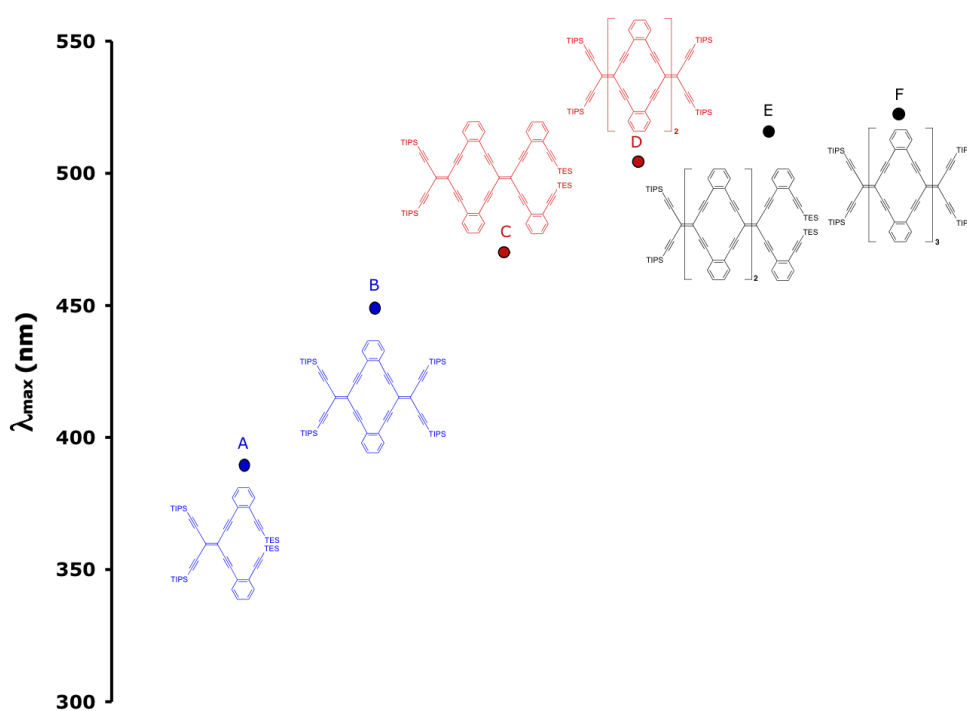


Figure 3-8. Scheme showing increase in λ_{\max} versus structure for compounds a) **3.32**, b) **3.7a**, c) **3.33**, d) **3.7b**, e) **3.34**, and f) **3.7c**, as measured in THF.

The optical properties of unsymmetrically substituted radiannulenes **3.21** and **3.35a–b** have also been investigated using UV-vis spectroscopy (in THF) and the results are summarized in Table 3-3 and Figure 3-9. The λ_{max} values for both radiannulene **3.35a** and **3.35b** are red shifted relative to the parent radiannulene **3.21** (17 nm and 21 nm, respectively). The lowest energy λ_{max} of radiannulene **3.35b** (471 nm) is slightly red-shifted (4 nm) relative to **3.35a**, as a result of adding the strong electron withdrawing nitrophenyl substituents. The λ_{max} values for both radiannulenes **3.35a** and **3.35b** are red-shifted relative to the phenyl-substituted radiannulene **3.5a** (54 nm and 58 nm, respectively) due to the increased conjugation resulting from the ethynyl spacers in **3.35a** and **3.35b**.⁶

Table 3-3. UV-vis spectral data for compounds **3.21**, **3.35a**, and **3.35b** in THF.

Compound	$\lambda_{\text{max}} / \text{nm} (\epsilon = \text{L mol}^{-1} \text{ cm}^{-1})$			$E_{\text{g}}^{\text{opt [a]}} / \text{eV}$
3.21	450 (63 200)	329 (28 900)	282 (82 700)	2.76
3.35a	467 (52 400)	338 (29 500)	285 (86 600)	2.66
3.35b	471 (56 900)	344 (54 400)	286 (74 600)	2.63

[a] Calculated from the lowest energy λ_{max} .

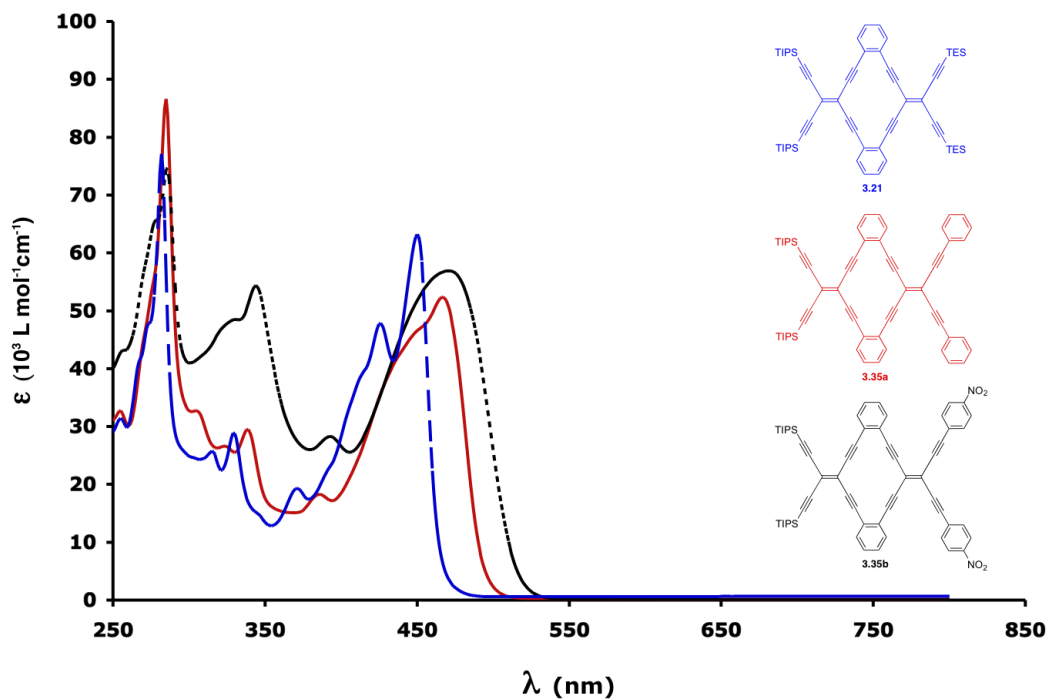


Figure 3-9. UV-vis spectra of compounds **3.21**, **3.35a**, and **3.35b** as measured in THF.

Electrochemical analysis of selected radiannulenes has been carried out in order to gain additional insight into their electronic properties. The results of this study are summarized in Table 3-4 and Figure 3-10. Cyclic voltammetry (CV) studies reveal each of the measured compounds shows an irreversible oxidation, and a least two quasi-reversible reductions. The smallest radiannulene **3.7a** shows an irreversible oxidation event at 1.14 V, as well as what appears to be a two-electron reduction at -1.50 V. Osteryoung square wave voltammetry (OSWV) of radiannulene **3.7a** shows the first reduction is broader than both the oxidation and second reduction waves, with an integration approximately double that of the other waves, further supporting a two electron reduction (Figure 3-11).¹⁸

Table 3-4. Electrochemical properties of compounds **3.7a**, **3.7b**, **3.33–3.34**, and **3.35a–b** in CH₂Cl₂ (vs Fc/Fc⁺ couple).^[a]

Cmpd	$E_{\text{red1}} / \text{V}$	$E_{\text{red2}} / \text{V}$	$E_{\text{red3}} / \text{V}$	$E_{\text{ox}} / \text{V}^{[b]}$	$E_{\text{g}}^{\text{electro}} / \text{eV}$	$E_{\text{g}}^{\text{opt} [d]} / \text{eV}$
3.7a	-1.50 ^[c]	-1.85	–	1.14	2.65	2.76
3.7b	-1.33	-1.57	2.00 ^[b]	1.00	2.33	2.46
3.33	-1.60	-1.80	–	1.16	2.76	2.64
3.34	-1.46	-1.63	-2.04 ^[b]	0.98	2.46	2.40
3.35a	-1.46	-1.56	-1.82 ^[b]	1.01	2.47	2.66
3.35b	-1.36	-1.54	-2.03 ^[b]	1.16	2.51	2.63

[a] Cyclic voltammetry was performed in CH₂Cl₂ solutions containing 0.1 M *n*-Bu₄NPF₆ as supporting electrolyte at a scan rate of 150 mV/s. The working electrode was a platinum disc, the counter electrode was a platinum wire, and the reference electrode was a non-aqueous Ag/AgCl [10 mM] in MeCN. The potential values (E) were calculated using the following equation (except where otherwise noted): $E = (E_{\text{pc}} + E_{\text{pa}})/2$, where E_{pc} and E_{pa} correspond to the cathodic and anodic peak potentials, respectively. Potentials are referenced to the ferrocene/ferrocenium (Fc/Fc⁺) couple used as an internal standard. All potentials represent a one-electron reduction or oxidation event (except where otherwise noted). $E_{\text{g}}^{\text{electro}}$ determined from the separation between the first oxidation and first reduction potentials. [b] Potentials were estimated as $E^{\circ} = (E_{\text{peak}} + E_{\text{onset}})/2$. [c] Two-electron reduction. [d] Calculated from the lowest energy λ_{max} .

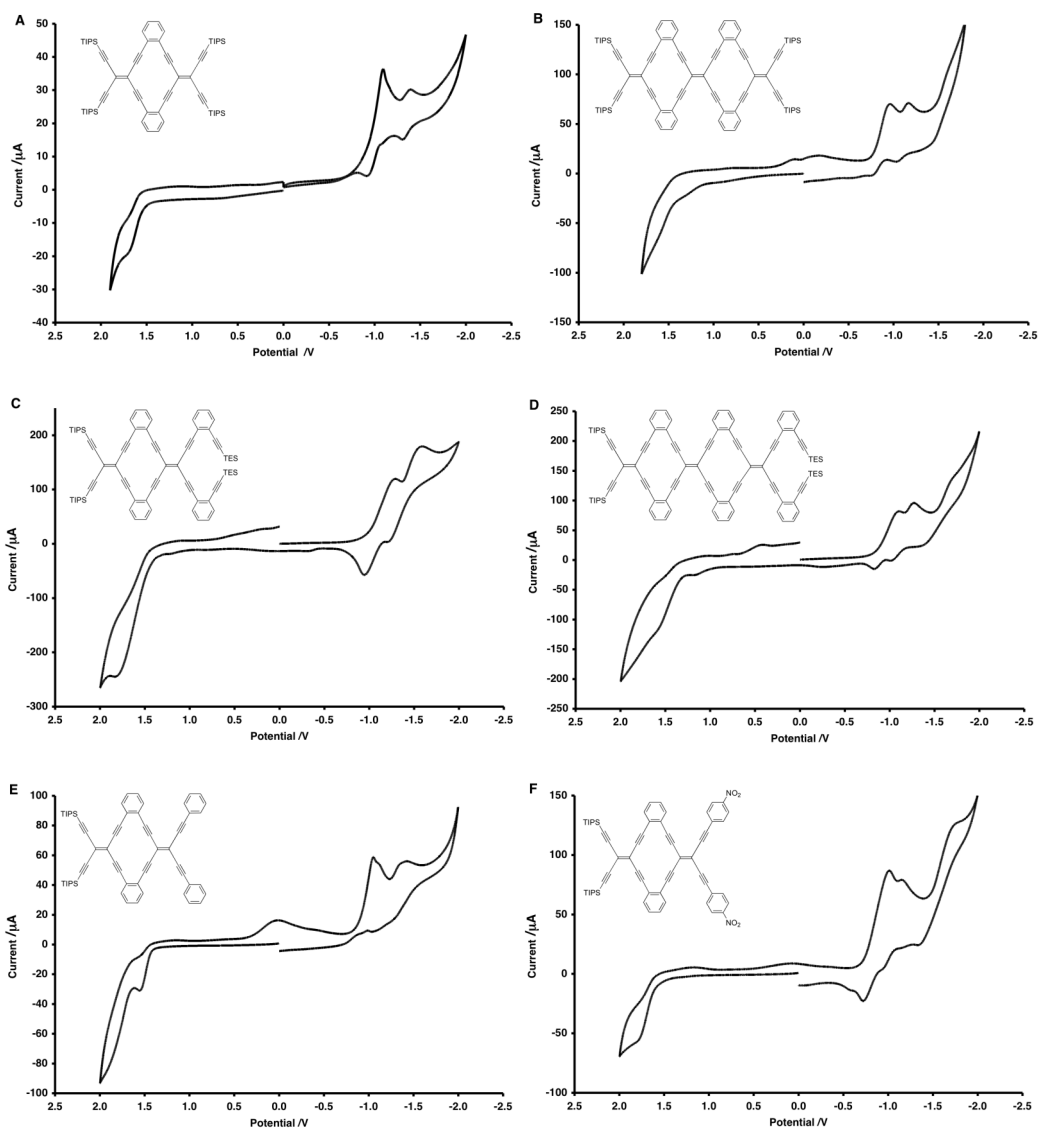


Figure 3-10. CV plots for compounds (a) **3.7a**, (b) **3.7b**, (c) **3.33**, (d) **3.34**, (e) **3.35a**, and (f) **3.35b** as measured in CH_2Cl_2 (vs Ag/AgCl).

Di-radiaannulene **3.7b** shows an irreversible oxidation step at 1.00 V, two reversible reductions, and a quasi-reversible third reduction, the first of which occurs at -1.33 V. It is apparent from the electrochemical data that extending the conjugation from the mono-radiaannulene **3.7a** to the di-radiaannulene **3.7b** results in approximately equal cathodic shift in the oxidation potential (0.14 V) and anodic shift in the first reduction

potential (0.17 V). Thus, the resulting decrease in HOMO-LUMO gap, by moving from the monomer **3.7a** ($E_g^{\text{electro}} = 2.65 \text{ eV}$, $E_g^{\text{opt}} = 2.76 \text{ eV}$) to dimer **3.7b** ($E_g^{\text{electro}} = 2.33 \text{ eV}$, $E_g^{\text{opt}} = 2.46 \text{ eV}$), can be attributed to an almost equal increase in HOMO energy and decrease in LUMO energy. Cyclic voltammetry measured for compounds **3.33** and **3.34** is qualitatively similar to that of **3.7a–b**. Thus, both **3.33** and **3.34** show an irreversible oxidation, while compound **3.33** displays two reversible reductions and the next higher homologue **3.34** displays three reversible or quasi-reversible reductions. Surprisingly, the E_g^{electro} calculated for compound **3.33** (2.76 eV) is higher than that for radiannulene **3.7a** (2.65 eV), despite the fact that **3.33** formally has a longer effective conjugation length. Similarly, E_g^{electro} for compound **3.34** (2.46 eV) is higher than that of di-radiannulene **3.7b** (2.33 eV). In both cases, estimates of E_g^{electro} for compounds **3.33–3.34** are higher than those predicted by UV-vis analysis (**3.33**, $E_g^{\text{opt}} = 2.64 \text{ eV}$; **3.34**, $E_g^{\text{opt}} = 2.40 \text{ eV}$).

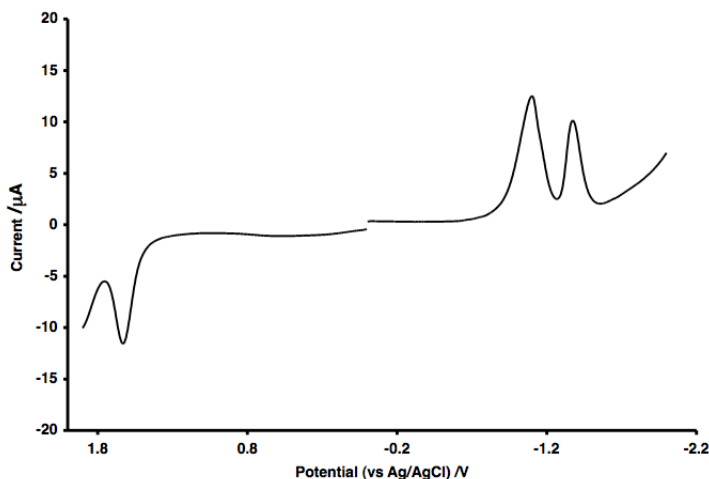


Figure 3-11. OSWV plot of radiannulene **3.7a** as measured in CH_2Cl_2 .

CV analysis of substituted radiannulenes **3.35a** and **3.35b** shows that both substituted compounds display an irreversible oxidation, and three reversible reductions. Phenyl substituted **3.35a** is markedly easier to oxidize than its electron deficient counterpart **3.35b** (1.01 V vs 1.16 V, respectively). Conversely, the electron withdrawing

nature of the nitro-phenyl substituents results in a more facile reduction of **3.35b** than **3.35a** (-1.36 V vs -1.46 V, respectively). Compared to the previously prepared phenyl substituted radiannulene **3.5a** ($E_{\text{ox}} = 0.78$ V, $E_{\text{red1}} = -1.94$ V, $E_{\text{g}}^{\text{electro}} = 2.72$ eV), radiannulene **3.35a** was more difficult to oxidize yet easier to reduce.⁶ This suggests that the extended π -conjugation imparted by the acetylene spacer in **3.35a** serves to enhance the electron accepting nature of the macrocycle core.

Notably present in most of the electrochemical studies was the emergence of a cathodic wave at *ca.* 0 V vs Ag/AgCl (Figure 3-10). This wave only appears after completion of the first oxidation cycle of the CV analysis, suggesting the formation of a new electrochemically active species as a result of oxidation. Zhao has previously reported similar irreversible oxidation behaviour for **3.3b**.⁴ It is speculated that this oxidative process follows an electrochemical-chemical (EC) mechanism, resulting in a possible rearrangement of the macrocycle core.¹⁹

Single crystals suitable for X-ray crystallographic analysis have been obtained for radiannulenes **3.7a**, **3.9**, **3.7b**, **3.35a**, and **3.35b** by slow evaporation from a solution of hexanes at room temperature (**3.7a** and **3.9**), by slow evaporation from a solution of CH_2Cl_2 /hexanes at room temperature (**3.7b** and **3.35a**), or from a CHCl_3 solution at 4 °C (**3.35b**). Trialkylsilyl substituted radiannulenes **3.7a** and **3.9** both share very similar structural features (Table 3-5, Table 3-6, Figure 3-12). Bond angles within the radiannulene core deviate slightly from the ideal 120° (i.e., for **3.7a**, $\text{C5-C4-C10} = 117.4(2)^\circ$, for **3.9** $\text{C5-C4-C10} = 117.5(2)^\circ$), as do the outer alkylidene bond angles (i.e., for **3.7a**, $\text{C2-C3-C11} = 116.0(2)^\circ$, for **3.9** $\text{C2-C3-C11} = 117.2(2)^\circ$). Exocyclic acetylene bonds in **3.7a** ($\text{Si1-C1-C2} = 174.6(2)^\circ$, $\text{C1-C2-C3} = 174.7(2)^\circ$) are slightly more distorted than those in **3.9** ($\text{Si1-C1-C2} = 176.0(2)^\circ$, $\text{C1-C2-C3} = 178.3(2)^\circ$). The bond lengths for **3.7a** and **3.9**, however, are overall comparable and unremarkable. Both

radiaannulenes **3.7a** and **3.9** pack in a slip-stacked fashion, arranging a phenyl ring of one molecule above the olefin unit of a neighbouring molecule (Figure 3-13). The smaller triethylsilyl groups present in **3.9** allow for slightly closer π - π interactions between the two neighbouring radiaannulene molecules (intermolecular C \cdots C, D, = 3.386 Å) when compared to the bulkier triisopropylsilyl groups in **3.7a** (D = 3.494 Å). Interplanar distances were calculated from the distance between the least squares plane generated from the 14 carbons of one radialene macrocycle and that of its nearest non-covalent neighbour.

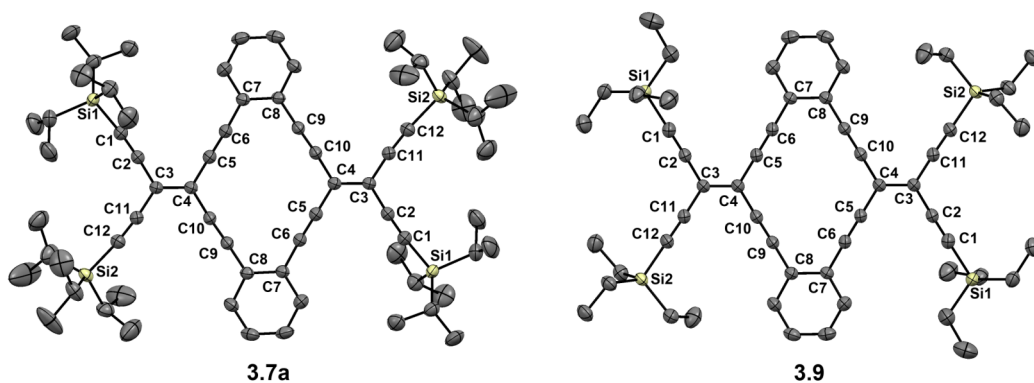


Figure 3-12. ORTEP representation of X-Ray data for radiaannulenes **3.7a** and **3.9** (atoms are represented by Gaussian ellipsoids at the 50% probability level, hydrogen atoms omitted for clarity).

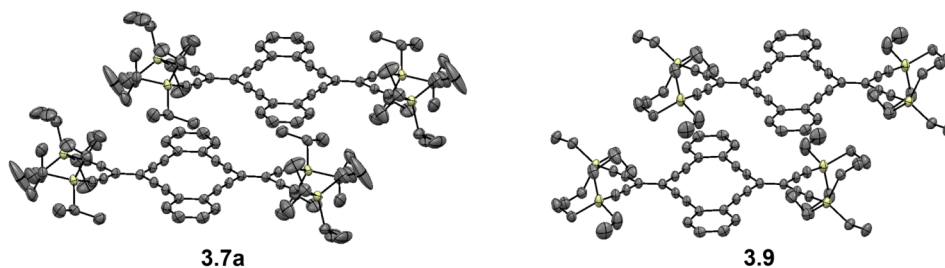


Figure 3-13. X-ray crystallographic structures of radiaannulenes **3.7a** and **3.9** illustrating solid-state packing (atoms are represented by Gaussian ellipsoids at the 50% probability level, hydrogen atoms omitted for clarity).

X-ray crystallography of di-radialene **3.7b** reveals a nearly planar structure, with a slight twist about the terminal olefins of about 1° (Figure 3-14). Bond angles within the macrocycle are similar to those of **3.7a** and **3.9**, with the “outer” endocyclic alkylidene angle C5–C4–C19 = 117.6(2)° and the “central” alkylidene angle C10–C13–C14 = 117.9(2)°. The “internal” alkynes of **3.7b** are slightly distorted, with a noted bending of a single alkyne unit in each macrocycle (i.e., C4–C19–C18 = 171.3(2)°, C17–C18–C19 = 177.5(2)°). The exocyclic acetylenes exhibit similar bending to those in **3.7a**. The planar nature of the large macrocycle also lends itself to π – π interactions, which are apparent from the close packing in the solid state ($D = 3.427\text{Å}$), which is just slightly closer than that observed for **3.7a** ($D = 3.494\text{Å}$). The interplanar distance of **3.7b** was calculated from the distance between the least squares plane generated from the 28 carbons of one di-radialene macrocycle and that of its nearest non-covalent neighbour.

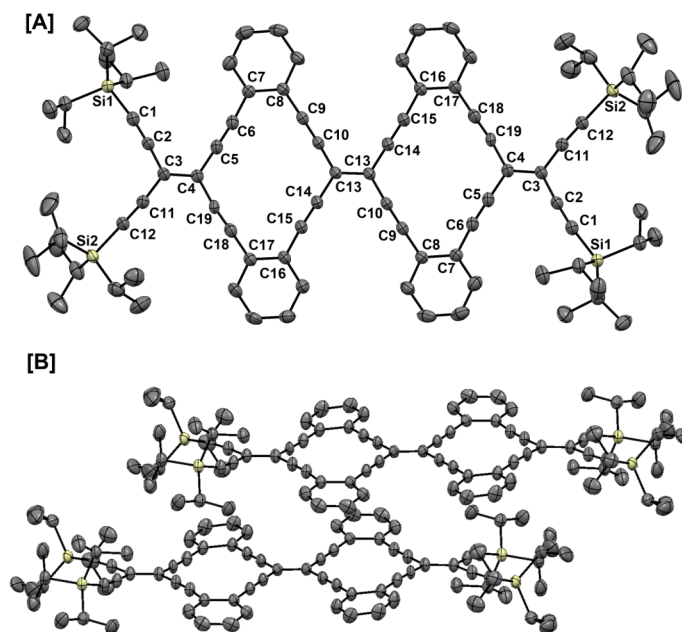


Figure 3-14. (a) ORTEP representation of X-Ray data for di-radiaannulene **3.7b** (b) Edge-on view illustrating solid-state packing (atoms are represented by Gaussian ellipsoids at the 50% probability level, hydrogen atoms omitted for clarity).

Table 3-5. Selected bond angles for radiannulenes **3.7a**, **3.9**, **3.7b**, **3.35a**, and **3.35b** (°).

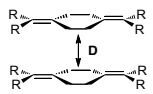
Cmpd	C2-C3-C11	C5-C4-C10	C6-C7-C8	Si1-C1-C2	C4-C5-C6	C20-C21-C22	
			C7-C8-C9	C1-C2-C3	C4-C10-C9	C21-C22-C25	
			C3-C11-C12	Si2-C12-C11	C5-C6-C7	C20-C23-C24	
					C8-C9-C10	C23-C24-C26	
3.7a	116.0(2)	117.4(2)	120.8(2)	174.6(2)	174.6(2), 178.6(2)	–	
			121.4(2)	174.7(2)	177.8(2), 176.6(2)		
				169.6(2)			
				175.2(2)			
3.9	117.2(2)	117.5(2)	120.5(2)	176.0(2)	178.2(2), 175.6(2)	–	
			120.6(2)	178.3(2)	178.6(2), 176.6(2)		
				177.5(2)			
				177.0(2)			
3.7b	115.7(2)	117.6(2) ^[a]	121.4(2)	166.8(2)	178.8(2), ^[e] 171.3(2) ^[f]	–	
		117.9(2) ^[b]	119.9(2)	175.7(2)	174.2(2), ^[g] 177.5(2) ^[h]		
			121.4(2) ^[c]	173.8(2)	176.5(2), ^[i] 179.3(2) ^[j]		
			120.9(2) ^[d]	174.3(2)	177.9(2), ^[k] 175.8(2) ^[l]		
3.35a	116.6(1)	117.5(1) ^[a]	121.3(1)	169.0(1)	177.4(2), ^[e] 176.3(2) ^[f]	176.7(2)	
		117.6(1) ^[m]	117.7(1) ^[b]	120.7(1)	176.2(2)	176.6(2), ^[g] 179.9(2) ^[h]	178.8(2)
				120.5(1) ^[c]	179.6(1)	176.3(2), ^[i] 174.9(2) ^[j]	177.3(2)
				120.8(1) ^[d]	176.2(2)	178.9(2), ^[k] 174.8(2) ^[l]	176.8(2)
3.35b	116.5(2)	118.4(2) ^[a]	119.7(2)	169.4(2)	179.1(2), ^[e] 179.0(2) ^[f]	174.5(2)	
		116.6(2) ^[m]	118.3(2) ^[b]	120.5(2)	176.0(2)	178.7(2), ^[g] 178.6(2) ^[h]	178.5(2)
				119.9(2) ^[c]	173.2(2)	177.8(2), ^[i] 177.3(2) ^[j]	176.0(2)
				120.4(2) ^[d]	174.4(2)	178.8(2), ^[k] 179.0(2) ^[l]	179.0(2)

[a]C5–C4–C19. [b]C10–C13–C14. [c]C15–C16–C17. [d]C16–C17–C18. [e]C4–C5–C6.

[f]C4–C19–C18. [g]C5–C6–C7. [h]C17–C18–C19. [i]C9–C10–C13. [j]C13–C14–C15.

[k]C8–C9–C10. [l]C14–C15–C16. [m]C21–C20–C23.

Table 3-6. Selected bond lengths and interplanar distances for radiaannulenes **3.7a**, **3.9**, **3.7b**, **3.35a**, and **3.35b** (Å).

Cmpd	C1–C2	C5–C6	C21–C22	
	C11–C12	C9–C10	C23–C24	
3.7a	1.206(3)	1.201(2)	–	3.494 ^[e]
	1.202(2)	1.199(2)	–	
3.9	1.206(3)	1.201(3)	–	3.386 ^[e]
	1.204(3)	1.197(3)	–	
3.7b	1.211(3)	1.192(3), ^[a] 1.172(3) ^[b]	–	3.427 ^[f]
	1.210(3)	1.201(2), ^[c] 1.198(3) ^[d]	–	
3.35a	1.209(2)	1.200(2), ^[a] 1.203(2) ^[b]	1.198(2)	3.362 ^[e]
	1.205(2)	1.206(2), ^[c] 1.201(2) ^[d]	1.203(3)	
3.35b	1.208(3)	1.203(3), ^[a] 1.203(3) ^[b]	1.200(3)	3.022 ^[e]
	1.203(3)	1.205(3), ^[c] 1.201(3) ^[d]	1.207(4)	

[a]C5–C6. [b]C18–C19. [c]C9–C10. [d]C14–C15. [e] Interplanar distances were calculated from the distance between the least squares plane generated from the 14 carbons of one radialene macrocycle and that of its nearest non-covalent neighbour. [f] Interplanar distances were calculated from the distance between the least squares plane generated from the 28 carbons of one di-radialene macrocycle and that of its nearest non-covalent neighbour.

X-ray crystallography of unsymmetrically substituted radiaannulenes **3.35a** and **3.35b** reveals that both molecules adopt a slight “saddle” shape (Figure 3-15). Bond lengths and angles of radiaannulenes **3.35a** and **3.35b** are comparable and similar to those of radiaannulenes **3.7a** and **3.9**. Compound **3.35a** packs in a similar fashion to that of **3.7a** and **3.9**, placing the electron-deficient olefin of one molecule above a macrocyclic phenyl ring of a neighbouring molecule. This places in the bulky triisopropylsilyl groups

of one molecule directly adjacent to the exocyclic phenyl rings of a neighbouring molecule, which forces the phenyl rings out of the radiannulene plane. Compound **3.35b**, however, packs in a different fashion than the previous radiannulenes. The phenyl rings of the radiannulene macrocycle in **3.35b** sit above the electron-withdrawing nitrophenyl groups of a neighbouring molecule, resulting in a closely packed dimer, with the smallest interplanar distance of all the measured radiannulenes ($D = 3.022 \text{ \AA}$). Interplanar distances were calculated from the distance between the least squares plane generated from the 14 carbons of one radialene macrocycle and that of its nearest non-covalent neighbour.

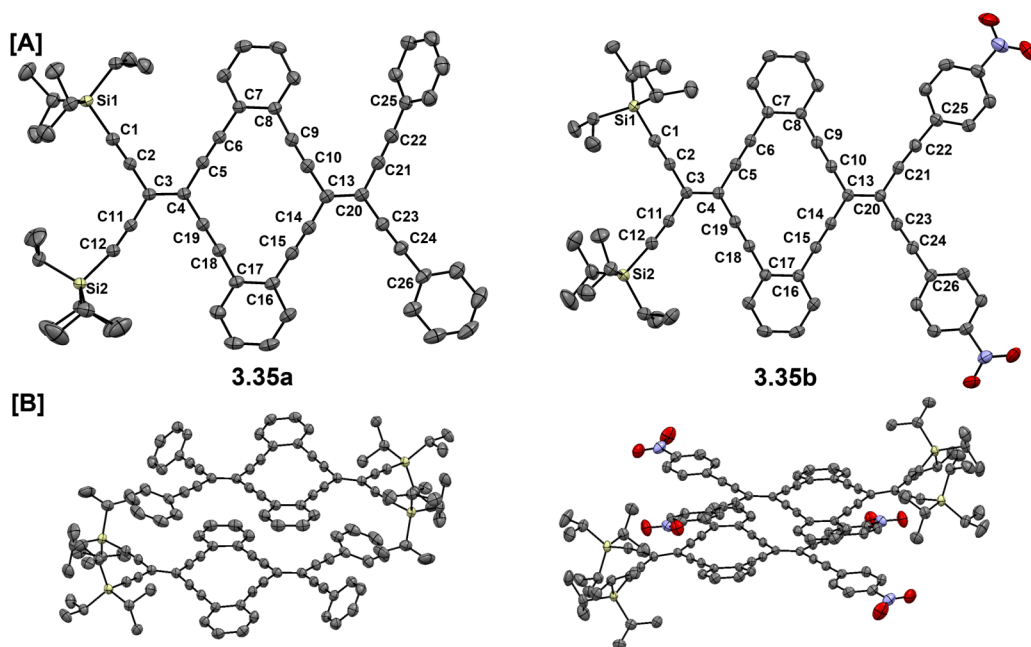


Figure 3-15. (a) ORTEP representation of X-Ray data for radiannulene **3.35a** and **3.35b** (b) Edge-on view for **3.35a** and **3.35b** illustrating solid-state packing (atoms are represented by Gaussian ellipsoids at the 50% probability level, hydrogen atoms and co-crystallized solvent molecules omitted for clarity).

3.7 Conclusion

A series of functionalized radiannulenes has been successfully prepared, including phenyl substituted radiannulene **3.35a**, nitro-phenyl substituted radiannulene **3.35b**, and aniline substituted radiannulene **3.35c**. In addition, an oligomeric series of radiannulenes **3.7a–c** has been prepared in an attempt to model some potential properties of 6,6,12-graphyne. Several synthetic routes have been explored, using a variety of different building blocks. The most promising of these routes involves the use of building block **3.29**. This molecule possesses both the dibromoolefin moiety required to close the radiannulene macrocycle, as well as the extended 1,2-diethynylaryl skeleton needed to extend the series. Molecule **3.29** allows for the stepwise synthesis of the target mono-radiannulene **3.7a**, di-radiannulene **3.7b**, and tri-radiannulene **3.7c**. Unfortunately, the stability of tri-radiannulene **3.7c** has yet to be established; this molecule decomposed prior to complete characterization when dissolved in CDCl₃. Sufficient material was recovered, however, to allow for investigation into its electronic properties via UV-vis spectroscopy. Based on the results of the UV-vis study, it appears that the effective conjugation length for the series of **3.7a–3.7c** has nearly been reached at the stage of the tri-radiannulene **3.7c**, with an $E_g^{\text{opt}} = 2.38$ eV. Further optimization of the synthetic procedure should allow for the extension of this protocol beyond tri-radiannulene **3.7c**. Regardless, this band gap appears to be sufficiently larger than that predicted for models of 6,6,12-graphyne, which is expected to possess a Dirac point and be a zero band-gap semiconductor.² Thus, an alternative structure may be needed to more effectively explore the potential properties of 6,6,12-graphyne.

3.8 References

1. Baughman, R. H.; Eckhardt, H.; Kertesz, M. *J. Phys. Chem.* **1987**, *87*, 6687–6699.
2. Malko, D.; Neiss, C.; Vines, F.; Görling, A. *Phys. Rev. Lett.* **2012**, *108*, 086804.
3. Wu, Y.-L.; Bures, F.; Jarowski, P. D.; Schweizer, W. B.; Boudon, C.; Gisselbrecht, J. P.; Diederich, F. *Chem. Eur. J.* **2010**, *16*, 9592–9605.
4. Chen, G.; Dawe, L.; Wang, L.; Zhao, Y. *Org. Lett.* **2009**, *11*, 2736–2739.
5. Lincke, K.; Frellsen, A. F.; Parker, C. R.; Bond, A. D.; Hammerich, O.; Nielsen, M. B. *Angew. Chem. Int. Ed.* **2012**, *51*, 6099–6102.
6. Gholami, M.; Chaur, M. N.; Wilde, M.; Ferguson, M. J.; McDonald, R.; Echegoyen, L.; Tykwinski, R. R. *Chem. Commun.* **2009**, 3038–3040.
7. Hasegawa, M.; Takatsuka, Y.; Kuwatani, Y.; Mazaki, Y. *Tetrahedron Lett.* **2012**.
In press. doi: 10.1016/j.tetlet.2012.07.109
8. Gholami, M. Ph.D Thesis, University of Alberta, 2009.
9. Zhou, Q.; Carroll, P. J.; Swager, T. M. *J. Org. Chem.* **1994**, *59*, 1294–1301.
10. Moore, J. S.; Weinstein, E. J.; Wu, Z. *Tetrahedron Lett.* **1991**, *32*, 2465–2466.
11. (a) Karpov, G. V.; Popik, V. V. *J. Am. Chem. Soc.* **2007**, *129*, 3892–3793. (b) Hatheway, G. J.; Hansch, C.; Kim, K. H.; Milstein, S. R.; Schmidt, C. L.; Smith, R. N. *J. Med. Chem.* **1978**, *21*, 563–574.
12. (a) Sandmeyer, T. *Ber. Dtsch. Chem. Ges.* **1884**, *17*, 1633–1635. (b) McClintock, S. P.; Zakharov, L. N.; Herges, R.; Haley, M. M. *Chem. Eur. J.* **2011**, *17*, 6798–6806. (c) Hwang, J.-J.; Tour, J. T. *Tetrahedron* **2002**, *58*, 10387–10405. (d) Kosynkin, D. V.; Tour, J. T. *Org. Lett.* **2001**, *3*, 993–995. (e) Doyle, M. P.; Bryker, W. J. *J. Org. Chem.* **1979**, *44*, 1572–1574.

13. Alvarez, R.; Martinez, C.; Madich, Y.; Denis, J. G.; Aurrecochea J. M.; de Lera, A. R. *Chem. Eur. J.* **2010**, *16*, 12746–12753.
14. Ohkita, M.; Ando, K.; Suzuki, T.; Tsuji, T. *J. Org. Chem.* **2000**, *65*, 4385–4390.
15. (a) Harris, S. J.; Walton, D. R. M. *Tetrahedron*, **1978**, *34*, 1037–1042. (b) Swindell, C. S.; Fan, W.; Klimko, P. G. *Tetrahedron Lett.* **1994**, *35*, 4959–4962. (c) Li, J.; Huang, P. *Beilstein J. Org. Chem.* **2011**, *7*, 426–431.
16. In this case, the HOMO-LUMO gap is estimated from the lowest energy λ_{\max} , as opposed to the lowest energy absorption edge with $\epsilon \geq 1000 \text{ L mol}^{-1} \text{ cm}^{-1}$. The use of λ_{\max} allows for a better comparison of molecules for which ϵ could not be measured, such as tri-radiaannulene **3.7c**.
17. (a) Kehoe, J. M.; Kiley, J. H.; English, J. J.; Johnson, C. A.; Peterson, R. C.; Haley, M. M. *Org. Lett.* **2000**, *2*, 969–972. (b) Johnson, C. A.; Lu, Y.; Haley, M. M. *Org. Lett.* **2007**, *9*, 3725–3728.
18. Bard, A. J.; Faulkner, L. R. (Eds.) *Electrochemical Methods: Fundamentals and Applications*, Wiley-VCH, Weinheim (**2000**).
19. Ramkumar, D.; Kalpana, M.; Varghese, B.; Sankararaman, S. *J. Org. Chem.* **1996**, *61*, 2247–2250.

Chapter 4 – Electrochemical Investigations of Functionalized Pentacenes and Pentacene Oligomers[†]

4.1 Introduction

Over the course of my PhD studies, I became interested in the electronic properties of the conjugated materials prepared in the Tykwinski group. I took particular interest in the electrochemical properties of the molecules being synthesized within the group, as electrochemical analysis of conjugated molecules such as acenes provides insight into the HOMO and LUMO energy these molecules. This knowledge is quite significant since an understanding of the HOMO and LUMO energy levels is important for the incorporation of molecules such as acenes into devices. My interest in the electrochemistry of such molecules led to the collaboration with my colleague, Dr. Dan Lehnherr, who focused on the synthesis of conjugated pentacenes. This collaboration led to the electrochemical analysis of several series of conjugated pentacene monomers and oligomers. As part of this study, I worked toward the synthesis of a series of several thienyl substituted pentacenes that might be used for electrochemical pentacene polymer formation.

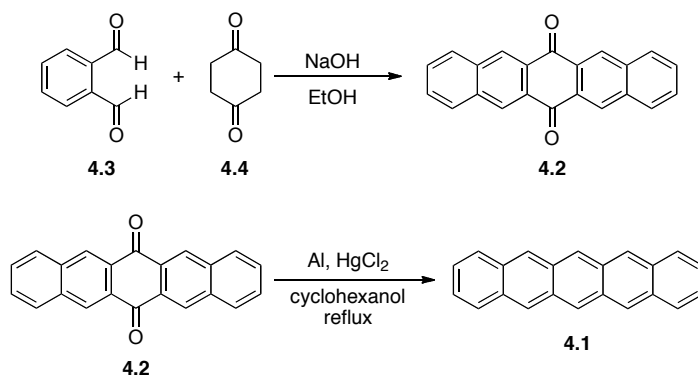
This chapter will describe five sub-projects focused on the electrochemical properties of substituted pentacenes; 1) The synthesis and electrochemistry of polarized

[†] Portions of this chapter have been published. (a) Lehnherr, D.; Murray, A. H.; MacDonald, R.; Ferguson, M. J.; Tykwinski, R. R. *Chem. Eur. J.* **2009**, *15*, 12580–12584. (b) Lehnherr, D.; Murray, A. H.; MacDonald, R.; Tykwinski, R. R. *Angew. Chem. Int. Ed.* **2010**, *49*, 6190–6194.

pentacenes, 2) The electrochemistry of pentacene/polycyclic aromatic hydrocarbon (PAH) dyads, 3) The electrochemistry of conjugated pentacene oligomers, 4) The synthesis and electrochemistry of conjugated pentacene dimers linked by π -spacers, and 5) The attempted polymerization of thienyl substituted pentacenes.

4.1.1 Introduction to Pentacene

There is a vast array of organic molecules that are of use as semiconductors, and pentacene **4.1** has garnered a great deal of attention over the past 10 years. Chemists, physicists and engineers alike have studied pentacene and its derivatives in an effort to develop new organic semiconductors.^{1,2} First prepared by Clar in 1929, pentacene can be synthesized by reductive aromatization of 6,13-pentacenequinone **4.2**, which can be obtained from a four-fold aldol condensation of 1,2-phthalaldehyde **4.3** with 1,4-cyclohexanedione **4.4** (Scheme 4-1).³⁻⁵

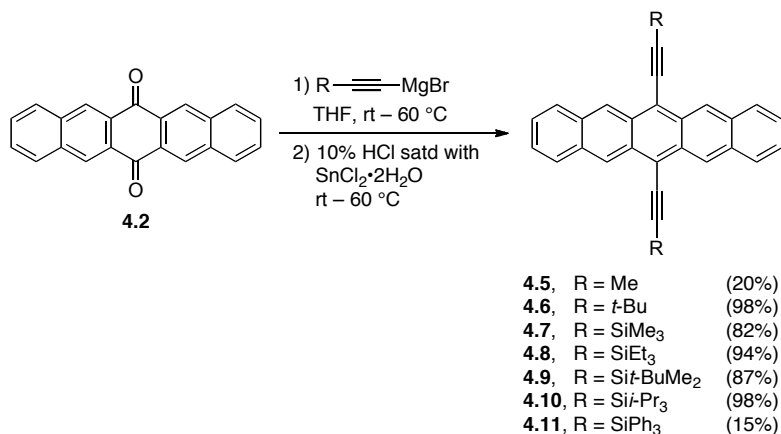


Scheme 4-1. Synthesis of pentacene **4.1**.

Pristine pentacene possesses a UV-vis absorption $\lambda_{\text{max}} = 576$ nm in benzene, and an electrochemically determined HOMO-LUMO gap ($E_{\text{g}}^{\text{electro}}$) of 2.09 eV.^{6,7} This corresponds to a first reduction potential (E_{red1}) of -1.87 V and first oxidation potential

(E_{ox1}) of 0.22 V vs the ferrocene/ferrocenium couple in *o*-dichlorobenzene (*o*-DCB).⁷ A promising material, pentacene has a number of limitations in regards to its application in semiconductor devices, notably poor solubility and low kinetic stability.

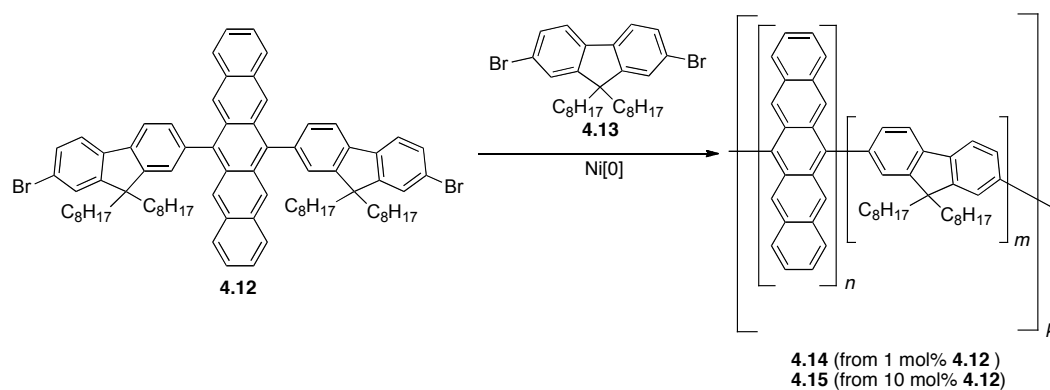
One way that the issue of solubility and stability of pentacene has been addressed is by synthetic functionalization, which also is a means of tuning the optical and electronic properties of the molecule. The most influential functionalized pentacenes were arguably 6,13-bis(silylethynyl)pentacenes (**4.5–4.11**), such as 6,13-bis(triisopropylsilylethynyl)pentacene **4.10**, discovered by Anthony and coworkers (Scheme 4-2).⁸ Pentacene **4.10** is a stable solid and readily soluble in most common organic solvents, which has allowed for easier processing, such as purification and solution deposition of thin films.



Scheme 4-2. Synthesis of 6,13-bis(ethynyl)pentacenes by Anthony and coworkers (**4.5–4.11**).

As a means of improving the properties of functionalized pentacenes, incorporation of the pentacene chromophore into oligomers and polymers is a logical progression. The solid-state morphology of pentacene is known to be important for device performance, and thus the ability to form processable polymer films could aid in

device fabrication. There have been, however, a limited number of pentacene oligomers and polymers reported in the literature.⁹ Tokito and coworkers reported the first pentacene polymers in 2001 (Scheme 4-3).¹⁰ Yamamoto coupling of dibromo compounds **4.12** and **4.13** resulted in random copolymers **4.14** and **4.15**, depending on the ratio of monomers used.

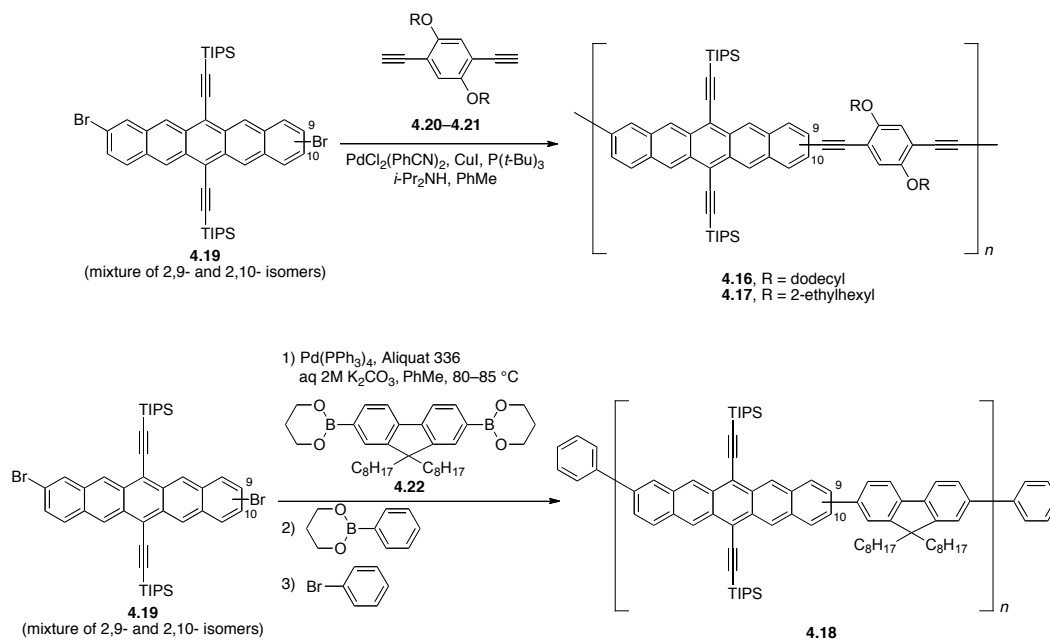


Scheme 4-3. Synthesis of pentacene-fluorene copolymers **4.14** and **4.15**.

Thin films of polymer **4.15** possess a UV-vis absorption λ_{max} of 623 nm and emission $\lambda_{\text{max,em}}$ at 625 nm (excitation wavelength, $\lambda_{\text{exc}} = 365$ nm). Polymer light emitting diodes (PLEDs) constructed using **4.15** (indium tin oxide (ITO)/polyethylenedioxythiophene (PEDOT)/**4.15**/Ca/Al) showed an operating voltage which was higher than that of the polyfluorene homopolymer, and that PLEDs of **4.15** had an insufficient half-life for practical applications.

Pentacene polymers **4.16–4.17** were prepared by Bao and coworkers in 2007, and they synthesized polymer **4.18** in 2008 (Scheme 4-4).¹¹ Pentacene **4.19** (a mixture of 2,9-dibromo and 2,10-dibromo isomers) underwent a Sonogashira cross-coupling reaction with 1,4-diethynylbenzenes **4.20–4.21** to yield copolymers **4.16** and **4.17**. Pentacene **4.19** was also used in a Suzuki cross-coupling reaction with fluorene-boronic ester **4.22** to give

copolymer **4.18**.



Scheme 4-4. Synthesis of pentacene copolymers **4.16–4.18**.

UV-vis spectroscopy of polymers **4.16–4.18** in *o*-DCB reveals absorption λ_{max} at *ca.* 670 nm, while absorption λ_{max} of thin films show almost no red-shift, suggesting poor electronic communication between polymer chains in the solid state. Electrochemical analysis of polymers **4.16–4.18** (Table 4-1) reveals that E_{red1} varied from -1.37 to -1.42 V for each polymer, while E_{ox1} varied from 0.24 to 0.32 V.

Table 4-1. Electrochemical properties of pentacene copolymers **4.16–4.18**.^[a]

Compound	$E_{\text{ox1}}^{\text{onset}}$	$E_{\text{red1}}^{\text{onset}}$	$E_{\text{red2}}^{\text{onset}}$	E_g^{electro}
	/ V	/ V	/ V	/ eV
4.16	0.32	-1.37	-1.80	1.69
4.17	0.28	-1.42	-1.82	1.70
4.18	0.24	-1.40	-1.89	1.64

[a] Potentials measured versus ferrocene/ferrocenium (Fc/Fc⁺) couple in *o*-DCB containing 0.05 M *n*-Bu₄NPF₆ as supporting electrolyte.

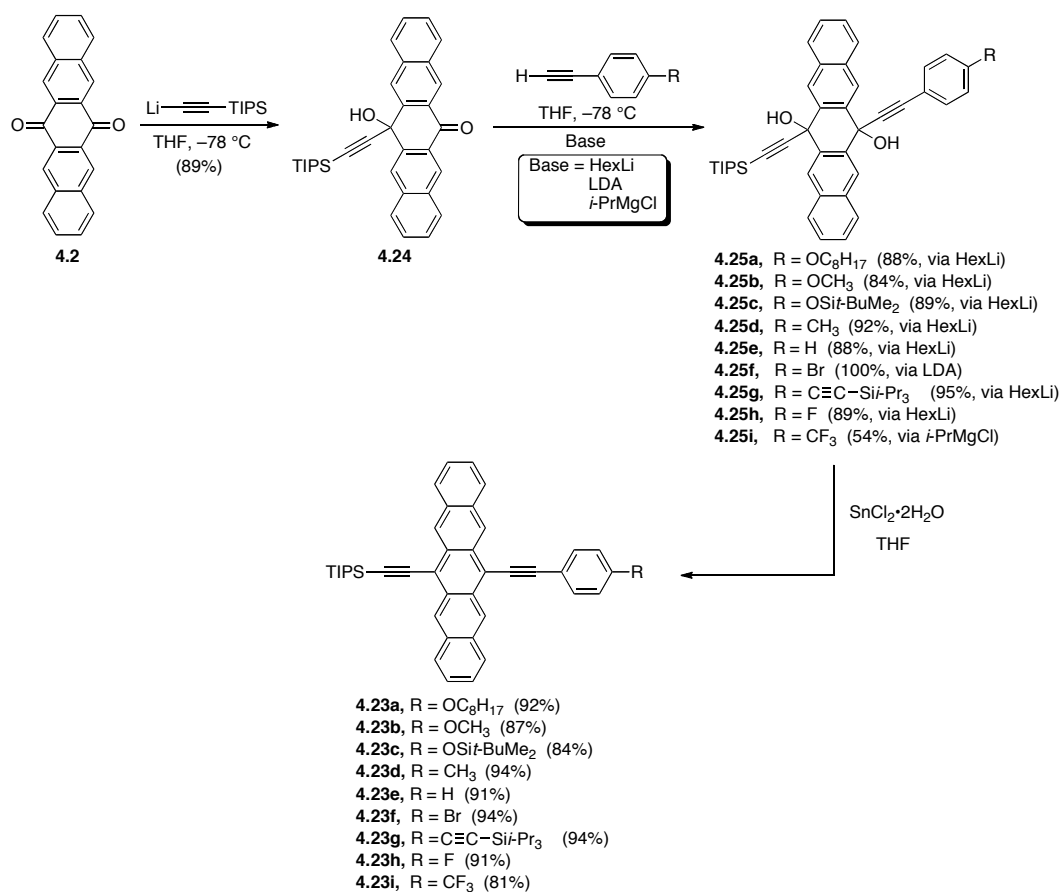
With the development of efficient functionalization methods for pentacene, it becomes possible to prepare an array of substituted pentacenes to be studied as possible candidates for use as optical and electronic materials. In addition, functionalization of pentacene could be used to prepare conjugated pentacene oligomers and polymers, an area of research that is still relatively unexplored. Analysis of the electrochemical properties of conjugated pentacene molecules offers vital insight into the HOMO and LUMO energy levels, an important attribute for developing acene molecules for use in organic devices.

4.2 Synthesis and Electrochemical Properties of Polarized Pentacenes

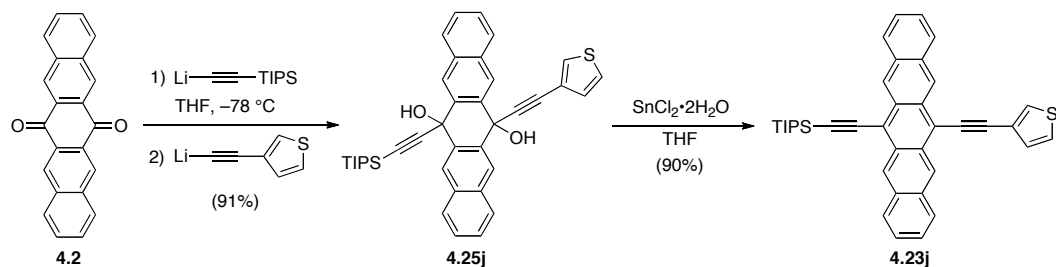
The first series of target molecules were unsymmetrically substituted pentacenes (**4.23a–i**) containing a conjugated aryl substituent. The goal was to examine the influence of the conjugated aryl substituent on the HOMO and LUMO levels of the pentacene molecules, using electrochemical analysis. Pentacenes **4.23a–i** molecules were prepared by, Dr. Dan Lehnerr.¹² The synthesis began by slow addition of the Li-acetylide of

TIPS-acetylene to a slurry of 6,13-pentacenequinone **4.2** in THF at $-78\text{ }^{\circ}\text{C}$, which yielded ketone **4.20** in 89% yield (Scheme 4-5). To a solution of ketone **4.20** was added an acetylide nucleophile (generated using HexLi, LDA, or *i*-PrMgCl) to yield diols **4.25a–i** in moderate to excellent yield (54–100%). Diols **4.25a–i** then underwent reductive aromatization in the presence of $\text{SnCl}_2 \cdot 2\text{H}_2\text{O}$ to afford unsymmetrical pentacenes **4.23a–i** in good yields (81–94%).

Toward development of a polymerizable pentacene derivative, I adapted the basic procedure from Dr. Lehnerr to provide unsymmetric pentacene **4.23j** directly from 6,13-pentacenequinone **4.2** without isolation of the ketone intermediate. Thus, addition of TIPS-acetylide to **4.2** followed by lithiated 3-ethynylthiophene afforded diol **4.25j** in 91% yield (Scheme 4-6). Diol **4.25j** then underwent reductive aromatization to yield pentacene **4.23j** in 90% yield.



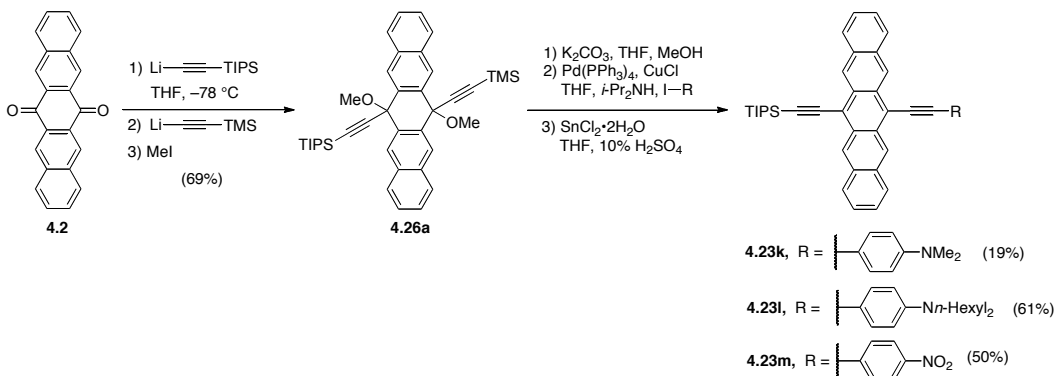
Scheme 4-5. Synthesis of unsymmetrically substituted pentacenes **4.23a-i**.



Scheme 4-6. Synthesis of unsymmetrically substituted pentacene **4.23j**.

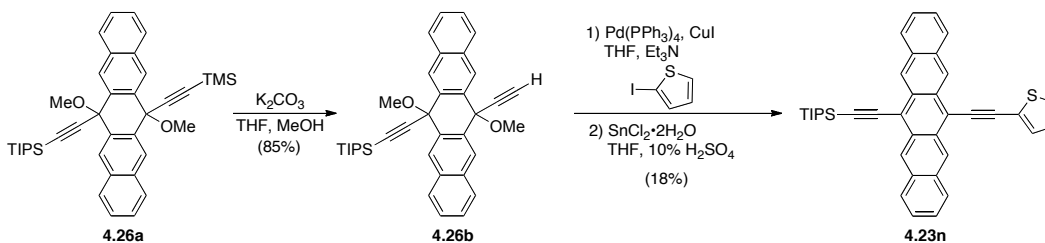
The synthesis of pentacenes incorporating strong electron donating or withdrawing groups, **4.23k-m**, was carried out via Sonogashira cross-coupling reaction. This was due to the difficulty in the synthesis of these molecules using nucleophilic addition. The synthesis began with the formation of di-methoxy pentacene **4.26a**

(Scheme 4-7). Stepwise addition of TIPS-acetylide and TMS-acetylide to 6,13-pentacenequinone **4.2** followed by trapping the resulting alkoxide with iodomethane afforded **4.26a** in 69% yield. Removal of the TMS groups of **4.26a** with K_2CO_3 in THF/MeOH and subsequent Sonogashira cross-coupling reaction of the resulting terminal acetylene with an aryl iodide, and final reductive aromatization yielded pentacenes **4.23k–m** in low to moderate yields (19–61%).



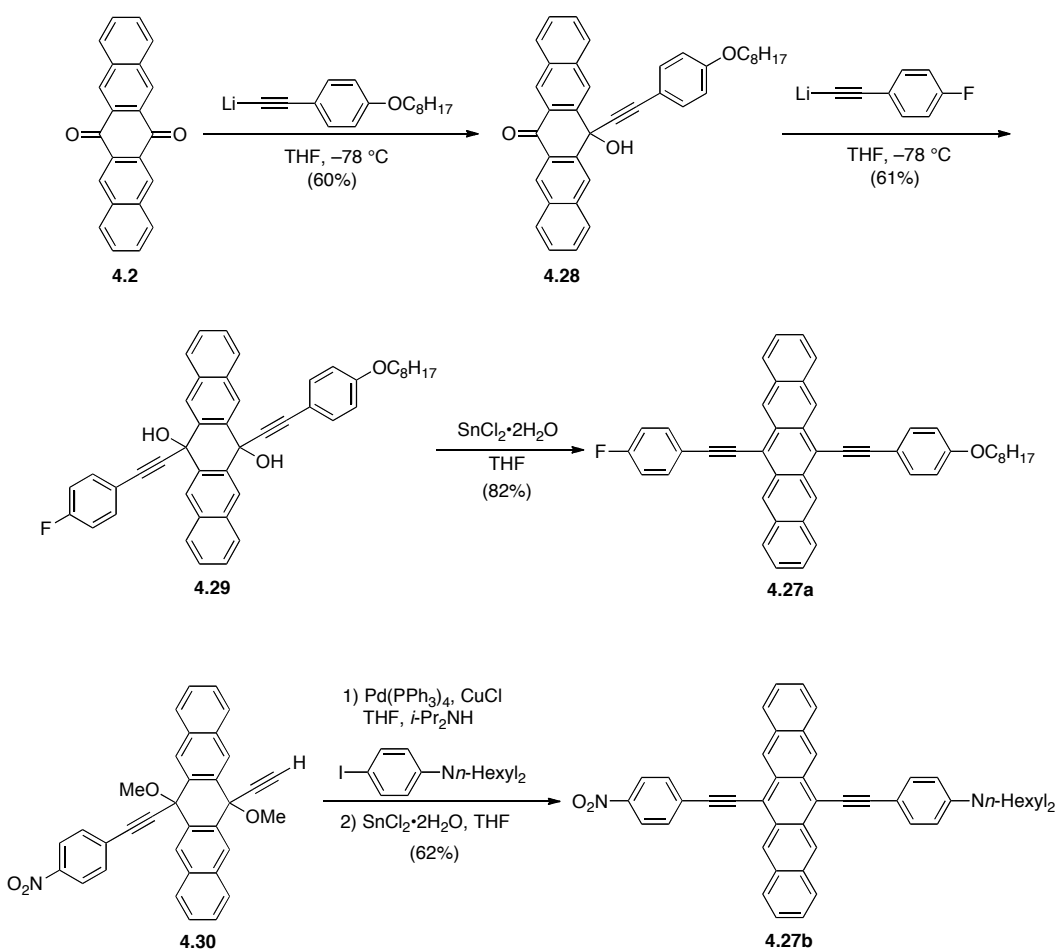
Scheme 4-7. Synthesis of unsymmetrically substituted pentacenes **4.23k–m**.

Using a similar procedure, I was able to construct 2-thienyl substituted pentacene **4.23n** in 18% yield (Scheme 4-8). While the yield of **4.23n** was low, this procedure remains unoptimized.



Scheme 4-8. Synthesis of unsymmetrically substituted pentacene **4.23n**.

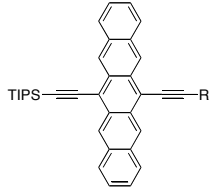
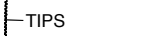
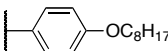
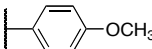
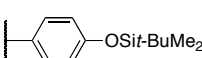
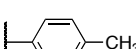
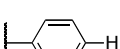
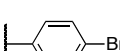
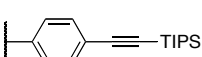

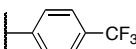
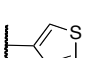
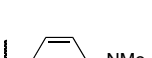
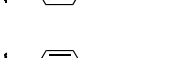
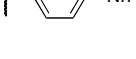
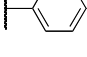
Substituted pentacene **4.27a** was prepared utilizing a stepwise nucleophilic addition of lithiated ethynylarenes to pentacenequinone **4.2** (Scheme 4-9). Addition of the lithium acetylide formed from 1-*n*-octyloxy-4-ethynylbenzene to **4.2** afforded ketone **4.28** in 60% yield. Subsequent addition of the lithium acetylide of 1-ethynyl-4-fluorobenzene to **4.28** led to the formation of diol **4.29** in 61% yield. Reductive aromatization of **4.29** yielded **4.27a** in 82% yield. Alternatively, bis-aryl substituted pentacene **4.27b** was prepared in a 62% yield using a sequence of Sonogashira cross-coupling reaction and reductive aromatization starting from di-methoxy pentacene **4.30**. Compounds **4.27a–b** were prepared by Dr. Dan Lehnerr.¹²



Scheme 4-9. Synthesis of polarized pentacenes **4.27a** and **4.27b**.

The electrochemical properties of pentacenes **4.23a–n** and **4.27a–b** have been investigated using cyclic voltammetry (CV, Table 4-2, Figure 4-1, Figure 4-2, Figure 4-3). Nearly all of the pentacenes exhibit three reversible or quasi-reversible electrochemical events; two reductions and one oxidation. There are several exceptions to this general trend. Pentacene **4.23j** exhibits two oxidations, the second of which is irreversible, corresponding to the thiophene moiety.¹³ *N,N*-Dialkylaniline substituted pentacenes **4.23k–l** also exhibit two irreversible oxidations, typical of aromatic amines.¹⁴ Pentacenes **4.23c** and **4.23m** exhibit three reversible or quasi-reversible reductions. It is also worth noting the presence in some CV the appearance of a small oxidation wave (*ca.* –0.40 to –0.70 V vs Ag/AgNO₃, Figure 4-1) after initial reductions. This oxidation is likely the result of an electrochemistry / chemistry (EC) process, in which adventitious water reacts with the generated radical anion and dianion of pentacene to generate a partially protonated product.¹⁵ Adventitious water proves problematic for **4.23n**, for which an aqueous reference electrode has been used, and failed to generate meaningful analysis.

Table 4-2. Electrochemical properties (vs Fc/Fc⁺ couple) and optical band gap of pentacenes **4.10**, **4.23a–n**, and **4.27a–b**.

Compound		$E_{\text{ox1}}^{[a]}$ / V	$E_{\text{red1}}^{[a]}$ / V	$E_{\text{red2}}^{[a]}$ / V	$E_{\text{g}}^{\text{electro [a]}}$ (PhH/MeCN) / eV	$E_{\text{g}}^{\text{opt [f]}}$ (CH ₂ Cl ₂) / eV
R =						
4.10		0.45	-1.45	-1.93	1.90	1.84
4.23a		0.34	-1.46	-1.93	1.80	1.78
4.23b		0.35	-1.46	-1.92	1.81	1.78
4.23c		0.36	-1.47	-1.92 -2.09 ^[c]	1.83	1.79
4.23d		0.37	-1.44	-1.91	1.81	1.80
4.23e		0.39	-1.44	-1.90	1.83	1.81
4.23f		0.41	-1.43	-1.87	1.84	1.80
4.23g		0.41	-1.42	-1.84	1.83	1.78
4.23h		0.40	-1.43	-1.88	1.83	1.81
4.23i		0.43	-1.42	-1.83	1.85	1.79
4.23j		0.34 0.89 ^[d]	-1.42	-1.91	1.76	1.76
4.23k		0.18 ^[c] 0.43 ^[d]	-1.47	-1.93	1.65	1.68
4.23l		0.16 0.41 ^[d]	-1.47	-1.94	1.63	1.66
4.23m		0.44	-1.33	-1.46 -2.09 ^[c]	1.77	1.72
4.23n ^[b]		–	–	–	–	1.76
4.27a	see Scheme 4-8	0.31	-1.43	-1.90	1.74	1.76
4.27b	see Scheme 4-8	0.18 0.39 ^[d]	-1.34	-1.48	1.52	1.49

[a] Cyclic voltammetry was performed in benzene/MeCN (3:1 v/v) solutions containing

0.1 M *n*-Bu₄NPF₆ as supporting electrolyte at a scan rate of 150 mV/s. The working electrode was a platinum disc, the counter electrode was a platinum wire, and the reference electrode was a non-aqueous Ag/AgNO₃ [10 mM] in MeCN. The potential values (*E*) were calculated using the following equation (except where otherwise noted): $E = (E_{pc} + E_{pa})/2$, where E_{pc} and E_{pa} correspond to the cathodic and anodic peak potentials, respectively. Potentials are referenced to the ferrocene/ferrocenium (Fc/Fc⁺) couple used as an internal standard. E_g^{electro} determined from the separation between the first oxidation and first reduction potentials. [b] The reference electrode was aqueous Ag/AgCl/NaCl [3M]. [c] This oxidation potential was estimated by reporting the E_{pa} of the oxidation wave. [d] E_{ox2} . [e] E_{red3} . [f] The wavelength used as the absorption edge for determining HOMO-LUMO energy gap corresponds to the lowest energy absorption that has molar absorption coefficient $\epsilon \geq 1000 \text{ L mol}^{-1} \text{ cm}^{-1}$.

Electron-donating groups (arylether and thienyl) appended to pentacene result in a slightly easier oxidation process, demonstrated by the lowering of oxidation potentials (i.e., raising HOMO energy) to $E_{ox1} = 0.34\text{--}0.36 \text{ V}$ for **4.23j** and **4.23a–c**, when compared to the phenyl derivative **4.23e** ($E_{ox1} = 0.39 \text{ V}$). *N,N*-Alkylaniline derivatives **4.23k–l** exhibit irreversible oxidations at 0.18 V and 0.16 V respectively, corresponding to the oxidation of the aniline moiety. Further oxidation of the pentacene chromophore appears at higher oxidation potentials, $E_{ox2} = 0.43 \text{ V}$ and 0.41 V, respectively. The presence of electron-withdrawing substituents (CF₃, **4.23i**, $E_{ox1} = 0.43 \text{ V}$, NO₂, **4.23m**, $E_{ox1} = 0.44 \text{ V}$) results in more difficult oxidation processes when compared to the phenyl derivative **4.23e**. These electron-withdrawing groups, however, facilitate the reduction process, with nitrophenyl substituted **4.23m** ($E_{red1} = -1.33 \text{ V}$) being considerably easier to reduce than **4.23e** ($E_{red1} = -1.44 \text{ V}$), indicative of a lower LUMO energy.

The overall trend in electrochemical HOMO-LUMO gap (E_g^{electro}) is consistent

with that determined using UV-vis absorption measurements (E_g^{opt}).¹² Most of the substituted pentacenes show E_g^{electro} in a narrow range (1.80–1.84 eV), while that of the 3-thiophene substituted pentacene **4.23j** ($E_g^{\text{electro}} = 1.76$ eV) and nitrophenyl substituted pentacene **4.23m** ($E_g^{\text{electro}} = 1.77$ eV) are slightly lower. *N,N*-Alkylaniline derivatives **4.23k–l** possess markedly lower band gaps, the result of raised HOMO energies localized on the *N,N*-dialkylaniline groups. Lastly, the donor / acceptor substituted pentacene **4.27b** shows a narrowed band gap (1.52 eV) when compared to mono-substituted electron-donating or electron-withdrawing derivatives **4.23l** and **4.23m**. It is also worth noting that many of these molecular pentacenes possess similar, and in some cases narrower, E_g^{electro} compared to polymeric pentacenes **4.16–4.18** ($E_g^{\text{electro}} = 1.64–1.70$ eV)¹¹, suggesting that functionalization in the 6- and 13-positions of pentacene more effectively tunes the band-gap than that in the 2,9- or 2,10-positions.

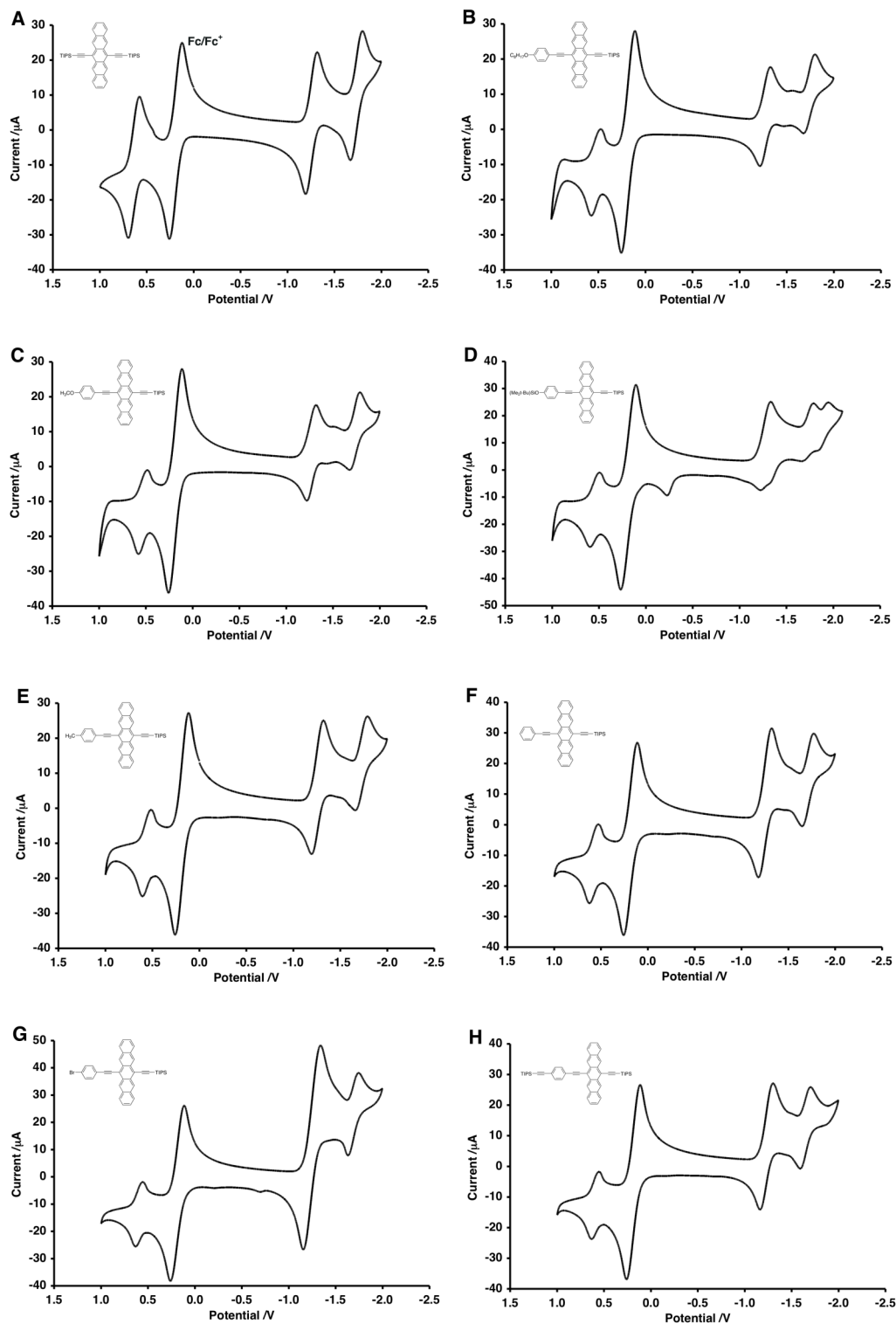


Figure 4-1. CV plots of pentacenes (a) **4.10**, (b) **4.23a**, (c), **4.23b**, (d), **4.23c**, (e) **4.23d**, (f) **4.23e**, (g) **4.23f**, and (h) **4.23g** as measured in 3:1 benzene/MeCN (vs Ag/Ag⁺).

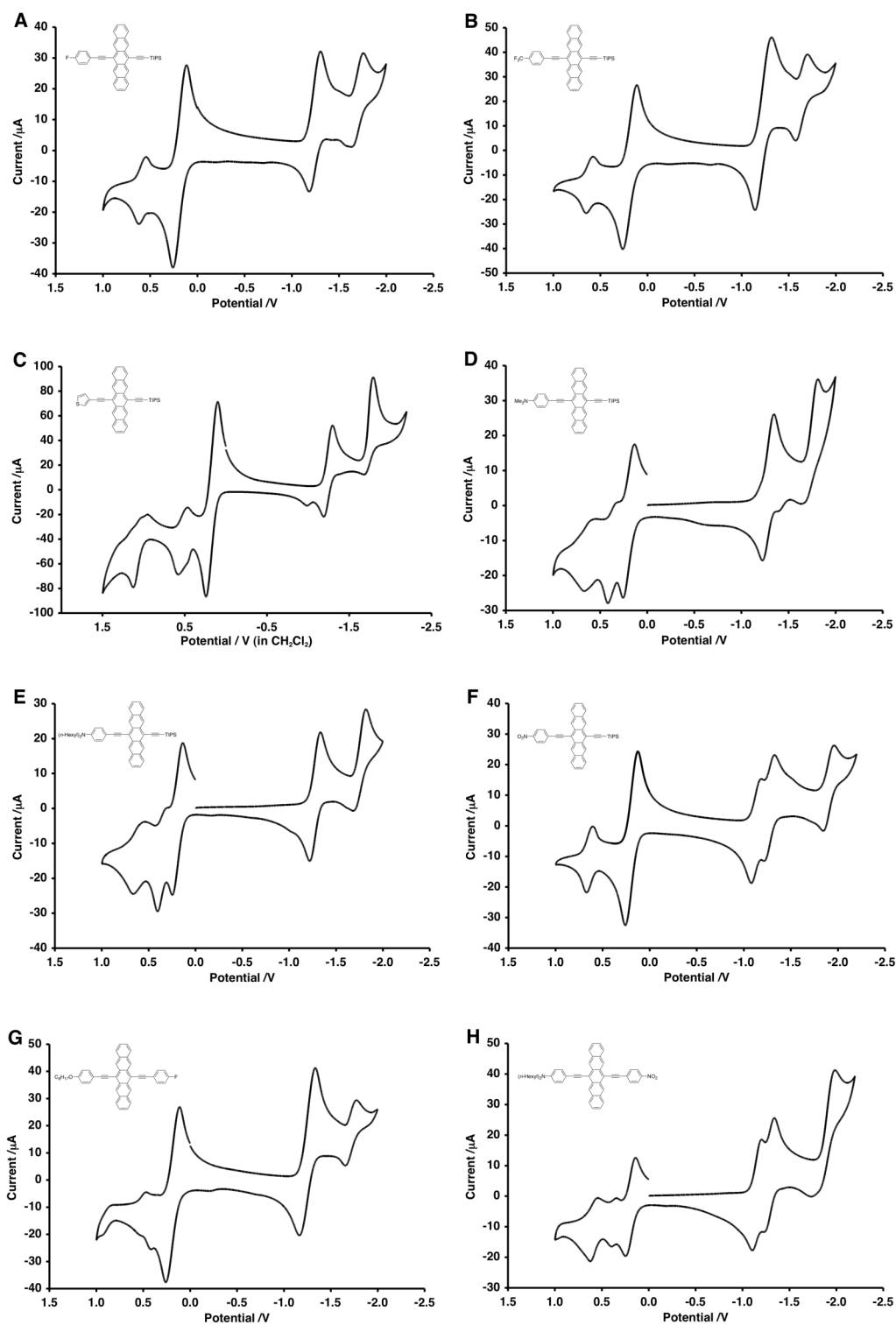


Figure 4-2. CV plots of pentacenes (a) **4.23h**, (b) **4.23i**, (c), **4.23j**, (d), **4.23k**, (e) **4.23l**, (f) **4.23m**, (g) **4.27a**, and (h) **4.27b** as measured in 3:1 benzene/MeCN (vs Ag/Ag⁺).

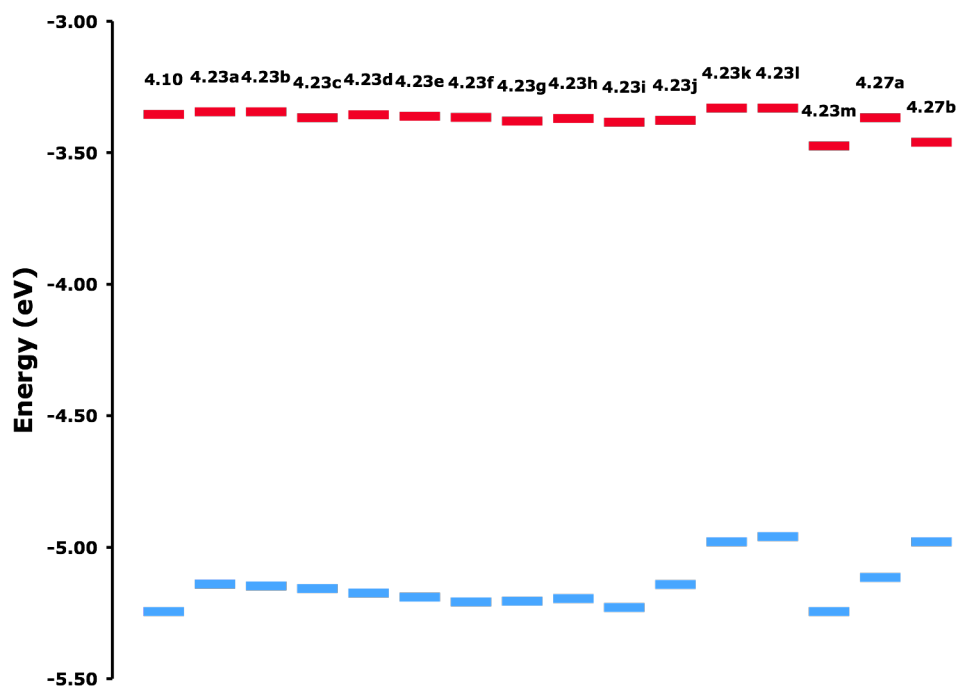
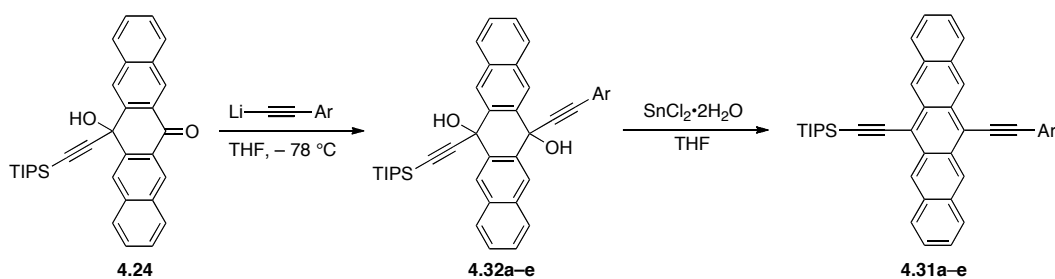
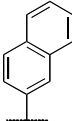
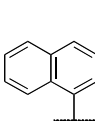
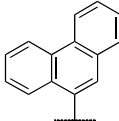
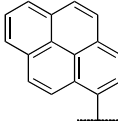
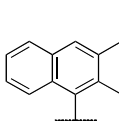


Figure 4-3. HOMO-LUMO energy levels of polarized pentacenes **4.10**, **4.23a–m** and **4.27a–b**.¹⁶

4.3 Synthesis and Electrochemical Properties of Pentacene/Polycyclic Aromatic Hydrocarbon Dyads

A series of polycyclic aromatic hydrocarbon (PAH) pentacene dyads **4.31a–e** was prepared by Dr. Dan Lehnerr, via acetylide addition to ketone **4.24** (Scheme 4-10).¹² Generation of the appropriate aryl acetylide using HexLi, and subsequent addition to ketone **4.24** afforded diols **4.32a–e** in moderate to excellent yields (41–99%). Reductive aromatization of diols **4.32a–e** in THF yielded pentacene-PAH dyads **4.31a–e** in good yields (83–98%).

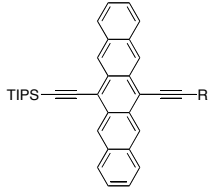
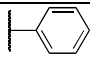
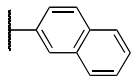
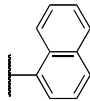
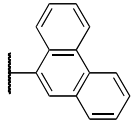
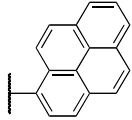
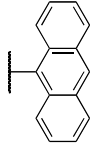


					
	a	b	c	d	e
4.32	99%	91%	95%	83%	41%
4.31	83%	90%	86%	98%	83%

Scheme 4-10. Synthesis of pentacene-polycyclic aromatic hydrocarbon dyads **4.31a–e**.

The electrochemical properties of pentacenes **4.31a–e** has been investigated in comparison to **4.23e** using cyclic voltammetry (CV, Table 4-3, Figure 4-4). There is a small variation in the oxidation and first reduction potentials of all the pentacene-PAH dyads as a function of the structure of the aryl group. Both oxidation and reduction processes, however, are made slightly easier as benzannulation of the aryl substituent is increased, suggesting that the HOMO energies levels rise while LUMO energies simultaneously lower (Figure 4-5). Similar to the polarized pentacenes **4.23a–n**, E_g^{electro} values for pentacene-PAH dyads are in good agreement with their corresponding E_g^{opt} values. Anthracene substituted pentacene-PAH dyad **4.31e** shows the lowest E_g^{electro} (1.71 eV), which is comparable to polymers **4.16** and **4.17** ($E_g^{\text{electro}} = 1.69\text{--}1.70$ V).¹¹ This again highlights the efficiency in conjugation when substitution occurs at the 6,13-positions of pentacene, compared to the 2,9- or 2,10-positions.

Table 4-3. Electrochemical properties (vs Fc/Fc⁺ couple) and optical band gap of pentacene-PAH dyads **4.23e** and **4.31a–e**

Cmpd		$E_{\text{ox1}}^{[a]}$ / V	$E_{\text{red1}}^{[a]}$ / V	$E_{\text{red2}}^{[a]}$ / V	$E_{\text{g}}^{\text{electro [a]}}$ (PhH/MeCN) / eV	$E_{\text{g}}^{\text{opt [c]}}$ (CH ₂ Cl ₂) / eV
4.23e		0.39	-1.44	-1.90	1.83	1.81
4.31a		0.38	-1.42	-1.86	1.80	1.79
4.31b		0.39	-1.42	-1.86	1.81	1.79
4.31c		0.38	-1.40	-1.83	1.78	1.78
4.31d		0.34	-1.40	-1.80	1.74	1.74
4.31e		0.33 ^[b]	-1.38 ^[b]	-1.77 ^[b]	1.71	1.74

[a] Cyclic voltammetry was performed in benzene/MeCN (3:1 v/v) solutions containing 0.1 M *n*-Bu₄NPF₆ as supporting electrolyte at a scan rate of 150 mV/s. The working electrode was a platinum disc, the counter electrode was a platinum wire, and the reference electrode was a non-aqueous Ag/AgNO₃ [10 mM] in MeCN. The potential values (*E*) were calculated using the following equation (except where otherwise noted): $E = (E_{\text{pc}} + E_{\text{pa}})/2$, where E_{pc} and E_{pa} correspond to the cathodic and anodic peak potentials, respectively. Potentials are referenced to the ferrocene/ferrocenium (Fc/Fc⁺) couple used as an internal standard. $E_{\text{g}}^{\text{electro}}$ determined from the separation between the first oxidation and first reduction potentials. [b] Scan rate of 200 mV/s. [c] The

wavelength used as the absorption edge for determining HOMO-LUMO energy gap corresponds to the lowest energy absorption that has molar absorption coefficient $\epsilon \geq 1000 \text{ L mol}^{-1} \text{ cm}^{-1}$.

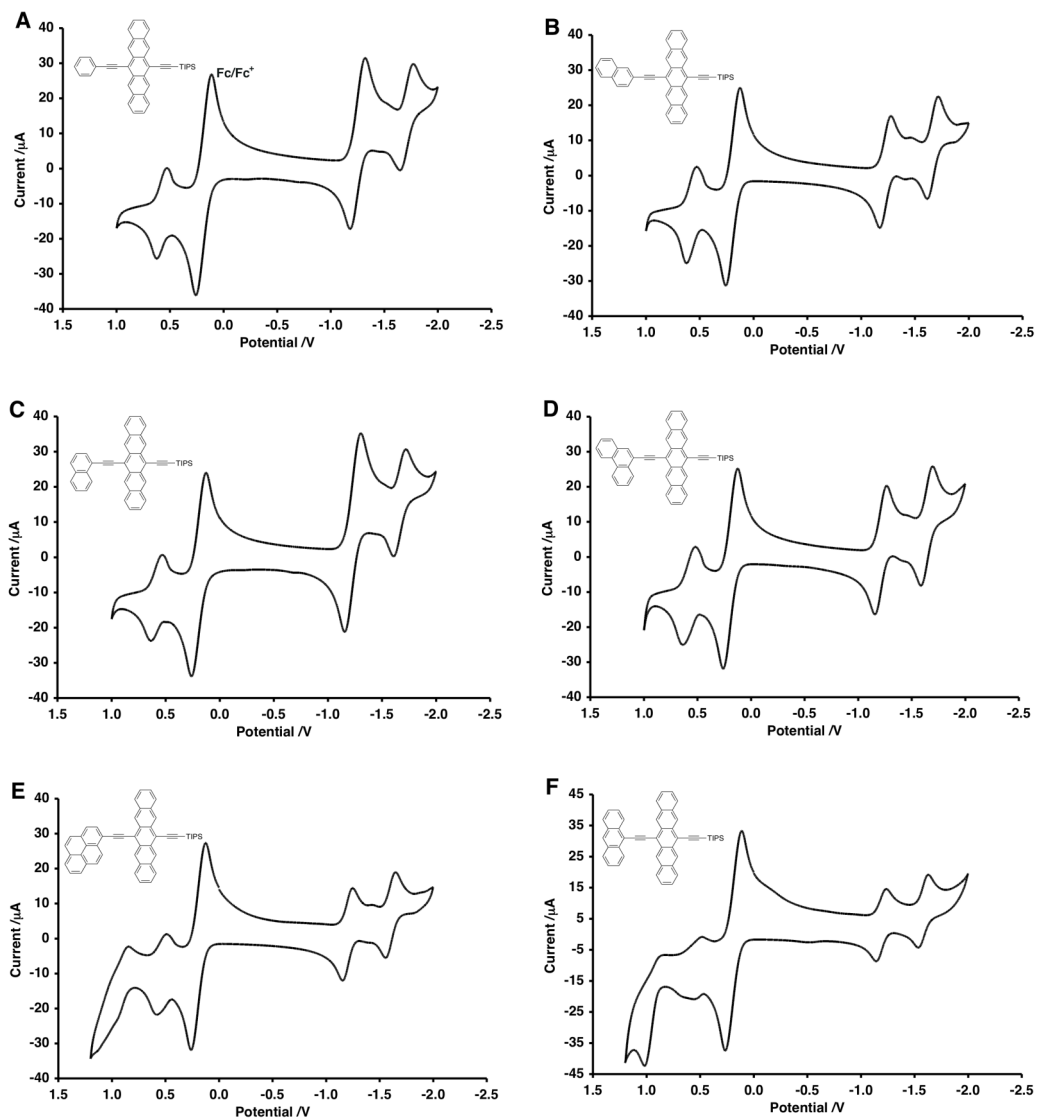


Figure 4-4. CV plots of pentacenes (a) **4.23e**, (b) **4.31a**, (c) **4.31b**, (d) **4.31c**, (e) **4.31d**, and (f) **4.31e** as measured in 3:1 benzene:acetonitrile (vs Ag/Ag⁺).

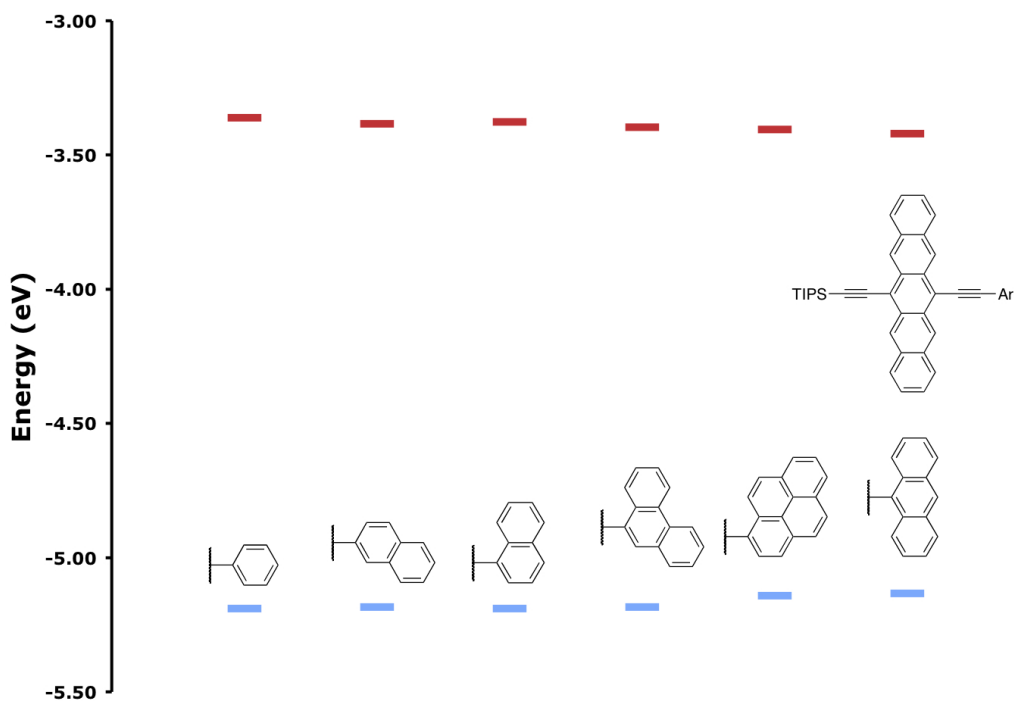


Figure 4-5. HOMO-LUMO energy levels of pentacene-PAH dyads **4.23e** and **4.31a-e**.¹⁶

4.4 Electrochemical Properties of Conjugated Pentacene Oligomers

In light of the narrowing E_g^{electro} for the pentacene-PAHs described in Section 4.2, a series of pentacene oligomers **4.33–4.36**, conjugated via butadiyne linkers at the 6,13-positions, were prepared by Dr. Dan Lehnerr (Figure 4-6). Tri-*n*-hexylsilyl groups provided the best solubility over the course of the series, and the series of oligomers with these terminal groups will thus be the focus discussion.

E_g^{electro} from 2.03 eV to 1.46 eV as oligomer length increases.

Table 4-4. Electrochemical properties of conjugated pentacene oligomers **4.33–4.35** in THF (vs Fc/Fc⁺ couple).^[a]

Cmpd	E_{ox1} / V	E_{ox2} / V	E_{red1} / V	E_{red2} / V	E_{red3} / V	E_{red4} / V	E_{red5} / V	E_{red6} / V	E_g^{electro} / eV
4.33	0.54	–	–1.49	–1.97	–	–	–	–	2.03
4.34	0.39	0.53	–1.25	–1.46	–1.96	–2.19	–	–	1.64
4.35	0.33 ^[b]	–	–1.13	–1.25	–1.56	–1.90	–2.05	–2.23	1.46

[a] Cyclic voltammetry was performed in THF solutions containing 0.1 M *n*-Bu₄NPF₆ as supporting electrolyte at a scan rate of 150 mV/s. The working electrode was a platinum disc, the counter electrode was a platinum wire, and the reference electrode was a non-aqueous Ag/AgNO₃ [10 mM] in MeCN. The potential values (E) were calculated using the following equation (except where otherwise noted): $E = (E_{\text{pc}} + E_{\text{pa}})/2$, where E_{pc} and E_{pa} correspond to the cathodic and anodic peak potentials, respectively. Potentials are referenced to the ferrocene/ferrocenium (Fc/Fc⁺) couple used as an internal standard. E_g^{electro} determined from the separation between the first oxidation and first reduction potentials. [b] The oxidation potential was estimated by reporting E_{pa} of the oxidation wave.

There are a total of two one-electron reductions per pentacene unit observed for each of the oligomers **4.33–4.35**. For example, monomer **4.33** shows two reductions, dimer **4.34** shows four reductions, and trimer **4.35** shows six reductions. This confirms electronic communication between pentacene moieties within the molecule, as the

formation of a pentacene radical anion hinders the introduction of a second radical anion on an adjacent pentacene moiety. It is also worth noting that reduction potential for adding a second electron to an individual pentacene moiety is similar regardless of oligomer length, i.e., for monomer **4.33** ($E_{\text{red}2} = -1.97$ V), dimer **4.34** ($E_{\text{red}3} = -1.96$ V), and trimer **4.35** ($E_{\text{red}4} = -1.90$ V). It should also be noted that CV of trimer **4.35** reveals an anodic wave (*ca.* -0.40 V vs Ag/Ag^+ , see Figure 4-7c), which only appeared after initial reduction of the molecule.

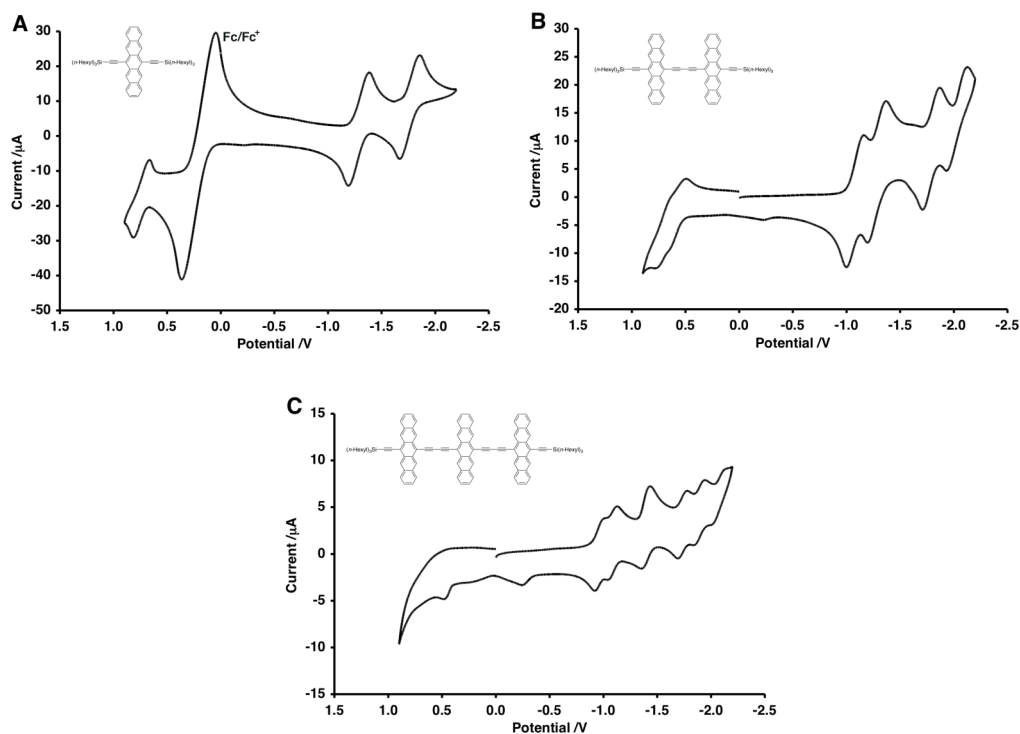


Figure 4-7. CV plots of pentacenes (a) **4.33**, (b) **4.34**, and (c) **4.35** as measured in THF (vs Ag/Ag^+).

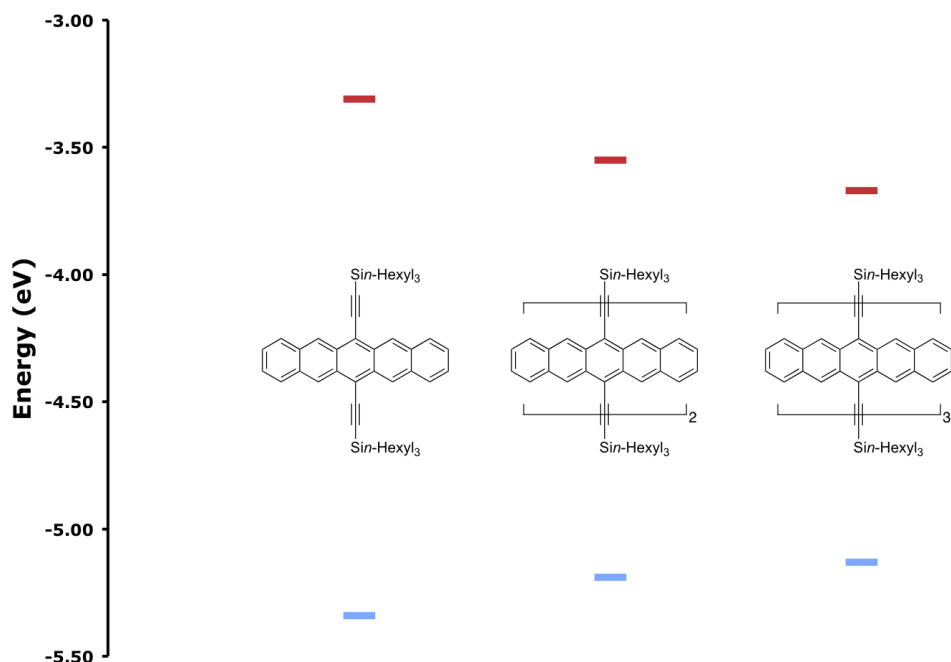


Figure 4-8. HOMO-LUMO energy levels of conjugated pentacenes **4.33–4.35** as measured in THF.¹⁶

CV of oligomers **4.33–4.35** in CH_2Cl_2 results in poor resolution of the cathodic waves. This is highlighted by the three broad reductions of trimer **4.35** ($E_{\text{red1}} = -1.20$ V, $E_{\text{red2}} = -1.58$ V, and $E_{\text{red3}} = -1.92$ V Figure 4-9c), when compared with the six individual reductions observed for **4.35** in THF (Figure 4-7c). It should also be noted the presence of a small anodic wave (*ca.* -0.7 to -1.0 V vs Ag/Ag^+) present after initial reduction, similar to that observed for polarized pentacene **4.23j**.¹⁵ The anodic waves of **4.33–4.35**, however, are better resolved in CH_2Cl_2 and cathodically shifted versus those in THF. For example, trimer **4.35** displays three oxidations, with $E_{\text{ox1}} = 0.14$ V in CH_2Cl_2 (versus $E_{\text{ox1}} = 0.34$ V in THF). This results in smaller HOMO-LUMO gaps for the series in CH_2Cl_2 than those observed in THF ($E_{\text{g}}^{\text{electro}} = 1.83\text{--}1.33$ eV in CH_2Cl_2 , vs $E_{\text{g}}^{\text{electro}} = 2.03\text{--}1.46$ eV in THF). $E_{\text{g}}^{\text{electro}}$ values for the series in CH_2Cl_2 were in better agreement with the UV-vis

determined E_g^{opt} values (for **4.33–4.35**, $E_g^{\text{opt}} = 1.86$ eV, 1.57 eV, and 1.39 eV, respectively). The HOMO-LUMO gap for the conjugated oligomers at the 6,13-positions of pentacene are significantly lower than those of regio-irregular polymers conjugated at the 2,9- and 2,10-positions, **4.16–4.18** ($E_g^{\text{electro}} = 1.64–1.70$ eV).

Table 4-5. Electrochemical properties of conjugated pentacene oligomers **4.33–4.35** in CH_2Cl_2 (vs Fc/Fc^+ couple).^[a]

Cmpd	E_{ox1} / V	E_{ox2} / V	E_{ox3} / V	E_{red1} / V	E_{red2} / V	E_{red3} / V	E_{red4} / V	E_g^{electro} / eV
4.33	0.34	–	–	–1.49	–1.97	–	–	1.83
4.34	0.25	0.47	–	–1.26	–1.42	–1.90	–2.13	1.51
4.35 ^[d]	0.14 ^[c]	0.34 ^[c]	0.56 ^[c]	–1.20 ^[b]	–1.58 ^[b]	–1.92 ^[b]	–	1.33

[a] Cyclic voltammetry was performed in THF solutions containing 0.1 M *n*-Bu₄NPF₆ as supporting electrolyte at a scan rate of 150 mV/s. The working electrode was a platinum disc, the counter electrode was a platinum wire, and the reference electrode was a non-aqueous Ag/AgNO₃ [10 mM] in MeCN. The potential values (E) were calculated using the following equation (except where otherwise noted): $E = (E_{\text{pc}} + E_{\text{pa}})/2$, where E_{pc} and E_{pa} correspond to the cathodic and anodic peak potentials, respectively. Potentials are referenced to the ferrocene/ferrocenium (Fc/Fc^+) couple used as an internal standard. E_g^{electro} determined from the separation between the first oxidation and first reduction potentials. [b] Represents a two-electron event. [c] The oxidation potential was estimated by reporting E_{pa} of the oxidation wave. [d] Scan rate of 200 mV/s.

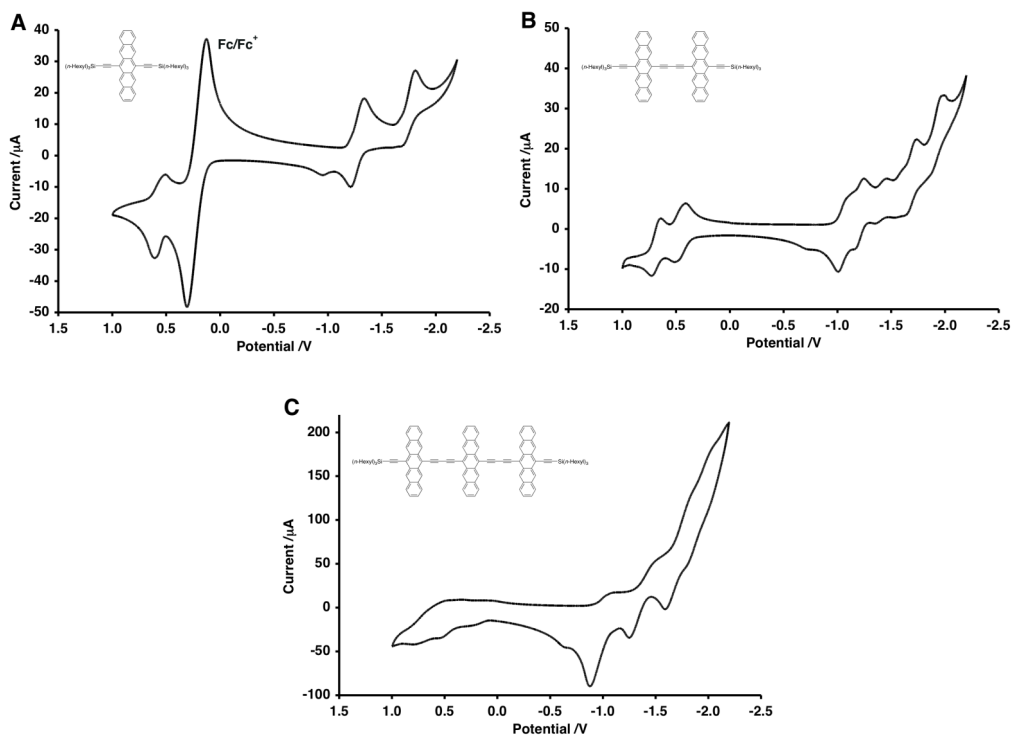


Figure 4-9. CV plots of pentacenes (a) **4.33**, (b) **4.34**, and (c) **4.35** as measured in CH_2Cl_2 (vs Ag/Ag^+).

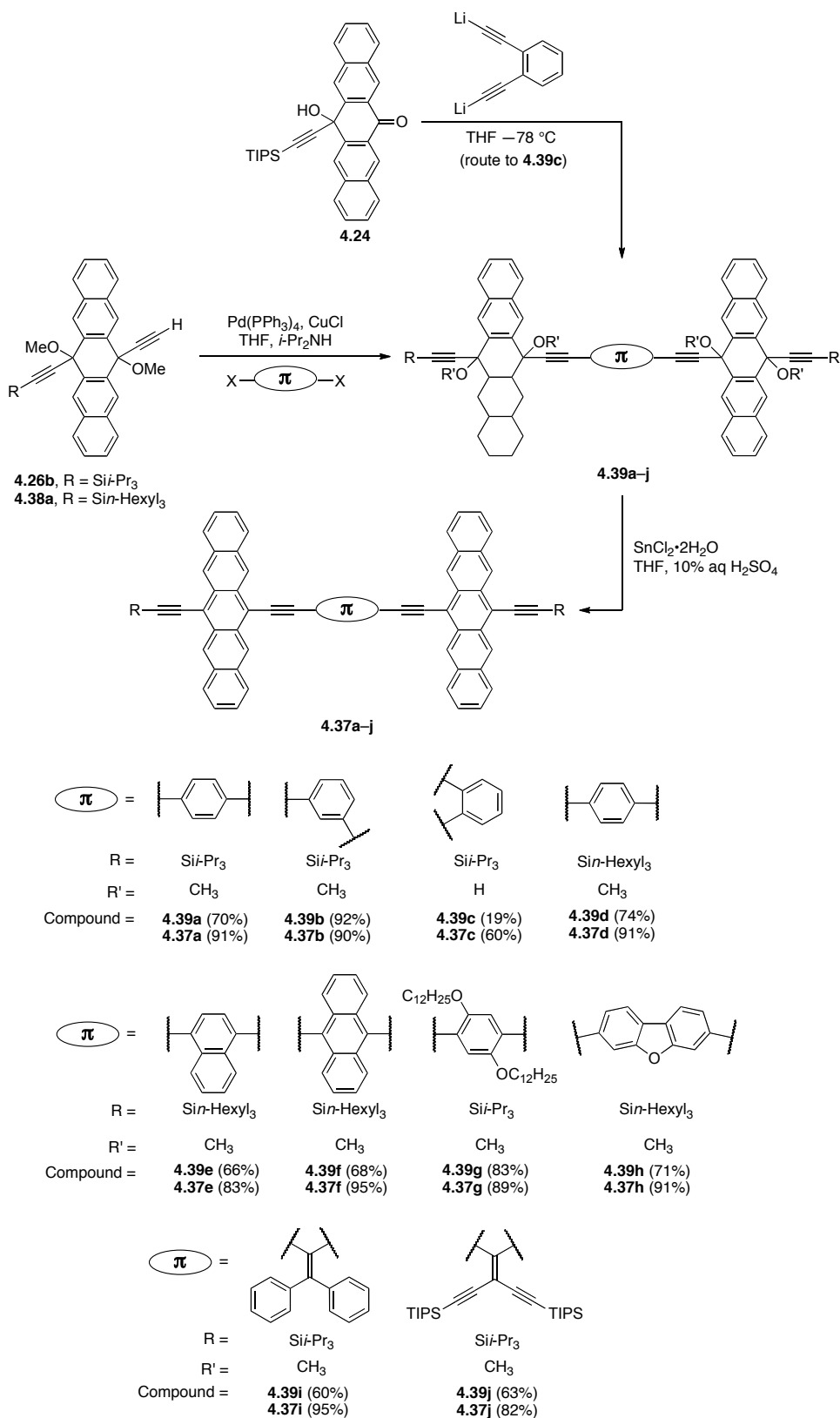
4.5 Synthesis and Electrochemical Properties of Conjugated Dimers of Diethynylpentacene Linked by π -Spacers

While the synthesis of conjugated pentacenes **4.33–4.36** highlights the efficient electronic communication between chromophores when substituted at the 6,13-positions of pentacene, the resulting poor solubility of the larger structures limits this approach to moving beyond tetramer **4.36**. An alternative approach would be to incorporate π -spacers between the pentacene units, which could serve as solubilizing groups. The synthesis of a series of conjugated pentacene dimers **4.37a–j** was carried out by a colleague, Dr. Dan Lehnerr (Scheme 4-11).¹² The synthesis began with the Sonogashira cross-coupling reaction of methylethers **4.26b** or **4.38a** with the appropriate dihalogenated arene, to yield the dimers **4.39a–j**. It should be noted that **4.39c** was prepared by an alternative route; the

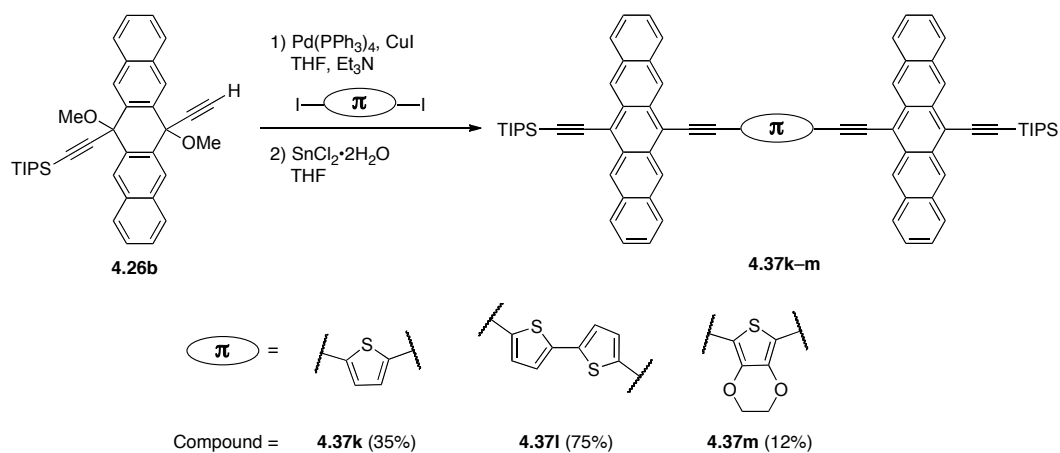
addition of lithiated *ortho*-diethynylbenzene to ketone **4.24**. Dimers **4.39a–j** were then reduced to pentacenes **4.37a–j** in moderate to good yields (60–91%).

Conjugated pentacene dimers containing thiophene linkers, **4.37k–m**, were prepared using methodology established by Dr. Lehnerr (Scheme 4-12). Sonogashira cross-coupling reaction of methylether **4.26b** with the appropriate diiodothiophene afforded dimeric **4.39k–m**, which were not isolated but directly reduced to conjugated pentacenes **4.37k–m** in moderate yields (12–75%).

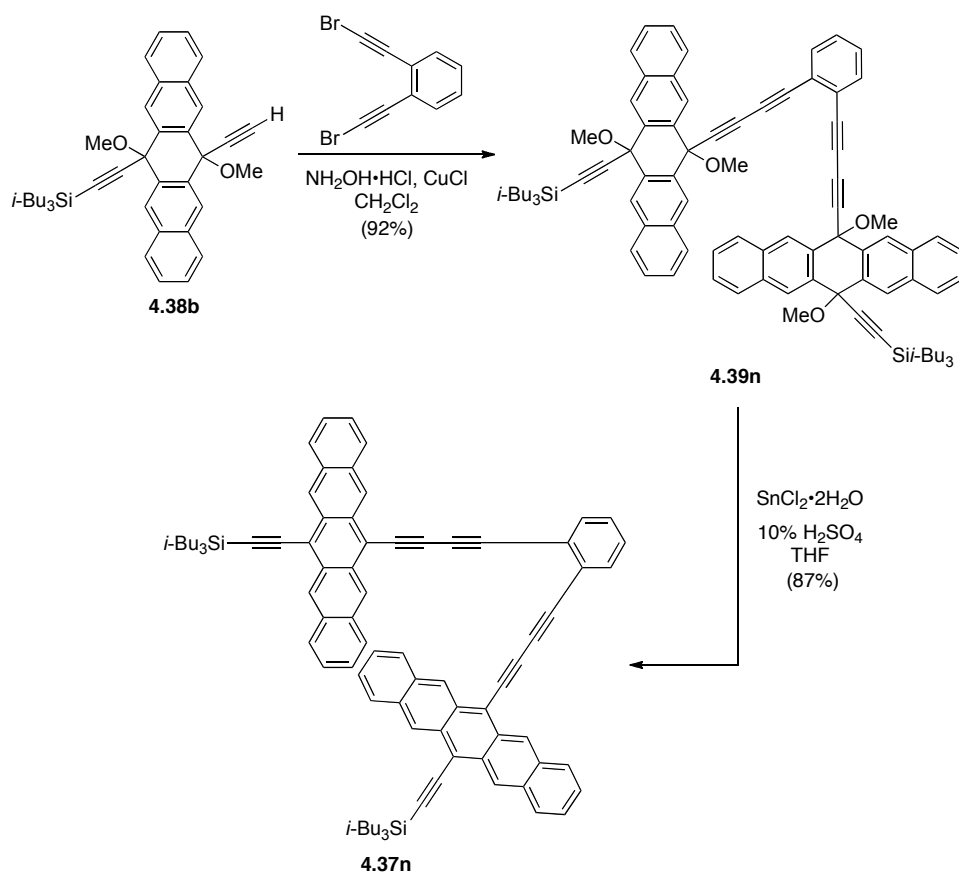
Butadiyne linked phenyl dimer **4.37n** was prepared through the use of a Cadiot-Chodkiewicz reaction (Scheme 4-13) by Dr. Dan Lehnerr. Cross-coupling of **4.38b** and 1,2-bis(bromoethynyl)benzene afforded **4.39n** in 92% yield. Reductive aromatization of **4.39n** gave **4.37n** in 87% yield.



Scheme 4-11. Synthesis of conjugated pentacene dimers **4.37a-j**.



Scheme 4-12. Synthesis of conjugated pentacene dimers **4.37k–m**.



Scheme 4-13. Synthesis of conjugated pentacene dimer **4.37n** via a Cadiot-Chodkiewicz reaction.


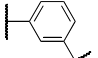
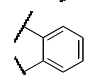
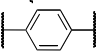
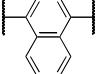
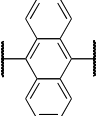
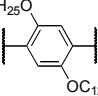
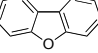
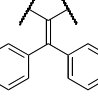
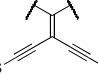
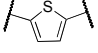
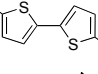
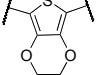
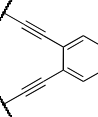
The electrochemical properties of pentacenes **4.37a–n** have been investigated using cyclic voltammetry (Table 4-6, Figure 4-10, Figure 4-11, Figure 4-12). The poor solubility of pentacenes **4.37f** and **4.37l–m** prevented their electrochemical analysis. Isomeric pentacenes **4.37a–c** display similar electrochemical behaviour, with a few notable differences. *Ortho*-isomer **4.37c** shows the lowest oxidation potential ($E_{\text{ox}1} = 0.26$ V), possibly a result of intramolecular π -stacking of the pentacene moieties as this would aid in stabilization of the resulting radical cation. An increased electron density on the pentacene moiety would also account for the cathodic shift in first reduction potential (0.08 V) of *ortho*-isomer **4.37c** when compared to the *para*-isomer **4.37a**. In addition, the second oxidation and reduction potentials of *ortho*-isomer **4.37c** ($E_{\text{ox}2} = 0.53$ V, $E_{\text{red}2} = -1.95$ V) are both higher than *para*-isomer **4.37a** ($E_{\text{ox}2} = 0.39$ V, $E_{\text{red}2} = -1.85$ V), which further supports a delocalized radical cation (or anion) across the two pentacene moieties via an intramolecular π -stacking interaction. Interestingly, *meta*-isomer **4.37b**, which does not contain a linear conjugation pathway between each pentacene moiety, possesses a HOMO-LUMO gap ($E_{\text{g}}^{\text{electro}} = 1.77$ eV), analogous to that of pentacene monomer **4.23e** ($E_{\text{g}}^{\text{electro}} = 1.83$ eV).

Benzannulation of the phenylene spacer results in a lowering of the band gap, as demonstrated by naphthylene-linked dimer **4.37e** ($E_{\text{g}}^{\text{electro}} = 1.63$ eV) versus phenylene-linked dimer **4.37d** ($E_{\text{g}}^{\text{electro}} = 1.72$ eV). However, the increase in benzannulation of the PAH spacer results in a marked decrease in solubility, with anthrylene-linked dimer **4.37f** being insufficiently soluble for electrochemical analysis.

The incorporation of heteroatoms into the π -spacer does not have a significant impact on the electrochemistry of the dimers. Alkoxy substituted phenylene linked dimer **4.37g** exhibited very similar electrochemistry to phenylene linked dimer **4.37a**, and possessed an identical band gap ($E_{\text{g}}^{\text{electro}} = 1.72$ eV). It was also noted that the long alkoxy chains did not result in improved solubility. Dibenzofuranylene linked dimer **4.37h**

possessed the same band gap as *meta*-substituted phenylene linked dimer **4.37b** ($E_g^{\text{electro}} = 1.77$ eV).

Table 4-6. Electrochemical properties (vs Fc/Fc⁺ couple)^[a] and optical band gap^[b] of pentacenes **4.37a–n**.

Cmpd	π -Spacer	End Group	E_{ox1} / V	E_{ox2} / V	E_{red1} / V	E_{red2} / V	E_{red3} / V	E_g^{electro} / eV	E_g^{opt} / eV
4.37a		<i>Sii</i> -Pr ₃	0.29	0.39	-1.43	-1.85	–	1.72	1.71
4.37b		<i>Sii</i> -Pr ₃	0.31	0.45	-1.46	-1.63	-1.92	1.77	1.75
4.37c		<i>Sii</i> -Pr ₃	0.26	0.53	-1.50	-1.95	-2.06	1.76	1.70
4.37d		<i>Sin</i> -Hexyl ₃	0.30	–	-1.42	-1.70	-2.12	1.72	1.71
4.37e		<i>Sin</i> -Hexyl ₃	0.20	0.31	-1.43	-1.82	-2.20	1.63	1.67
4.37f		<i>Sin</i> -Hexyl ₃	– ^[d]	– ^[d]	– ^[d]	– ^[d]	– ^[d]	– ^[d]	1.58
4.37g		<i>Sii</i> -Pr ₃	0.31	–	-1.41	-1.79	-2.01	1.72	1.59
4.37h		<i>Sin</i> -Hexyl ₃	0.30	0.40	-1.47	-1.73	-1.93	1.77	1.77
4.37i		<i>Sii</i> -Pr ₃	0.29	0.45	-1.46	-2.01	-2.12	1.75	1.71
4.37j		<i>Sii</i> -Pr ₃	0.37	0.49	-1.34	-1.54	-1.82 ₂ , -2.11 ^[f]	1.71	1.64
4.37k^[c]		<i>Sii</i> -Pr ₃	0.36	0.74	-1.38	-1.91	-2.12	1.74	1.61
4.37l		<i>Sii</i> -Pr ₃	– ^[d]	– ^[d]	– ^[d]	– ^[d]	– ^[d]	– ^[d]	1.63
4.37m		<i>Sii</i> -Pr ₃	– ^[d]	– ^[d]	– ^[d]	– ^[d]	– ^[d]	– ^[d]	1.62
4.37n		<i>Sii</i> -Bu ₃	0.32	0.35	-1.38	-1.85	–	1.70	1.69

[a] Cyclic voltammetry was performed in CH₂Cl₂ solutions containing 0.1 M *n*-Bu₄NPF₆ as supporting electrolyte at a scan rate of 150 mV/s. The working electrode was a

platinum disc, the counter electrode was a platinum wire, and the reference electrode was a non-aqueous Ag/AgNO₃ [10 mM] in MeCN. The potential values (E) were calculated using the following equation (except where otherwise noted): $E = (E_{pc} + E_{pa})/2$, where E_{pc} and E_{pa} correspond to the cathodic and anodic peak potentials, respectively. Potentials are referenced to the ferrocene/ferrocenium (Fc/Fc⁺) couple used as an internal standard. E_g^{electro} determined from the separation between the first oxidation and first reduction potentials. [b] The wavelength used as the absorption edge for determining HOMO-LUMO energy gap corresponds to the lowest energy absorption that has molar absorption coefficient $\epsilon \geq 1000 \text{ L mol}^{-1} \text{ cm}^{-1}$. [c] The reference electrode was an aqueous Ag/AgCl/NaCl [3M]. [d] Data not measured due to poor soluble. [e] E_{red4} .

Thienylene linked dimer **4.37l** was the most difficult of the functionalized aryl linked pentacenes to oxidize ($E_{\text{ox1}} = 0.36 \text{ V}$), despite the electron donating behaviour of the thiophene unit. The band gap of **4.37l** ($E_g^{\text{electro}} = 1.74 \text{ eV}$) is similar to that of 3-thienyl substituted monomer **4.23j** ($E_g^{\text{electro}} = 1.76 \text{ eV}$). Bithienylene linked **4.37l** and ethylenedioxythienylene linked **4.37m** are both too insoluble for electrochemical analysis.

Tetraethynylethylenylene (TEE) linked dimer **4.37j** and diphenyldiethynylethylenylene (DPDEE) linked dimer **4.37i** exhibited similar electrochemistry to the phenylene-linked dimers. TEE linked dimer **4.37j** was more difficult to oxidize ($E_{\text{ox1}} = 0.37 \text{ V}$) than DPDEE linked dimer **4.37i** ($E_{\text{ox1}} = 0.29 \text{ V}$), yet much more readily reduced ($E_{\text{red1}} = -1.34 \text{ V}$ for **4.37j**, versus $E_{\text{red1}} = -1.46 \text{ V}$ for **4.37i**). This can be explained by strong electron withdrawing nature of TEEs, and their increased delocalization relative to DPDEEs. While the pentacene moieties are connected via cross-conjugation, they are linearly conjugated to the *i*-Pr₃Si-C≡C unit in **4.37j**, resulting in a band gap ($E_g^{\text{electro}} = 1.72 \text{ eV}$) similar to *para*-phenylene linked dimer **4.37a** ($E_g^{\text{electro}} = 1.71$

eV).

Ortho-phenylene butadiyne linked pentacene **4.37n** shows electrochemical behaviour similar to that of *para*-phenylene linked dimer **4.37a**. While the geometry is similar to that of *ortho*-isomer **4.37c**, the butadiyne spacers seem to provide sufficient distance between the pentacene moieties to prevent significant intramolecular π -stacking interactions. This is supported by the more difficult oxidation of **4.37n** ($E_{\text{ox1}} = 0.32$ V) versus **4.37c** ($E_{\text{ox1}} = 0.26$ V). Instead of facilitating π -stacking, the butadiyne linker serves to increase the linear conjugation length, resulting in an easier reduction of **4.37n** ($E_{\text{red1}} = -1.38$ V) in comparison to **4.33c** ($E_{\text{red1}} = -1.50$ V). This results in a HOMO-LUMO gap for pentacene **4.37n** ($E_{\text{g}}^{\text{electro}} = 1.70$ eV) closer to that of the *para*-isomer **4.37a** ($E_{\text{g}}^{\text{electro}} = 1.72$ eV) than to **4.37c**.

Cyclic voltammetry of the majority of conjugated dimers **4.37a–n** reveals the presence of a small anodic wave (*ca.* -0.75 to -1.0 V, versus Ag/Ag^+), which was only present after initial reduction of the pentacenes. This is consistent with the electrochemically generated radical dianion reacting with adventitious water to generate small amounts of a partially protonated product, similar to that observed for the polarized pentacenes.¹⁵

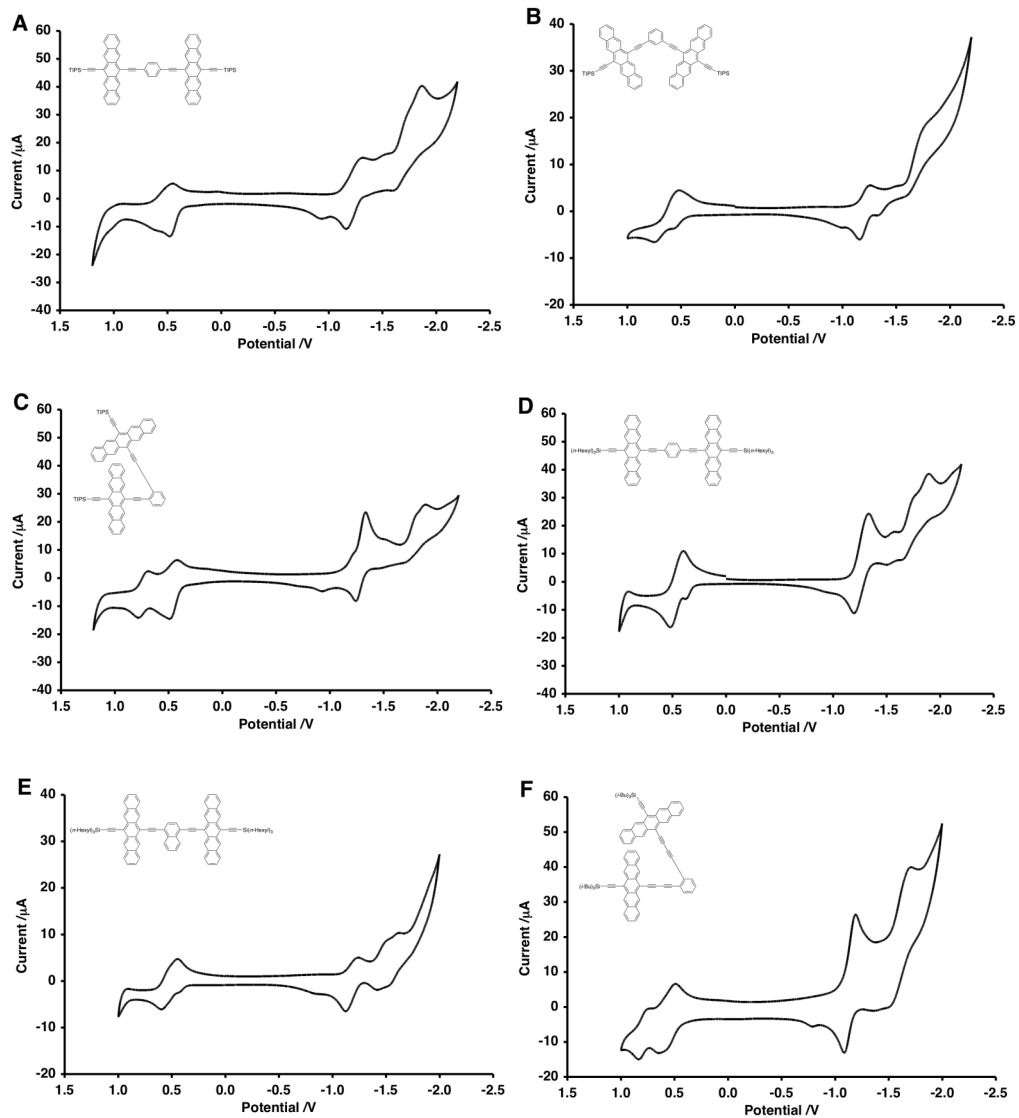


Figure 4-10. CV plots of pentacenes (a) **4.37a**, (b) **4.37b**, (c) **4.37c**, (d) **4.37d**, (e) **4.37e**, and (f) **4.37f** as measured in CH_2Cl_2 (vs Ag/Ag^+).

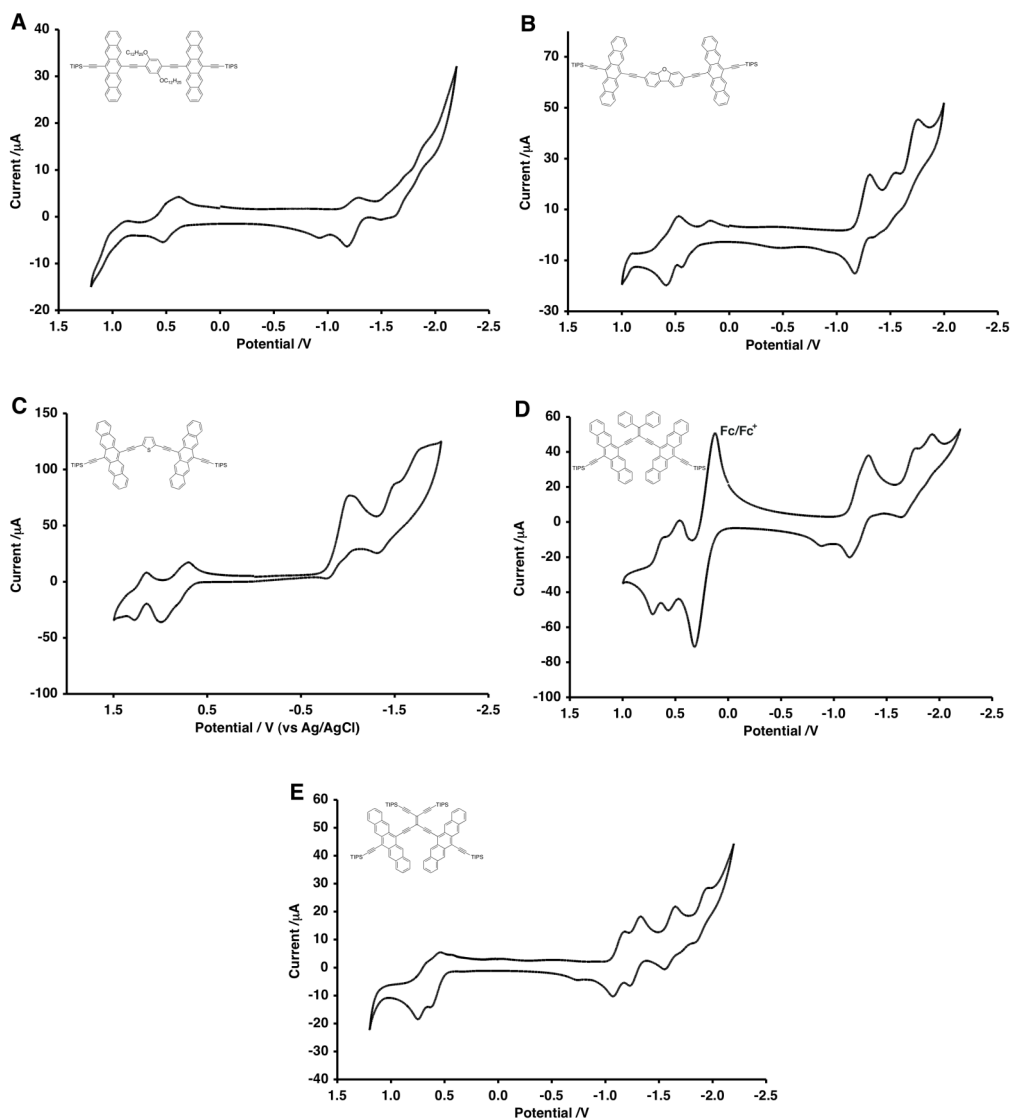


Figure 4-11. CV plots of pentacenes (a) 4.37g, (b) 4.37h, (c) 4.37k, (d) 4.37i, and (e) 4.37j as measured in CH_2Cl_2 (vs Ag/Ag^+).

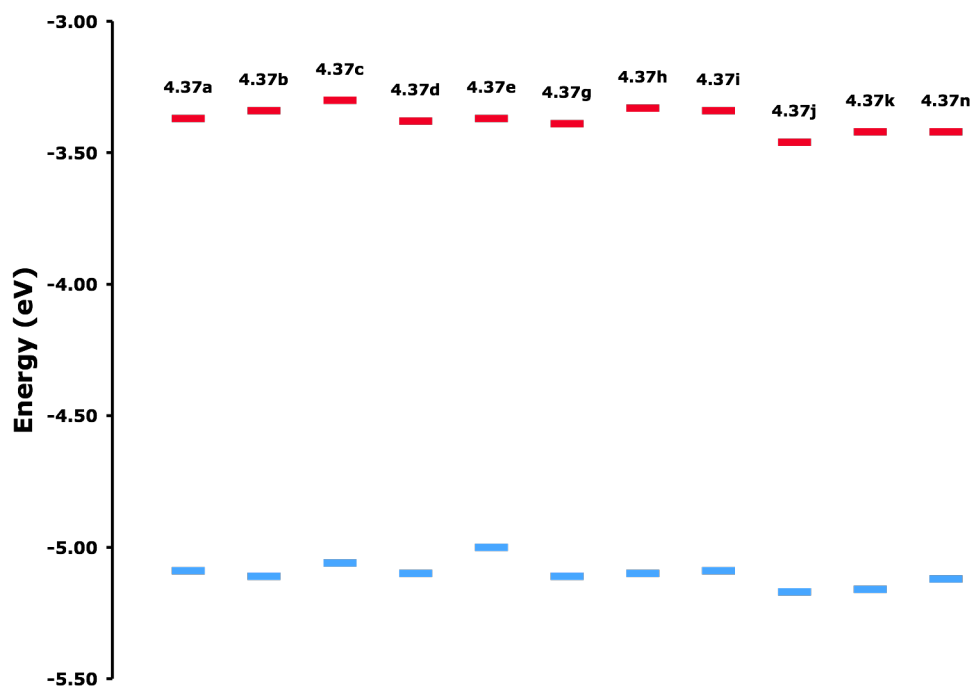
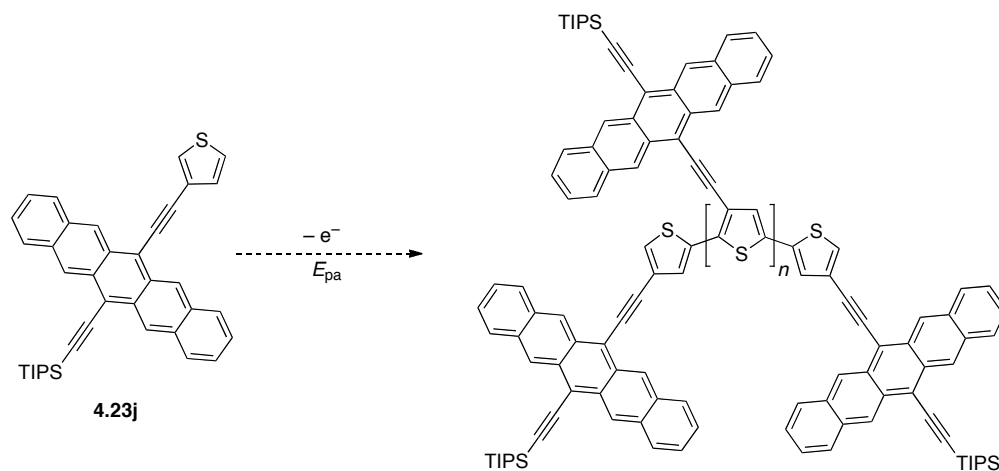


Figure 4-12. HOMO-LUMO energy levels of conjugated pentacene dimers **4.37a–n**.¹⁶

4.6 Attempted Electrochemical Polymerization of **4.23j**

It is known that thiophenes undergo oxidative polymerization, which can be initiated electrochemically.¹³ The incorporation of the thiophene moiety to the pentacene framework opens the possibility of forming conjugated pentacene-thiophene polymers via an electrochemical reaction. Thus, the polymerization of thienyl substituted pentacene **4.23j** was attempted using cyclic voltammetry (Scheme 4-14, Figure 4-13). Following the initial redox scan, successive sweeps showed no increase in current, suggesting that no conducting polymer was being deposited on the electrode. Varying the scan rate and increasing the concentration of **4.23j** had no effect on the formation of a polymer film.



Scheme 4-14. Attempted electrochemical polymerization of pentacene **4.23j**.

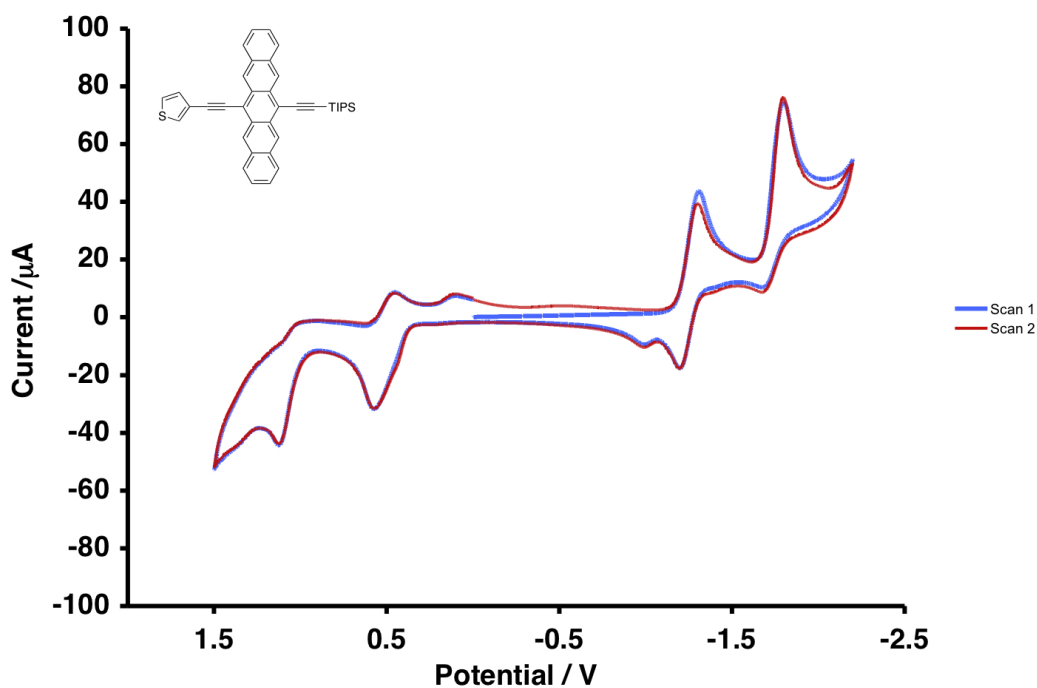


Figure 4-13. Attempted electrochemical polymerization of **4.23j** using CV as measured in CH_2Cl_2 (vs Ag/Ag^+).

4.7 Conclusion

The electronic properties of several series of conjugated pentacene molecules have been studied using cyclic voltammetry. In addition, a series of thienyl substituted

pentacenes have been prepared and studied using cyclic voltammetry. Varying the substitution of the groups appended to pentacene at the 6,13-positions shows a stronger influence than previously reported for substitution at the 2,9- and 2,10- positions. Linking multiple pentacene chromophores together via the 6,13-position has the most dramatic impact on the electronic properties, with butadiyne linker giving the largest decrease in band gap. The trend of decreasing band gap with oligomer length is also accompanied by a marked decrease in solubility, which unfortunately limits the application of this approach.

4.8 References

1. (a) Anthony, J. E. *Chem. Rev.* **2006**, *106*, 5028–5048. (b) Anthony, J. E. *Angew. Chem. Int. Ed.* **2008**, *47*, 452–483.
2. Bendikov, M.; Wudl, F.; Perepichka, D. F. *Chem. Rev.* **2004**, *104*, 4891–4945.
3. (a) Clar, E.; John, F. *Chem. Ber.* **1930**, *63*, 2967–2977. (b) Clar, E.; John, F. *Chem. Ber.* **1931**, *63*, 2194–2200.
4. Reid, W.; Anthöfer, F. *Angew. Chem.* **1954**, *66*, 604–604.
5. Bruckner, V.; Karczag, A.; Kormendy, K.; Meszaros, M.; Tomasz, J. *Tetrahedron Lett.* **1961**, *1*, 5–6.
6. Mauldings, D. R.; Roberts, B. G. *J. Org. Chem.* **1969**, *34*, 1734–1736.
7. Sakamoto, Y.; Suzuki, T.; Kobayashi, M.; Gao, Y.; Fukai, Y.; Inoue, Y.; Sato, F.; Tokito, S. *J. Am. Chem. Soc.* **2004**, *126*, 8138–8140.
8. (a) Anthony, J. E.; Brooks, J. S.; Eaton, D. L.; Parkin, S. R. *J. Am. Chem. Soc.* **2001**, *123*, 9482–9483. (b) Anthony, J. E.; Eaton, D. L.; Parkin, S. R. *Org. Lett.* **2002**, *4*, 15–18.
9. Lehnerr, D.; Tykwinski, R. R. *Aust. J. Chem.* **2011**, *64*, 919–929.

10. Tokito, S.; Weinfurter, K.-H.; Fujikawa, H. Tsutsui, T.; Taga, Y. *Proc. SPIE-Int. Opt. Soc. Eng.* **2001**, *4105*, 69–74.
11. (a) Okamoto, T.; Bao, Z. *J. Am. Chem. Soc.* **2007**, *129*, 10308–10309. (b) Okamoto, T.; Jiang, Y.; Qu, F.; Mayer, A. C.; Parmer, J. E.; McGehee, M. D.; Bao, Z. *Macromolecules* **2008**, *41*, 6977–6980.
12. Lehnherr, D. PhD Thesis, University of Alberta, 2010.
13. Roncali, J. *Chem. Rev.* **1992**, *92*, 711–738.
14. *The Chemistry of Anilines*, Parts 1 and 2 (Ed.: Rappoport, Z.), Wiley-VCH, Weinheim, **2007**.
15. This EC mechanism has been reported for anthracene, see: Parker, V. D.; Tilset, M.; Hammerich, O. *J. Am. Chem. Soc.* **1987**, *109*, 7906–7908.
16. The HOMO and LUMO energy levels were estimated from the first oxidation and reduction potentials vs Fc/Fc^+ , using the equation $E = -1 \cdot (E_{\text{ox1/red1}} + 4.8 \text{ eV})$, based on the premise that the energy level of ferrocene/ferrocenium is 4.8 eV below the vacuum level. a) Bard, A. J.; Faulkner, L. R. (Eds.) *Electrochemical Methods: Fundamentals and Applications*, Wiley-VCH, Weinheim (**2000**). b) Pommerehne, J.; Vestweber, H.; Guss, W.; Mahrt, R. F.; Bässler, H.; Porsch, M.; Daub, J. *Adv. Matter.* **1995**, *7*, 551–554.

Chapter 5 – Conclusions and Future Outlook

5.1 Conclusions

The work presented in this thesis has focused on the synthesis and study of conjugated carbon materials, namely 1) the synthesis of graphyne model compounds and the study of their optical and electronic properties, and 2) the electrochemical investigations of a series of functionalized pentacene molecules.

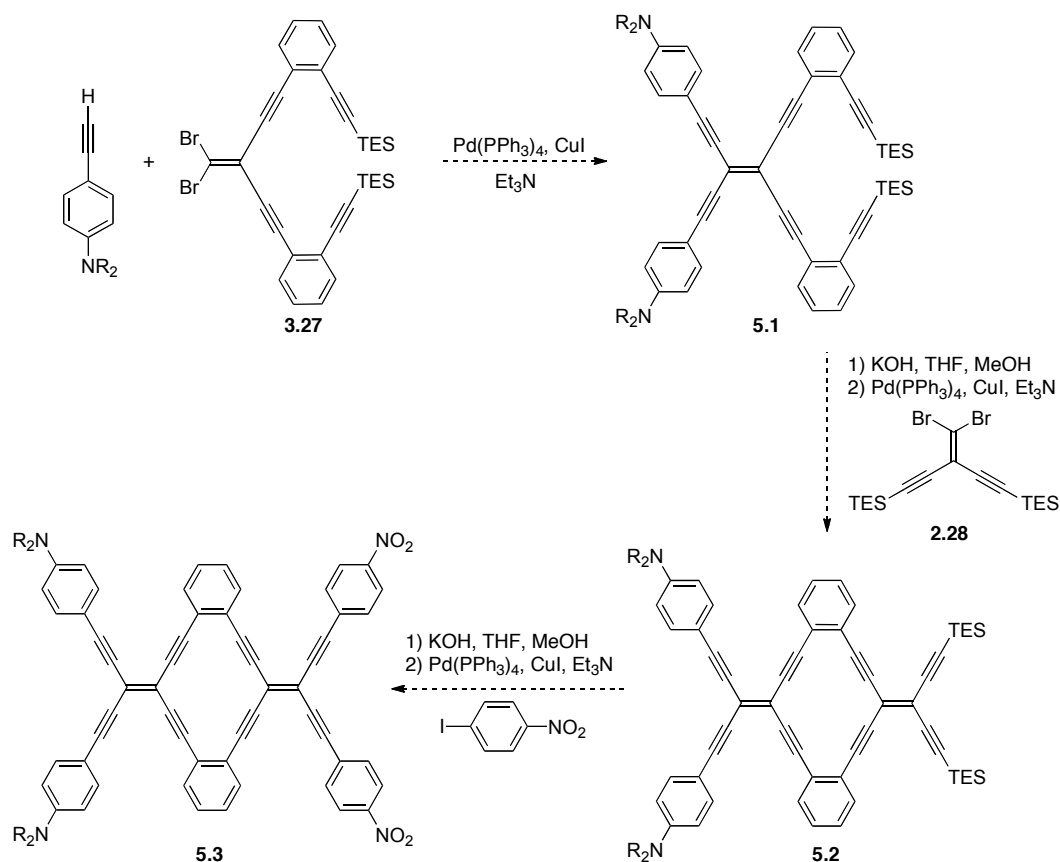
Chapter 2 focused on synthetic efforts to prepare model compounds for 12,12,12-graphyne. The goal was to prepare a series of expanded radialenes to serve as model structures of this form graphyne. Unfortunately, the formation of undesirable side products and low yielding reactions prevented realization of the target radialenes. Many of the intermediate building blocks, however, served as valuable precursors to other conjugated structures, such as the radiaannulenes described in Chapter 3.

Chapter 3 described efforts to prepare model compounds of 6,6,12-graphyne, via the synthesis of a series of oligomeric radiaannulenes. A variety of synthetic routes were attempted, including a one-pot approach and several stepwise routes. While the one-pot method could rapidly provide monomeric radiaannulenes in the fewest possible steps (*ca.* 10% yield in one step), it was not efficient for the preparation of longer oligomers. Instead, a stepwise approach using building block **3.27** allowed for the synthesis of mono-, di-, and trimeric radiaannulenes. Unfortunately, trimeric radiaannulene **3.7c** was unexpectedly unstable in CDCl₃, and could not be fully characterized. Sufficient material was recovered, however, to provide UV-vis analysis, which suggested that the effective conjugation length in this graphyne series had been effectively reached by the stage of the trimer ($E_g^{\text{opt}} = 2.38 \text{ eV}$). The result suggested a significantly higher band gap for the model compounds than predicted for 6,6,12-graphyne (predicted to be a zero band-gap semiconductor). Thus, this may not be an effective model structure for 6,6,12-graphyne.¹

Chapter 4 focused on the electrochemical analysis of several series of functionalized pentacene molecules. A large number of substituted pentacenes were studied using CV to determine the impact of substitution on the properties of the pentacene framework. Electrochemical analysis revealed substitution at the 6,13-positions of pentacene had a much stronger influence on the electronic properties than substitution at the 2,9- and 2,10-positions.² A conjugated series of pentacenes connected at the 6,13-positions by butadiyne linkers showed the most dramatic decrease in bandgap (down to $E_g \approx 1.4$ eV), reaching the effective conjugation length by the stage of the tetramer.

5.2 Outlook

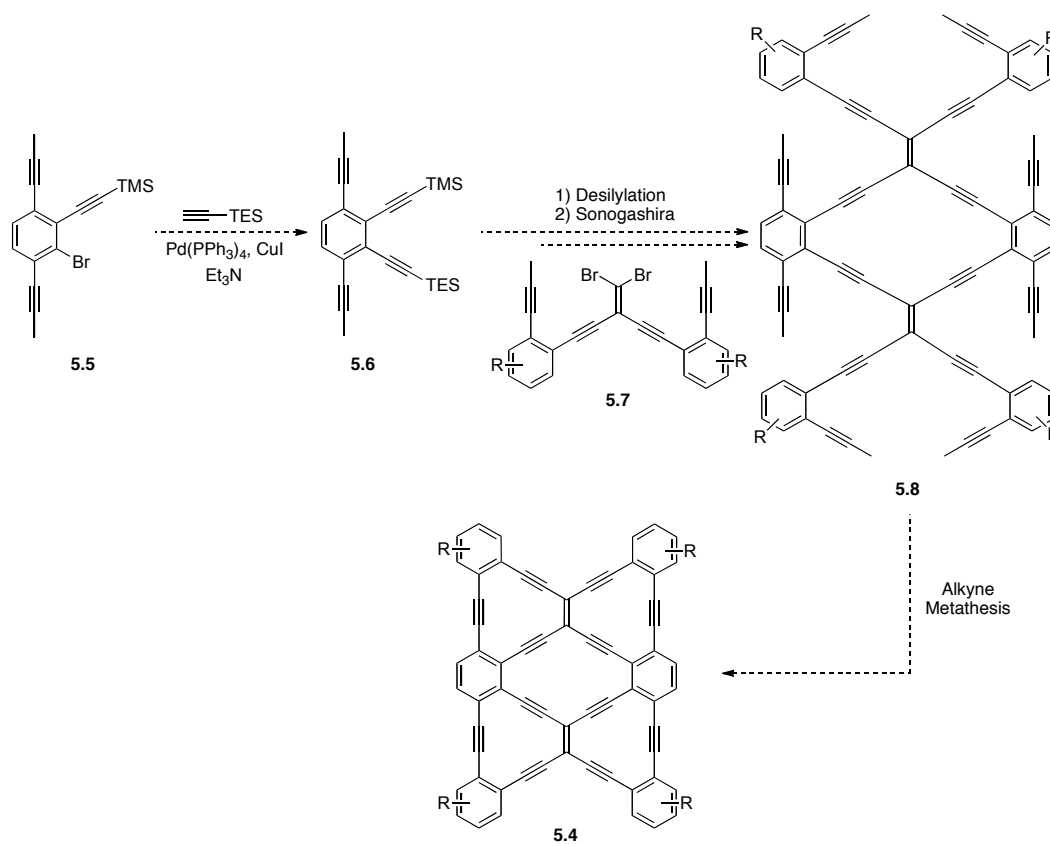
There are many possibilities for extension of the graphyne research project, particularly in the area of radiannulenes and 6,6,12-graphyne. First, the synthesis of unsymmetrical radiannulene **3.20** allows for the synthesis of differently functionalized radiannulenes. However, the approach described in this thesis fails to provide radiannulenes functionalized with electron-donating substituents. Further optimization of this procedure should allow for the synthesis of these donor-substituted materials. Alternatively, it should be possible to attach the electron-donating substituents to compound **3.27** to give functionalized **5.1**, and subsequent cyclization to give donor substituted radiannulene **5.2** would be possible (Scheme 5-1). Subsequent desilylation and cross-coupling should then allow for the synthesis of a donor-acceptor radiannulene **5.3** (Scheme 5-1).



Scheme 5-1. Proposed synthesis of donor functionalized radiannulene **5.2** and donor / acceptor radiannulene **5.3**.

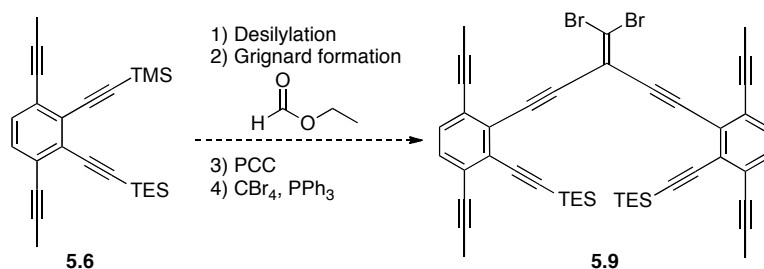
When examining the electronic characteristics of the series of radiannulenes **7a–c** prepared to study 6,6,12-graphyne, it was clear from the band gap corresponding to the effective conjugation length was much higher than that predicted for 6,6,12-graphyne. Thus, an alternative molecular scaffold may need to be considered to better model 6,6,12-graphyne. One such series of molecules would be available through fusion of the outer benzene rings with an acetylene linker, such as radiannulene **5.4**. It should be possible to prepare such a compound using a combination of methodology developed in this thesis, and building blocks developed using methodology developed by Vollhardt in combination with alkyne metathesis used by Haley (Scheme 5-2).^{3,4} For example,

triethynylbenzenes similar to **5.5** have been prepared by Vollhardt, and could serve as a precursor tetraethynylbenzene **5.6**. This could be carried through a series of Sonogashira cross-coupling reactions with dibromoolefin **5.7** to yield radiannulene **5.8**. Intramolecular alkyne metathesis, similar to that used by Haley, should provide fused radiannulene **5.4**.



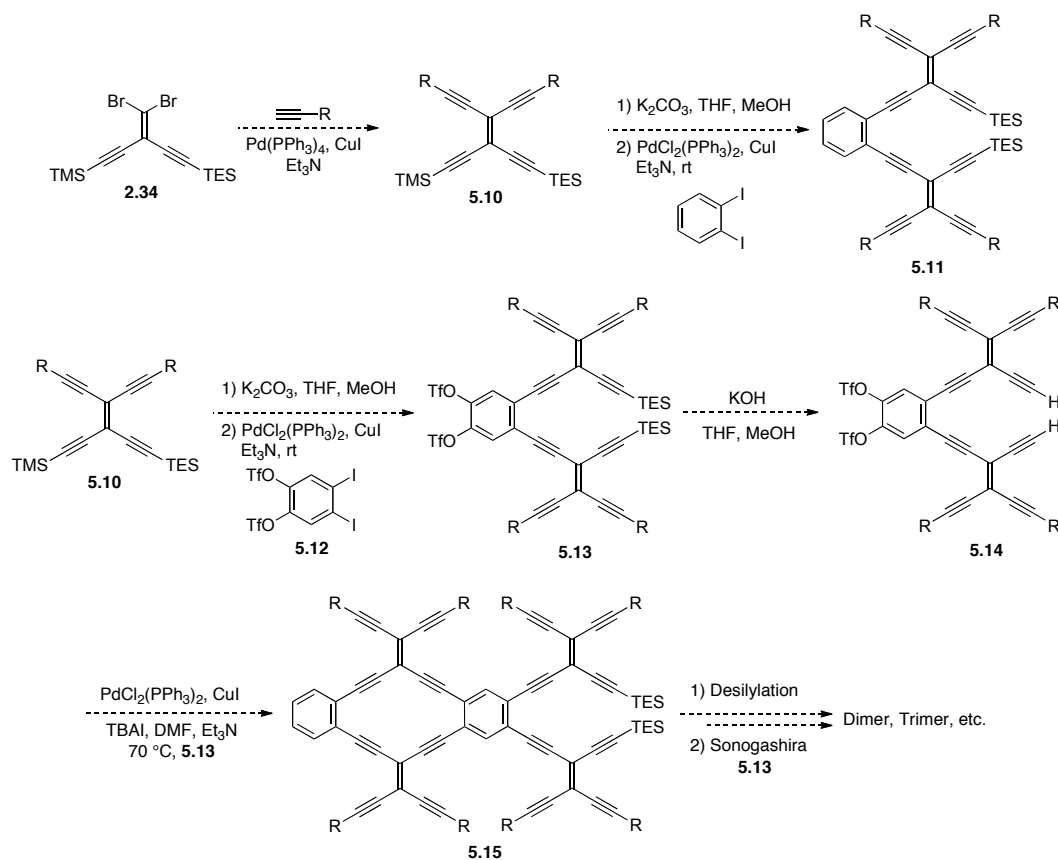
Scheme 5-2. Proposed synthesis of fused radiannulene **5.4**.

Similar to the use of **3.27** in the synthesis of radiannulene oligomers **3.7a–c**, compound **5.9** could serve as the key building block in the stepwise synthesis of fused radiannulene oligomers (Scheme 5-3).



Scheme 5-3. Proposed synthesis of compound **5.9**.

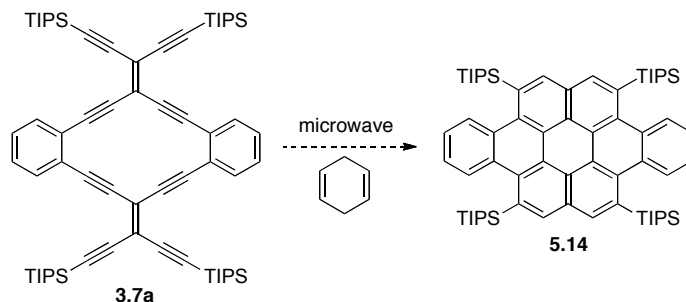
If the synthesis of synthesis of radiannulene oligomers **3.7a–c** is thought of as expansion in a north-south direction, an alternative approach would be to expand the structure of the model compounds in an east-west direction. This could be accomplished using TEEs such as **5.10** as a starting point, prepared from dibromoolefin **2.34** (Scheme 5-4). Selective desilylation and Sonogashira cross-coupling reaction with 1,2-diodobenzene would give end unit **5.11**. Alternatively, desilylation of **5.10** and selective Sonogashira cross-coupling with 4,5-diodo-1,2-phenylene bis-triflate **5.12**, as described by Dussault and coworkers⁵ would yield building block **5.13**. Finally, a combination of **5.14** and **5.13** would give radiannulene **5.15**, which could undergo several iterations of desilylation and cross-coupling reaction with **5.13** to extend the series.



Scheme 5-4. Proposed synthesis to east-west radiannulene oligomers.

It is also worth considering that radiannulenes such as **3.7a** do not need to be thought of as final target molecules, but instead intermediates to other interesting structures. An intriguing observation made during the synthesis of the oligomeric series of radiannulenes was their exothermic transitions in DSC. Similar observations have been reported for a series of 1,2-bis(ethynyl)benzenes. Etzkorn and coworkers used the DSC transition as the temperature required to induce a microwave assisted Bergman cyclization to produce a series of naphthalene derivatives.⁶ Utilizing these reaction conditions, microwave assisted Bergman cyclization of **3.7a** in the presence of 1,4-cyclohexadiene could produce dibenzo[A,J]coronene **5.14** (Scheme 5-5). Considering the methodology developed in this thesis for the synthesis of radiannulenes **3.7a** and its

derivatives, Bergman cyclization of these molecules could provide a novel route to a variety of functionalized coronenes.



Scheme 5-5. Proposed synthesis of dibenzo[A,J]coronene **5.14** via Bergman cyclization of **3.7a**.

5.3 References

1. Malko, D.; Neiss, C.; Vines, F.; Görling, A. *Phys. Rev. Lett.* **2012**, *108*, 086804.
2. (a) Okamoto, T.; Bao, Z. *J. Am. Chem. Soc.* **2007**, *129*, 10308–10309. (b) Okamoto, T.; Jiang, Y.; Qu, F.; Mayer, A. C.; Parmer, J. E.; McGehee, M. D.; Bao, Z. *Macromolecules* **2008**, *41*, 6977–6980.
3. Miljanic, O. S.; Holmes, D.; Vollhardt, K. P. C. *Org. Lett.* **2005**, *7*, 4001–4004.
4. (a) Johnson II, C. A.; Lu, Y.; Haley, M. M. *Org. Lett.* **2007**, *9*, 3725–3728. (b) Schrock, R. R. *Acc. Chem. Res.* **1986**, *19*, 342–348. (c) Schrock, R. R. *Polyhedron* **1995**, *14*, 3177–3195. (d) Zhang, W.; Kraft, S.; Moore, J. S. *J. Am. Chem. Soc.* **2004**, *126*, 329–335. (e) Zhang, W.; Moore, J. S. *J. Am. Chem. Soc.* **2005**, *127*, 11863–11870. (f) Zhang, W.; Moore, J. S. *Adv. Synth. Catal.* **2007**, *349*, 93–120.
5. Fisher, T. J.; Dussault, P. H. *Eur. J. Org. Chem.* **2012**, 2831–2836.
6. (a) Kane, C. M.; Meyers, T. B.; Yu, X.; Gerken, M.; Etzkorn, M. *Eur. J. Org.*

Chem. **2011**, 2969–2980. (b) Jones, R. R.; Bergman, R. G. *J. Am. Chem. Soc.*
1972, *94*, 660–661.

Chapter 6 – Experimental Section

6.1 General Experimental Details

Reagents were purchased in reagent grade from commercial suppliers and used without further purification. THF, Et₂O, and benzene were distilled from sodium/benzophenone ketyl. Hexanes, CH₂Cl₂, and MeCN were distilled from CaH₂. *i*-Pr₂NH was distilled from NaOH pellets; Ethylformate was distilled from molecular sieves (Type 4Å, 0.125 inch); Et₃N was distilled over NaOH pellets. Evaporation and concentration *in vacuo* was done at water-aspirator pressure. All reactions were performed in standard, dry glassware under an inert atmosphere of nitrogen or argon. Column chromatography and “plugging”: silica gel-60 (230–400 mesh). Thin Layer Chromatography (TLC): pre-coated plastic sheets covered with 0.20 mm silica gel with fluorescent indicator UV 254 nm; visualization by UV light or KMnO₄ stain. Melting points are uncorrected.

¹H and ¹³C NMR spectra were collected at 27 °C in CDCl₃, CD₂Cl₂, and (CD₃)₂CO; solvent peaks as reference. Coupling constants are reported as observed (±0.5 Hz). For simplicity, the coupling constants of the aryl protons for *para*-substituted aryl groups have been reported as pseudo first-order (i.e., doublets), even though they are second-order (AA'XX') spin systems.

UV-vis absorption spectra were acquired at rt using a Varian Cary 400 Scan Spectrometer or a Varian Cary 5000 UV-vis-NIR spectrometer; λ_{max} in nm (ε in L·mol⁻¹·cm⁻¹). Emission spectra were recorded using Photon Technology International (PTI) MP1 Fluorescence system. Solutions for fluorescence experiments were deoxygenated with nitrogen or argon. The excitation wavelength and maximum intensity emission

wavelength are denoted as λ_{exc} and $\lambda_{\text{max,em}}$, respectively.

For mass spectral analyses, low-resolution data are provided in cases when M^+ is not the base peak; otherwise, only high-resolution data are provided. The samples for ESI mass spectrometry were dissolved in $\text{ClCH}_2\text{CH}_2\text{Cl}$ and made use of a 3:1 MeOH/toluene mixture as the carrier solvent. MALDI mass spectrometry used the matrix *trans*-2-[3-(4-*tert*butylphenyl)-2-methyl-2-propenylidene]malononitrile (DCTB). The samples for APPI were dissolved in THF/MeOH.

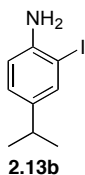
Differential scanning calorimetry (DSC) measurements were measured on a Perkin Elmer Pyris 1 DSC instrument. Thermogravimetric analyses (TGA) were carried out on a Perkin Elmer Pyris 1 TGA instrument. All thermal analyses were carried out under a flow of nitrogen with a heating rate of 10 °C/min. Thermal decomposition temperature as measured by TGA (as sample weight loss) are reported as T_d in which the temperature listed corresponds to the intersection of the tangent lines of the baseline and the edge of the peak corresponding to the first significant weight loss, typically >5%. Melting points from DSC analysis are reported as the peak maxima, except in cases when the sample decomposed, in which case the onset temperature of the decomposition exothermic peak is reported, as well as the exothermic maxima corresponding to the decomposition.

Cyclic voltammetry experiments were done using a Bioanalytical Systems, Inc. (BASi) Epsilon Rotating-Disk Electrode (Model RDE-2). Data was analyzed by BASi Epsilon-EC Ver. 2.00.71–USB, BASi ComServer Ver. 1.03 on a PC computer. A three-electrode cell was used, using platinum disk working electrode and a platinum wire counter electrode. A Ag/AgCl (3M NaCl) aqueous reference electrode or Ag/Ag⁺ (0.01

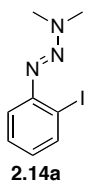
M AgNO₃, 0.1 M *n*-Bu₄NPF₆ solution in MeCN) quasi-reference electrode was used. Ferrocenium/ferrocene (Fc⁺/Fc) couple was used as an internal standard. The potential values (*E*) were calculated using the following equation (except where otherwise noted): $E = (E_{pc} + E_{pa})/2$, where *E*_{pc} and *E*_{pa} correspond to the cathodic and anodic peak potentials, respectively. The potential values obtained in reference to Ag/Ag⁺ were converted to potentials versus ferrocenium/ferrocene (Fc⁺/Fc). Solution cyclic voltammetry was performed using ca. 1 mM solution of the analyte in CH₂Cl₂ or THF or a mixture of benzene/MeCN (as noted in the figure or table captions) containing 0.1 M *n*-Bu₄NPF₆ as supporting electrolyte at a scan rate of 150 mV·s⁻¹, except where noted otherwise. All solutions were deoxygenated with N₂ before each experiment and a blanket of N₂ was used over the solution during the experiment. The working electrode was polished with 0.05 μm alumina polish prior to each scan.

X-ray analysis was carried out on a Nonius KappaCCS diffractometer by Dr. Frank Hampel at the Friedrich-Alexander-Universität Erlangen-Nürnberg. X-ray crystallographic data for unpublished compounds is available from the X-ray Crystallographic Laboratory, Department Chemie und Pharmazie, Universität Erlangen-Nürnberg, Henkestraße 42, 91054, Erlangen, Germany; phone: 09131 85-22988, -22952, fax: 09131 85-23031, -26865. These data can be obtained by using the ADM code provided.

6.2 Experimental Details for Chapter 2

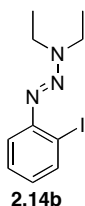


To a solution of 4-isopropylaniline (10 mL, 9.9 g, 73 mmol) in CH_2Cl_2 (150 mL) and MeOH (75 mL) was added benzyltriethylammonium dichloroiodate (28.24 g, 72.36 mmol) and CaHCO_3 (12.44 g, 148.1 mmol) at 0 °C. The solution was warmed to rt and stirred for 1 h. The reaction was quenched via the addition of saturated H_2O (200 mL). The aq phase was extracted with CH_2Cl_2 (2 x 25 mL). The combined organic phase was washed with H_2O (100 mL) and saturated aq NaCl (100 mL), dried with MgSO_4 , filtered, and the solvent removed *in vacuo*. Column chromatography (silica gel, 2:1 Hex/ CH_2Cl_2) afforded **2.13b** (16.65 g, 87%) as a yellow oil. $R_f = 0.35$ (2:1 CH_2Cl_2 /Hex). IR (neat film): 3446 (m), 3357 (m), 3014 (w), 2954 (s), 2865 (m), 1611 (s), 1494 (s). ^1H NMR (300 MHz, CDCl_3) δ 7.48 (dd, $J = 2.0$ Hz, 0.3 Hz, 1H), 7.00 (ddd, $J = 8.0$ Hz, 2.0 Hz, 0.5 Hz, 1H), 6.68 (d, $J = 8.2$ Hz, 1H), 3.81 (s, 2H), 2.75 (sept, $J = 6.9$ Hz, 1H), 1.17 (d, $J = 6.9$ Hz, 6H). ^{13}C NMR (75 MHz, CDCl_3) δ 144.5, 140.9, 136.6, 127.5, 114.7, 84.5, 32.8, 24.1. EI MS m/z 261.0 (M^+ , 55) 246.0 ($[\text{M} - \text{Me}]^+$, 100]. EI HRMS m/z calcd for $\text{C}_9\text{H}_{12}\text{NI}$ (M^+) 261.0015, found 261.0014.



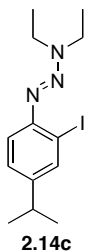
To a solution of 2-iodoaniline (10.02 g, 45.76 mmol) in THF (40 mL), MeCN (60 mL) and H_2O (40 mL) was slowly added conc HCl (48 mL) and NaNO_2 (6.616 g, 95.90 mmol) at -5 °C. The bright yellow slurry was stirred under N_2 for 30 min, maintaining a temperature between -5 °C and 0 °C, and then transferred via cannula to a flask charged

with aq Me₂NH (51.88 g, 454.5 mmol, 40%) and K₂CO₃ (31.58 g, 228.5 mmol) dissolved in MeCN (60 mL) and H₂O (100 mL). The reaction was warmed to rt over 30 min and quenched via the addition of H₂O (100 mL). The aq phase was extracted with Et₂O (2 x 100 mL). The combined organic phase was washed with H₂O (50 mL) and saturated aq NaCl (50 mL), dried with MgSO₄, filtered, and the solvent removed *in vacuo*. Purification by column chromatography (silica gel, 3:1 Hex/CH₂Cl₂) afforded **2.14a** (10.15 g, 81%) as an orange oil. *R*_f = 0.5 (2:1 Hex/CH₂Cl₂). IR (ATR): 3053 (w), 2900 (m), 2785 (w), 1562 (w), 1452 (m). ¹H NMR (300 MHz, CDCl₃) δ 7.83 (dd, *J* = 7.8, 1.3, 1H), 7.36 (dd, *J* = 8.1, 1.6, 1H), 7.26 (ddd, *J* = 8.2, 7.1, 1.2, 1H), 6.83 (ddd, *J* = 7.9, 7.1, 1.7, 1H), 3.51 (br s, 3H), 3.26 (br s, 3H). ¹³C NMR (75 MHz, CDCl₃) δ 150.0, 139.0, 128.7, 126.7, 117.6, 96.5, 43.0, 36.5. ESI MS *m/z* 276 ([M + H]⁺, 100), 231 ([M – NMe₂]⁺, 40). ESI HRMS *m/z* calcd for C₈H₁₁IN₃ ([M + H]⁺) 275.9992, found 275.9989.

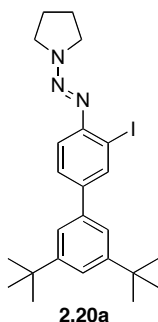


To a solution of 2-iodoaniline (2.411 g, 11.01 mmol) in THF (15 mL), MeCN (10 mL) and H₂O (10 mL) was slowly added conc HCl (11 mL) and NaNO₂ (1.595 g, 23.12 mmol) at –5 °C. The bright yellow slurry was stirred under N₂ for 30 min, maintaining a temperature between –5 °C and 0 °C, then transferred via cannula to a flask charged with Et₂NH (12 mL, 8.5 g, 120 mmol) and K₂CO₃ (7.6 g, 55 mmol) dissolved in MeCN (25 mL) and H₂O (15 mL). The reaction was warmed to rt over 30 min and quenched via the addition of H₂O (50 mL). The aq phase was extracted with Et₂O (2 x 50 mL). The combined organic phase was washed with H₂O (20 mL) and saturated aq NaCl (20 mL), dried with MgSO₄, filtered, and the solvent removed *in vacuo*. Purification by column chromatography (silica gel, 2:1 Hex/CH₂Cl₂) afforded **2.14b** (2.736 g, 82%) as an orange

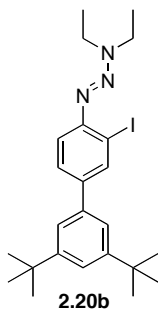
oil. $R_f = 0.5$ (2:1 Hex/CH₂Cl₂). IR (ATR): 3055 (w), 2968 (s), 2929 (s), 2868 (m), 1610 (m), 1576 (m). ¹H NMR (400 MHz, CDCl₃) δ 7.2 (dd, $J = 7.8, 1.2$, 1H), 7.34 (dd, $J = 8.0, 1.6$, 1H), 7.25 (ddd, $J = 8.1, 7.1, 1.4$, 1H), 6.81 (ddd, $J = 7.9, 7.1, 1.7$, 1H), 3.78 (q, $J = 7.2$, 4H), 1.31 (t, $J = 7.0$, 6H). ¹³C NMR (100 MHz, CDCl₃) δ 150.4, 139.0, 128.6, 126.5, 117.5, 96.5, 49.0, 42.1, 14.6, 11.0. MALDI MS m/z 304 ([M + H]⁺, 100).



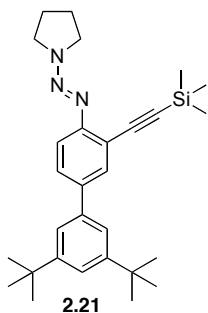
To a solution of **2.13b** (5.231 g, 20.03 mmol) in THF (15 mL), MeCN (35 mL) and H₂O (15 mL) was slowly added conc HCl (18 mL) and NaNO₂ (2.924 g, 42.38 mmol) at -5 °C. The bright yellow slurry was stirred under N₂ for 30 min, maintaining a temperature between -5 °C and 0 °C, then transferred via cannula to a flask charged with Et₂NH (20 mL, 15 g, 204 mmol) and K₂CO₃ (19.837 g, 143.53 mmol) dissolved in MeCN (50 mL) and H₂O (65 mL). The reaction was warmed to rt over 30 min and quenched via the addition of H₂O (50 mL). The aq phase was extracted with Et₂O (2 x 50 mL). The combined organic phase was washed with H₂O (20 mL) and saturated aq NaCl (20 mL), dried with MgSO₄, filtered, and the solvent removed *in vacuo*. Purification by column chromatography (silica gel, 2:1 CH₂Cl₂/Hex) afforded **2.14c** (6.399 g, 93%) as an orange oil. $R_f = 0.75$ (2:1 CH₂Cl₂/Hex). ¹H NMR (400 MHz, CDCl₃) δ 7.66 (d, $J = 1.9$ Hz, 1H), 7.22 (d, $J = 3.1$ Hz, 1H), 7.10 (dd, $J = 8.3$ Hz, 1.9 Hz, 1H), 3.74 (q, $J = 7.1$ Hz, 4H), 2.79 (sept, $J = 6.9$ Hz, 1H), 1.27 (t, $J = 7.1$ Hz, 6H), 1.19 (d, $J = 6.9$ Hz, 6H). EI MS m/z 345.07 (M⁺, 45), 272.99 ([M - NEt₂]⁺, 45), 244.98 ([M - N₃Et₂]⁺, 100].



To a solution of **2.19** (3.004 g, 7.375 mmol) in THF (20 mL), MeCN (13 mL) and H₂O (13 mL) was slowly added conc HCl (7 mL) and NaNO₂ (1.026 g, 14.87 mmol) at -5 °C. The bright yellow slurry was stirred under N₂ for 30 min, maintaining a temperature between -5 °C and 0 °C, then transferred via cannula to a flask charged with pyrrolidine (6.2 mL, 5.2 g, 73 mmol) and K₂CO₃ (5.092 g, 36.84 mmol) dissolved in MeCN (20 mL) and H₂O (30 mL). The reaction was warmed to rt over 30 min and quenched via the addition of H₂O (50 mL). The aq phase was extracted with Et₂O (2 x 50 mL). The combined organic phase was washed with H₂O (20 mL) and saturated aq NaCl (20 mL), dried with MgSO₄, filtered, and the solvent removed *in vacuo*. Purification by column chromatography (silica gel, 3:1 Hex/CH₂Cl₂) afforded **2.20a** (3.280 g, 91%) as an orange oily solid. *R_f* = 0.4 (3:1 Hex/CH₂Cl₂). IR (CH₂Cl₂ cast film): 3060 (w), 2963 (s), 2903 (m), 2869 (m), 1594 (m). ¹H NMR (400 MHz, CDCl₃) δ 8.06 (d, *J* = 1.9 Hz, 1H), 7.51 (dd, *J* = 8.3 Hz, 1.9 Hz, 1H), 7.43–7.37 (m, 4H), 2.96 (br s, 2H), 3.79 (br s, 2H), 2.11–2.00 (m, 4H), 1.38 (s, 18H). ¹³C NMR (100 MHz, CDCl₃) δ 151.2, 149.5, 140.8, 139.0, 137.7, 127.9, 121.6, 121.4, 117.3, 96.9, 51.1, 47.3, 35.0, 31.5, 24.0, 23.6. ESI HRMS *m/z* calcd for C₂₄H₃₃N₃I ([M + H]⁺) 490.1714, found 490.1713.

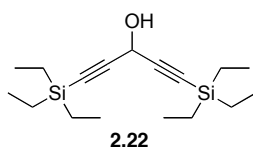


To a solution of **2.19** (2.319 g, 5.694 mmol) in THF (10 mL), MeCN (5 mL) and H₂O (5 mL) was slowly added conc HCl (6 mL) and NaNO₂ (0.828 g, 12.00 mmol) at -5 °C. The bright yellow slurry was stirred under N₂ for 30 min, maintaining a temperature between -5 °C and 0 °C, then transferred via cannula to a flask charged with diethylamine (6.0 mL, 4.3 g, 58 mmol) and K₂CO₃ (4.000 g, 28.94 mmol) dissolved in MeCN (20 mL) and H₂O (30 mL). The reaction was warmed to rt over 30 min and quenched via the addition of H₂O (50 mL). The aq phase was extracted with Et₂O (2 x 50 mL). The combined organic phase was washed with H₂O (20 mL) and saturated aq NaCl (20 mL), dried with MgSO₄, filtered, and the solvent removed *in vacuo*. Purification by column chromatography (silica gel, 5:1 Hex/CH₂Cl₂) afforded **2.20b** (2.086 g, 75%) as a yellow oil. *R*_f = 0.6 (3:1 Hex/CH₂Cl₂). ¹H NMR (300 MHz, CDCl₃) δ 8.04 (d, *J* = 1.9 Hz, 1H), 7.50 (dd, *J* = 8.3 Hz, 1.9 Hz, 1H), 7.41–7.36 (m, 4H), 3.81 (q, *J* = 7.1 Hz, 4H), 1.36 (s, 18H), 1.32 (t, *J* = 7.2 Hz, 6H).



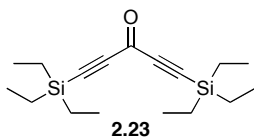
To a solution of **2.20a** (3.133 g, 6.401 mmol) in deoxygenated, dry *i*-Pr₂NH (50 mL) was added PdCl₂(PPh₃)₂ (0.116 g, 0.165 mmol) and CuI (0.061 g, 0.32 mmol). The solution

was purged with argon for an additional 10 min after which trimethylsilylacetylene (3.7 mL, 2.6 g, 27 mmol) was added. The flask was sealed under argon with a rubber septum and stirred for 18 h. The reaction was quenched via the addition of saturated aq NH₄Cl (100 mL). The aq phase was extracted with Et₂O (2 x 50 mL). The combined organic phase was washed with H₂O (50 mL) and saturated aq NaCl (50 mL), dried with MgSO₄, filtered, and the solvent removed *in vacuo*. Purification by column chromatography (silica gel, 1:1 CH₂Cl₂/Hex) afforded **2.21** (2.512 g, 85%) as a pale yellow, oily solid. *R*_f = 0.35 (1:1 Hex/CH₂Cl₂). IR (microscope): 3064(w), 2962(s), 2902 (m), 2966 (m), 2155 (m), 1593 (m). ¹H NMR (500 MHz, CDCl₃) δ 7.69 (d, *J* = 1.3 Hz, 1H), 7.50–7.46 (m, 2H), 7.40–7.39 (m, 3H), 3.97 (br s, 2H), 3.77 (br s, 2H), 2.06 (br s, 4H), 1.39 (s, 18H), 0.29 (s, 9H). ¹³C NMR (100 MHz, CDCl₃) δ 151.20, 151.1, 139.6, 138.7, 131.7, 128.4, 121.4, 121.3, 117.9, 117.1, 103.7, 98.2, 51.0, 46.6, 35.0, 31.5, 23.9, 23.8, 0.2. ESI HRMS *m/z* for C₂₉H₄₂N₃Si ([M + H]⁺) 460.3143, found 460.3144.

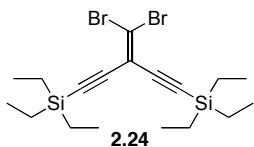


To a solution of triethylsilylacetylene (10.3 mL, 8.06 g, 57.5 mmol) in dry THF (125 mL) was added *n*-hexyl lithium (25 mL, 58 mmol, 2.3 M in hexanes) at –78 °C. The solution was stirred for 30 min at –78 °C, and ethyl formate (2.2 mL, 2.0 g, 27 mmol) was then added. The solution was gradually warmed to rt and stirred under argon for 1 h. The reaction was quenched via the addition of saturated aq NH₄Cl (150 mL). The aq phase was extracted with Et₂O (2 x 100 mL). The combined organic phase was washed with H₂O (50 mL) and saturated aq NaCl (50 mL), dried with MgSO₄, filtered, and the solvent removed *in vacuo*. Column chromatography (silica gel, 2:1 Hex/CH₂Cl₂) afforded **2.22** (8.0 g, 95%) as a yellow oil. *R*_f = 0.40 (1:1 Hex/CH₂Cl₂). IR (neat film): 3600–3300 (br,

m), 2956 (s), 2937 (m) 2877 (s) 2176 (w) ^1H NMR (400 MHz, CDCl_3) δ 5.07 (d, $J = 6.7$ Hz, 1H), 2.17 (d, $J = 7.2$ Hz, 1H), 0.97 (t, $J = 7.9$ Hz, 18H), 0.59 (q, $J = 7.9$ Hz, 12H). ^{13}C NMR (100 MHz, CDCl_3) δ 103.4, 87.1, 53.1, 7.4, 4.2. ESI MS m/z 331.2 ($[\text{M} + \text{Na}]^+$, 100)

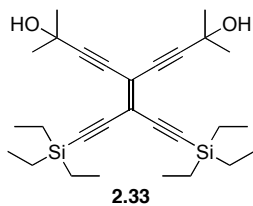


To a solution of **2.22** (1.10 g, 3.56 mmol) in dry CH_2Cl_2 (150 mL) was added 4Å mol. sieves (1.5 g), celite (1.5 g) and PCC (1.17 g, 5.44 mmol). The solution was stirred for 24 h at rt. The reaction was passed through a plug of silica gel with CH_2Cl_2 . Solvent removal *in vacuo* afforded **2.23** (1.04 g, 95%) as a yellow oil. $R_f = 0.65$ (1:1 Hex/ CH_2Cl_2). IR (neat film): 2957 (s), 2938 (m) 2914 (m) 2878 (s) 2158 (m), 1636 (s). ^1H NMR (400 MHz, CDCl_3) δ 1.00 (t, $J = 7.9$ Hz, 18H), 0.67 (q, $J = 7.9$ Hz, 12H). ^{13}C NMR (100 MHz, CDCl_3) δ 160.1, 104.2, 98.0, 7.2, 3.8. ESI MS m/z 329.2 ($[\text{M} + \text{Na}]^+$, 100), 307.2 ($[\text{M} + \text{H}]^+$, 90). ESI HRMS m/z calcd for $\text{C}_{17}\text{H}_{31}\text{OSi}_2$ ($[\text{M} + \text{H}]^+$) 307.1908, found 307.1909.

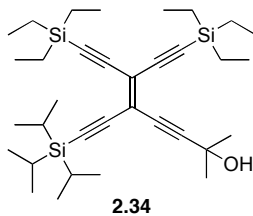


To a solution of PPh_3 (3.540 g, 13.49 mmol) and CBr_4 (2.24 g, 6.75 mmol) in dry CH_2Cl_2 (40 mL) was added a solution of **2.23** (0.970 g, 3.16 mmol) in dry CH_2Cl_2 (10 mL). The solution was stirred for 3 h at rt. The reaction was quenched via the addition of hexanes, followed by a passing through a plug of silica gel with hexanes. Solvent removal *in vacuo* afforded **2.24** (1.226 g, 83%) as a yellow oil. $R_f = 0.60$ (Hexanes). IR (neat film): 2957 (s) 2936 (m) 2912 (s) 2876 (s), 2155 (w), 2131 (w). ^1H NMR (400 MHz, CDCl_3) δ 1.00 (t, $J = 7.9$ Hz, 18H), 0.63 (q, $J = 7.9$ Hz, 12H). ^{13}C NMR (100 MHz, CDCl_3) δ 114.7,

109.5, 101.5, 100.4, 7.4, 4.1. EI HRMS m/z calcd for $C_{18}H_{30}^{79}Br^{81}BrSi_2$ (M^+) 462.0232, found 462.0241.

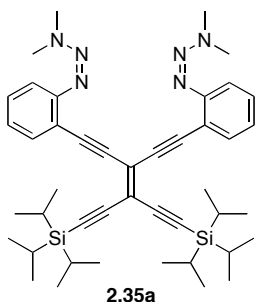


To a solution of **2.24** (460 mg, 0.98 mmol) and 2-methyl-3-butyn-2-ol (0.30 mL, 250 mg, 3.6 mmol) in dry, deoxygenated *i*-Pr₂NH (5 mL) was added Pd(PPh₃)₄ (66 mg, 0.057 mmol) and CuI (25 mg, 0.13 mmol). The flask was sealed under argon with a rubber septum and stirred at rt for 18 h. The reaction was quenched via the addition of saturated aq NH₄Cl (25 mL). The aq phase was extracted with Et₂O (2 x 15 mL). The combined organic phase was washed with H₂O (20 mL) and saturated aq NaCl (20 mL), dried with MgSO₄, filtered, and the solvent removed *in vacuo*. Column chromatography (silica gel, 3:1 Hex/EtOAc) afforded **2.33** (457 mg, 99%) as an amber oily solid. $R_f = 0.35$ (3:1 Hex/EtOAc). IR (neat): 3500–3200 (br), 2982 (s), 2957 (s), 2876 (m), 2207 (w), 2146 (w). ¹H NMR (400 MHz, CDCl₃) δ 1.99 (s, 2H), 1.54 (s, 12H), 0.99 (t, $J = 7.9$ Hz, 18H), 0.62 (q, $J = 7.9$ Hz, 12H). ¹³C NMR (100 MHz, CDCl₃) δ 117.8, 116.8, 102.9, 102.5, 102.2, 79.6, 65.7, 31.1, 7.4, 4.2. EI HRMS m/z calcd for $C_{28}H_{44}O_2Si_2$ (M^+) 468.2880, found 468.2883.



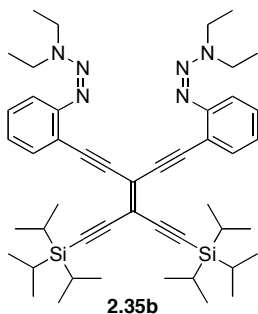
To a solution of **2.24** (655 mg, 1.42 mmol), PdCl₂(PPh₃)₂ (50 mg, 0.07 mmol) and CuI (25 mg, 0.13 mmol) in dry, deoxygenated THF (20 mL) and Et₃N (10 mL) was added 2-methyl-3-butyn-2-ol (0.12 mL, 100 mg, 1.2 mmol). The flask was sealed under argon

with a rubber septum and stirred at rt for 2 h. To this solution was added triisopropylsilylacetylene (0.60 mL, 490 mg, 2.7 mmol) and the reaction was left to stir an additional 16 h. The reaction was quenched via the addition of saturated aq NH₄Cl (25 mL). The aq phase was extracted with Et₂O (2 x 15 mL). The combined organic phase was washed with H₂O (20 mL) and saturated aq NaCl (20 mL), dried with MgSO₄, filtered, and the solvent removed *in vacuo*. Column chromatography (silica gel, 3:1 Hex/EtOAc) afforded **2.34** (322 mg, 40%) as an amber oily solid. *R_f* = 0.55 (4:1 Hex/EtOAc). IR (neat): 3500–3200 (br), 2957 (s), 2875 (s), 2218 (w), 2152 (w). ¹H NMR (500 MHz, CDCl₃) δ 1.90 (s, 1H), 1.53 (s, 6H), 1.10–1.07 (m, 21H), 1.00 (t, *J* = 7.9 Hz, 9H), 0.97 (t, *J* = 7.9 Hz, 9H), 0.62 (q, *J* = 7.9 Hz, 6H), 0.61 (q, *J* = 7.9 Hz, 6H). ¹³C NMR (125 MHz, CDCl₃) δ 117.5, 117.3, 103.3, 102.9, 102.7, 102.65, 102.64, 102.5, 102.3, 80.1, 65.7, 31.1, 18.7, 11.2, 7.5, 7.4, 4.3, 4.2. EI HRMS *m/z* calcd for C₃₄H₅₈OSi₃ (M⁺) 566.3796, found 566.3795.



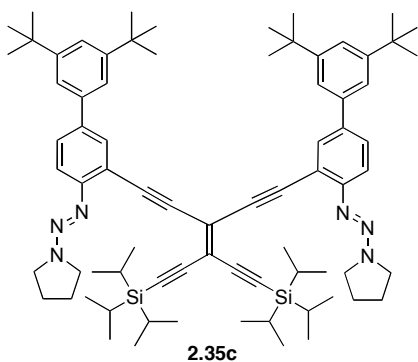
To a solution of **2.31** (0.501 g, 0.862 mmol) in THF (3 mL) and MeOH (3 mL) was added KOH (2.0 mL, 2.0 mmol, 1.0M in H₂O). The reaction was stirred for 20 min and then quenched via the addition of saturated aq NH₄Cl (15 mL). The aq phase was extracted with Et₂O (2 x 15 mL). The combined organic phase was washed with H₂O (10 mL) and saturated aq NaCl (10 mL), dried with MgSO₄, filtered, and the solvent reduced to *ca.* 5 mL *in vacuo*. The solution was then transferred to a flask charged with **2.14a** (0.508 g, 1.85 mmol) dissolved in deoxygenated, dry Et₃N (20 mL). To this solution was added PdCl₂(PPh₃)₂ (0.030 g, 0.043 mmol) and CuI (0.017 g, 0.089 mmol). The flask was

sealed under argon with a rubber septum and stirred for 24 h. The reaction was quenched via the addition of saturated aq NH_4Cl (50 mL). The aq phase was extracted with Et_2O (2 x 25 mL). The combined organic phase was washed with H_2O (20 mL) and saturated aq NaCl (20 mL), dried with MgSO_4 , filtered, and the solvent removed *in vacuo*. Column chromatography (silica gel, 2:1 Hex/ CH_2Cl_2) afforded **2.35a** (0.214 g, 34%) as a yellow/brown solid. $R_f = 0.40$ (1:1 Hex/ CH_2Cl_2). $\text{Mp} = 98\text{ }^\circ\text{C}$. IR (ATR): 3052 (w), 2937 (s), 2890 (m), 2860 (s), 2200 (w), 2181 (w), 2137 (w), 1462 (s). ^1H NMR (300 MHz, CDCl_3) δ 7.39 (td, $J = 7.9$ Hz, 1.1 Hz, 4H), 7.25 (td, $J = 7.7$ Hz, 1.4 Hz, 2H), 7.03 (td, $J = 7.5$ Hz, 1.2 Hz, 2H), 3.40 (br s, 6H), 3.05 (br s, 6H), 1.14–0.99 (m, 42H). ^{13}C NMR (75 MHz, CDCl_3) δ 152.3, 132.6, 129.4, 124.5, 119.3, 117.7, 117.0, 114.9, 104.3, 100.7, 97.5, 91.8, 42.9 (br), 36.2 (br), 18.6, 11.3. EI MS m/z 730 (M^+ , 100), 687 ($[\text{M} - \text{NMe}_2]^+$, 40).



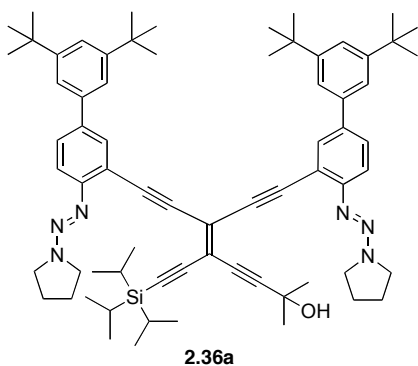
To a solution of **2.31** (1.008 g, 1.734 mmol) in THF (6 mL) and MeOH (6 mL) was added KOH (3.40 mL, 3.40 mmol, 1.0M in H_2O). The reaction was stirred for 20 min and then quenched via the addition of saturated aq NH_4Cl (25 mL). The aq phase was extracted with Et_2O (2 x 25 mL). The combined organic phase was washed with H_2O (20 mL) and saturated aq NaCl (20 mL), dried with MgSO_4 , filtered, and the solvent reduced to *ca.* 5 mL *in vacuo*. The solution was then transferred to a flask charged with **2.14b** (1.232 g, 4.064 mmol) dissolved in deoxygenated, dry THF (6 mL) and *i*- Pr_2NH (2 mL). To this solution was added $\text{Pd}(\text{PPh}_3)_4$ (0.106 g, 0.092 mmol) and CuI (0.043 g, 0.23

mmol). The flask was sealed under argon with a rubber septum and stirred for 24 h. The reaction was quenched via the addition of saturated aq NH₄Cl (50 mL). The aq phase was extracted with Et₂O (2 x 25 mL). The combined organic phase was washed with H₂O (20 mL) and saturated aq NaCl (20 mL), dried with MgSO₄, filtered, and the solvent removed *in vacuo*. Column chromatography (silica gel, 2:1 CH₂Cl₂/Hex) afforded **2.35b** (0.564 g, 41%) as an orange/yellow solid. *R*_f = 0.60 (1:1 CH₂Cl₂/Hex). Mp = 98 °C. IR (ATR): 3048 (w), 2937 (s), 2889 (m), 2861 (s), 2198 (m), 2181 (m), 2137 (m), 1461 (s). ¹H NMR (400 MHz, CDCl₃) δ 7.41 (dd, *J* = 7.7 Hz, 1.2 Hz, 2H), 7.36 (dd, *J* = 8.2 Hz, 0.8 Hz, 2H), 7.23 (ddd, *J* = 8.3 Hz, 7.2 Hz, 1.3 Hz, 2H), 7.00 (td, *J* = 7.5 Hz, 1.1 Hz, 2H), 3.65 (bs, 8H), 1.21 (bs, 12H), 1.11–1.00 (m, 42H). ¹³C NMR (100 MHz, CDCl₃) δ 152.7, 132.7, 129.3, 124.2, 119.4, 117.8, 116.7, 114.9, 104.4, 100.6, 97.7, 91.3, 18.6, 11.3 (two signals coincident or not observed). MALDI MS *m/z* 788 ([M + H]⁺, 25), 686 ([M – N₃Et₂]⁺, 100).



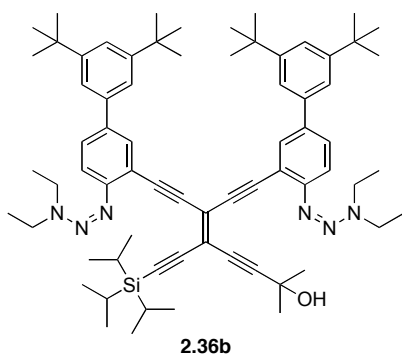
To a solution of **2.31** (281 mg, 0.483 mmol) in THF (4 mL) was added K₂CO₃ (139 mg, 1.03 mmol). The reaction was for 30 min, and then quenched via the addition of saturated aq NH₄Cl (25 mL). The aq phase was extracted with Et₂O (2 x 25 mL). The combined organic phase was washed with H₂O (20 mL) and saturated aq NaCl (20 mL), dried with MgSO₄, filtered, and the solvent reduced to *ca.* 5 mL *in vacuo*. The solution was then transferred to a flask charged with **2.20a** (502 mg, 1.03 mmol) dissolved in deoxygenated, dry THF (5 mL) and *i*-Pr₂NH (3 mL). To this solution was added

Pd(PPh₃)₄ (6 mg, 0.004 mmol), CuI (5 mg, 0.03 mmol). The flask was sealed under argon with a rubber septum and stirred for 24 h. The reaction was quenched via the addition of saturated aq NH₄Cl (25 mL). The aq phase was extracted with Et₂O (2 x 25 mL). The combined organic phase was washed with H₂O (20 mL) and saturated aq NaCl (20 mL), dried with MgSO₄, filtered, and the solvent removed *in vacuo*. Column chromatography (silica gel, 5:1 Hex/EtOAc) afforded **2.35c** (319 mg, 57%) as a yellow solid. *R*_f = 0.15 (5:1 Hex/EtOAc). Mp = 208–210 °C. IR (neat): 3062 (w), 2961 (s), 2890 (m), 2866 (s), 2189 (w), 2140 (w), 1594 (m), 1464 (m). ¹H NMR (400 MHz, CDCl₃) δ 7.64 (d, *J* = 2.0 Hz, 2H), 7.50–1.48 (m, 2H), 7.44 (d, *J* = 8.5 Hz, 2H), 7.40–7.38 (m, 6H), 3.81 (br s, 4H), 3.60 (br s, 4H), 1.77 (br s, 4H), 1.53 (br s, 4H), 1.37 (s, 36H), 1.08–1.06 (m, 42H). ¹³C NMR (100 MHz, CDCl₃) δ 152.2, 151.1, 139.6, 138.4, 130.6, 128.7, 121.4, 121.2, 117.8, 117.0, 104.5, 100.8, 98.0, 92.5, 35.0, 31.6, 18.7, 11.3 (two signals coincident or not observed). EIMS *m/z* 1158.8 (M⁺, 100).



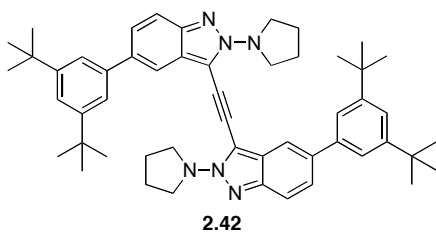
To a solution of **2.34** (0.163 g, 0.287 mmol) in THF (2 mL) and MeOH (5 mL) was added KOH (0.049 g, 0.87 mmol). The reaction was stirred for 20 min and then quenched via the addition of saturated aq NH₄Cl (15 mL). The aq phase was extracted with Et₂O (2 x 15 mL). The combined organic phase was washed with H₂O (10 mL) and saturated aq NaCl (10 mL), dried with MgSO₄, filtered, and the solvent reduced to *ca.* 5 mL *in vacuo*. The solution was then transferred to a flask charged with **2.20a** (0.311 g, 0.635 mmol) dissolved in deoxygenated, dry THF (20 mL) and Et₃N (10 mL). To this solution was

added PdCl₂(PPh₃)₂ (0.012 g, 0.017 mmol) and CuI (0.006 g, 0.03 mmol). The flask was sealed under argon with a rubber septum and stirred for 24 h. The reaction was quenched via the addition of saturated aq NH₄Cl (30 mL). The aq phase was extracted with Et₂O (2 x 25 mL). The combined organic phase was washed with H₂O (20 mL) and saturated aq NaCl (20 mL), dried with MgSO₄, filtered, and the solvent removed *in vacuo*. Column chromatography (silica gel, 10:1 Hex/EtOAc) afforded **2.36a** (0.073 g, 24%) as a yellow oily solid. *R*_f = 0.30 (4:1 Hex/EtOAc). IR (neat film): 3600–3200 (br), 3059 (w), 2962 (s), 2866 (s), 2190 (w), 2137 (w), 1594 (m). ¹H NMR (500 MHz, CDCl₃) δ 7.71 (d, *J* = 2.0 Hz, 2H), 7.56–7.50 (m, 2H), 7.50–7.46 (m, 2H), 7.46–7.40 (m, 6H), 3.84 (bs, 2H), 3.76 (bs, 4H), 3.66 (bs, 2H), 2.27 (s, 1H), 1.80–1.72 (bs, 8H), 1.60 (s, 6H), 1.40 (s, 18H), 1.39 (s, 18H), 1.12–1.08 (m, 21H). ¹³C NMR (125 MHz, CDCl₃) δ 152.25, 152.18, 151.2, 151.1, 139.6, 139.4, 138.5, 138.4, 130.8, 130.6, 128.78, 128.75, 121.5, 121.4, 121.16, 121.12, 120.3, 117.7, 117.6, 117.4, 117.0, 113.8, 103.8, 101.9, 101.4, 97.9, 97.6, 92.3, 92.0, 80.7, 65.7, 51.0 (br), 47.0 (br), 35.0, 31.61, 31.59, 31.4, 23.9 (br), 23.6 (br), 18.8, 11.3 (one signal coincident or not observed). ESI MS *m/z* 1083.70 ([M + Na]⁺, 20), 990.64 ([M – C₄H₈N]⁺, 100]. ESI HRMS *m/z* calcd for C₇₀H₉₂N₆NaOSi ([M + Na]⁺) 1083.6994, found 1083.6966.



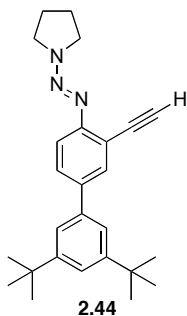
To a solution of **2.34** (0.103 g, 0.182 mmol) in THF (2 mL) and MeOH (5 mL) was added KOH (0.2 mL, 0.2 mmol, 1.0M in H₂O). The reaction was stirred for 20 min and then quenched via the addition of saturated aq NH₄Cl (15 mL). The aq phase was

extracted with Et₂O (2 x 15 mL). The combined organic phase was washed with H₂O (10 mL) and saturated aq NaCl (10 mL), dried with MgSO₄, filtered, and the solvent reduced to *ca.* 5 mL *in vacuo*. The solution was then transferred to a flask charged with **2.20b** (0.181 g, 0.368 mmol) dissolved in deoxygenated, dry THF (8 mL) and *i*-Pr₂NH (4 mL). To this solution was added Pd(PPh₃)₄ (0.013 g, 0.011 mmol) and CuI (0.005 g, 0.03 mmol). The flask was sealed under argon with a rubber septum and stirred for 24 h. The reaction was quenched via the addition of saturated aq NH₄Cl (30 mL). The aq phase was extracted with Et₂O (2 x 25 mL). The combined organic phase was washed with H₂O (20 mL) and saturated aq NaCl (20 mL), dried with MgSO₄, filtered, and the solvent removed *in vacuo*. Column chromatography (silica gel, 10:1 Hex/EtOAc) afforded **2.36b** (0.063 g, 33%) as a yellow oily solid. *R*_f = 0.40 (5:1 Hex/EtOAc). ¹H NMR (400 MHz, CDCl₃) δ 7.68 (d, *J* = 1.5 Hz, 1H), 7.64 (d, *J* = 1.6 Hz, 1H), 7.54–7.43 (m, 4H), 7.41–7.38 (m, 6H), 3.72–3.68 (m, 8H), 2.13 (bs, 1H), 1.56 (s, 1H), 1.371 (s, 18H), 1.367 (s, 18H), 1.24–1.13 (m, 12H), 1.07–1.01 (m, 21H). ¹³C NMR (100 MHz, CDCl₃) δ 152.1, 152.0, 151.4, 151.3, 139.8, 139.7, 138.7, 138.5, 131.1, 131.0, 129.0, 128.9, 121.64, 121.57, 121.40, 121.36, 120.3, 118.2, 118.1, 117.4, 117.1, 114.6, 111.2, 104.0, 102.0, 101.5, 98.0, 97.9, 91.6, 91.2, 80.8, 65.9, 35.2, 31.8, 31.6, 18.9, 11.5 (four signals coincident or not observed).



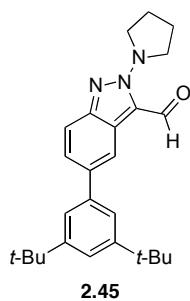
To a solution of **2.21** (293 mg, 0.638 mmol) in THF (5 mL) and MeOH (5 mL) was added K₂CO₃ (103 mg, 0.745 mmol). The reaction was stirred for 1 h, and then quenched via the addition of saturated aq NH₄Cl (25 mL). The aq phase was extracted with Et₂O (2 x 25 mL). The combined organic phase was washed with H₂O (20 mL) and saturated aq

NaCl (20 mL), dried with MgSO₄, filtered, and the solvent reduced to *ca.* 5 mL *in vacuo*. The solution was then transferred to a flask charged with **2.38** (77 mg, 0.20 mmol) dissolved in deoxygenated, dry THF (5 mL) and *i*-Pr₂NH (10 mL). To this solution was added PdCl₂(PPh₃)₂ (5 mg, 0.007 mmol), CuI (3 mg, 0.02 mmol). The flask was sealed under argon with a rubber septum and stirred for 24 h. The reaction was quenched via the addition of saturated aq NH₄Cl (25 mL). The aq phase was extracted with Et₂O (2 x 25 mL). The combined organic phase was washed with H₂O (20 mL) and saturated aq NaCl (20 mL), dried with MgSO₄, filtered, and the solvent removed *in vacuo*. Column chromatography (silica gel, 5:1 Hex/EtOAc) afforded **2.42** (88 mg, 36%) as a bright yellow solid. *R*_f = 0.15 (5:1 Hex/EtOAc). Mp = 300–305 °C. UV-vis (CH₂Cl₂) λ_{max}: 258, 384, 406 nm. Fluorescence (CH₂Cl₂): λ_{exc} = 406 nm, λ_{max,em} = 424 nm. IR (microscope): 3050 (w), 2963 (s), 2871 (s), 1940 (w), 1593 (s). ¹H NMR (400 MHz, CDCl₃) δ 7.89 (dd, *J* = 1.7 Hz, 0.8 Hz, 2H), 7.78 (dd, *J* = 8.9 Hz, 0.8 Hz, 2H), 7.63 (dd, *J* = 8.9 Hz, 1.7 Hz, 2H), 7.47 (d, *J* = 1.8 Hz, 4H), 7.43 (t, *J* = 1.8 Hz, 2H), 3.62–3.59 (m, 8H), 2.09–2.07 (m, 8H), 1.37 (s, 36H). ¹³C NMR (100 MHz, CDCl₃) δ 151.2, 144.9, 140.9, 137.6, 123.1, 121.86, 121.42, 121.3, 118.1, 117.5, 117.4, 88.1, 55.2, 35.0, 31.4, 23.2. ESI HRMS *m/z* calcd for C₅₂H₆₅N₆ ([M + H]⁺) 773.5265, found 773.5261.

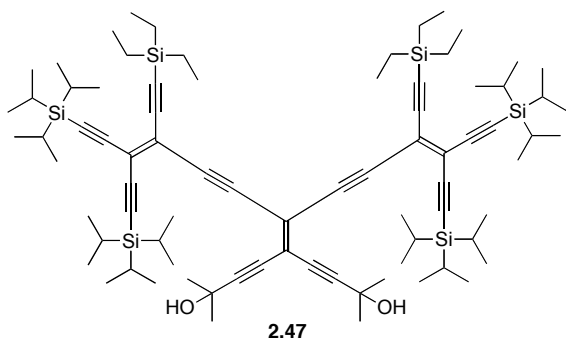


To a solution of **2.21** (523 mg, 1.15 mmol) in THF (20 mL) and MeOH (20 mL) was added aq KOH (74 mg, 1.3 mmol). The reaction was stirred at rt for 2 h, and then quenched via the addition of H₂O (50 mL). The aq phase was extracted with CH₂Cl₂ (2 x

25 mL). The combined organic phase was washed with H₂O (25 mL) and saturated aq NaCl (25 mL), dried with MgSO₄, filtered, and the solvent removed *in vacuo*. Column chromatography (silica gel, 1.5:1 Hex/CH₂Cl₂) afforded **2.44** (338 mg, 76%) as a yellow solid. *R*_f = 0.35 (1.5:1 Hex/CH₂Cl₂). Mp = 130–131 °C IR (microscope): 3289 (m), 3062 (w), 2962 (s), 2868 (m), 2106 (w), 1593 (m). ¹H NMR (400 MHz, CDCl₃) δ 7.74 (d, *J* = 2.0 Hz, 1H), 7.53 (dd, *J* = 8.5 Hz, 2.1 Hz, 1H), 7.48 (d, *J* = 8.5 Hz, 1H), 7.41 (s, 3H), 3.93 (br s, 2H), 3.79 (br s, 2H), 3.30 (s, 1H), 2.04 (br s, 4H), 1.37 (s, 18H). ¹³C NMR (75 MHz, CDCl₃) δ 152.1, 151.1, 139.5, 138.7, 132.2, 128.6, 121.5, 121.3, 117.3, 116.9, 82.3, 80.8, 51.2, 46.8, 35.0, 31.6, 23.8. EI HRMS *m/z* calcd for C₂₆H₃₄N₃ ([M + H]⁺) 388.2747, found 388.2744.



The synthesis of **2.44** occasionally gave **2.45** in small amounts (1–3%) which could be isolated via column chromatography (silica gel, 3:2 Hex/CH₂Cl₂) as a bright orange semi-solid. *R*_f = 0.15 (1:1 Hex/CH₂Cl₂). ¹H NMR (300 MHz, CDCl₃) δ 10.44 (s, 1H), 8.36 (dd, *J* = 1.7 Hz 0.9 Hz, 1H), 7.82 (dd, *J* = 8.9 Hz, 0.8 Hz, 1H), 7.68 (dd, *J* = 8.9 Hz, 1.8 Hz, 1H), 7.47–7.39 (m, 3H), 3.58–3.54 (m, 4H), 2.14–2.10 (m, 4H), 1.38 (s, 18H).



Synthesis of **2.47** using original conditions

To a solution of **2.33** (246 mg, 0.525 mmol) in THF (6 mL) was added TBAF (1.1 mL, 1.1 mmol, 1.0 M in THF) at 0 °C. The reaction was stirred at 0 °C for 15 min, and then quenched via the addition of saturated aq NH₄Cl (25 mL). The aq phase was extracted with Et₂O (2 x 25 mL). The combined organic phase was washed with H₂O (20 mL) and saturated aq NaCl (20 mL), dried with MgSO₄, filtered, and the solvent reduced to *ca.* 5 mL *in vacuo*. The solution was then transferred to a flask charged with **2.37** (894 mg, 1.32 mmol) dissolved in deoxygenated, dry THF (6 mL) and *i*-Pr₂NH (6 mL). To this solution was added Pd(PPh₃)₄ (25 mg, 0.022 mmol) and CuI (4 mg, 0.02 mmol). The flask was sealed under argon with a rubber septum, stirred for 24 h, and the reaction quenched via the addition of saturated aq NH₄Cl (25 mL). The aq phase was extracted with Et₂O (2 x 25 mL). The combined organic phase was washed with H₂O (20 mL) and saturated aq NaCl (20 mL), dried with MgSO₄, filtered, and the solvent removed *in vacuo*. Column chromatography (silica gel, 7:1 Hex/EtOAc) afforded **2.47** (25 mg, 4%) as an oily brown solid.

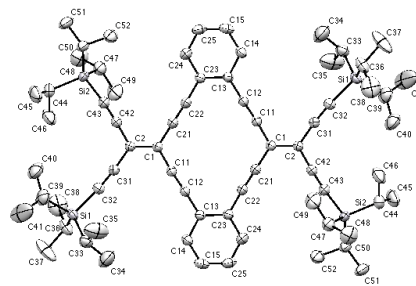
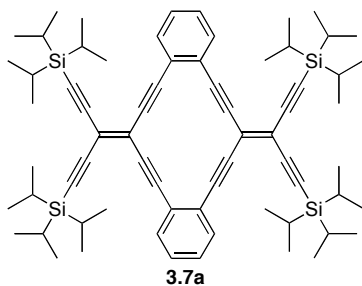
Synthesis of **2.47** using “optimized” conditions

To a solution of **2.33** (143 mg, 0.305 mmol) in THF (6 mL) was added TBAF (0.65 mL, 0.65 mmol, 1.0 M in THF) at 0 °C. The reaction was stirred at 0 °C for 15 min, and then quenched via the addition of saturated aq NH₄Cl (25 mL). The aq phase was extracted with Et₂O (2 x 25 mL). The combined organic phase was washed with H₂O (20 mL) and

saturated aq NaCl (20 mL), dried with MgSO₄, filtered, and the solvent reduced to *ca.* 5 mL *in vacuo*. The solution was then transferred to a flask charged with **2.37** (623 mg, 0.923 mmol) dissolved in deoxygenated, dry THF (4 mL) and *i*-Pr₂NH (3 mL). To this solution was added PdCl₂(PPh₃)₂ (14 mg, 0.019 mmol), CuI (5 mg, 0.03 mmol) and P(*t*-Bu)₃ (0.15 mL, 0.050 mmol, 0.33 M in toluene). The flask was sealed under argon with a rubber septum, heated to 50 °C, and stirred for 48 h. The solution was cooled to rt and the reaction quenched via the addition of saturated aq NH₄Cl (25 mL). The aq phase was extracted with Et₂O (2 x 25 mL). The combined organic phase was washed with H₂O (20 mL) and saturated aq NaCl (20 mL), dried with MgSO₄, filtered, and the solvent removed *in vacuo*. Column chromatography (silica gel, 7:1 Hex/EtOAc) afforded **2.47** (40 mg, 10%) as an oily brown solid.

Data for **2.47** (sample obtained from “optimized” reaction): $R_f = 0.15$ (5:1 Hex/EtOAc). IR (neat): 3500–3200 (br), 2891 (s), 2867 (s), 2210 (w), 2150 (w). ¹H NMR (400 MHz, CDCl₃) δ 2.00 (s, 2H), 1.56 (s, 12H), 1.08 (s, 42H), 1.06 (s, 42H), 0.97 (t, $J = 7.9$ Hz, 18H), 0.61 (q, $J = 7.9$ Hz, 12H). ¹³C NMR (100 MHz, CDCl₃) δ 119.6, 117.8, 117.7, 116.0, 104.2, 103.9, 103.8, 103.32, 103.27, 103.1, 101.9, 95.3, 93.9, 79.5, 65.7, 31.1, 18.62, 18.60, 11.3, 11.2, 7.5, 4.2. MALDI HRMS (DCTB) m/z calcd for C₈₀H₁₂₈O₂Si₆ (M⁺) 1288.8524, found 1288.8535.

6.3 Experimental Details for Chapter 3



Synthesis of **3.7a** via one-pot reaction:

To a solution of **2.25** (736 mg, 1.35 mmol) and 1,2-diethynylbenzene (171 mg, 1.36 mmol) in deoxygenated, dry Et₃N (10 mL) was added Pd(PPh₃)₄ (158 mg, 0.137 mmol) and CuI (52 mg, 0.273 mmol). The flask was sealed under argon with a rubber septum, heated to 60 °C, and stirred for 24 h. The solution was cooled to rt and the reaction quenched via the addition of saturated aq NH₄Cl (30 mL). The aq phase was extracted with Et₂O (2 x 25 mL). The combined organic phase was washed with H₂O (20 mL) and saturated aq NaCl (20 mL), dried with MgSO₄, filtered, and the solvent removed *in vacuo*. Column chromatography (alumina, neutral, 4:1→2:1 Hex/CH₂Cl₂) afforded a dark yellow solid. The solid was further purified by dissolving into a small amount of CH₂Cl₂ and precipitated by the addition of MeOH to yield **3.7a** (83 mg, 12%) as a bright yellow solid.

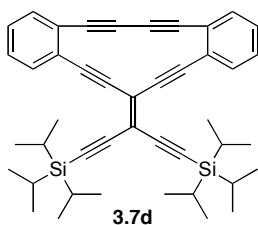
Synthesis of **3.7a** via stepwise reaction:

To a solution of **3.32** (100 mg, 0.113 mmol) in THF (2 mL) and MeOH (10 mL) was added KOH (65 mg, 1.2 mmol). The reaction was stirred at rt for 3 h and then quenched via the addition of saturated aq NH₄Cl (20 mL). The aq phase was extracted with Et₂O (2 x 20 mL). The combined organic phase was washed with H₂O (10 mL) and saturated aq NaCl (10 mL), dried with MgSO₄, filtered, and the solvent reduced to *ca.* 5 mL *in vacuo*. This solution was transferred to a solution of **2.25** (62 mg, 0.11 mmol) in deoxygenated,

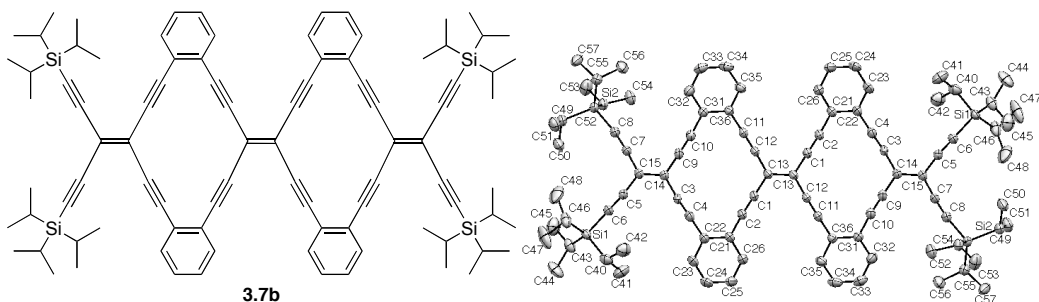
dry Et₃N (5 mL), and purged with argon for 15 min. To the reaction was added Pd(PPh₃)₄ (7 mg, 0.006 mmol) and CuI (3 mg, 0.02 mmol). The flask was sealed under argon with a rubber septum, heated to 50 °C, and stirred for 18 h. The solution was cooled to rt and the reaction quenched via the addition of saturated aq NH₄Cl (25 mL). The aq phase was extracted with Et₂O (2 x 25 mL). The combined organic phase was washed with H₂O (20 mL) and saturated aq NaCl (20 mL), dried with MgSO₄, filtered, and the solvent removed *in vacuo*. Column chromatography (alumina, neutral, 4:1→2:1 Hex/CH₂Cl₂) afforded a dark yellow solid. The solid was further purified by dissolving into a small amount of CH₂Cl₂ and precipitated by the addition of MeOH to yield **3.7a** (45 mg, 39%) as a bright yellow solid.

Data for **3.7a** (obtained from samples via stepwise reaction): $R_f = 0.50$ (4:1 Hex/CH₂Cl₂). UV-vis (THF) λ_{\max} (ϵ): 282 (82 700), 313 (28 200), 330 (32 300), 371 (22 400), 426 (51 800), 450 (65 900) nm. IR (ATR): 2939 (m), 2890 (w), 2862 (m), 2134 (w), 1460 (m). ¹H NMR (300 MHz, CDCl₃) δ 7.52–7.46 (m, 4H), 7.30–7.22 (m, 4H), 1.14–1.11 (m, 84H) ¹³C NMR (75 MHz, CDCl₃) δ 132.1, 128.5, 125.4, 117.4, 116.8, 104.4, 102.8, 96.8, 91.3, 18.7, 11.3. MALDI HRMS (DCTB) m/z calcd for C₆₈H₉₂Si₄ (M⁺) 1020.6271, found 1020.6278. DSC: decomposition, 254 °C (onset), 266 °C (peak).

Crystals suitable for X-ray crystallography by slow evaporation of solutions of **3.7a** in hexanes left standing in the dark at rt for several days. X-ray crystallographic data for **3.7a** (ADM01): C₆₈H₉₂Si₄, $M_r = 1021.78$; crystal dimensions (mm) 0.3094 × 0.1924 × 0.1574; triclinic space group $P\bar{1}$ (no. 2); $a = 8.4669(5)$ Å, $b = 12.5501(7)$ Å, $c = 15.4542(11)$ Å; $\alpha = 90.022(5)^\circ$, $\beta = 96.448(6)^\circ$, $\gamma = 97.093(5)^\circ$; $V = 1619.12(17)$ Å³; $Z = 1$; $\rho_{\text{calcd}} = 1.048$ mg mm⁻³; $\mu = 1.115$ mm⁻¹; $\lambda = 1.54178$ Å; $T = -100$ °C; $2\theta_{\text{max}} = 146.82^\circ$; total data collected = 9735; $R_1 = 0.0503$; $wR_2 = 0.1407$ for 337 variables, 6214 unique reflections, and 0 restraints; residual electron density = 0.714 and -0.621 e Å⁻³.



The stepwise route to **3.7a** occasionally gave **3.7d** in small amounts (1–3%) which could be isolated via column chromatography (alumina, neutral, 4:1→2:1 Hex/CH₂Cl₂) as a bright yellow solid. $R_f = 0.55$ (4:1 Hex/CH₂Cl₂). IR (ATR): 3064 (w), 2943 (s), 2892 (m), 2865 (s), 2211 (w), 2198 (w), 2175 (w), 2138 (w), 1469 (s). ¹H NMR (300 MHz, CDCl₃) δ 7.48–7.44 (m, 2H), 7.36–7.32 (m, 2H), 7.30–7.26 (m, 4H), 1.16–1.12 (m, 42H). ¹³C NMR (75 MHz, CDCl₃) δ 131.3, 129.5, 129.1, 128.8, 128.7, 125.5, 118.1, 116.7, 104.4, 103.7, 97.3, 92.6, 87.0, 81.4, 18.8, 11.4. MALDI HRMS (DCTB) m/z calcd for C₄₄H₅₀Si₂ (M⁺) 634.3446, found 634.3447.



Synthesis of **3.7b** via one-pot reaction:

To a solution of **3.10** (80 mg, 0.15 mmol) and **2.25** (166 mg, 0.30 mmol) in deoxygenated, dry THF (15 mL) and *i*-Pr₂NH (15 mL) was added Pd(PPh₃)₄ (37 mg, 0.032 mmol) and CuI (6 mg, 0.03 mmol). The flask was sealed under nitrogen with a rubber septum, heated to 60 °C, and stirred for 18 h. The solution was cooled to rt and the reaction quenched via the addition of saturated aq NH₄Cl (30 mL). The aq phase was extracted with Et₂O (2 x 30 mL). The combined organic phase was washed with H₂O (25 mL) and saturated aq NaCl (25 mL), dried with MgSO₄, filtered, and the solvent removed *in vacuo*. Column chromatography (alumina, neutral, 5:1→2:1 Hex/CH₂Cl₂) afforded a

dark red solid. The solid was further purified by dissolving into a small amount of THF and precipitated by the addition of MeOH and cooling to $-78\text{ }^{\circ}\text{C}$ to yield **3.7b** (10 mg, 5%) as a deep red solid.

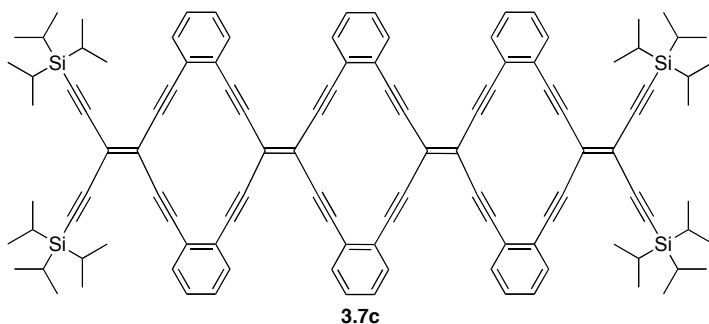
Synthesis of **3.7b** via stepwise reaction:

To a solution of **3.33** (58 mg, 0.051 mmol) in THF (4 mL) and MeOH (10 mL) was added KOH (30 mg, 0.53 mmol). The reaction was stirred at rt for 4 h and quenched via the addition of saturated aq NH_4Cl (20 mL). The aq phase was extracted with Et_2O (2 x 20 mL). The combined organic phase was washed with H_2O (10 mL) and saturated aq NaCl (10 mL), dried with MgSO_4 , filtered, and the solvent reduced to *ca.* 5 mL *in vacuo*. This solution was transferred to a solution of **2.25** (28 mg, 0.051 mmol) in deoxygenated dry Et_3N (5 mL), and purged with argon for 15 min. To the reaction was added $\text{Pd}(\text{PPh}_3)_4$ (3 mg, 0.003 mmol) and CuI (1 mg, 0.005 mmol). The flask was sealed under argon with a rubber septum, heated to $50\text{ }^{\circ}\text{C}$, and stirred for 16 h. The solution was cooled to rt and the reaction quenched via the addition of saturated aq NH_4Cl (25 mL). The aq phase was extracted with Et_2O (2 x 25 mL). The combined organic phase was washed with H_2O (20 mL) and saturated aq NaCl (20 mL), dried with MgSO_4 , filtered, and the solvent removed *in vacuo*. Column chromatography (alumina, neutral, 4:1 \rightarrow 2:1 Hex/ CH_2Cl_2) afforded **3.7b** (12 mg, 18%) as a deep red solid.

Data for **3.7b** (obtained from samples via one-pot reaction): $R_f = 0.44$ (2:1 Hex/ CH_2Cl_2). Mp = $200\text{ }^{\circ}\text{C}$ (decomp). UV-vis (THF) λ_{max} : 287, 343, 415, 485, 504 nm. IR (CHCl_3 cast film): 3058 (w), 2943 (s), 2892 (m), 2865 (s), 2185 (w), 2136 (w), 1485 (m), 1463 (m). ^1H NMR (400 MHz, CDCl_3) δ 7.64–7.62 (m, 4H), 7.55–7.53 (m, 4H), 7.38–7.30 (m, 8H), 1.16–1.12 (m, 84H) ^{13}C NMR (100 MHz, CDCl_3) δ 132.3, 131.8, 128.73, 128.67, 128.5, 125.5, 125.4, 117.8, 117.0, 116.8, 104.4, 103.0, 97.9, 96.8, 92.0, 91.5, 18.7, 11.4. ESI

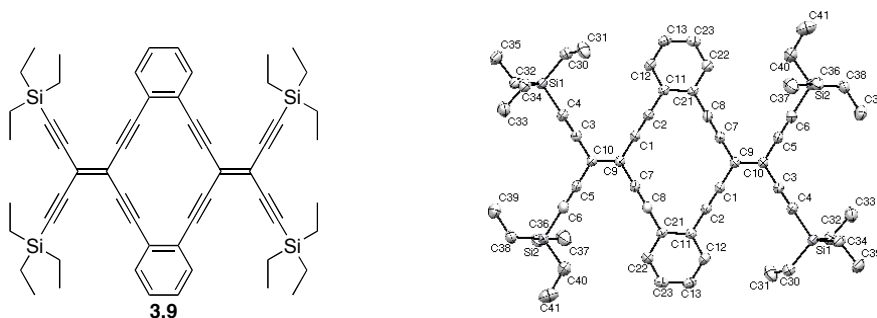
HRMS m/z calcd for $C_{90}H_{100}NaSi_4$ ($[M + Na]^+$) 1315.6794, found 1315.6759. DSC: decomposition, 280 °C (onset), 285 °C (peak).

Crystals suitable for X-ray crystallography by slow evaporation of solutions of **3.7b** in hexanes left standing in the dark at rt for several days. X-ray crystallographic data for **3.7b** (ADM04): $C_{90}H_{100}Si_4$, $M_r = 1294.06$; crystal dimensions (mm) $0.373 \times 0.1684 \times 0.0756$; triclinic space group $P\bar{1}$ (No. 2); $a = 8.9732(7)$ Å, $b = 13.1109(9)$ Å, $c = 18.0827(12)$ Å; $\alpha = 71.321(6)^\circ$, $\beta = 80.336(6)^\circ$, $\gamma = 79.647(6)^\circ$; $V = 1968.6(2)$ Å³; $Z = 1$; $\rho_{\text{calcd}} = 1.092$ mg mm⁻³; $\mu = 1.018$ mm⁻¹; $\lambda = 1.54178$ Å; $T = -100$ °C; $2\theta_{\text{max}} = 147.34^\circ$; total data collected = 11687; $R_1 = 0.0493$; $wR_2 = 0.1461$ for 436 variables, 7538 unique reflections, and 0 restraints; residual electron density = 0.56 and -0.28 e Å⁻³.



To a solution of **3.34** (65 mg, 0.046 mmol) in THF (5 mL) and MeOH (8 mL) was added KOH (30 mg, 0.53 mmol). The reaction was stirred at rt for 4 h, and then quenched via the addition of saturated aq NH_4Cl (25 mL). The aq phase was extracted with CH_2Cl_2 (2 x 25 mL). The combined organic phase was washed with H_2O (20 mL) and saturated aq NaCl (20 mL), dried with $MgSO_4$, filtered, and the solvent reduced to *ca.* 5 mL *in vacuo*. The solution was then transferred to a flask charged with **2.25** (25 mg, 0.046 mmol) dissolved in Et_3N (5 mL) and the combined solution purged with argon for 15 min. To this solution was added $Pd(PPh_3)_4$ (3 mg, 0.003 mmol) and CuI (1 mg, 0.005 mmol). The flask was sealed under argon with a rubber septum, heated to 50 °C, and stirred for 16 h. The solution was cooled to rt and the reaction quenched via the addition of saturated aq

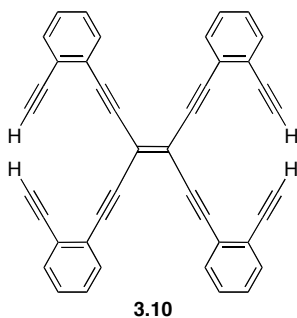
NH₄Cl (25 mL). The aq phase was extracted with CH₂Cl₂ (2 x 25 mL). The combined organic phase was washed with H₂O (20 mL) and saturated aq NaCl (20 mL), dried with MgSO₄, filtered, and the solvent removed *in vacuo*. Preparative TLC (silica gel, 3:2 Hex/CH₂Cl₂) afforded **3.7c** (3.5 mg, 5%) as a dark red solid, which decomposed when dissolved in CDCl₃. *R*_f = 0.4 (3:2 Hex/CH₂Cl₂). UV-vis (THF) λ_{max}: 284, 490, 522 nm. MALDI HRMS (DCTB) *m/z* calcd for C₁₁₂H₁₀₈Si₄ (M⁺) 1564.7523, found 1564.7532.



To a solution of **2.24** (816 mg, 1.76 mmol) and 1,2-diethynylbenzene (222 mg, 1.76 mmol) in deoxygenated, dry THF (10 mL) and *i*-Pr₂NH (2 mL) was added Pd(PPh₃)₄ (203 mg, 0.176 mmol) and CuI (65 mg, 0.34 mmol). The flask was sealed under nitrogen with a rubber septum, heated to 60 °C, and stirred for 24 h. The solution was cooled to rt and the reaction quenched via the addition of saturated aq NH₄Cl (30 mL). The aq phase was extracted with Et₂O (2 x 25 mL). The combined organic phase was washed with H₂O (20 mL) and saturated aq NaCl (20 mL), dried with MgSO₄, filtered, and the solvent removed *in vacuo*. Column chromatography (alumina, neutral, 10:1 Hex/CH₂Cl₂) afforded a dark yellow solid. The solid was further purified by crystallization from hexanes to yield **3.9** (116 mg, 15%) as a bright yellow solid. *R*_f = 0.60 (2:1 Hex/CH₂Cl₂). Mp = 225–230 °C (decomp). UV-vis (THF) λ_{max} (ε): 280 (75 300), 312 (30 700), 328 (33 700), 370 (21 600), 424 (52 200), 448 (71 100) nm. IR (CHCl₃ cast film): 3018 (w), 2956 (m), 2935 (m), 2875 (m), 2193 (w), 2140 (w), 1485 (w). ¹H NMR (300 MHz, CDCl₃) δ 7.51–7.46 (m, 4H), 7.32–7.26 (m, 4H), 1.04 (t, *J* = 7.8 Hz, 36H), 0.70 (q, *J* = 7.9 Hz,

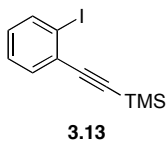
24H). ^{13}C NMR (75 MHz, CDCl_3) δ 132.1, 128.6, 125.4, 117.7, 117.2, 103.6, 103.3, 97.0, 91.3, 7.5, 4.3. MALDI HRMS (DCTB) m/z calcd for $\text{C}_{56}\text{H}_{68}\text{Si}_4$ (M^+) 852.4393, found 852.4396. DSC: decomposition, 232 °C (onset), 236 °C (peak).

Crystals suitable for X-ray crystallography by slow evaporation of solutions of **3.9** in hexanes left standing in the dark at rt for several days. X-ray crystallographic data for **3.9** (ADM03): $\text{C}_{56}\text{H}_{68}\text{Si}_4$, $M_r = 853.46$; crystal dimensions (mm) $0.305 \times 0.1584 \times 0.1164$; triclinic space group $P\bar{1}$ (no. 2); $a = 8.4415(6)$ Å, $b = 11.9793(9)$ Å, $c = 13.3120(9)$ Å; $\alpha = 79.899(6)^\circ$, $\beta = 86.040(6)^\circ$, $\gamma = 88.457(6)^\circ$; $V = 1321.98(16)$ Å³; $Z = 1$; $\rho_{\text{calcd}} = 1.072$ mg mm⁻³; $\mu = 1.283$ mm⁻¹; $\lambda = 1.54178$ Å; $T = -100$ °C; $2\theta_{\text{max}} = 151.42^\circ$; total data collected = 9637; $R_1 = 0.0562$; $wR_2 = 0.1652$ for 277 variables, 5351 unique reflections, and 0 restraints; residual electron density = 1.13 and -0.46 e Å⁻³.



To a solution of **3.18** (104 mg, 0.106 mmol) THF (10 mL) was TBAF (0.50 mL, 0.50 mmol, 1.0 M in THF) at 0 °C. The solution was stirred at 0 °C for 10 min, warmed to rt, and stirred for an additional 20 min. The reaction was quenched via the addition of saturated aq NH_4Cl (20 mL). The aq phase was extracted with Et_2O (2 x 15 mL). The combined organic phase was washed with H_2O (10 mL) and saturated aq NaCl (10 mL), dried with MgSO_4 , filtered, and the solvent removed *in vacuo*. The yellow solid was dissolved in minimum amount of CH_2Cl_2 and precipitated by the addition of hexanes to yield **3.10** (49 mg, 88%) as a bright yellow solid. $R_f = 0.25$ (2:1 Hex/ CH_2Cl_2). Mp = 150–155 °C (decomp). IR (ATR): 3295 (m), 3280 (m), 3062 (w), 2209 (w), 2184 (w), 1475

(m), 1440 (m). ^1H NMR (400 MHz, CDCl_3) δ 7.57–7.49 (m, 8H), 7.33–7.28 (m, 8H), 3.18 (s, 4H). ^{13}C NMR (100 MHz, CDCl_3) δ 132.6, 132.5, 128.7, 128.4, 125.8, 124.9, 117.3, 97.4, 91.1, 82.2, 81.6. MALDI MS (DCTB) m/z 524 (M^+ , 100). ESI HRMS m/z calcd for $\text{C}_{42}\text{H}_{20}\text{Na}$ ($[\text{M} + \text{Na}]^+$) 547.1457, found 547.1456.

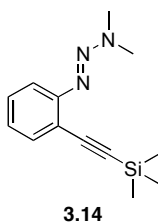


Synthesis of **3.13** via triazene decomposition of **3.14**

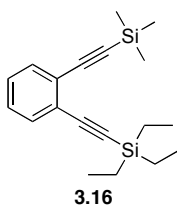
A solution of **3.14** (1.706 g, 6.952 mmol) in MeI (10 mL) was sealed under nitrogen in an Ace-glassware pressure tube. The reaction was heated to 140 °C and stirred for 24 h. The reaction was cooled to rt and the remaining MeI was removed under vacuum, condensed, and quenched with MeOH. The residual product was purified by passed through a plug of silica gel with hexanes to give **3.13** (1.356 g, 65%) as an orange oil.

Synthesis of **3.13** via a modified Sandmeyer reaction

A solution of **3.15a** (11.973 g, 63.239 mmol) in dry THF (100 mL) was added dropwise to $\text{BF}_3 \cdot \text{Et}_2\text{O}$ (32 mL) at -20 °C and stirred for 20 min. To this solution was added dropwise a solution of *t*-BuONO (26 mL, 22 g, 220 mmol) dissolved in dry THF (50 mL). The reaction was stirred for 1 h, after which the diazonium salt was precipitated by addition of Et_2O (300 mL). The supernatant was carefully decanted, the solid was dissolved in MeCN (150 mL), and cooled to 0 °C. To this solution was added Et_4NI (20.696 g, 80.482 mmol) in small portions. The reaction was warmed to rt, stirred for 30 min, and quenched via the addition of saturated aq $\text{Na}_2\text{S}_2\text{O}_3$ (200 mL). The aq phase was extracted with hexanes (2 x 100 mL). The combined organic phase was washed with H_2O (100 mL) and saturated aq NaCl (100 mL), dried with MgSO_4 , filtered, and the solvent removed *in vacuo*. Column chromatography (silica gel, Hex) afforded **3.13** (12.091 g, 64%) as an orange oil. Spectroscopic data matches that previously reported.¹

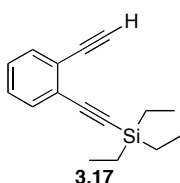


To a solution of **2.14a** (2.02 g, 7.34 mmol) in deoxygenated, dry Et₃N (50 mL) was added PdCl₂(PPh₃)₂ (0.26 g, 0.37 mmol) and CuI (0.16 g, 0.81 mmol). The solution was purged with argon for an additional 10 min after which trimethylsilylacetylene (2.1 mL, 1.5 g, 15 mmol) was added. The flask was sealed under argon with a rubber septum and stirred for 18 h. The reaction was quenched via the addition of saturated aq NH₄Cl (100 mL). The aq phase was extracted with Et₂O (2 x 50 mL). The combined organic phase was washed with H₂O (50 mL) and saturated aq NaCl (50 mL), dried with MgSO₄, filtered, and the solvent removed *in vacuo*. Column chromatography (silica gel, 2:1 Hex/CH₂Cl₂) afforded **3.14** (1.71 g, 95%) as an amber solid. *R*_f = 0.15 (2:1 Hex/CH₂Cl₂). Mp = 39–40 °C. IR (ATR): 3048 (w), 2954 (s), 2898 (m), 2154 (s), 1468 (s). ¹H NMR (300 MHz, CDCl₃) δ 7.45 (dd, *J* = 7.7 Hz, 1.4 Hz, 1H), 7.39 (dd, *J* = 8.2 Hz, 0.9 Hz, 1H), 7.23 (td, *J* = 7.7 Hz, 1.4 Hz, 1H), 7.03 (td, *J* = 7.5 Hz, 1.2 Hz, 1H), 3.49 (br s, 3H), 3.25 (br s, 3H), 0.23 (s, 9H). ¹³C NMR (75 MHz, CDCl₃) δ 152.3, 133.1, 129.1, 124.8, 117.9, 116.9, 103.3, 98.2, 0.1 (one signal coincident or not observed). ESI HRMS *m/z* calcd for C₁₃H₁₉N₃NaSi ([M + Na]⁺) 268.1241, found 268.1238.

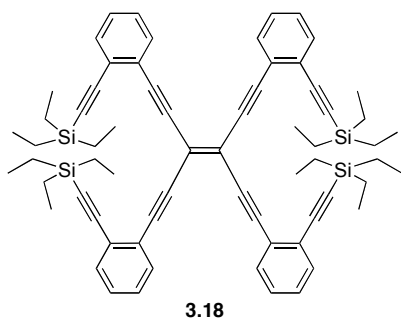


To a solution of **3.13** (0.883 g, 2.94 mmol), PdCl₂(PPh₃)₄ (0.103 g, 0.147 mmol), and CuI (0.055 g, 0.29 mmol) in deoxygenated Et₃N (8 mL) was added triethylsilylacetylene (1.3 mL, 1.0 g, 7.2 mmol). The flask was sealed under argon with a rubber septum and stirred

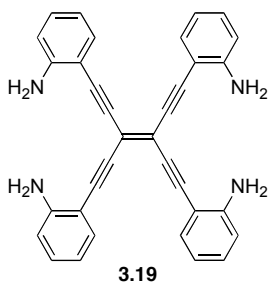
at rt for 16 h. The reaction was quenched via the addition of saturated aq NH₄Cl (25 mL). The aq phase was extracted with Et₂O (2 x 25 mL). The combined organic phase was washed with H₂O (20 mL) and saturated aq NaCl (20 mL), dried with MgSO₄, filtered, and the solvent removed *in vacuo*. Column chromatography (silica gel, Hexanes) afforded **3.16** (0.894 g, 97%) as a yellow oil. *R*_f = 0.3 (Hexanes). IR (CH₂Cl₂ cast film): 3061 (w), 2954 (s), 2911 (m), 2874 (m), 2159 (m), 1476 (m). ¹H NMR (300 MHz, CDCl₃) δ 7.48–7.41 (m, 2H), 7.23–7.20 (m, 2H), 1.05 (t, *J* = 7.8 Hz, 9H), 0.68 (q, *J* = 7.8 Hz, 6H), 0.24 (s, 9H). ¹³C NMR (75 MHz, CDCl₃) δ 132.64, 132.57, 128.0, 127.9, 125.8, 125.6, 104.4, 103.3, 98.3, 96.0, 7.8, 4.4, 0.0. EIMS *m/z* 312.2 (M⁺, 59), 283.1 ([M – Et]⁺, 83). EI HRMS *m/z* calcd for C₁₉H₂₈Si₂ (M⁺) 312.1729, found 312.1724.



To a solution of **3.16** (9.994 g, 31.81 mmol) in THF (5 mL) and MeOH (25 mL) was added K₂CO₃ (4.421 g, 31.99 mmol). The solution was stirred for 1 h after which the reaction was quenched via the addition of saturated aq NH₄Cl (50 mL). The aq phase was extracted with Et₂O (2 x 50 mL). The combined organic phase was washed with H₂O (50 mL) and saturated aq NaCl (50 mL), dried with MgSO₄, filtered, and the solvent removed *in vacuo*. Column chromatography (silica gel, 10:1 Hex/CH₂Cl₂) afforded **3.17** (7.306, 96%) as an orange oil. *R*_f = 0.25 (10:1 Hex/CH₂Cl₂). IR (neat film): 3305 (m), 3062 (w), 2954 (s), 2910 (m), 2874 (s), 2158 (s), 1474 (m). ¹H NMR (300 MHz, CDCl₃) δ 7.50–7.43 (m, 2H), 7.29–7.20 (m, 2H), 3.26 (s, 1H), 1.05 (t, *J* = 7.8 Hz, 9H), 0.67 (q, *J* = 7.9 Hz, 6H). ¹³C NMR (75 MHz, CDCl₃) δ 132.4, 132.3, 128.3, 128.0, 126.4, 125.0, 104.1, 96.4, 82.1, 81.0, 7.5, 4.4. EIMS *m/z* 240.1 (M⁺, 30), 211.1 ([M – Et]⁺, 100). EI HRMS *m/z* calcd for C₁₆H₂₀Si (M⁺) 240.1334, found 240.1332.

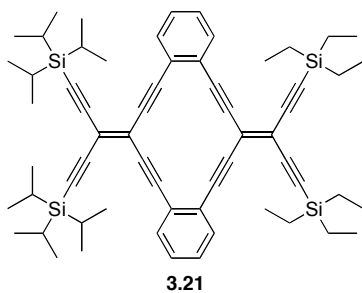


To a solution of **3.17** (126 mg, 0.524 mmol) and tetrabromoethene (40 mg, 0.12 mmol) in THF (2 mL) and *i*-Pr₂NH (1 mL) was added Pd(PPh₃)₄ (10 mg, 0.008 mmol) and CuI (1 mg, 0.005 mmol). The flask was sealed under argon with a rubber septum, heated to 60 °C, and stirred for 24 h. The solution was cooled to rt and the reaction quenched via the addition of saturated aq NH₄Cl (10 mL). The aq phase was extracted with Et₂O (2 x 15 mL). The combined organic phase was washed with H₂O (10 mL) and saturated aq NaCl (10 mL), dried with MgSO₄, filtered, and the solvent removed *in vacuo*. Column chromatography (silica gel, 5:1 Hex/CH₂Cl₂) afforded **3.18** (56 mg, 50%) as a bright yellow/orange oily solid. *R*_f = 0.53 (2:1 Hex/CH₂Cl₂). IR (ATR): 2951 (s), 2908 (m), 2871 (s), 2193 (w), 2154 (w), 1476 (m). ¹H NMR (400 MHz, CDCl₃) δ 7.49–7.45 (m, 8H), 7.25–7.16 (m, 8H), 0.93 (t, *J* = 7.9 Hz, 36H), 0.56 (q, *J* = 7.9 Hz, 24H). ¹³C NMR (75 MHz, CDCl₃) δ 132.6, 132.4, 128.3, 127.8, 125.8, 125.6, 118.3, 103.9, 97.6, 97.0, 90.7, 7.5, 4.3. ESI HRMS *m/z* calcd for C₆₆H₇₆NaSi₄ ([M + Na]⁺) 1003.4916, found 1003.4893.



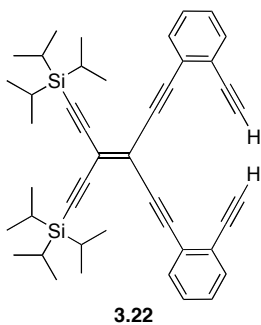
To a solution of **2.31** (1.002 g, 1.724 mmol) in THF (20 mL) cooled to 0 °C was added TBAF (7.0 mL, 7.0 mmol, 1.0M in THF). The reaction was stirred for 30 min, and then

quenched via the addition of saturated aq NH_4Cl (25 mL). The aq phase was extracted with Et_2O (2 x 25 mL). The combined organic phase was washed with H_2O (20 mL) and saturated aq NaCl (20 mL), dried with MgSO_4 , filtered, and the solvent reduced to *ca.* 5 mL *in vacuo*. The solution was then transferred to a flask charged with 2-iodoaniline (1.588 g, 7.250 mmol) dissolved in deoxygenated, dry Et_3N (40 mL). To this solution was added $\text{PdCl}_2(\text{PPh}_3)_2$ (0.122 g, 0.174 mmol) and CuI (0.070 g, 0.368 mmol). The flask was sealed under argon with a rubber septum and stirred for 24 h. The reaction was quenched via the addition of saturated aq NH_4Cl (50 mL). The aq phase was extracted with CH_2Cl_2 (2 x 25 mL). The combined organic phase was washed with H_2O (20 mL) and saturated aq NaCl (20 mL), dried with MgSO_4 , filtered, and the solvent removed *in vacuo*. Column chromatography (silica gel, 2:1 $\text{CH}_2\text{Cl}_2/\text{EtOAc}$) afforded **3.19** (0.110 g, 13%) as red/brown solid. $R_f = 0.20$ (CH_2Cl_2). $\text{Mp} = 205$ °C. IR (ATR): 3447 (w), 3429 (w), 3359 (w), 3333 (w), 3028 (w), 2919 (w), 2206 (m), 2171 (m), 1607 (s). ^1H NMR (300 MHz, Acetone- d_6) δ 7.32 (d, $J = 7.7$ Hz, 1H), 7.16 (d, $J = 8.3$ Hz, 1H), 6.82 (d, $J = 8.3$ Hz, 1H), 6.63 (d, $J = 7.7$ Hz, 1H). ^{13}C NMR (75 MHz, Acetone- d_6) δ 150.7, 132.7, 131.6, 117.4, 115.0, 114.9, 106.0, 96.8, 93.5. ESI HRMS m/z calcd for $\text{C}_{34}\text{H}_{24}\text{N}_4\text{Na}$ ($[\text{M} + \text{Na}]^+$) 511.1893, found 511.1899.



To a solution of **3.22** (719 mg, 1.13 mmol) and **2.24** (521 mg, 1.13 mmol) in deoxygenated, dry THF (50 mL) and *i*- Pr_2NH (15 mL) was added $\text{Pd}(\text{PPh}_3)_4$ (65 mg, 0.056 mmol) and CuI (65 mg, 0.34 mmol). The flask was sealed under argon with a rubber septum, heated to 60 °C, and stirred for 18 h. The solution was cooled to rt and the

reaction quenched via the addition of saturated aq NH_4Cl (25 mL). The aq phase was extracted with Et_2O (2 x 25 mL). The combined organic phase was washed with H_2O (20 mL) and saturated aq NaCl (20 mL), dried with MgSO_4 , filtered, and the solvent removed *in vacuo*. Column chromatography (alumina, neutral, 10:1 Hex/ CH_2Cl_2) afforded a dark yellow solid. The solid was further purified by crystallization from hexanes to yield **3.21** (505 mg, 48%) as a bright yellow solid. $R_f = 0.45$ (5:1 Hex/ CH_2Cl_2). Mp = 215 °C. UV-vis (THF) λ_{max} (ϵ): 282 (82 700), 315 (25 700), 329 (28 900), 371 (19 300), 426 (47 800), 450 (63 200) nm. IR (ATR): 2943 (m), 2865 (m), 2137 (w), 1459 (m). ^1H NMR (400 MHz, CDCl_3) δ 7.52–7.46 (m, 4H), 7.30–7.25 (m, 4H), 1.14–1.11 (m, 42H), 1.04 (t, $J = 7.9$ Hz, 18H), 0.70 (q, $J = 7.9$ Hz, 12H). ^{13}C NMR (100 MHz, CDCl_3) δ 132.12, 132.06, 128.5, 125.4, 117.8, 117.6, 117.1, 116.8, 104.4, 103.5, 103.3, 102.9, 97.1, 96.8, 91.4, 18.7, 11.4, 7.5, 4.4 (three signals coincident or not observed). APPI HRMS m/z calcd for $\text{C}_{62}\text{H}_{81}\text{Si}_4$ ($[\text{M} + \text{H}]^+$) 937.5410, found 937.5407 DSC: decomposition, 231 °C (onset), 234 °C (peak).



Synthesis of **3.22** via **3.25**

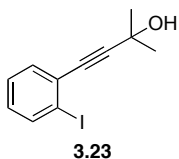
To a solution of **3.25** (605 mg, 0.803 mmol) in benzene (50 mL) was added KOH (452 mg, 8.06 mmol). The reaction was heated to reflux and stirred for 24 h, cooled to rt, and quenched via the addition of saturated aq NH_4Cl (50 mL). The aq phase was extracted with Et_2O (2 x 25 mL). The combined organic phase was washed with H_2O (15 mL) and saturated aq NaCl (15 mL), dried with MgSO_4 , filtered, and the solvent removed *in*

vacuo. Column chromatography (silica gel, 5:1 Hex/CH₂Cl₂) afforded **3.22** (149 mg, 30%) as an amber oil.

Synthesis of **3.22** via **3.26**

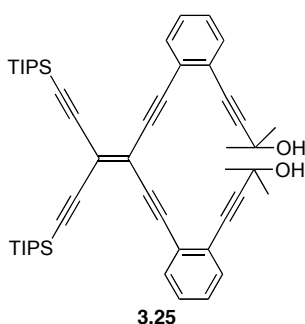
To a solution of **3.26** (62 mg, 0.079 mmol) in THF (3 mL) and MeOH (8 mL) was added aq KOH (0.2 mL, 0.2 mmol, 1.0 M). The reaction was stirred at rt for 3 h, and then quenched via the addition of saturated aq NH₄Cl (15 mL). The aq phase was extracted with Et₂O (2 x 10 mL). The combined organic phase was washed with H₂O (10 mL) and saturated aq NaCl (10 mL), dried with MgSO₄, filtered, and the solvent removed *in vacuo*. Column chromatography (silica gel, 4:1 Hex/CH₂Cl₂) afforded **3.22** (49 mg, 97%) as an amber oil.

Data for **3.22** (obtained from samples via **3.26**): $R_f = 0.6$ (5:1 Hex/CH₂Cl₂). IR (ATR): 3298 (m), 2060 (w), 2940 (s), 2891 (m), 2862 (s), 2187 (w), 2138 (w), 1463 (m). ¹H NMR (400 MHz, CDCl₃) δ 7.50–7.44 (m, 4H), 7.29–7.25 (m, 4H), 3.30 (s, 2H), 1.09–1.05 (m, 42H). ¹³C NMR (75 MHz, CDCl₃) δ 132.4, 132.0, 128.5, 128.2, 125.8, 124.9, 117.8, 117.5, 103.9, 102.4, 96.8, 90.6, 82.1, 81.7, 18.6, 11.2. APPI MS 669.39 ([M + H + MeOH]⁺, 100), 637.36 ([M + H]⁺, 60). APPI HRMS m/z calcd for C₄₄H₅₃Si₂ ([M + H]⁺) 637.3680, found 637.3672.



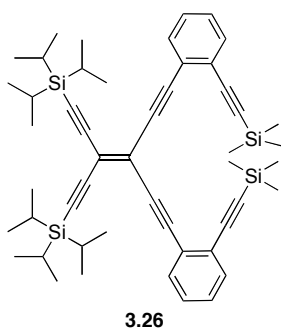
To a solution of 1,2-diiodobenzene (2.5 g, 7.6 mmol) and 2-methyl-3-propyn-2-ol (0.65 g, 7.7 mmol) in deoxygenated THF (10 mL) and *i*-Pr₂NH (1 mL) was added Pd(PPh₃)₄ (0.451 g, 0.390 mmol) and CuI (0.159 g, 0.835 mmol) at 0 °C. The flask was sealed under argon with a rubber septum, warmed to rt, and stirred for 18 h. The reaction was quenched via the addition of saturated aq NH₄Cl (25 mL). The aq phase was extracted with Et₂O (2 x 25 mL). The combined organic phase was washed with H₂O (20 mL) and

saturated aq NaCl (20 mL), dried with MgSO₄, filtered, and the solvent removed *in vacuo*. Column chromatography (silica gel, 2:1 Hex/EtOAc) afforded **3.23** (1.729 g, 79%) as an orange oily solid. *R*_f = 0.50 (2:1 Hex/EtOAc). IR (CH₂Cl₂ cast film): 3340 (br), 3054 (w), 2977 (m), 1459 (m) ¹H NMR (300 MHz, CDCl₃) δ 7.83–7.80 (m, 1H), 7.42–7.38 (m, 1H), 7.29–7.24 (m, 1H), 7.00–6.94 (m, 1H), 1.64 (s, 6H) ¹³C NMR (75 MHz, CDCl₃) δ 138.6, 132.4, 129.4, 129.1, 127.8, 101.3, 97.5, 84.5, 65.8, 31.3. EIMS *m/z* 286 (M⁺, 89), 271 ([M – Me]⁺, 100), 159 ([M – I]⁺, 95).



To a solution of **3.24** (646 mg, 2.52 mmol) in THF (10 mL) at 0 °C was added TBAF (2.6 mL, 2.6 mmol, 1.0 M). The reaction was stirred at 0 °C for 30 min, and then quenched via the addition of saturated aq NH₄Cl (25 mL). The aq phase was extracted with Et₂O (2 x 25 mL). The combined organic phase was washed with H₂O (20 mL) and saturated aq NaCl (20 mL), dried with MgSO₄, filtered, and the solvent reduced to *ca.* 5 mL *in vacuo*. The solution was then transferred to a flask charged with **2.25** (653 mg, 1.19 mmol) dissolved in dry, deoxygenated THF (6 mL) and *i*-Pr₂NH (1 mL), and purged with argon for 15 min. To this solution was added Pd(PPh₃)₄ (140 mg, 0.121 mmol) and CuI (42 mg, 0.22 mmol). The flask was sealed under argon with a rubber septum and stirred for 20 h. The reaction was quenched via the addition of saturated aq NH₄Cl (25 mL). The aq phase was extracted with Et₂O (2 x 25 mL). The combined organic phase was washed with H₂O (20 mL) and saturated aq NaCl (20 mL), dried with MgSO₄, filtered, and the solvent removed *in vacuo*. Column chromatography (silica gel, 5:1 Hex/EtOAc) afforded **3.25**

(666 mg, 74%) as an oily yellow solid. $R_f = 0.35$ (2:1 Hex/EtOAc). $M_p = 47\text{ }^\circ\text{C}$. IR (neat film): 2500–3200 (br), 3062 (w), 2944 (s), 2892 (m), 2866 (s), 2208 (w), 2188 (w), 2140 (w), 1483 (m), 1463 (m) ^1H NMR (400 MHz, CDCl_3) δ 7.45–7.39 (m, 4H), 7.28–7.21 (m, 4H), 2.74 (s, 2H), 1.53 (s, 12H), 1.08–1.04 (m, 42H). ^{13}C NMR (100 MHz, CDCl_3) δ 132.0, 131.7, 128.7, 127.8, 125.5, 125.3, 118.3, 116.9, 103.9, 102.7, 99.0, 97.1, 90.4, 80.6, 65.6, 31.1, 18.6, 11.3. ESI HRMS m/z calcd for $\text{C}_{50}\text{H}_{64}\text{NaO}_2\text{Si}_2$ ($[\text{M} + \text{Na}]^+$) 775.4337, found 775.4334.



Synthesis of **3.26** via **2.31**

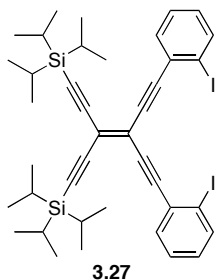
To a solution of **2.31** (1.00 g, 1.72 mmol) in THF (4 mL) and MeOH (10 mL) was added K_2CO_3 (0.530 g, 3.84 mmol). The reaction was stirred at rt for 1 h, and then quenched via the addition of saturated aq NH_4Cl (25 mL). The aq phase was extracted with Et_2O (2 x 25 mL). The combined organic phase was washed with H_2O (20 mL) and saturated aq NaCl (20 mL), dried with MgSO_4 , filtered, and the solvent reduced to *ca.* 5 mL *in vacuo*. The solution was then transferred to a flask charged with **3.13** (1.10 g, 3.67 mmol) dissolved in deoxygenated, dry THF (10 mL) and *i*- Pr_2NH (2 mL) and purged with argon for 15 min. To this solution was added $\text{Pd}(\text{PPh}_3)_4$ (100 mg, 0.0865 mmol) and CuI (33 mg, 0.17 mmol). The flask was sealed under argon with a rubber septum, heated to $50\text{ }^\circ\text{C}$, and stirred for 24 h. The solution was cooled to rt and the reaction quenched via the addition of saturated aq NH_4Cl (25 mL). The aq phase was extracted with Et_2O (2 x 25 mL). The combined organic phase was washed with H_2O (20 mL) and saturated aq NaCl

(20 mL), dried with MgSO₄, filtered, and the solvent removed *in vacuo*. Column chromatography (silica gel, 10:1 Hex/CH₂Cl₂) afforded **3.26** (1.117 g, 83%) as an amber oil.

Synthesis of **3.26** via **3.27**

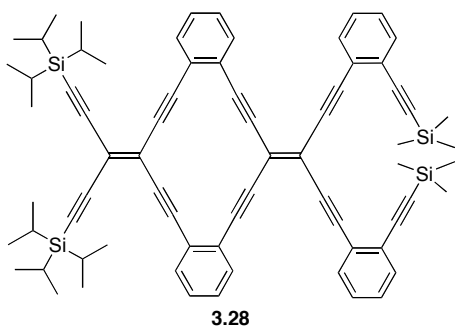
To a solution of **3.27** (0.105 g, 0.125 mmol) and trimethylsilylacetylene (0.10 mL, 0.068 g, 0.69 mmol) dissolved in deoxygenated, dry THF (5 mL) and *i*-Pr₂NH (1 mL) was added Pd(PPh₃)₄ (0.013 g, 0.011 mmol) and CuI (0.008 g, 0.04 mmol). The reaction was sealed under argon with a rubber septum, heated to 50 °C, and stirred for 4h. The solution was cooled to rt and the reaction quenched via the addition of saturated aq NH₄Cl (15 mL). The aq phase was extracted with Et₂O (2 x 15 mL). The combined organic phase was washed with H₂O (10 mL) and saturated aq NaCl (10 mL), dried with MgSO₄, filtered, and the solvent removed *in vacuo*. Column chromatography (silica gel, 4:1 Hex/CH₂Cl₂) afforded **3.26** (0.062 g, 63%) as an amber oil.

Data for **3.26** (obtained from samples via **2.31**): $R_f = 0.4$ (4:1 Hex/CH₂Cl₂). IR (ATR): 2942 (m), 2893 (m), 2863 (m), 2159 (w), 2144 (w), 1463 (m) ¹H NMR (400 MHz, CDCl₃) δ 7.44–7.40 (m, 4H), 7.25–7.18 (m, 4H), 1.07–1.02 (m, 42H), 0.14 (s, 18H). ¹³C NMR (75 MHz, CDCl₃) δ 132.0, 131.9, 128.3, 127.7, 126.0, 125.8, 118.2, 104.0, 103.0, 102.1, 99.6, 97.0, 90.4, 18.6, 11.3, 0.2 (one signal coincident or not observed). ESI HRMS m/z calcd for C₅₀H₆₈NaSi₄ ([M + Na]⁺) 803.4290, found 803.4305.



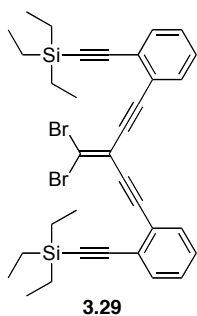
A solution of **2.35b** (100 mg, 0.127 mmol) in MeI (5 mL) was sealed under nitrogen in an Ace-glassware pressure tube. The reaction was heated to 140 °C and stirred for 24 h. The

reaction was cooled to rt and the remaining MeI was removed under vacuum, condensed, and quenched with MeOH. The residual product was purified by passed through a plug of silica gel with 4:1 Hex/CH₂Cl₂ to give **3.27** (105 mg, 98%) as an orange oily solid. $R_f = 0.40$ (4:1 Hex/CH₂Cl₂). IR (ATR): 2939 (s), 2890 (m), 2861 (s), 2202 (w), 2138 (w), 1460 (s). ¹H NMR (300 MHz, CDCl₃) δ 7.85–7.82 (m, 2H), 7.46 (dd, $J = 7.8$ Hz, 1.7 Hz, 2H), 7.28 (td, $J = 7.6$ Hz, 1.2 Hz, 2H), 7.00 (ddd, $J = 8.0$ Hz, 7.5 Hz, 1.7 Hz, 2H), 1.09–1.04 (m, 42H). ¹³C NMR (75 MHz, CDCl₃) δ 138.8, 133.0, 129.9, 129.3, 127.5, 117.8, 117.0, 103.9, 102.8, 101.0, 100.4, 89.9, 18.6, 11.2. MALDI m/z 713 ($[M - I]^+$, 100).

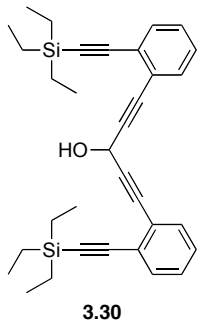


To a solution of **3.21** (85 mg, 0.091 mmol) in THF (5 mL) and MeOH (7 mL) was added KOH (25 mg, 0.45 mmol). The reaction was stirred at rt for 2 h, and then quenched via the addition of saturated aq NH₄Cl (25 mL). The aq phase was extracted with Et₂O (2 x 25 mL). The combined organic phase was washed with H₂O (20 mL) and saturated aq NaCl (20 mL), dried with MgSO₄, filtered, and the solvent reduced to *ca.* 5 mL *in vacuo*. The solution was then transferred to a flask charged with **3.13** (185 mg, 0.616 mmol) dissolved in deoxygenated, dry THF (4 mL) and *i*-Pr₂NH (2 mL). To this solution was added Pd(PPh₃)₄ (6 mg, 0.005 mmol) and CuI (1 mg, 0.005 mmol). The flask was sealed under nitrogen with a rubber septum and stirred for 24 h. The reaction was quenched via the addition of saturated aq NH₄Cl (15 mL). The aq phase was extracted with Et₂O (2 x 15 mL). The combined organic phase was washed with H₂O (10 mL) and saturated aq NaCl (10 mL), dried with MgSO₄, filtered, and the solvent removed *in vacuo*. Column

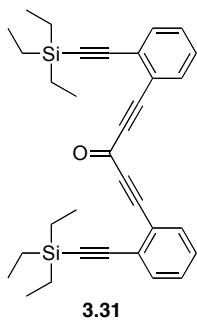
chromatography (silica gel, 10:1 Hex/CH₂Cl₂) afforded **3.28** (9 mg, 9%) as an orange film. $R_f = 0.40$ (2:1 Hex/CH₂Cl₂). ¹H NMR (400 MHz, CDCl₃) δ 7.90 (d, $J = 7.9$ Hz, 2H), 7.62–7.58 (m, 4H), 7.53–7.51 (m, 2H), 7.36 (t, $J = 7.5$ Hz, 2H), 7.32–7.28 (m, 4H), 7.06 (t, $J = 7.7$ Hz, 2H), 1.07–1.05 (m, 42H), 0.05 (s, 18H). ¹³C NMR (100 MHz, CDCl₃) δ 139.0, 133.1, 132.7, 132.2, 130.1, 129.4, 128.63, 128.60, 127.8, 125.5, 125.2, 117.7, 117.3, 116.7, 116.5, 104.4, 103.0, 101.1, 100.9, 97.7, 96.8, 91.8, 91.5, 90.6, 18.7, 11.3, 1.0 (two signals coincident or not observed).



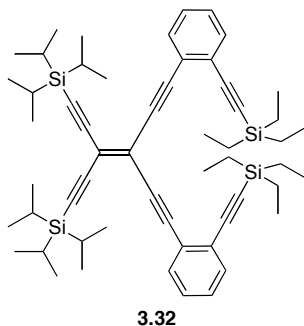
To a solution of PPh₃ (7.130 g, 27.18 mmol) and CBr₄ (4.468g, 13.47 mmol) in dry, deoxygenated CH₂Cl₂ (90 mL) was added a solution of **3.31** (3.226 g, 6.365 mmol) in dry, deoxygenated CH₂Cl₂ (10 mL). The solution was stirred for 3 h at rt. The reaction was quenched via the addition of hexanes, followed by a plug through silica gel with hexanes. Solvent removal *in vacuo* afforded **3.29** (3.849 g, 91%) as a yellow oil. $R_f = 0.60$ (2:1 Hex/CH₂Cl₂). IR (CH₂Cl₂ cast film): 3061 (w), 2955 (s) 2934 (s) 2910 (s) 2874 (s), 2204 (w), 2158 (m), 1480 (m) ¹H NMR (500 MHz, CDCl₃) δ 7.50–7.47 (m, 4H), 7.29–7.23 (m, 4H), 0.99 (t, $J = 7.9$ Hz, 18H), 0.63 (q, $J = 7.9$ Hz, 12H). ¹³C NMR (125 MHz, CDCl₃) δ 132.7, 132.2, 128.6, 127.9, 125.8, 124.9, 114.4, 108.6, 104.0, 97.0, 94.3, 89.2, 7.5, 4.4. EIMS m/z 583.2 ([M – Br]⁺, 5), 115.1 ([SiEt₃]⁺, 40). MALDI HRMS (DCTB) m/z calcd for C₃₄H₃₈⁷⁹Br⁸¹BrSi₂ (M⁺) 660.0873, found 662.0857.



To a solution of **3.17** (7.306 g, 30.39 mmol) in dry THF (150 mL) was added MeMgBr (9.2 mL, 28 mmol, 3.0 M in Et₂O). The solution was stirred for 30 min at rt, and ethyl formate (1.0 mL, 0.92 g, 12 mmol) was then added. The solution was gently heated to reflux and stirred under argon for 1 h. The solution was cooled to rt and the reaction quenched via the addition of saturated aq NH₄Cl (150 mL). The aq phase was extracted with Et₂O (2 x 100 mL). The combined organic phase was washed with H₂O (50 mL) and saturated aq NaCl (50 mL), dried with MgSO₄, filtered, and the solvent removed *in vacuo*. Column chromatography (silica gel, 7:1 Hex/EtOAc) afforded **3.30** (3.522 g, 56%) as a yellow oil. *R*_f = 0.20 (5:1 Hex/EtOAc). IR (CH₂Cl₂ cast film): 3550–3300 (br, m), 3061 (w), 2955 (s) 2935 (s) 2911 (s) 2875 (s), 2234 (w), 2158 (m) 1478 (m), 1442 (m) ¹H NMR (500 MHz, CDCl₃) δ 7.47–7.45 (m, 4H), 7.26–7.24 (m, 4H), 5.58 (d, *J* = 7.0 Hz, 1H), 2.24 (d, *J* = 8.0 Hz, 1H), 1.03 (t, *J* = 8.0 Hz, 18H), 0.64 (q, *J* = 8.0 Hz, 12H). ¹³C NMR (125 MHz, CDCl₃) δ 132.4, 132.2, 128.4, 126.1, 124.8, 104.2, 96.4, 89.6, 83.3, 53.4, 7.5, 4.4. EIMS *m/z* 508.3 (M⁺, 10), 493.2 ([M – Me]⁺, 45), 479.2 ([M – Et]⁺, 100). EI HRMS *m/z* calcd for C₃₃H₄₀OSi₂ (M⁺) 508.2619, found 508.2620.

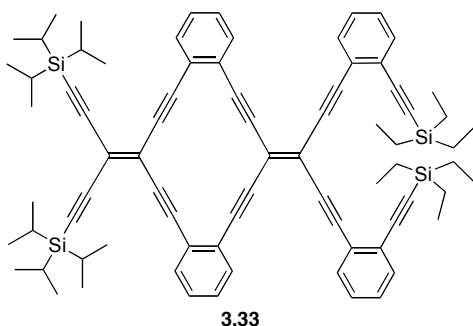


To a solution of **3.30** (3.522 g, 6.922 mmol) in dry, deoxygenated CH₂Cl₂ (150 mL) was added 4Å mol. sieves (5 g), celite (5 g) and PCC (2.249 g, 10.43 mmol). The solution was stirred for 24 h at rt. The reaction was quenched via a plug through silica gel with CH₂Cl₂. Solvent removal *in vacuo* afforded **3.31** (3.226 g, 92%) as a yellow oil. *R*_f = 0.40 (5:1 Hex/EtOAc). IR (CH₂Cl₂ cast film): 3063 (w), 2955 (s), 2935 (s), 2911 (s), 2875 (s), 2217 (s), 2185 (s), 2160 (m), 1622 (s), 1477 (m). ¹H NMR (500 MHz, CDCl₃) δ 7.56 (ddd, *J* = 7.7 Hz, 1.4 Hz, 0.6 Hz, 2H), 7.51 (ddd, *J* = 7.8 Hz, 1.3 Hz, 0.6 Hz, 2H), 7.4 (td, *J* = 7.7 Hz, 1.4 Hz, 2H), 7.30 (td, *J* = 7.3 Hz, 1.4 Hz, 2H), 0.99 (t, *J* = 7.9 Hz, 18H), 0.64 (q, *J* = 7.9 Hz, 12H). ¹³C NMR (125 MHz, CDCl₃) δ 160.3, 133.1, 132.5, 130.3, 128.0, 127.4, 122.6, 103.0, 98.6, 92.0, 89.5, 7.5, 4.3. EIMS *m/z* 491.1 ([M – Me]⁺, 10), 477.2 ([M – Et]⁺, 100). MALDI HRMS (DCTB) *m/z* calcd for C₃₃H₃₉OSi₂ ([M + H]⁺) 507.2534, found 507.2534.



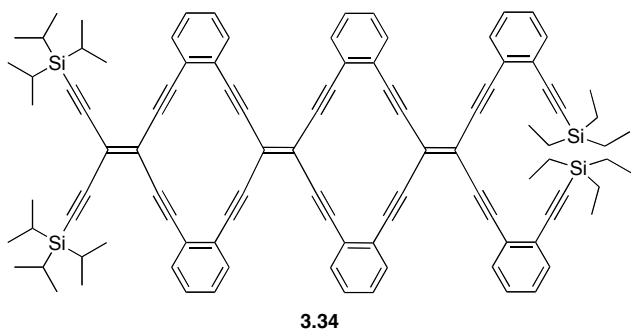
To a solution of **3.29** (1.244 g, 1.877 mmol) in deoxygenated, dry Et₃N (10 mL) was added Pd(PPh₃)₄ (0.125 g, 0.108 mmol) and CuI (0.039 g, 0.205 mmol). The solution was purged with argon for an additional 10 min after which triisopropylsilylacetylene (2.2

mL, 1.8 g, 9.8 mmol) was added. The flask was sealed under argon with a rubber septum and stirred for 4 h at 50 °C. The solution was cooled to rt and the reaction was quenched via the addition of saturated aq NH₄Cl (25 mL). The aq phase was extracted with Et₂O (2 x 25 mL). The combined organic phase was washed with H₂O (20 mL) and saturated aq NaCl (20 mL), dried with MgSO₄, filtered, and the solvent removed *in vacuo*. Column chromatography (silica gel, 5:1 Hex/CH₂Cl₂) afforded **3.32** (1.493 g, 92%) as a dark amber oil. *R*_f = 0.60 (5:1 Hex/CH₂Cl₂). UV-vis (THF) λ_{max}: 238, 322, 362, 372, 390 nm. IR (CH₂Cl₂ cast film): 2956 (s), 2866 (s), 2159 (w), 1463 (m) ¹H NMR (500 MHz, CDCl₃) δ 7.46–7.42 (m, 4H), 7.24–7.19 (m, 4H), 1.05–1.02 (m, 42H), 0.93 (t, *J* = 7.9 Hz, 18H), 0.58 (q, *J* = 7.9 Hz, 12H). ¹³C NMR (125 MHz, CDCl₃) δ 132.2, 132.0, 128.2, 127.5, 126.1, 125.7, 118.3, 117.8, 104.04, 103.97, 101.9, 97.04, 96.97, 90.2, 18.6, 11.2, 7.4, 4.3. MALDI HRMS (DCTB) *m/z* calcd for C₅₆H₈₀Si₄ (M⁺) 864.5331, found 864.5335.



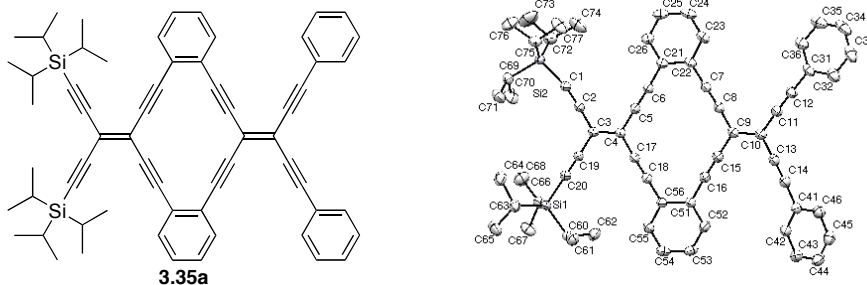
To a solution of **3.32** (754 mg, 0.871 mmol) in THF (4 mL) and MeOH (15 mL) was added KOH (490 mg, 8.73 mmol). The reaction was stirred at rt for 6 h, and then quenched via the addition of saturated aq NH₄Cl (25 mL). The aq phase was extracted with Et₂O (2 x 25 mL). The combined organic phase was washed with H₂O (20 mL) and saturated aq NaCl (20 mL), dried with MgSO₄, filtered, and the solvent reduced to *ca.* 5 mL *in vacuo*. The solution was then transferred to a flask charged with **3.29** (574 mg, 0.866 mmol) dissolved in Et₃N (12 mL), and purged with argon for 15 min. To this

solution was added Pd(PPh₃)₄ (53 mg, 0.046 mmol) and CuI (16 mg, 0.084 mmol). The flask was sealed under argon with a rubber septum, heated to 50 °C, and stirred for 16 h. The solution was cooled to rt and the reaction quenched via the addition of saturated aq NH₄Cl (25 mL). The aq phase was extracted with Et₂O (2 x 25 mL). The combined organic phase was washed with H₂O (20 mL) and saturated aq NaCl (20 mL), dried with MgSO₄, filtered, and the solvent removed *in vacuo*. Column chromatography (silica gel, 3:1 Hex/CH₂Cl₂) afforded **3.33** (391 mg, 40%) as a bright yellow solid. *R*_f = 0.33 (2:1 Hex/CH₂Cl₂). UV-vis (THF) λ_{max} (ε): 286 (87 100), 328 (37 800), 338 (35 200), 388 (24 800), 450 (52 300), 470 (59 300) nm. IR (CHCl₃ cast film): 3060 (w), 2955 (s), 2887 (s), 2867 (s), 2188 (w), 2157 (w), 1481 (m), 1463 (m) ¹H NMR (500 MHz, CDCl₃) δ 7.60–7.57 (m, 2H), 7.54–7.50 (m, 4H), 7.49–7.46 (m, 2H), 7.31–7.29 (m, 4H), 7.27–7.21 (m, 4H), 1.15–1.11 (m, 42H), 0.92 (t, *J* = 7.9 Hz, 18H), 0.54 (q, *J* = 7.9 Hz, 12H). ¹³C NMR (125 MHz, CDCl₃) δ 132.6, 132.5, 132.1, 132.0, 128.6, 128.5, 128.4, 127.9, 126.0, 125.53, 125.48, 125.3, 118.1, 117.6, 117.2, 116.9, 104.5, 103.8, 102.8, 97.9, 97.43, 97.35, 96.9, 91.9, 91.3, 90.6, 18.7, 11.4, 7.5, 4.3. MALDI HRMS (DCTB) *m/z* calcd for C₇₈H₈₈Si₄ (M⁺) 1136.5958, found 1136.5957.



To a solution of **3.33** (391 mg, 0.344 mmol) in THF (7 mL) and MeOH (15 mL) was added KOH (195 mg, 3.46 mmol). The reaction was stirred at rt for 4 h, and then quenched via the addition of saturated aq NH₄Cl (25 mL). The aq phase was extracted with Et₂O (2 x 25 mL). The combined organic phase was washed with H₂O (20 mL) and

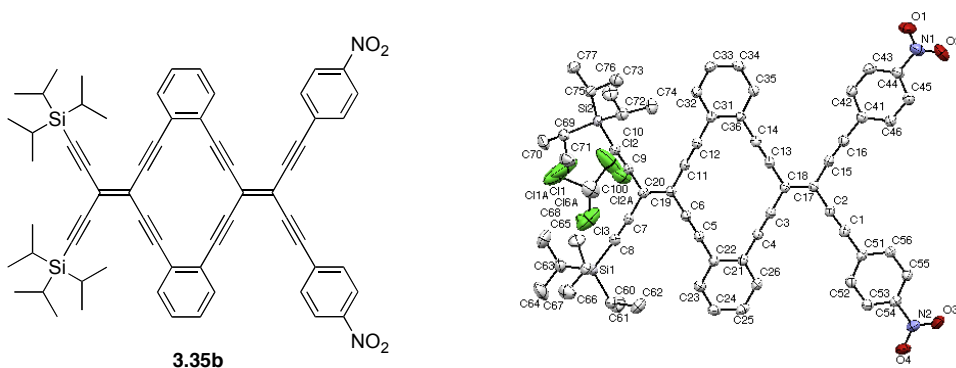
saturated aq NaCl (20 mL), dried with MgSO₄, filtered, and the solvent reduced to *ca.* 5 mL *in vacuo*. The solution was then transferred to a flask charged with **3.29** (223 mg, 0.336 mmol) dissolved in deoxygenated, dry Et₃N (6 mL), and purged with argon for 15 min. To this solution was added Pd(PPh₃)₄ (20 mg, 0.017 mmol) and CuI (8 mg, 0.040 mmol). The flask was sealed with a rubber septum under argon, heated to 50 °C, and stirred for 16 h. The solution was cooled to rt and the reaction quenched via the addition of saturated aq NH₄Cl (25 mL). The aq phase was extracted with Et₂O (2 x 25 mL). The combined organic phase was washed with H₂O (20 mL) and saturated aq NaCl (20 mL), dried with MgSO₄, filtered, and the solvent removed *in vacuo*. Column chromatography (alumina, neutral, 4:1→2:1 Hex/CH₂Cl₂) afforded **3.34** (88 mg, 19%) as a dark red solid. *R*_f = 0.50 (1:1 Hex/CH₂Cl₂). UV-vis (THF) λ_{max}: 288, 388, 494, 516 nm. IR (CHCl₃ cast film): 3061 (w), 2954 (s), 2889 (s), 2867 (s), 2184 (w), 2157 (w), 2138 (w), 1484 (m), 1462 (m) ¹H NMR (500 MHz, CDCl₃) δ 7.66–7.63 (m, 4H), 7.61–7.59 (m, 2H), 7.55–7.50 (m, 6H), 7.39–7.25 (m, 12H), 1.17–1.08 (m, 42H), 0.94 (t, *J* = 7.9 Hz, 18H), 0.56 (q, *J* = 7.9 Hz, 12H). ¹³C NMR (125 MHz, CDCl₃) δ 132.7, 132.6, 132.2, 132.1, 131.74, 131.70, 128.8, 128.73, 128.68, 128.6, 128.5, 127.9, 126.0, 125.54, 125.52, 125.47, 125.43, 125.35 118.1, 117.6, 117.4, 117.11, 117.09, 116.8, 104.4, 103.8, 102.9, 98.00, 97.87, 97.49, 97.39, 96.8, 92.16, 92.11, 92.07, 91.5, 90.7, 18.7, 11.3, 7.5, 4.3 (one signal coincident or not observed). MALDI HRMS (DCTB) *m/z* calcd for C₁₀₀H₉₆Si₄ (M⁺) 1408.6584, found 1408.6596.



To a solution of **3.21** (31 mg, 0.033 mmol) in THF (6 mL) and MeOH (8 mL) was added KOH (20 mg, 0.36 mmol). The reaction was stirred at rt for 1 h, and then quenched via the addition of saturated aq NH₄Cl (25 mL). The aq phase was extracted with Et₂O (2 x 25 mL). The combined organic phase was washed with H₂O (20 mL) and saturated aq NaCl (20 mL), dried with MgSO₄, filtered, and the solvent reduced to *ca.* 5 mL *in vacuo*. The solution was then transferred to a flask charged with iodobenzene (11 μL, 20 mg, 0.099 mmol) dissolved in deoxygenated, dry THF (5 mL) and *i*-Pr₂NH (1 mL). To this solution was added Pd(PPh₃)₄ (2 mg, 0.002 mmol) and CuI (1 mg, 0.005 mmol). The flask was sealed with a rubber septum under N₂ and stirred for 1 h. The reaction was quenched via the addition of saturated aq NH₄Cl (15 mL). The aq phase was extracted with Et₂O (2 x 15 mL). The combined organic phase was washed with H₂O (10 mL) and saturated aq NaCl (10 mL), dried with MgSO₄, filtered, and the solvent removed *in vacuo*. Column chromatography (alumina, neutral, Hexanes → 2:1 Hex/CH₂Cl₂) afforded **3.35a** (21 mg, 75%) as a bright orange solid. *R*_f = 0.6 (2:1 Hex/CH₂Cl₂). Mp = 195–200 °C (decomp). UV-vis (THF) λ_{max} (ε): 285 (86 600), 305 (32 700), 338 (29 500), 386 (18 300), 467 (52 400) nm. IR (CH₂Cl₂ cast film): 3062 (w), 2943 (s), 2891 (m), 2865 (s), 2187 (w), 2137 (w), 1486 (m). ¹H NMR (400 MHz, CDCl₃) δ 7.64–7.59 (m, 4H), 7.55–7.50 (m, 4H), 7.40–7.37 (m, 6H), 7.31–7.27 (m, 4H), 1.15–1.11, (m, 42H). ¹³C NMR (75 MHz, CDCl₃) δ 132.2, 131.9, 131.8, 129.2, 128.7, 128.6, 128.5, 125.4, 122.6, 117.7, 117.2, 117.0, 116.7, 104.4, 103.0, 99.5, 97.3, 96.8, 91.7, 91.4, 87.6, 18.7, 11.3 (one signal

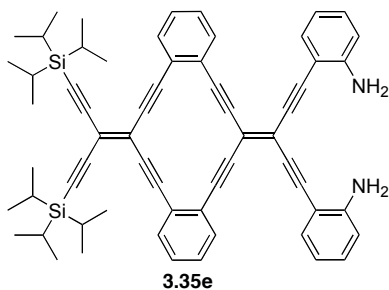
coincident or not observed). ESI HRMS m/z calcd for $C_{62}H_{60}NaSi_2$ ($[M + Na]^+$) 883.4126, found 883.4126. DSC: decomposition, 190 °C (onset), 195 °C (peak).

Crystals suitable for X-ray crystallography by slow evaporation of solutions of **3.35a** in dichloromethane/hexanes left standing in the dark at rt for several days. X-ray crystallographic data for **3.35a** (ADM05): $C_{62}H_{60}Si_2$, $M_r = 861.28$; crystal dimensions (mm) $0.3139 \times 0.0789 \times 0.0355$; triclinic space group $P\bar{1}$ (no. 2); $a = 14.5441(8)$ Å, $b = 14.7350(9)$ Å, $c = 15.0170(10)$ Å; $\alpha = 118.291(7)^\circ$, $\beta = 107.091(5)^\circ$, $\gamma = 96.452(5)^\circ$; $V = 2584.8(3)$ Å³; $Z = 2$; $\rho_{\text{calcd}} = 1.107$ mg mm⁻³; $\mu = 0.894$ mm⁻¹; $\lambda = 1.54178$ Å; $T = -100$ °C; $2\theta_{\text{max}} = 147.1^\circ$; total data collected = 15535; $R_1 = 0.0378$; $wR_2 = 0.1071$ for 589 variables, 9871 unique reflections, and 0 restraints; residual electron density = 0.31 and -0.36 e Å⁻³.



To a solution of **3.21** (42 mg, 0.045 mmol) in THF (8 mL) and MeOH (10 mL) was added KOH (25 mg, 0.45 mmol). The reaction was stirred at rt for 2 h, and then quenched via the addition of saturated aq NH_4Cl (25 mL). The aq phase was extracted with Et_2O (2 x 25 mL). The combined organic phase was washed with H_2O (20 mL) and saturated aq $NaCl$ (20 mL), dried with $MgSO_4$, filtered, and the solvent reduced to *ca.* 5 mL *in vacuo*. The solution was then transferred to a flask charged with 4-iodo-nitrobenzene (34 mg, 0.14 mmol) dissolved in deoxygenated, dry THF (5 mL) and *i*- Pr_2NH (1 mL). To this solution was added $Pd(PPh_3)_4$ (3 mg, 0.003 mmol) and CuI (1 mg, 0.005 mmol). The

flask was sealed with a rubber septum under N₂ and stirred for 1 h. The reaction was quenched via the addition of saturated aq NH₄Cl (15 mL). The aq phase was extracted with Et₂O (2 x 15 mL). The combined organic phase was washed with H₂O (10 mL) and saturated aq NaCl (10 mL), dried with MgSO₄, filtered, and the solvent removed *in vacuo*. Column chromatography (alumina, neutral, 1:1 Hex/CH₂Cl₂) afforded **3.35b** (38 mg, 88%) as a bright orange solid. $R_f = 0.35$ (1:1 Hex/CH₂Cl₂). Mp = 225 °C (decomp). UV-vis (THF) λ_{\max} (ϵ): 286 (74 600), 330 (48 500), 344 (54 400), 393 (28 200), 471 (56 900) nm. IR (ATR): 2940 (m), 2891 (m), 2863 (m), 2182 (w), 2133 (w), 1590 (m). ¹H NMR (400 MHz, CDCl₃) δ 8.25 (d, $J = 8.9$, 4H), 7.74, (d, $J = 8.9$, 4H) 7.56–7.43 (m, 2H), 7.47–7.45 (m, 2H), 7.36–7.30 (m, 4H), 1.16–1.12, (m, 42H). ¹³C NMR (100 MHz, CDCl₃) δ 147.6, 132.4, 131.8, 129.3, 129.1, 128.8, 125.8, 124.7, 123.9, 120.6, 118.3, 116.3, 114.4, 104.3, 103.5, 99.4, 97.1, 96.5, 91.7, 91.5, 91.3, 18.7, 11.4 (one signal coincident or not observed). ESI HRMS m/z calcd for C₆₂H₅₈N₂NaO₄Si₂ ([M + Na]⁺) 973.3827, found 973.3811. DSC: decomposition, 221 °C (onset), 228 °C (peak). Crystals suitable for X-ray crystallography by slow evaporation of a solution of **3.35b** in CDCl₃ left standing in the dark at 4 °C for several days. X-ray crystallographic data for **3.35b** (ADM02): C₆₃H₅₉N₂O₄Si₂Cl₃, $M_r = 1070.65$; crystal dimensions (mm) 0.2492 × 0.0922 × 0.0574; triclinic space group $P\bar{1}$ (no. 2); $a = 7.5624(4)$ Å, $b = 16.0301(8)$ Å, $c = 25.9429(13)$ Å; $\alpha = 107.327(5)^\circ$, $\beta = 93.017(4)^\circ$, $\gamma = 100.290(4)^\circ$; $V = 2935.1(3)$ Å³; $Z = 2$; $\rho_{\text{calcd}} = 1.211$ mg mm⁻³; $\mu = 2.175$ mm⁻¹; $\lambda = 1.54178$ Å; $T = -100$ °C; $2\theta_{\text{max}} = 146.88^\circ$; total data collected = 17654; $R_1 = 0.0505$; $wR_2 = 0.1419$ for 707 variables, 11177 unique reflections, and 15 restraints; residual electron density = 0.41 and -0.44 e Å⁻³. One disordered CHCl₃ per asymmetric unit. Three Cl atoms split positions refined to 50:50 occupation.

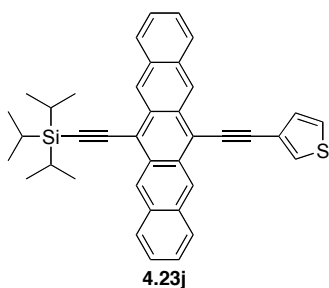


To a solution of **3.21** (52 mg, 0.055 mmol) in THF (5 mL) and MeOH (10 mL) was added KOH (33 mg, 0.59 mmol). The reaction was stirred at rt for 1 h and then quenched via the addition of saturated aq NH₄Cl (25 mL). The aq phase was extracted with Et₂O (2 x 25 mL). The combined organic phase was washed with H₂O (20 mL) and saturated aq NaCl (20 mL), dried with MgSO₄, filtered, and the solvent reduced to *ca.* 5 mL *in vacuo*. The solution was then transferred to a flask charged with 2-iodoaniline (37 mg, 0.17 mmol) dissolved in deoxygenated, dry THF (5 mL) and *i*-Pr₂NH (1 mL) that had been purged with N₂ for 15 min. To this solution was added Pd(PPh₃)₄ (3 mg, 0.003 mmol) and CuI (1 mg, 0.005 mmol). The flask was sealed under N₂ with a rubber septum and stirred for 2 h. The reaction was quenched via the addition of saturated aq NH₄Cl (15 mL). The aq phase was extracted with Et₂O (2 x 15 mL). The combined organic phase was washed with H₂O (10 mL) and saturated aq NaCl (10 mL), dried with MgSO₄, filtered, and the solvent removed *in vacuo*. Column chromatography (alumina, neutral, 1:2 Hex/CH₂Cl₂) afforded **3.35e** (36 mg, 73%) as a dark orange solid. *R*_f = 0.4 (1:1 Hex/CH₂Cl₂). ¹H NMR (300 MHz, CDCl₃) δ 7.57–7.50 (m, 4H), 7.42 (dd, *J* = 7.8 Hz, 1.2 Hz, 2H), 7.34–7.26 (m, 4H), 7.18 (d, *J* = 7.7 Hz, 2H), 6.74–6.70 (m, 4H), 4.42 (s, 4H), 1.23–1.06, (m, 42H). ¹³C NMR (75 MHz, CDCl₃) δ 148.5, 132.6, 132.2, 132.1, 130.9, 128.7, 128.4, 125.4, 125.1, 117.8, 117.6, 117.5, 116.7, 114.2, 114.1, 106.7, 104.3, 102.9, 96.8, 96.7, 93.4, 92.0, 91.4, 18.7, 11.3 (one signal coincident or not observed). ESI HRMS *m/z* calcd for C₆₂H₆₂N₂NaSi₂ ([M + Na]⁺) 913.4344, found 913.4320.

6.4 Experimental Details for Chapter 4

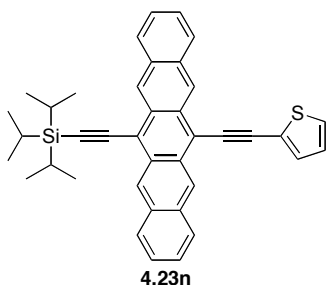
General Procedure A – Thienyl-substituted pentacene synthesis.

Unless otherwise noted in the individual procedures, a solution of **4.26b** (*ca.* 1 equiv per thienyl halide) and thienyl halide (1 equiv) in deoxygenated, dry THF and Et₃N was added Pd(PPh₃)₄ (*ca.* 0.05 equiv) and CuI (*ca.* 0.1 equiv). The flask was sealed under argon with a rubber septum and stirred for 24 h. The reaction was quenched via the addition of saturated aq NH₄Cl (25 mL). The aq phase was extracted with CH₂Cl₂ (2 x 25 mL). The combined organic phase was washed with H₂O (20 mL) and saturated aq NaCl (20 mL), dried with MgSO₄, filtered, and the solvent removed *in vacuo*. The crude product was passed through a plug of silica gel with hexanes:CH₂Cl₂ (1:1) and the solvent removed *in vacuo*. The product was dissolved in deoxygenated, dry THF to which SnCl₂•2H₂O (*ca.* 2.5 equiv per **4.26b**) and 1–2 drops 10% H₂SO₄ were added. The flask was sealed under argon with a rubber septum, covered with aluminum foil, and stirred for 24 h. The reaction was quenched by passing through a plug of silica gel with CH₂Cl₂. Precipitation from EtOAc with hexanes or CH₂Cl₂ with MeOH at –78 °C and/or column chromatography afforded the desired thiophenyl substituted pentacene.



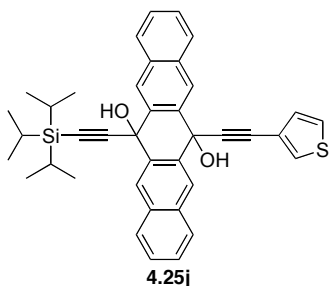
To a solution of **4.25j** (0.152 g, 0.254 mmol) in deoxygenated, dry THF (8 mL) was added SnCl₂•2H₂O (0.148 g, 0.579 mmol). The flask was sealed under argon with a rubber septum, covered in aluminum foil, and stirred at rt for 5 h. The reaction was quenched by passing through a plug of silica gel with 1:1 Hex:CH₂Cl₂ and the solvent removed *in vacuo*. Column chromatography (silica gel, 2:1 Hex/CH₂Cl₂) afforded **4.23j**

(0.129 g, 90%) as a dark blue solid. $R_f = 0.30$ (2:1 Hex/CH₂Cl₂). Mp = 165–170 °C (decomp). UV-vis (CH₂Cl₂) λ_{\max} (ϵ): 310 (173 600), 354 (20 000), 438 (3 900), 598 (12 500), 652 (21 900) nm. IR (CH₂Cl₂ cast film): 3047 (w), 2941 (s), 2890 (m), 2863 (s), 2123 (m), 1463 (m). ¹H NMR (500 MHz, CDCl₃) δ 9.32 (s, 2H), 9.25 (s, 2H), 8.04–8.01 (m, 2H), 7.97–7.94 (m, 2H), 7.88 (dd, $J = 2.9$ Hz, 1.0 Hz, 1H), 7.55 (dd, $J = 4.9$ Hz, 1.0 Hz, 1H), 7.49 (dd, $J = 4.9$ Hz, 3.0 Hz, 1H), 7.42–7.38 (m, 4H), 1.41–1.35 (m, 21H). ¹³C NMR (125 MHz, CDCl₃) δ 132.24, 132.16, 130.6, 130.12, 130.07, 129.1, 128.7, 128.6, 128.4, 125.96, 125.88, 125.8, 122.8, 118.2, 118.0, 107.0, 104.9, 99.4, 87.5, 19.1, 11.8. ESI HRMS m/z calcd for C₃₉H₃₇SSi ([M + H]⁺) 565.2380, found 565.2392. TGA: $T_d \approx 375$ °C. DSC: decomp, 159 °C (onset), 172 °C (peak). Anal. calcd for C₃₉H₃₆SSi: C, 82.93, H, 6.42; S, 5.68. Found; C, 82.98; H, 6.52; S, 5.52.



A solution of **4.26b** (200 mg, 0.367 mmol) and 2-bromothiophene (0.10 mL, 170 mg, 1.0 mmol) in deoxygenated, dry THF (10 mL) and Et₃N (2 mL) was subjected to general procedure A. Column chromatography (silica gel, 2:1 Hex/CH₂Cl₂) afforded **4.23n** (37 mg, 18%) as a dark blue/green solid. $R_f = 0.50$ (2:1 Hex/CH₂Cl₂). Mp = 210–215 °C. UV-vis (CH₂Cl₂) λ_{\max} (ϵ): 274 (35 400), 312 (88 200), 378 (12 800), 602 (6 600), 656 (10 400) nm. IR (CH₂Cl₂ cast film): 3048 (w), 2941 (s), 2890 (m), 2864 (s), 2129 (w), 1462 (m). ¹H NMR (300 MHz, CD₂Cl₂) δ 9.32 (s, 2H), 9.23 (s, 2H), 8.10–7.98 (m, 4H), 7.68 (dd, $J = 3.6$ Hz, 1.0 Hz, 1H), 7.54 (dd, $J = 5.2$ Hz, 1.0 Hz, 1H), 7.48–7.42 (m, 4H), 7.23 (dd, $J = 5.2$ Hz, 3.7 Hz, 1H), 1.45–1.37 (m, 21H). ¹³C NMR (125 MHz, CD₂Cl₂) δ 133.0, 132.7, 130.9, 128.93, 128.88, 128.0, 126.7, 126.64, 126.58, 126.1, 118.9, 117.9, 108.2,

104.9, 98.2, 92.0, 19.2, 12.1. MALDI HRMS (DCTB) m/z calcd for $C_{38}H_{36}SSi$ (M^+) 564.2302, found 564.2295.

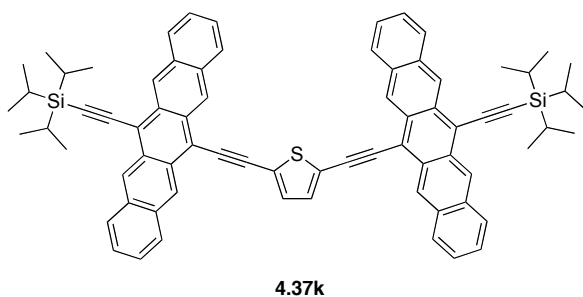


To a solution of triisopropylsilylacetylene (0.24 mL, 0.20 g, 1.1 mmol) in dry THF (5 mL) cooled to -78 °C was added *n*-BuLi (0.35 mL, 0.88 mmol, 2.5 M in hexanes). The solution was stirred for 10 min at -78 °C, before being transferred via cannula to a suspension of 6,13-pentacenequinone (0.299 g, 0.969 mmol) in THF (10 mL) at rt. The suspension was stirred at rt for 2 h. The reaction was then cooled to -78 °C and stirring stopped to allow undissolved 6,13-pentacenequinone to settle to the bottom of the flask. The supernatant was transferred via cannula to a solution of lithiated 3-ethynylthiophene (see below) cooled to -78 °C. The reaction was warmed to rt and stirred for 5 h. The reaction mixture was cooled to -78 °C and quenched via the addition of saturated aq NH_4Cl (25 mL). The aq phase was extracted with CH_2Cl_2 (2 x 25 mL). The combined organic phase was washed with H_2O (50 mL) and saturated aq NaCl (50 mL), dried with $MgSO_4$, filtered, and the solvent removed *in vacuo*. Column chromatography (silica gel, 2:1 Hex/EtOAc) afforded **4.25j** (0.477 g, 91%) as a pale brown solid. $R_f = 0.40$ (2:1 CH_2Cl_2 /Hex). IR (CH_2Cl_2 cast film): 3550–3300 (br, m), 3055 (w), 2943 (s), 2890 (m), 2865 (s), 2231 (w), 2173 (w) 1495 (m). 1H NMR (500 MHz, $CDCl_3$) δ 8.77 (s, 2H), 8.59 (s, 2H), 7.96–7.93 (m, 2H), 7.91–7.88 (m, 2H), 7.55–7.51 (m, 4H), 7.38 (dd, $J = 3.0$ Hz, 1.1 Hz, 1H), 7.16 (dd, $J = 5.1$ Hz, 3.0 Hz, 1H), 7.01 (dd, $J = 5.1$ Hz, 1.1 Hz, 1H), 3.43 (s, 1H), 3.42 (s, 1H), 1.21–1.16 (m, 21H). ^{13}C NMR (125 MHz, $CDCl_3$) δ 137.3, 135.3, 133.4, 133.2, 129.80, 129.77, 128.3, 128.2, 127.03, 126.97, 126.9, 125.3, 125.1, 120.8,

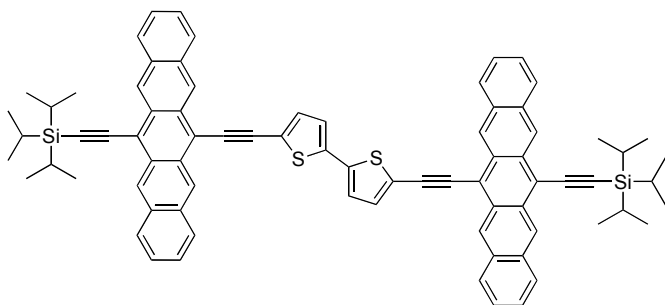
108.2, 91.6, 90.7, 82.5, 70.9, 68.8, 18.8, 11.4. ESI HRMS m/z calcd for $C_{39}H_{38}NaO_2SSi$ ($[M + Na]^+$) 621.2254, found 621.2245.

Preparation of lithiated 3-ethynylthiophene solution:

To a solution of 3-ethynylthiophene (0.229 g, 2.12 mmol) in dry THF (5 mL) cooled to -78 °C was added *n*-BuLi (0.8 mL, 2.0 mmol, 2.5 M in hexanes) and the solution was stirred for 30 min.

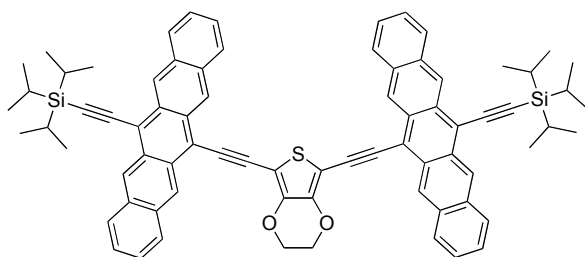


A solution of **4.26b** (175 mg, 0.321 mmol) and 2,5-diiodothiophene (51 mg, 0.15 mmol) in deoxygenated, dry THF (2 mL) and Et_3N (5 mL) was subjected to general procedure A. Precipitation from CH_2Cl_2 with MeOH afforded **4.37k** (55 mg, 35%) as a deep blue/green solid. $R_f = 0.55$ (2:1 Hex/ CH_2Cl_2). Mp = > 300 °C. UV-vis (CH_2Cl_2) λ_{max} (ϵ): 314 (174 400), 406 (21 100), 704 (28 200) nm. IR (CH_2Cl_2 cast film): 3048 (m), 2941 (s), 2890 (m), 2864 (s), 2127 (m), 1463 (m). 1H NMR (500 MHz, CD_2Cl_2) δ 9.35 (br s, 2H), 9.27 (br s, 2H), 9.22 (br s, 2H), 9.14 (br s, 2H), 8.13 (br s, 2H), 8.05 (br s, 2H), 7.99 (br s, 4H), 7.72 (br s, 2H), 7.47 (br s, 8H), 1.46–1.34 (m, 42H). ^{13}C NMR (125 MHz, CD_2Cl_2) δ 132.72, 132.68, 130.7, 130.2, 129.0, 128.8, 126.7, 126.02, 125.99, 125.93, 125.92, 19.2, 12.1 (five signals coincident or not observed). MALDI HRMS (DCTB) m/z calcd for $C_{74}H_{68}SSi_2$ (M^+) 1044.4575, found 1044.4569.



4.37I

A solution of **4.26b** (200 mg, 0.367 mmol) and 5,5-diiodo-2,2'-bithiophene (69 mg, 0.17 mmol) in deoxygenated, dry THF (2 mL) and Et₃N (2 mL) was subjected to general procedure A. Precipitation from EtOAc with hexanes afforded **4.37I** (143 mg, 75%) as a dark blue/green solid that was insoluble in common organic solvents. The product was insufficiently soluble for meaningful NMR spectroscopic analysis. $R_f = 0.40$ (2:1 Hex/CH₂Cl₂). Mp = > 300 °C. UV-vis (CH₂Cl₂) λ_{max} (ϵ): 272 (42 500), 314 (211 600), 440 (24 200), 628 (19 200), 684 (34 800) nm. IR (CH₂Cl₂ cast film): 3047 (w), 2941 (s), 2891 (m), 2864 (s), 2124 (m), 1463 (m). MALDI HRMS (DCTB) m/z calcd for C₇₈H₇₀S₂Si₂ (M⁺) 1126.4452, found 1126.4440.



4.37m

A solution of **4.26b** (175 mg, 0.321 mmol) and 2,5-diiodo-3,4-ethylenedioxythiophene (60 mg, 0.15 mmol) in deoxygenated, dry THF (2 mL) and Et₃N (5 mL) was subjected to general procedure A. Precipitation from EtOAc with hexanes afforded **4.37m** (21 mg, 12%) as a dark blue/green that was insoluble in common organic solvents. The product was insufficiently soluble for meaningful NMR spectroscopic analysis. $R_f = 0.6$ (2:1 Hex/CH₂Cl₂). Mp = > 300 °C. UV-vis (CH₂Cl₂) λ_{max} : 316, 422, 720 nm. IR (CH₂Cl₂ cast

film): 3050 (w), 2942 (s), 2890 (m), 2865 (s), 2121 (w), 2065 (w), 1527 (m). MALDI HRMS (DCTB) m/z calcd for $C_{76}H_{70}O_2SSi_2$ (M^+) 1102.4630, found 1102.4621.

6.5 References

1. Karpov, G. V.; Popik, V. V. *J. Am. Chem. Soc.* **2007**, *129*, 3892–3793.